Structure and Dynamics of Block Copolymer Micelles

A DISSERTATION

SUBMITTED TO THE FACULTY OF

UNIVERSITY OF MINNESOTA

BY

En Wang

IN PARTIAL FULFILLMENT OF THE REQUIREMENTS

FOR THE DEGREE OF

DOCTOR OF PHILOSOPHY

Advisors: Frank S. Bates and Timothy P. Lodge

August 2019

Acknowledgement

I would like to first thank my advisors Prof. Frank Bates and Prof. Timothy Lodge for their guidance for the last 5 years of my graduate school. Their broad knowledge in polymer science deeply impressed me throughout every conversation and meeting. I greatly appreciate the big picture and elaborate details that they shared with me, without which this dissertation would not be possible. When I had challenges in research, they are always there supporting me to resolve tough questions. This drives me to cultivate problem solving skills and critical thinking ability. I am grateful for offering me opportunity to present my work in public, e.g., American Physics Society annual conferences and IPRIME annual meetings, and guiding me to write professional proposals and manuscripts.

Also, I want to thank my preliminary written and oral exam committee, Prof. Marc Hillmyer, Prof. Mahesh Mahanthappa, Prof. Xiang Cheng and Prof. David Flannigan, for their thoughts and suggestions on my research. I appreciate discussions with Prof. David Morse and Prof. Chris Macoskco as well. It is great experience to interact with many talented professors in the Department of Chemical Engineering and Materials Science at the University of Minnesota.

I would thank Infineum Company for funding this project and giving me the opportunity to collaborate with industry fellows. In particular, I want to thank Stuart Briggs, Jun Cui, Ewan Galbraith, and Nga Nguyen for helpful comments on my work. This collaboration reinforces my confidence in leveraging fundamental knowledge to innovate new products.

It is a great experience to work in the Bates group and Lodge group. I would like to thank Dr. Jie Lu for getting me aboard on this project, Dr. Siddharth Chanpuriya for training me on anionic polymerization, and Dr. Yuanchi Ma for discussing experimental

details. I benefited a lot through collaborations with Dr. Dan Zhao, Shuyi Xie, Dr. Sujay Chopade and Dr. Andrew Peters, to whom I owe thanks. I am also glad to mentor a first-year student, Jiahao Zhu, and an undergraduate student, Anirudh Raghavendran, who contributed to part of this dissertation. I would thank Bates group and Lodge group members for helpful discussions: Dr. Tuoqi Li, Dr. Yiming Zeng, Dr. Qile (Paul) Chen, Dr. Jun Xu, Dr. Ziang Li, Dr. Kailong Jin, Dr. Boxin Tang, Dr. Jiuyang Zhang, Dr. Christopher Thurber, Dr. Robert Hickey, Dr. Jennifer Laaser, Dr. Svetlana Morozova, Dr. Yaming Jiang, Dr. Peter Schmidt, Dr. Ronald Lewis, Dr. Matthew Irwin, Dr. Timothy Gillard, Dr. Alex Mannion, Dr. Tessie Panthani, Dr. Sam Dalsin, Dr. Karen Haman, Dr. Ralm Ricarte, Dr. Seyoung Jung, Dr. Kyungtae Kim, Dr. Mihee Kim, Dr. Piril Ertem, Dr. Jimin Shim, Dr. Nayereh Dadoo, Wenjia Zhang, Aakriti Kharel, Julia Early, McKenzie Coughlin, Aaron Lindsay, Bo Zhang, Zhengyuan (Donny) Shen, and many others who help me during my graduate school. I would thank Dr. Yiming Mao and Dr. Paul Butler at NIST, and Dr. Lilin He at Oak Ridge National Lab, for helping with small-angle neutron scattering experiments; Dr. David Giles for setting me up on rheology and thermal analysis; Dr. Wei Zhang, Dr. Fang Zhou, and Dr. Robert Halfner at Characterization Facility at University of Minnesota for helping with transmission electron microscopy.

In addition, I would like to thank my friends, Tianqi Wang, Motao Cao, Lian Bai, Han Xiao, Yan Wu, Yuyang Du, Yangming Kou, Xiayu Peng, Hongshi Li, Qi Han, Yunlong Zou, Wentao Tang, Yueke (Kevin) Yang, and Chenyang Zhang for sharing happiness and accompanying with me in the last 5 years.

Finally, I must thank my wife, my parents, and my parents-in-law for their love and support behind me. Without them, I cannot make this accomplishment. Thank you, with my sincere love!

To My Family

Abstract

Block copolymers (BCPs) containing two or more distinct chains linked end-to-end will self-assemble into various nanostructures when dissolved in a selective solvent, including spherical and cylindrical micelles, and bilayer vesicles. The equilibrium structure and thermodynamic and dynamic properties are essential factors for processing BCP micelles in various applications. This work is motivated by a desire to investigate structure and chain exchange kinetics of BCP micelles. In this work, nanostructured micelles are formed by poly(styrene)-*b*-poly(ethylene-*alt*-propylene) (SEP) diblock, poly(ethylene-*alt*-propylene)-*b*-poly(styrene)-*b*-poly(ethylene-*alt*-propylene) (EPSEP'), and poly(styrene)-*b*-poly(ethylene-*alt*-propylene)-*b*-poly(styrene) (SEPS') triblock copolymers in either squalane or binary mixtures of squalane and 1-phenyldodecane, where PEP and PEP', and PS and PS', refer to different chain lengths. The solvents are selective to the PEP block, leading to aggregation of PS blocks into the core, and swelling of PEP blocks as the corona.

Micelle structures and thermodynamic properties of micelle solutions were characterized by static and dynamic light scattering (SLS and DLS), small-angle X-ray scattering (SAXS) and small-angle neutron scattering (SANS), while the kinetics of chain exchange was investigated by time-resolved small-angle neutron scattering (TR-SANS). These experiments and analyses quantitatively address the effects of corona block length, solvent selectivity, and corona block asymmetry on structure and chain exchange rates in BCP micelles. First, smaller core radii and aggregation numbers, but significantly thicker corona layers were observed in SEP diblock micelles with increasing corona block length. Two orders of magnitude faster kinetics was observed with increasing corona block length by four times. Second, the kinetics of chain exchange kinetics was accelerated by 10 orders of magnitude upon mixing squalane with 50 vol% 1-phenyldodecane for the same SEP block micelle. Third, the aggregation number, core radius, hydrodynamic

radius, and critical micelle temperature decreased when varying the corona block asymmetry from asymmetric to symmetric EPSEP' triblock micelles. The two asymmetric triblocks exhibited one order of magnitude faster exchange rates than the diblock, while the symmetric triblock was two orders of magnitude faster. Another symmetric triblock with two 1.6 times longer corona blocks accelerated the kinetics of chain exchange 10 times more. Finally, micelle ordering were suppressed up to 50 vol% in asymmetric EPSEP' triblocks, while the equivalent SEP diblock micelles and symmetric EPSEP triblock micelles packed onto body-centered cubic structure at 10 – 30 vol% polymer concentration. These results offer a better understanding of the roles of corona block length, core block–solvent interaction parameter χ, and corona block length asymmetry in structure and chain exchange kinetics, which will ultimately aid in designing optimal block copolymer micelles (i.e., core and corona block length, chain architecture and solvent selectivity) for specific applications.

Table of Contents

List of Tables

List of Figures

Chapter I.
Introduction and Background

1.1 Introduction

Polymers are long chain macromolecules composed of dozens to several thousands of repeating units known as monomers. They are widely found in all aspects of our lives, such as human DNA, automotive bumpers, sneakers, and 3D printing resins. Block copolymers (BCPs) are a special class of polymers containing two or more distinct chains linked end-to-end. The simplest example is an AB diblock copolymer that contains a long chain of type A monomers covalently bonded to a chain of type B monomers. When dissolved in a solvent that selectively favors one of the blocks, block copolymers can produce various nanostructures, including spherical and cylindrical micelles, and bilayer vesicles. The simplest and most studied structure is the spherical micelle illustrated in Figure 1.1 for an AB diblock copolymer. Here the A blocks (blue chains) associate to form a nearly pure micelle core (blue region) due to thermodynamically unfavorable interactions with the solvent and B blocks (green chains), while the solvent swollen B blocks radiate from the core surface as a corona (green region).

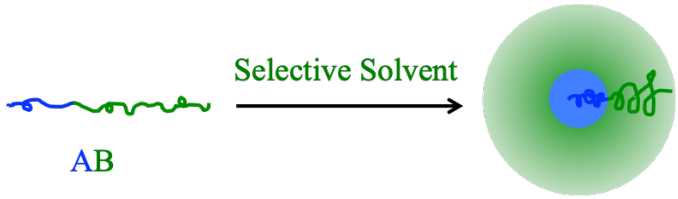

Figure 1.1 Self-assembly of block copolymers into a spherical micelle.

Self-assembled block copolymer micelles have useful solution properties, offering a

variety of applications, including nanolithography,[1-3] drug delivery,[4-6] plastics toughening,[7-10] and viscosity modification[11] for use in enhanced oil recovery and motor lubricants.

For all such applications, the micelle structure (e.g., aggregation number of chains in a micelle N_{agg}, core radius R_{core}, corona layer thickness L_{corona}, and overall micelle radius $R_{micelle}$) is an essential factor to achieve desirable properties. Moreover, the thermodynamic properties of micelles, i.e., critical micelle concentration (CMC) and critical micelle temperature (CMT), are also important parameters for design, preparation and processing. Both the micelle structure and thermodynamic properties are functions of the BCP molecular characteristics, including the core block length N_{core}, corona block length N_{corona}, polymer chain architecture (diblock, triblock, multiblock and non-linear variants), solvent quality, polymer concentration, and temperature. These are discussed with respect to experimental and theoretical considerations in the next section.

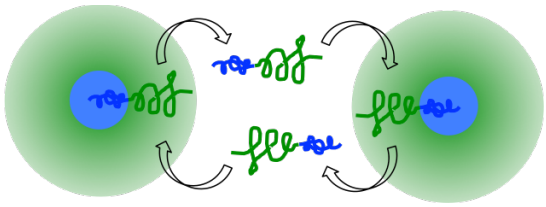

Figure 1.2 Schematic illustration of chain exchange between BCP micelles.

The dynamics of BCP micelles govern the kinetic pathways leading to an equilibrium state. Two distinct mechanisms may be operative during the micelle equilibration process: micelle fusion/fission and single chain exchange between micelles. Chain exchange is believed to be dominant when the BCP micelle system is near equilibrium. Figure 1.2 illustrates the chain exchange process, where a polymer chain escapes from a micelle, diffuses through the solvent, and ultimately inserts into another micelle. This

chain exchange process redistributes the polymer molecules among micelles, thus adjusting the aggregation number of chains within the micelles and their overall structure. We note that the total number of micelles stays almost constant during the chain exchange process, while this is not the case with micelle fusion or fission.

Although the subject of significant investigation during the past decade, a comprehensive understanding of the kinetics of chain exchange in BCP micelles with regard to the many available variables is still lacking. This doctoral thesis was motivated by a desire to elucidate some of the detailed mechanisms of chain exchange in BCP micelles. Our model system is poly(styrene)-*b*-poly(ethylene-*alt*-propylene) (PS-PEP) diblock, poly(ethylene-*alt*-propylene)-*b*-poly(styrene)-*b*-poly(ethylene-*alt*-propylene) (PEP-PS-PEP') and poly(styrene)-*b*-poly(ethylene-*alt*-propylene)-*b*-poly(styrene) (PS-PEP-PS') triblock copolymers (where PEP and PEP', and PS and PS', refer to different chain lengths). Squalane and binary mixtures of squalane and 1-phenyldodecane have been used as selective solvents for the PEP block. Thus, the corona PEP blocks swell while the PS blocks aggregate into compact micelle cores. This model system was chosen to investigate the factors that affect the rate of chain exchange in BCP micelles for several reasons. For example, temperature is one of the key factors in the kinetics study. The glass transition temperature (T_g) of the core block is approximately 70 ºC in dry micelle cores,[12] which offers the ability to conveniently turn on and off molecular exchange by heating and cooling the solution above and below T_g. The micelle structure is frozen during sample preparation at room temperature (below T_g). Upon heating to a target temperature ($> T_g$), the micelle system starts to chain exchange, which is recorded over time during the kinetic study (see below). Moreover, PS-PEP block copolymers, squalane and 1-phenyldodecane are thermally and chemically stable within experimental temperatures (up to about 200 ºC).

Before going further into the experimental details, we briefly review the prior theories and experiments on the thermodynamics and dynamics of BCP micelles in the next sections of this chapter. Chain exchange kinetics are emphasized since this represents the major part of this thesis work. Chapters III, IV, and V describe experiments and analyses that quantitatively address the effects of corona block length, solvent selectivity, and corona block asymmetry on chain exchange rates.

1.2 Structure and Thermodynamics of Block Copolymers Micelles

1.2.1 Overview of Micelle Formation and Structure

Micellization of BCPs is a consequence of the Gibbs free energy difference ($\Delta G = G_{\text{micelle}} - G_{\text{unimer}}$) between a polymer chain within a micelle (G_{micelle}) and as a unimer in solvent (G_{unimer}). The free energy change during micellization can also be described as the competition between enthalpy and entropy, i.e., $\Delta G = \Delta H - T\Delta S$, where ΔH is the enthalpy gain of micellization ($\Delta H < 0$) as the number of segment–solvent contacts decreases, and ΔS is the entropy cost ($\Delta S < 0$) as polymer chain conformations are significantly reduced when confined within the micelle. When $\Delta G < 0$ at low temperatures, polymer chains spontaneously aggregates into micelles. Conversely, micelles dissolve as free chains when $\Delta G > 0$. At the critical micelle temperature (CMT), i.e., T_{CMT}, the enthalpy gain compensates the entropy cost of micellization. This is called an upper critical micelle temperature (UCMT), which usually occurs in organic solvents. By contrast, some lower critical micelle temperature (LCMT) systems also have been investigated in the literature, typically in aqueous media and ionic liquids. The PS-PEP micelle systems studied here belongs to the UCMT category.

In terms of concentration, there are only free polymer chains in the solvent when the concentration is below the critical micelle concentration (CMC). Above the CMC, micelles will form. For a narrow dispersity BCP micelle system with a large aggregation

number, the relationship between free energy of micellization per polymer chain ΔG and the CMC is given by $\Delta G/kT = \ln(\text{CMC})$ in the dilute regime. When the concentration is above the overlap concentration, micelles will interact with each other, leading to ordering, such as body-centered cubic (BCC), face-centered cubic (FCC), or hexagonally close-packed (HCP) structures for spherical micelles. These ordered structures will melt above the order-disorder transition temperature (T_{ODT}), but reorder when cooled below the T_{ODT}.

Another interesting feature of block copolymer self-assembly is that BCP micelles can have different morphologies (e.g., spheres, cylinders, bilayers) and the transition of these morphologies can be conveniently achieved by adjusting the polymer composition (N_{core} or N_{corona}) or solvent selectivity without changing the chemistry of the block polymer. Analogous to low molecular weight surfactants, a packing parameter (P) is defined to simply explain the morphology transition: $P = V_{core} / (A_{int} \times l_{core})$. Here V_{core} is the volume of micelle core per chain, A_{int} is the interfacial area per chain, and l_{core} is the effective length of the core block. For $P < 1/3$, block copolymers generally assemble into a spherical shape. Upon increasing the core block fraction in the polymers, or alternatively increasing the solvent selectivity (i.e., increasing interfacial tension between the core block and solvent), the interfacial area per chain A_{int} will decrease, leading to the transition from spheres to cylinders ($1/3 < P < 1/2$) and to bilayers ($1/2 < P < 1$).

A block copolymer can form micelles of a certain shape in a selective solvent at a given temperature T (< CMT) and concentration c (> CMC). One key question is: what is the equilibrium micelle structure? From a thermodynamic point of view, minimizing the micelle free energy per chain ($G_{micelle}$) with respect to micelle parameters (e.g., N_{agg}, R_{core}, L_{corona}) determines the equilibrium structure. $G_{micelle}$ is the sum of interface (G_{int}), core (G_{core}) and corona (G_{corona}) free energy contributions, i.e., $G_{micelle} = G_{int} + G_{core} + G_{corona}$.

The first contribution G_{int} is an enthalpic interaction and the latter two (G_{core} and G_{corona}) are entropically based. Researchers adopted different models and assumptions to depict $G_{micelle}$ as a function of polymer characteristics (e.g., N_{core} and N_{corona}) and the interfacial tension between the core blocks and the solvent (γ). Thus, several theories have been proposed to predict the equilibrium structure of BCP micelles.

1.2.2 Theoretical Approaches

De Gennes described crew-cut spherical micelles whose core blocks are relatively longer than the corona blocks (i.e., $N_{core} >> N_{corona}$), as shown in Figure 1.3.[13] Later, Daoud and Cotton proposed a model to give the conformation of hairy (or so-called star-like) micelles (i.e., $N_{core} << N_{corona}$) also shown in the Figure 1.3.[14] The authors employed the concept of blobs to describe the concentration profile of corona blocks as a function of distance. Based on the Daoud-Cotton model, Halperin predicted the scaling correlation for hairy micelles.[15] In collaboration with Tirrell and Lodge, the author reviewed the scaling models for tethered polymer chains on both flat and curved surfaces.[16] Later, Zhulina et al. developed theories for both spherical and non-spherical BCP micelles (e.g., cylinders and bilayers).[17] This model, which indicated that the core free energy contributed relatively smaller than the corona and interface, predicted the transitions between different morphologies.

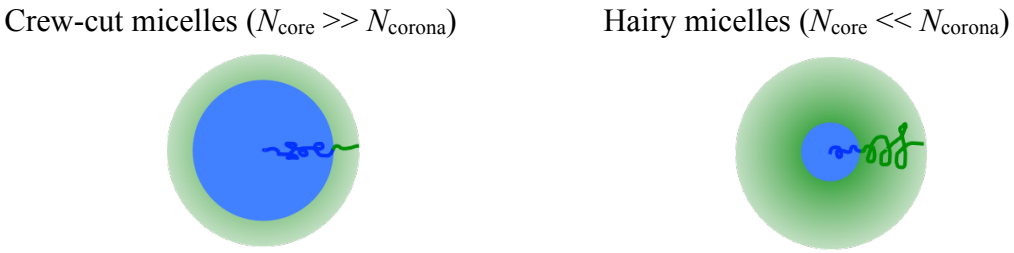

Figure 1.3 Schematic illustration of crew-cut micelles and hairy micelles

1.2.3 Experimental Results

Along with scaling models that predict the correaltions between micelle properties and polymer characteristics, extensive computational simulations[18-25] and experiments[26-35,41-47] have been designed to investigate the self-assembly of BCP micelles in organic solvents, aqueous solutions, and ionic liquids. Since our model system is comprised of PS-PEP diblock and triblock copolymers in squalane, we focus here on the literature dealing with systems that have similar self-assembly behavior, e.g., PS-PEP/alkanes and poly(styrene)-*b*-poly(isoprene) (PS-PI)/alkane systems. The thermodynamics of these micelle systems have been well documented using a variety of experimental techniques including microscopy and scattering techniques.

Early work visualized PS-PEP micelles isolated from dilute solutions using transmission electron microscopy (TEM).[26,27] In these studies, alkanes served as the preferential solvents for PEP, so that PEP swelled as the corona while PS aggregated into compact cores. The results showed spherical micelles with a narrow size distribution, and provided support for the use of the hard sphere model to represent micelle cores when fitting the scattering data (see next chapter).

Quintana et al. performed static light scattering (SLS) to determine the CMC and CMT of PS-PEP micelle solutions, and reported values of the Gibbs free energy ΔG, enthalpy ΔH, and entropy ΔS of micellization.[28,29] The large and negative values of ΔH suggested that the micellization of PS-PEP in *n*-alkanes is mainly driven by enthalpic factors. The different thermodynamic properties were attributed to the differences in the PS/*n*-alkane interactions, which was influenced by the number of carbon atoms in the *n*-alkanes and temperature. However, this influence was relatively small on the micelle dimensions (e.g., weight-averaged molecular weight of micelles M_w, micelle radius of gyration R_g, and hydrodynamic radius R_h). The authors further studied the effect of solvent selectivity on micelle structure and thermodynamic properties, where they

observed lower micelle molecular weight, smaller micelle size, lower CMT, and higher CMC for PS-PEP micelles in less selective solvents.[30-33]

Choi et al. demonstrated this effect after systematically investigating a series of PS-PEP diblock copolymers in pure squalane, and binary mixtures of squalane and 1-phenyldodecane via dynamic light scattering (DLS) and small-angle X-ray scattering (SAXS).[34,35] In comparison with the light scattering technique, SAXS offers larger values of the accessible scattering wave vector q (typically 0.001 $Å^{-1}$ – 1.0 $Å^{-1}$) to probe structural details at smaller length scales. Choi and co-workers adopted a hard sphere model which was originally developed by Pedersen and co-workers,[36-40] to extract micelle structural information from SAXS patterns. The scaling behavior $R_{core} \sim N_{core}^{0.5}$ was reported for PS-PEP micelles, which is analogous to the unperturbed end-to-end chain length of PS in melts, indicating that the core blocks were not stretched. Our recent work found that the micelle core size R_{core} is also influenced by N_{corona},[41] which was previously observed in PS-PI micelles as well.[42] This influence on R_{core}, however, was not as significant as N_{core}. These results were not anticipated by the simple scaling theories. It was also reported that the corona layer scaled as $L_{corona} \sim N_{corona}^{0.7}$ and the layers were thicker than predicted by theory.

The unsaturated PS-PI block copolymers should exhibit similar self-assembly behaviors to PS-PEP in organic solvents. McConnell et al. observed BCC and FCC ordered structures with PS-PI micelles in concentrated solutions, and explored the order-disorder transitions through SAXS and small-angle neutron scattering (SANS).[43,44] SANS is also a powerful tool to probe micelle structure. One big advantage with neutron scattering is the contrast matching technique, which permits isolation of particular components via deuterium labeling of individual polymer blocks and the solvent. Using the contrast matching method, Bang et al. systematically studied the temperature-

dependent micelle structures of PS-PI dispersed either in diethyl phthalate, which favors the PS block, or in tetradecane, which favors the PI block.[45] The SANS results showed a decrease in N_{agg} and R_{core} with increasing the temperature, i.e., reducing the interfacial tension. When increasing the solvent selectivity by mixing different selective solvents for the PS blocks, the authors observed micelle shape changes from spheres to cylinders to bilayer vesicles under cryogenic transmission electron microscopy (cyro-TEM).[46] Likewise, LaRue et al. studied several PS-PI samples in heptane, and reported a reversible transition from vesicles to cylindrical micelles for one sample, and transition from cylindrical to spherical micelles for another sample, by changing temperature to adjust the solvent selectivity.[47] These micelle morphologies were visualized by atomic force microscopy (AFM). Unlike the scattering techniques, microscopy offers direct visualization of micelle structure individually without any prior knowledge or model assumption. However, the major limitation is that those micrographs only show micelle morphologies in some selected regions, which might not be representative. Therefore, scattering techniques are complementary to overcome this limitation. In the two examples of micelle morphology transition studies, Bang et al. incorporated cyro-TEM with SAXS characterization,[46] while LaRue et al. combined AFM with SLS measurements.[47]

In summary, PS-PEP block copolymers will self-assemble into micelles when immersed into alkanes with c > CMC. PS blocks aggregate into compact cores, while corona PEP blocks swell. The system has an upper critical micellization temperature (UCMT), above which micelles will spontaneously dissolve into unimers. By tailoring the molecular characteristics or tuning the solvent selectivity, these micelles will adjust their sizes, and/or even change morphologies from spheres to cylinders, and to bilayers. At high concentrations, they will pack into ordered BCC and FCC structures, and undergo an order-disorder transition when heated above the T_{ODT}.

1.3 Dynamics of Block Copolymer Micelles

1.3.1 Overview of Micelle Equilibration Mechanisms

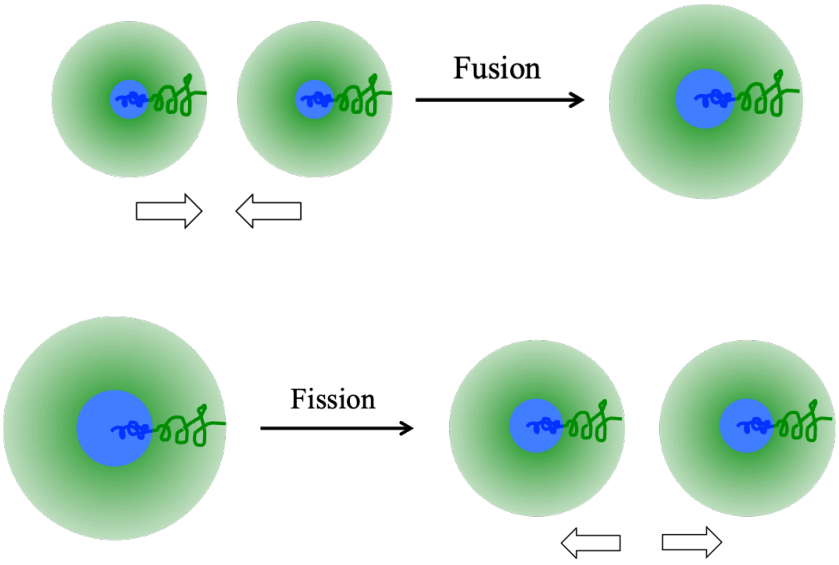

Figure 1.4 Schematic illustration of micelle fusion and fission mechanisms

Compared to the large number of studies dealing with the thermodynamic aspects, the dynamics of BCP micelles have been investigated much less extensively. Two distinct mechanisms of micelle equilibration need to be considered: micelle fusion/fission and single chain exchange. Figure 1.4 illustrates the micelle fusion/fission mechanism, where a large micelle breaks into two smaller micelles when its aggregation number of chains is much larger than the equilibrium value, or two small micelles merge into a larger micelle when their sizes are much smaller than the equilibrium size. We note that the total number of micelles will change after fusion or fission events. The single chain exchange mechanism is believed to be the dominant dynamical mode when the BCP micelle system is near equilibrium. As shown in Figure 1.2, a single polymer chain escapes from a micelle into the solvent, while individual free chains insert into micelles. This chain

exchange process redistributes the polymer chains among micelles. Most arguments dealing with micelle kinetics have been proposed based on these two mechanisms.

This section provides a literature review of progress made in understanding micelle equilibration mechanisms with regard to theoretical predictions and experimental results. A particular emphasis is placed on chain exchange kinetics near equilibrium, which is the focus of this thesis.

1.3.2 Theoretical approaches

Aniansson and Wall pioneered investigation of the kinetics of micelle equlibration using low molecular weight surfactant systems.[48,49] In their description, a fast relaxation process was attributed to single chain expulsion from or insertion into micelles, and a slower process was associated with the redistribution of micelle sizes. Lessner et al. included the micelle fusion/fission mechanism to explain the relaxation experiments in aqueous micelle systems.[50,51]

Block copolymer micelles are expected to exhibit significantly slower equilibration kinetics than small molecule surfactants due to the relatively long chains. Based on the Aniansson and Wall's model, Halperin and Alexander proposed a scaling theory for relaxation kinetics in BCP micelles near equilibrium.[52] The authors argued that the single chain exchange mechanism is dominant in polymeric micelles due to the high steric repulsion between sizable coronas, hindering micelle fusion/fission. Second, they assumed the expulsion of a polymer chain as the rate-limiting step during chain exchange. Halperin and Alexander considered the extraction of a polymer chain as occurring in two steps: (i) the core block escapes from the core into the corona/solvent matrix, collapsing into a bud with an associated surface area, and (ii) the entire polymer chain travels through the micelle corona. Thus, the activation energy (E_a) of chain expulsion is proportional to the surface free energy of a collapsed core block, i.e.,

$\gamma N_{core}^{2/3} a^2$, which is purely enthalpic. By adapting the Kramers rate theory, the unimer expulsion rate constant (k_{ex}) is given by:

$$k_{ex} \sim f(N_{core}, N_{corona}) \exp(-\gamma N_{core}^{2/3} a^2 / kT) \quad (1.1)$$

where γ is the interfacial tension between the core block segments and solvent, a is the size of core block repeat unit, k is Boltzmann's constant, and T is temperature. The pre-exponential factor $f(N_{core}, N_{corona})$ is, however, different between crew-cut micelles ($N_{core} >> N_{corona}$) and hairy micelles due to the effects of passage through the thick corona in hairy micelles. In solutions well above the CMC, $f(N_{core}, N_{corona})$ scales as $N_{core}^{7/3}$ for crew-cut micelles ($N_{core} >> N_{corona}$) and as $N_{core}^{22/25} N_{corona}^{9/5}$ for hairy micelles ($N_{core} >> N_{corona}$).

Dormidontova et al. further developed the scaling model for micellization kinetics with a larger perturbation from the equilibrium state.[53] The authors calculated the association/dissociation rate constants for single chain insertion/expulsion and micelle fusion/fission, and concluded that collectively combining these two mechanisms equilibrated the micelle system more effectively than either mechanism alone. At early stages of micellization, micelle fusion is dominant leading to an increase in the aggregation number of chains per micelle. When the system is near the equilibrium, the single chain exchange mechanism becomes dominant over micelle fusion/fission. The contributions of two aforementioned mechanisms to kinetics of micellization was further studied by Haliloğlu et al. using dynamic Monte Carlo simulations.[54] Later, Rharbi experimentally showed the presence of micelle fusion/fission at equilibrium, but with significant slower rate than chain expulsion/insertion in poly(ethylene oxide)-*b*-

poly(propylene oxide)-*b*-poly(ethylene oxide) (PEO-PPO-PEO) triblock copolymer micelles.[55]

Recently, prompted by interesting questions resulting from experimental observations, Halperin re-examined the role of the insertion penalty in the micelle chain exchange kinetics.[56] The author made corrections to the activation energy of chain insertion, and predicted a slower chain exchange kinetics due to the corona screening effect, which would be evident in two senarios: (i) coronal overlap upon increasing the micelle concentration, as observed by Choi et al. in concentrated micelle solutions,[57] and (ii) upon adding homopolymers, chemically identical to the corona blocks, to dilute solutions of non-overlapping micelles, as later confirmed by Lu et al.[58]

1.3.3 Experimental Results

Various computational simulation and experimental techniques have been applied to study the kinetics of micellization away from equilibrium and the kinetics of chain exchange near equilibrium. This section will begin with the former topic, and highlight work on chain exchange kinetics that inspires this thesis work.

Studies of micellization kinetics monitor the time-dependent signal after applying an abrupt perturbation to the micelle system. This abrupt perturbation includes changing the solvent composition, temperature jump (usually across the CMT), and pressure jump. The change of micelle size (or even morphology) is then characterized by time-resolved techniques, including imaging analysis such as TEM and AFM, and scattering techniques such as LS and SAXS. For example, in a temperature jump scattering experiment, an abrupt change of temperature is applied to the initial state of unimers at $t = 0$. After this temperature perturbation, unimers aggregate into micelles, until the system reaches the equilibrium. A scattering detector monitors the change of intensity and distribution of micelle sizes as a function of time. This time-dependent information provides insight into

the micellization process. Most works reported two distinct relaxation process in the kinetics of micellization.[59-65] The micelles initially approached a state near the equlibrium through a fast process, and finally reached the equilibrium state via a slow process. Furthermore, Lund et al., showed the time-dependent mean-average aggregation number by time-resolved SAXS, and proposed a nucleation and growth type process for micellization which was governed by single chain exchange.[66]

On the other hand, the experiments on the kinetics of chain exchange are typically designed near the equilibrium so that other mechanisms can be negligible. The fluorescence quenching method was first employed to study the equilibrium kinetics. This method requires a pair of block copolymers tagged with different fluorescent labels, i.e., donors and acceptors. The fluorescence intensity decreases with the exchange between donor- and acceptor-chains, which is recorded by the detector. Relaxation times of this dynamic process are extracted from fluorescence decay curves. However, some results by the fluorescence studies were not clear yet, where more than one relaxation time occurred near equilibrium other than single chain insertion/expulsion.[67,68] These were attributed to the presence of bulky chemical labels and multiple quenching pathways in the fluorescence quenching method.

Time-resolved SANS (TR-SANS) has recently been performed as a more accurate technique to investigate equilibrium chain exchange kinetics, because it only requires deuterium labeling and therefore minimizes experimental perturbations. The idea of TR-SANS is similar to the fluorescence quenching method, requiring a pair of block copolymers that are selectively protonated (h) or deuterated (d). SANS detector monitors the time-dependent scattering intensity when a fraction of h- and d-chains exchange between protonated and deuterated micelle cores. The evolution of excess scattering intensity reflects the change of contrast between the micelle cores and solvent: $I(t) - I(\infty)$

$\sim (\rho_{core}(t) - \rho_{solvent})^2$, where I(t) is the instantaneous intensity at time t, and $I(\infty)$ is the intensity to infinite time (i.e., completely exchanged state), and ρ_{core} and $\rho_{solvent}$ are scattering length density of core block and solvent, respectively. Figure 1.5 illustrates the evolution of contrast via micelle chain exchange during the TR-SANS experiment, where micelle cores are isotopically labeled, blue for protonated cores and red for deuterated cores, and the contrast of solvent is matched with molecularly mixed cores.

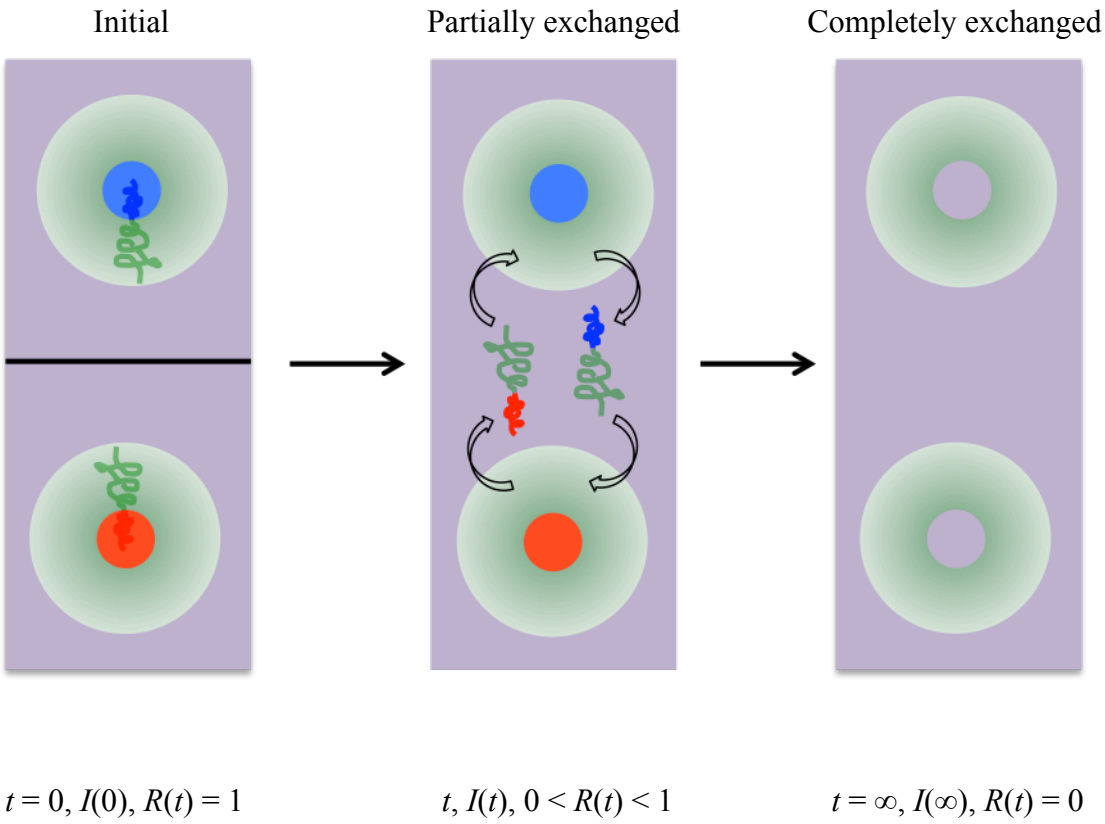

Figure 1.5 Evolution of contrast change via chain exchange in a TR-SANS experiment

Hence, a normalized relaxation function $R(t)$ is defined to represent the rate of chain exchange,

$$R(t) = \sqrt{\frac{I(t) - I(\infty)}{I(0) - I(\infty)}} \tag{1.2}$$

where $I(0)$ is the initial intensity ($t = 0$), $I(t)$ is the instantaneous intensity at time t, and $I(\infty)$ is the intensity at infinite time ($t = \infty$). $R(t)$ decreases over time as the contrast between micelle cores and solvent decreases via h- and d-chain exchange where the decay rate of $R(t)$ directly reflects the rate of chain exchange.

Willner and coworkers first performed TR-SANS experiment for the determination of chain exchange kinetics in poly(ethylene-*alt*-propylene)-*b*-poly(ethylene oxide) (PEP-PEO) micelles in dimethylformamide (DMF).[69] The authors further tuned the rate of chain exchange to accessible time scales by adjusting the interfacial tension γ between PEP and solvent, as a consequence of mixing DMF with water and changing temperatures.[71-72] The relaxation functions $R(t)$, however, showed a broad logarithmical decay over several decades in time, which was contradictory to Halperin and Alexander's theory. Similar logarithmic relaxation behavior was also observed in organic solvent systems: poly(styrene)-*b*-(butadiene) (PS-PB) diblocks and PB-PS-PB triblocks micelles in *n*-alkanes,[73] and poly(styrene)-*b*-poly(ethylene-*alt*-propylene) (PS-PEP) micelles in squalane.[74]

Choi et al. established a quantitative model to interpret the apparent logarithmic time dependence of chain exchange based on TR-SANS results of dilute PS-PEP diblock copolymer micelles in squalane. Choi's model expresses the relaxation function $R(t)$ by:

$$R(t) = \int P(N_{core}) \exp[-t \frac{6\pi^2 kT}{N_{core}^2 b^2 \zeta} \exp(-\alpha\chi N_{core})] \mathrm{d}N_{core} \quad (1.3)$$

$$P(N_i) = \frac{z^{z+1}}{\Gamma(z+1)} \frac{N_i^{z-1}}{N_n^z} \exp\left(-\frac{zN_i}{N_n}\right) \quad (1.4)$$

Here N_{core} is the core block degree of polymerization, and $P(N_{\mathrm{core}})$ is a Schulz-Zimm distribution function for disperse core blocks, given by eqn 1.4, where $z = [N_w/N_n - 1]^{-1}$, Γ is the gamma function, N_w and N_n are the weight average and number average degrees of polymerization of the core block, respectively. ζ is the monomeric friction factor and b is the statistical segment length of the core block, α is a pre-factor of order unity, and χ represents the Flory-Huggins interaction parameter between the core block and solvent (i.e., $\chi_{\mathrm{core\text{-}solvent}}$). The following assumptions are made in this model: (i) single chain exchange mechanism is dominant near equilibrium; (ii) the chain expulsion step is the rate limiting step; (iii) core blocks follow Rouse dynamics when buried in the micelle cores, i.e., $\tau_1 \approx N_{\mathrm{core}}^2 b^2 \zeta / 6\pi^2 kT$; and (iv) the energy barrier E_a of chain expulsion is proportional to χN_{core}. Choi's model successfully described the TR-SANS results in the PS-PEP micelle system, thus revealing the dramatic influence of the core block length, dispersity of core block lengths, and solvent selectivity on chain exchange kinetics.

Following this work, Lund et al. re-analyzed the data from the PEP-PEO micelle system, and reported consistency with the Choi's model.[75] Later, Zinn and co-workers designed an *n*-alkyl-PEO micelle system with strictly monodisperse core-forming blocks and examined the chain exchange kinetics.[76] The authors demonstarted a single exponential relaxation function $R(t)$ for this monodisperse system. This experiment verified that the dispersity of core block accounted for the logarithmic time dependence of exchange kinetics in BCP micelles, as accounted for with Choi's model.

To further confirm the dramatic sensitivity of chain exchange rate on the core block lengths and the dispersity, Lu et al. investigated a binary mixture of PS-PEP diblock copolymers with short and long PS blocks in two sets of experiments.[77,78] The first experiment isotopically labeled both short and long blocks, and measured the chain exchange rate for the binary mixture of micelles formed by two monomodal populations of core blocks. The relaxation function $R(t)$ was found to be simply the average of the relaxation functions corresponding to the single block copolymer component micelles, i.e., $R(t)_{\text{binary}} = \nu_1 R_1(t)_{\text{single}} + (1-\nu_1) R_2(t)_{\text{single}}$, where ν_i and $R_i(t)_{\text{single}}$ are the mole fraction and relaxation function for species i in the corresponding single micelle, respectively. The second experiment matched the contrast of one species of PS blocks with the solvent, and thus, the chain exchange of the other labeled PS blocks was monitored. The chain exchange rates for the labeled chains in such binary micelles were identical to the result obtained in the corresponding single micelles, i.e., $R_i(t)_{\text{binary}} = R_i(t)_{\text{single}}$. This result, evaluated without any adjustable parameters, proved that each chain undergoes an independent exchange process.

While these experiments confirmed the consequence of dispersity of core blocks on the chain exchange process, a coarse-grained single-chain mean-field simulation by Daza et al., recently reported a logarithmic decay in micelles formed by a strictly monodisperse distribution of chain lengths.[79,80] The authors suggested that such a logarithmic relaxation process was not necessarily the result of core block dispersity, but was ascribed to a broad distribution of energy barriers when the core block escapes from the core.

In addition to this recent result, there are more open questions beyond Choi's model with regard to factors that influence the kinetics of chain exchange. The first interesting question is the scaling of the core block length N_{core} for the activation energy E_a. As proposed by Halperin and Alexander, $E_a \sim N_{\text{core}}^{2/3}$ corresponds to the surface free energy

of a collapsed core block, i.e., $\gamma N_{core}^{2/3} a^2$, where γ is the interfacial tension between core blocks and the corona/solvent matrix and a is the monomer size. Choi's model, however, suggested $E_a \sim N_{core}$, assuming that the ejected core block is solvated and that E_a is attributed to unfavorable monomer–solvent interactions captured by $kT\chi N_{core}$. Although most of the experimental results in different micelle systems favored the N_{core} expressions rather than $N_{core}^{2/3}$, the exact N_{core} dependence on the activation energy term E_a is still subject to debate. This topic becomes more complicated when introducing a crystallized or semi-crystallized core block. Zinn and co-works proposed an additional term, i.e., the enthalpy of fusion ΔH_{fus} of *n*-alkyl chains for the crystalized micelle core, to the activation energy E_a.[81] Later, the authors showed a cooperative melting transition of different core blocks in the micelle core, followed by a decoupled chain exchange process in micelles formed by a binary mixture of *n*-alkyl-PEO with different *n*-alkyl lengths.[82]

Second, the role of corona blocks in chain exchange was not addressed by Choi's model since E_a was assumed to be purely the enthalpic penalty from the core block–solvent incompatibility. Dissipative particle dynamics (DPD) simulations by Li and Dormidontova[83] showed an acceleration of the chain exchange kinetics when increasing the corona block length at constant core block length, which was attributed to a higher solubility and higher critical micelle concentration (CMC) of the copolymer. However, Zinn et al. found that the kinetics slowed down as the corona block length increased in the C_{27}-PEO/H_2O system.[84] They attributed this slowing down to chain diffusion through a thicker corona layer, as predicted by Halperin and Alexander for hairy micelles with the scaling of $k_{ex} \sim N_{corona}^{-9/5}$. In the current work, we observed two orders of magnitude increase in chain exchange rate of PS-PEP micelles by increasing the corona block length four times at constant core block length, which was attributed to the entropic gain arising from the relief of corona chain stretching upon chain expulsion.[41]

In concentrated micelle solutions where micelles pack into a BCC lattice, Choi et al. found the rate of chain exchange in PS-PEP micelles decreased by one order of magnitude.[57] Another observation was a slowing down of chain exchange kinetics in non-overlapping PS-PEP micelles upon adding PEP homopolymers.[58] Since the polymer characteristics were not changed, this reduced chain exchange rate is a consequence of the corona screening. Halperin proposed an increase in insertion energy to account for the corona screening effect.[56] Alternatively, from our recent study, it can be argued that the stretching of corona blocks is relieved in a crowded corona environment, and thus less entropy benefit is gained when a polymer chain escapes from the micelle into the solution.[41]

Third, despite the use of different parameters (interfacial tension γ or Flory-Huggins interaction parameter χ) to represent the incompatibility between the core block and solvent, it is still an unresolved issue as to the exact dependence on χ. Choi's model assumes a simple relation $E_a \sim \chi N_{core}$. But there is a problem when imagining the scenario where the micelle system is approaching the critical micelle temperature (CMT). At T_{CMT}, there should be literally no energy barrier for chain expulsion, i.e., $E_a \approx 0$. However, the solvent quality is approximately the theta condition for the core block at T_{CMT}, i.e., $\chi \approx 0.5$ (taking the solvent volume as the reference volume). Ma and Lodge proposed an elaborate χ-dependent function $f(\chi)$,[85] so that $E_a \sim f(\chi)N_{core}$, with $f(\chi)$ given by,

$$f(\chi) = \frac{v_2}{v_1}\left(\chi - \frac{v_2}{v_1}\right) + \frac{1}{a\chi^2 + b\chi + c} \tag{1.5}$$

where v_1 and v_2 are molar volume of solvent and core block repeat unit, respectively, and a, b, c in the second term are empirical constants. It is worth noting that $f(\chi)$ is derived in

the context of Flory-Huggins theory, that the quantity of χ in this expression is converted by taking the volume of core block repeat unit as reference volume, and that high segregation strength χN_{core} is assumed. The authors found good performance of this modified function in poly(*n*-butyl methacrylate)-*b*-poly(methyl methacrylate) (PnBMA-PMMA) micelles in ionic liquids. An aspect of this thesis was motivated by a desire to test the universality of this χ-dependent function with PS-PEP micelles in different hydrocarbon solvents. We note that our micelle system has an upper critical temperature (UCMT) while the previously studied PnBMA-PMMA/ionic liquids are LCMT systems. Details of this work will be discussed in Chapter IV.

The diversity of molecular architectures such as triblock, multi-block, branched or grafted copolymers have not been thoroughly explored in the field of chain exchange kinetics in nanoscale micelles. The first study on the polymer architectural effect was done by Lund et al.[73] Their TR-SANS results reported 10 times slower exchange rate of a symmetric PB-PS-PB triblock copolymer micelle relative to a PS-PB diblock copolymer micelle in *n*-alkane solvents (which favor the PB blocks), where the triblock had the same composition but twice the molecular weight of the diblock, and the micelle structure formed by the triblock was similar to the diblock. By contrast, Lu et al. found a symmetric PEP-PS-PEP triblock copolymer exchanged chains three orders of magnitude faster than the equivalent PS-PEP diblock.[86] In this work, the authors prepared triblocks with an additional PEP corona block while the PS core block length was kept similar to the diblock, resulting in a smaller micelle aggregation number than with the diblock. Dissipative particle dynamics (DPD) simulations by Peters and Lodge revealed faster exchange kinetics in asymmetric B_1AB_2 triblocks than in the AB diblock analogs, where A is the core block and B is the corona, and the B_1 and B_2 corona blocks are a different length with $B_1 + B_2 = B$.[87] Using DPD simulations, Prhashanna and Chen investigated a

series of symmetric BAB triblocks, and reported slower kinetics with an increase of the core block length, and with an increase of the corona block length as well, although the retarding effect by the longer corona blocks was not appreciable.[88] Despite these discrepancies, we propose that the additional corona block in the PEP-PS-PEP triblock accelerates the kinetics due to the relief of more stretched corona chains in a more crowded corona environment with higher graft density at the interface. In addition, the looped conformation of the core block in the BAB-type triblocks further reduced the energy barrier of core block expulsion. This argument is supported by Peters and Lodge's observation that linear B_1AB_2 triblock exchanged chains faster than the equivalent branched AB_1B_2,[87] and by Prhashanna and Dormidontova's work that micelles formed by tadpole-shaped diblock copolymers (containing a loop-shaped core block and a linear corona block) exhibited faster chain exchange rate than the linear diblock.[89] The slower kinetics shown in Lund's work[73] is mainly attributed to the significant slowing down effect of the twice longer core blocks in the triblock. However, the possibility cannot be excluded that the re-insertion probability would be higher and that the diffusion time through a thicker corona layer would be longer for the triblock micelles with longer corona blocks, as observed by Prhashanna and Chen.[88] To find direct evidence to test this argument, we systematically investigated the effect of corona block length asymmetry on chain exchange kinetics of PEP-PS-PEP' triblock micelles, where PEP and PEP' have different molecular weights, while the core block length and overall corona block length (PEP + PEP') are held constant.

The chain exchange behavior of ABA-type triblock copolymer micelles with two core blocks is also interesting, since the hypersensitivity to core block length has been confirmed in the diblocks. Lu et al. reported a symmetric PS-PEP-PS triblock to exhibit exchange dynamics four orders of magnitude slower than the equivalent PS-PEP diblock,

yet faster than expected assuming uncorrelated extraction of the two core blocks.[86] Following this work, Peters and Lodge measured the relaxation times of gels formed by the same PS-PEP-PS triblock copolymer in Lu's experiments but at higher concentrations.[90] By comparison with the relaxation time of one core block in the diblock from TR-SANS, the authors explored the mechanism of core block pullout in these triblock micelles: (i) the relatively shorter core blocks ejected faster because of the dispersity of two core blocks, even though their average lengths were almost the same, and (ii) the effective energy barrier of one core block pull out was reduced in the ABA triblock architecture. To directly test the first hypothesis, an asymmetric PS-PEP-PS' triblock micelle system can be designed and investigated, where PS and PS' are different lengths.

In addition to the effects of molecular characteristics of the BCPs and solvents, the exchange rate of a single chain can also be influenced by the geometric structure of the micelle. Lund and co-workers investigated the exchange kinetics in PEP-PEO micelles across the irreversible cylinder-to-sphere transition, and observed a small but distinguishable increase in the exchange kinetics in the spherical micelles comparing to the cylindrical morphology.[91] Recently, Zhao et al. reported an approximate three times slowing down in exchange rate of the same polymer chain in micelles of two different sizes, both of which maintained stable structures during the TR-SANS experiment.[92] With a careful analysis of these two micelle dimensions, the polymer chain within the larger micelle had smaller interfacial area per chain at the interface and a larger corona density, which could account for the slower chain exchange.

1.4 Thesis Outline

Overall, this thesis is comprised of 7 chapters. This chapter serves as the introduction and background literature review for this thesis work, which focuses on the structure and

chain exchange kinetics of BCP micelles. Chapter II describes the experimental techniques that were frequently performed in this research. The experimental section gives a general overview of the block copolymer synthesis and characterization, micelle solution preparation, and the characterization of micelle structures and solution properties. We also introduce the hard sphere model used to fit the scattering data of block copolymer micelles. Chapters III – V each aim to answer one specific question in the chain exchange kinetics of BCP micelles. Chapter III quantifies the role of the corona block, leading to a more comprehensive model that explicitly includes a corona dependent term. Chapter IV validates the exact χ dependence of activation energy in chain exchange kinetics by varying the solvent selectivity. Chapter V systematically investigates the effect of corona block asymmetry on the kinetics of PEP-PS-PEP' triblock copolymer micelles, where PEP and PEP' have different lengths, but PS and the overall corona molecular weight (PEP + PEP') are held constant. Following up the investigation of PEP-PS-PEP' triblock micelles, Chapter VI shows how a mixed corona of shorter and longer PEP blocks suppresses the onset of micelle ordering at higher concentrations, and modifies the ordered state symmetry from the typically observed body-centered cubic packing. Finally, Chapter VII summarizes the thesis research and proposes several future directions of this research project.

1.5 References

[1] Lazzari, M.; López-Quintela, M. A. Block Copolymers as a Tool for Nanomaterial Fabrication. *Adv. Mater*. **2003**, *15*, 1583−1594.

[2] Glass, R.; Möller, M.; Spatz, J. P. Block Copolymer Micelle Nanolithography. *Nanotechnology* **2003**, *14*, 1153−1160.

[3] Hamley, I. W. Nanostructure Fabrication using Block Copolymers. *Nanotechnology* **2003**, *14*, 39−54.

[4] Jeong, B.; Bae, Y. H.; Lee, D. S.; Kim, S. W. Biodegradable Block Copolymers as Injectable Drug-Delivery Systems. *Nature* **1997**, *388*, 860−862.

[5] Li, Z.; Johnson L. M.; Ricarte R. G.; Yao, L. J.; Hillmyer M. A.; Bates, F. S.; Lodge, T. P. Enhanced Performance of Blended Polymer Excipients in Delivering a Hydrophobic Drug through the Synergistic Action of Micelles and HPMCAS. *Langmuir* **2017**, *33*, 2837−2848.

[6] Li, Z.; Lenk T. I.; Yao, L. J.; Bates, F. S.; Lodge, T. P. Maintaining Hydrophobic Drug Supersaturation in a Micelle Corona Reservoir. *Macromolecules* **2018**, *51*, 540–551.

[7] Declet-Perez C.; Francis, L. F.; Bates, F. S. Deformation Processes in Block Copolymer Toughened Epoxy. *Macromolecules* **2015**, *48*, 3672–3684.

[8] Li, T.; Heinzer, M. J.; Francis, L. F.; Bates, F. S. Engineering Superior Toughness in Commercially Viable Block Copolymer Modified Epoxy Resin. *J. Polym. Sci. B: Polym. Phys.* **2016**, *54*, 189–204.

[9] Li, T.; Zhang J.; Schneiderman, D. K.; Francis, L. F.; Bates, F. S. Toughening Glassy Poly(lactide) with Block Copolymer Micelles. *ACS Macro Lett.* **2016**, *5*, 359−364.

[10] Xu J.; Howard, M. J.; Mittal, V.; Bates, F. S. Block Copolymer Micelle Toughened Isotactic Polypropylene. *Macromolecules* **2017**, *50*, 6421–6432.

[11] Anderson, W. Block Copolymers as Viscosity Index Improvers for Lubricating Oils. US3763044A, **1973**.

[12] Lai C.; Russel, W. B.; Register, R. A. Phase Behavior of Styrene-Isoprene Diblock Copolymers in Strongly Selective Solvents. *Macromolecules* **2002**, *35*, 841–849.

[13] de Gennes, P. G. Conformations of Polymers Attached to an Interface. *Macromolecules* **1980**, *13*, 1069–1075.

[14] Daoud, M.; Cotton, J. P. Star Shaped Polymers: A Model for the Conformation and its Concentration Dependence. *J. Phys. France* **1982**, *43*, 531–538.

[15] Halperin, A. Polymeric Micelles: A Star Model. *Macromolecules* **1987**, *20*, 2943–2946.

[16] Halperin, A.; Tirrell, M.; Lodge, T. P. Tethered Chains in Polymer Microstuctures. *Adv. Polym. Sci.* **1992**, *100*, 31–71.

[17] Zhulina, E. B.; Adam, M.; LaRue, I.; Sheiko, S. S.; Rubinstein, M. Diblock Copolymer Micelles in a Dilute Solution. *Macromolecules* **2005**, *38*, 5330–5351.

[18] Nelson P. H.; Rutledge G. C.; Hatton T. A. On the Size and Shape of Self-Assembled Micelles. *J. Chem. Phys.* **1997**, *107*, 10777–10781.

[19] Viduna, D.; Milchev, A.; Binder, K. Monte Carlo Simulation of Micelle Formation in Block Copolymer Solutions. *Macromol. Theory Simul.* **1998**, *7*, 649–658.

[20] Milchev, A.; Bhattacharya A.; Binder K. Formation of Block Copolymer Micelles in Solution: A Monte Carlo Study of Chain Length Dependence. *Macromolecules* **2001**, *34*, 1881–1893.

[21] Srinivas G.; Shelley J. C.; Nielsen, S. O.; Discher, D. E.; Klein M. L. Simulation of Diblock Copolymer Self-Assembly, Using a Coarse-Grain Model. *J. Phys. Chem. B* **2004**, *108*, 8153–8160.

[22] Srinivas G.; Discher, D. E.; Klein M. L. Self-Assembly and Properties of Diblock Copolymers by Coarse-Grain Molecular Dynamics. *Nat. Mater*. **2004**, *3*, 638–644.

[23] Ortiz, V.; Nielsen, S. O.; Discher, D. E.; Klein M. L. Lipowsky R.; Shillcock, J. Dissipative Particle Dynamics Simulations of Polymersomes. *J. Phys. Chem. B* **2005**, *109*,17708–17714.

[24] Uneyama, T.; Doi, M. Calculation of the Micellar Structure of Polymer Surfactant on the Basis of the Density Functional Theory. *Macromolecules* **2005**, *38*, 5817–5825.

[25] Jiang, Y.; Chen T.; Ye, F.; Liang, H.; Shi, A.-C. Effect of Polydispersity on the Formation of Vesicles from Amphiphilic Diblock Copolymers. *Macromolecules* **2005**, *38*, 6710–6717.

[26] Price, C.; Hudd, A. L; Stubbersfield, R. B. A study of Micelle Formation by a Polystyrene-poly (ethylene/propylene) Block Copolymer in a Base Lubricating Oil. *Polymer* **1980**, *21*, 9.

[27] Candau, F.; Heatley, F.; Price, C.; Stubbersfield, R. B. An Investigation of the Structure of Micelles Formed by a Polystyrene-*b*-poly(ethylene/propylene) Block Copolymer in Paraffinic Solvents using ^{1}H and ^{13}C-Nuclear Magnetic Resonance. *Eur. Polym. J.* **1984**, *20*, 685–690.

[28] Quintana, J. R.; Villacampa, M.; Muñoz, M.; Andrio, A.; Katime, I. A. Micellization of a Polystyrene-*block*-poly(ethylene/propylene) Copolymer in *n*-Alkanes. 1. Thermodynamic Study. *Macromolecules* **1992**, *25*, 3125–3128.

[29] Quintana, J. R.; Villacampa, M.; Andrio, A.; Muñoz, M.; Katime, I. A. Micellization of a Polystyrene-*block*-poly(ethylene/propylene) Copolymer in *n*-Alkanes. 2. Structural Study. *Macromolecules* **1992**, *25*, 3129–3136.

[30] Quintana, J. R.; Villacampa, M.; Katime, I. A. Micellization of a Polystyrene-*b*-poly(ethylene/propylene) Block Copolymer in *n*-Dodecane/1.4-Dioxane Mixtures. 1. Thermodynamics of Micellization. *Macromolecules* **1993**, *26*, 601–605.

[31] Quintana, J. R.; Villacampa, M.; Katime, I. A. Micellization of a Polystyrene-*b*-poly(ethylene/propylene) Block Copolymer in *n*-Dodecane/1.4-Dioxane Mixtures. 2. Structure and Dimensions of Micelles. *Macromolecules* **1993**, *26*, 606–611.

[32] Quintana, J. R.; Jáñez, M. D.; Villacampa, M.; Katime, I. Diblock Copolymer Micelles in Solvent Binary Mixtures. 1. Selective Solvent/Precipitant. *Macromolecules* **1995**, *26*, 4139–4143.

[33] Villacampa, M.; de Apodaca, E. D.; Quintana, J. R.; Katime, I. Diblock Copolymer Micelles in Solvent Binary Mixtures. 2. Selective Solvent/Good Solvent. *Macromolecules* **1995**, *26*, 4144–4149.

[34] Choi, S.; Bates, F. S.; Lodge, T. P. Structure of Poly(styrene-*b*-ethylene-*alt*-propylene) Diblock Copolymer Micelles in Squalane. *J. Phys. Chem. B* **2009**, *113*, 13840–13848.

[35] Choi, S.; Lee, W. B.; Lodge, T. P.; Bates, F. S. Structure of Poly(styrene-*b*-ethylene-*alt*-propylene) Diblock Copolymer Micelles in Binary Solvent Mixtures. *J. Polym. Sci. B: Polym. Phys.* **2016**, *54*, 22–31.

[36] Pedersen, J. S.; Gerstenberg, M. C. Scattering Form Factor of Block Copolymer Micelles. *Macromolecules* **1996**, *29*, 1363–1365.

[37] Pedersen, J. S.; Hamley, I. W.; Ryu, C. Y.; Lodge, T. P. Contrast Variation Small-Angle Neutron Scattering Study of the Structure of Block Copolymer Micelles in a Slightly Selective Solvent at Semidilute Concentrations. *Macromolecules* **2000**, *33*, 542–550.

[38] Pedersen, J. S. Structure Factors Effects in Small-Angle Scattering from Block Copolymer Micelles and Star Polymers. *J. Chem. Phys.* **2001**, *114*, 2839–2846.

[39] Pedersen, J. S.; Svaneborg, C. Scattering from Block Copolymer Micelles. *Curr. Opin. Colloid Interface Sci.* **2002**, *7*, 158–166.

[40] Pedersen, J. S.; Svaneborg, C.; Almdal, K.; Hamley, I. W.; Young, R. N. A Small-Angle Neutron and X-ray Contrast Variation Scattering Study of the Structure of Block Copolymer Micelles: Corona Shape and Excluded Volume Interactions. *Macromolecules* **2003**, *36*, 416–433.

[41] Wang, E.; Lu, J.; Bates, F. S.; Lodge, T. P. Effect of Corona Block Length on the Structure and Chain Exchange Kinetics of Block Copolymer Micelles. *Macromolecules* **2018**, *51*, 3563–3571.

[42] LaRue, I.; Adam, M.; Zhulina, E. B.; Rubinstein, M.; Pitsikalis, M.; Hadjichristidis, N.; Ivanov, D. A.; Gearba, R. I.; Anokhin, D. V.; Sheiko, S. S. Effect of the Soluble Block Size on Spherical Diblock Copolymer Micelles. *Macromolecules* **2008**, *41*, 6555–6563.

[43] McConnell, G. A.; Gast, A. P.; Huang, J. S.; Smith, S. D. Disorder-Order Transitions in Soft Sphere Polymer Micelles. *Phys. Rev. Lett.* **1993**, *71*, 2102.

[44] McConnell, G. A.; Lin, E. K.; Gast, A. P.; Huang, J. S.; Lin, M. Y.; Smith, S. D. Structure and Interactions in Tethered-Chain Systems. *Faraday Discuss.* **1994**, *98*, 121–138.

[45] Bang, J.; Viswanathan, K.; Lodge, T. P.; Park, M. J.; Char, K. Temperature-Dependent Micellar Structures in Poly(styrene-*b*-isoprene) Diblock Copolymer Solutions near the Critical Micelle Temperature. *J. Chem. Phys.* **2004**, *121*, 11489–11500.

[46] Bang, J.; Jain, S.; Li, Z.; Lodge, T. P.; Pedersen, J. S.; Kesselman, E.; Talmon, Y. Sphere, Cylinder, and Vesicle Nanoaggregates in Poly(styrene-*b*-isoprene) Diblock Copolymer Solutions. *Marcomolecules* **2006**, *39*, 1199–1208.

[47] LaRue, I.; Adam, M.; Pitsikalis, M.; Hadjichristidis, N.; Rubinstein, M.; Sheiko, S. S. Reversible Morphological Transitions of Polystyrene-*b*-polyisoprene Micelles. *Macromolecules* **2006**, *39*, 309–314.

[48] Aniansson, E. A. G.; Wall, S. N. On the Kinetics of Step-Wise Micelle Association. *J. Phys. Chem.* **1974**, *78*, 1024–1030.

[49] Aniansson, E. A. G.; Wall, S. N.; Almgren, M.; Hoffmann, H.; Kielmann, I.; Ulbricht, W.; Zana, R.; Lang, J.; Tondre, C. Theory of the Kinetics of Micellar Equilibria and Quantitative Interpretation of Chemical Relaxation Studies of Micellar Solutions of Ionic Surfactants. *J. Phys. Chem.* **1976**, *80*, 905–922.

[50] Lessner, E.; Teubner, M.; Kahlweit, M. Relaxation Experiments in Aqueous Solutions of Ionic Micelles. 1. Theory and Experiments on the System H_2O-Sodium Tetradecyl Sulfate-$NaClO_4$. *J. Phys. Chem.* **1981**, *85*, 1529–1536.

[51] Lessner, E.; Teubner, M.; Kahlweit, M. Relaxation Experiments in Aqueous Solutions of Ionic Micelles.2. Experiments on the System H_2O-NaDS-$NaClO_4$ and Their Theoretical Interpretation. *J. Phys. Chem.* **1981**, *85*, 3167–3175.

[52] Halperin, A.; Alexander, S. Polymeric Micelles: Their Relaxation Kinetics. *Macromolecules* **1989**, *22*, 2403–2412.

[53] Dormidontova, E. E. Micellization Kinetics in Block Copolymer Solutions: Scaling Model. *Macromolecules* **1999**, *32*, 7630–7644.

[54] Haliloğlu, T.; Bahar, I.; Erman, B.; Mattice, W. L. Mechanisms of the Exchange of Diblock Copolymers between Micelles at Dynamic Equilibrium. *Macromolecules* **1996**, *29*, 4764–4771.

[55] Rharbi, Y. Fusion and Fragmentation Dynamics at Equilibrium in Triblock Copolymer Micelles. *Macromolecules* **2012**, *45*, 9823−9826.

[56] Halperin, A. On Micellar Exchange: The Role of the Insertion Penalty. *Macromolecules* **2011**, *44*, 5072–5074.

[57] Choi, S.; Bates, F. S.; Lodge, T. P. Molecular Exchange in Ordered Diblock Copolymer Micelles. *Macromolecules* **2011**, *44*, 3594–3604.

[58] Lu, J.; Bates, F. S.; Lodge, T. P. Addition of Corona Block Homopolymer Retards Chain Exchange in Solutions of Block Copolymer Micelles. *Macromolecules* **2016**, *49*, 1405−1413.

[59] Honda, C.; Hasegawa, Y.; Hirunuma, R.; Nose, T. Micellization Kinetics of Block Copolymers in Selective Solvent. *Macromolecules* **1994**, *27*, 7660–7668.

[60] Honda, C.; Abe, Y.; Nose, T. Relaxation Kinetics of Micellization in Micelle-Forming Block Copolymer in Selective Solvent. *Macromolecules* **1996**, *29*, 6778–6785.

[61] Goldmints, I.; Holzwarth, J. F.; Smith, K. A.; Hatton, T. A. Micellar Dynamics in Aqueous Solutions of PEO-PPO-PEO Block Copolymers. *Langmuir* **1997**, *13*, 6130–6134.

[62] Michels, B.; Waton, G.; Zana R. Dynamics of Micelles of Poly(ethylene oxide)-Poly(propylene oxide)-Poly(ethylene oxide) Block Copolymers in Aqueous Solutions. *Langmuir* **1997**, *13*, 3111–3118.

[63] Kositza, M. J.; Bohne, C.; Alexandridis, P.; Hatton, T. A.; Holzwarth, J. F. Micellization Dynamics and Impurity Solubilization of the Block-Copolymer L64 in an Aqueous Solution. *Langmuir* **1999**, *15*, 322–325.

[64] Kositza, M. J.; Bohne, C.; Alexandridis, P.; Hatton, T. A.; Holzwarth, J. F. Dynamics of Micro- and Macrophase Separation of Amphiphilic Block-Copolymers in Aqueous Solution. *Macromolecules* **1999**, *32*, 5539–5551.

[65] Waton, G.; Michels, B.; Zana, R. Dynamics of Block Copolymer Micelles in Aqueous Solution. *Macromolecules* **2001**, *34*, 907–910.

[66] Lund, R.; Willner, L.; Monkenbusch, M.; Panine, P.; Narayanan, T.; Colmenero, J.; Richter, D. Structural Observation and Kinetic Pathway in the Formation of Polymeric Micelles. *Phys. Rev. Lett.* **2009**, *102*, 188301.

[67] Procházka, K.; Bednář, B.; Mukhtar, E.; Svoboda, P.; Trněná, J.; Almgren, M. Nonradiative Energy Transfer in Block Copolymer Micelles. *J. Phys. Chem.* **1991**, *95*, 4563–4568.

[68] Underhill, R. S.; Ding, J.; Birss, V. I.; Liu, G. Chain Exchange Kinetics of Polystyrene-*block*-poly(2-cinnamoylethyl methacrylate) Micelles in THF/Cyclopentane Mixtures. *Macromolecules* **1997**, *30*, 8298–8303.

[69] Willner, L.; Poppe, A.; Allgaier, J.; Monkenbusch, M.; Richter, D. Time-Resolved SANS for the Determination of Unimer Exchange Kinetics in Block Copolymer Micelles. *Europhys. Lett.* **2001**, *55*, 667–673.

[70] Lund, R.; Willner, L.; Stellbrink, J.; Radulescu, A.; Richter, D. Tuning of Structure and Kinetics of Chain Exchange in Star-Like PEP-PEO Block Copolymer Micelles. *Physica B* **2004**, *350*, 909−912.

[71] Lund, R.; Willner, L.; Richter, D.; Dormidontova, E. E. Equilibrium Chain Exchange Kinetics of Diblock Copolymer Micelles: Tuning and Logarithmic Relaxation. *Macromolecules* **2006**, *39*, 4566–4575.

[72] Lund, R.; Willner, L.; Stellbrink, J.; Lindner, P.; Richter, D. Logarithmic Chain-Exchange Kinetics of Diblock Copolymer Micelles. *Phys. Rev. Lett.* **2006**, *96*, 068302.

[73] Lund, R.; Willner, L.; Richter, D.; Iatrou, H.; Hadjichristidisc, N.; Lindner, P. Unraveling the Equilibrium Chain Exchange Kinetics of Polymeric Micelles using Small-

Angle Neutron Scattering – Architectural and Topological Effects. *J. Appl. Cryst.* **2007**, *40*, 327−331.

[74] Choi, S.; Lodge, T. P.; Bates, F. S. Mechanism of Molecular Exchange in Diblock Copolymer Micelles: Hypersensitivity to Core Chain Length. *Phys. Rev. Lett.* **2010**, *104*, 047802–047804.

[75] Lund, R.; Willner, L.; Stellbrink, J.; Lindner, P.; Richter, D. Erratum: Logarithmic Chain-Exchange Kinetics of Diblock Copolymer Micelles. *Phys. Rev. Lett.* **2010**, *104*, 049902.

[76] Zinn, T.; Willner, L.; Lund, R.; Pipich, V.; Richter, D. Equilibrium Exchange Kinetics in n-alkyl–PEO Polymeric Micelles: Single Exponential Relaxation and Chain Length Dependence. *Soft Matter* **2012**, *8*, 623−626.

[77] Lu, J.; Bates, F. S.; Lodge, T. P. Molecular Exchange in Diblock Copolymer Micelles: Bimodal Distribution in Core-Block Molecular Weights. *ACS Macro Lett.* **2012**, *1*, 982−985.

[78] Lu, J.; Bates, F. S.; Lodge, T. P. Chain Exchange in Binary Copolymer Micelles at Equilibrium: Confirmation of the Independent Chain Hypothesis. *ACS Macro Lett.* **2013**, *2*, 451−455.

[79] Daza, F. A. G.; Avalos, J. B.; Mackie, A. D. Logarithmic Exchange Kinetics in Monodisperse Copolymeric Micelles. *Phys. Rev. Lett.* **2017**, *118*, 248001.

[80] Daza, F. A. G.; Avalos, J. B.; Mackie, A. D. Simulation Analysis of the Kinetic Exchange of the Copolymer Surfactants in Micelles. *Langmuir* **2017**, *33*, 6794–6803.

[81] Zinn, T.; Willner, L.; Pipich, V.; Richter, D.; Lund, R. Effect of Core Crystallization and Conformational Entropy on the Molecular Exchange Kinetics of Polymeric Micelles. *ACS Macro Lett.* **2015**, *4*, 651−655.

[82] König, N.; Willner, L.; Pipich, V.; Zinn, T.; Lund, R. Cooperativity during Melting and Molecular Exchange in Micelles with Crystalline Cores. *Phys. Rev. Lett.* **2019**, *122*, 078001.

[83] Li, Z.; Dormidontova, E. E. Equilibrium Chain Exchange Kinetics in Block Copolymer Micelle Solutions by Dissipative Particle Dynamics Simulations. *Soft Matter* **2011**, *7*, 4179–4188.

[84] Zinn, T.; Willner, L.; Pipich, V.; Richter, D.; Lund, R. Molecular Exchange Kinetics of Micelles: Corona Chain Length Dependence. *ACS Macro Lett.* **2016**, *5*, 884−888.

[85] Ma Y.; Lodge, T. P. Chain Exchange Kinetics in Diblock Copolymer Micelles in Ionic Liquids: The Role of χ. *Macromolecules* **2016**, *49*, 9542−9552.

[86] Lu, J.; Bates, F. S.; Lodge, T. P. Remarkable Effect of Molecular Architecture on Chain Exchange in Triblock Copolymer Micelles. *Macromolecules* **2015**, *48*, 2667−2676.

[87] Peters, A. J.; Lodge, T. P. Chain Exchange Kinetics of Asymmetric B_1AB_2 Linear Triblock and AB_1B_2 Branched Triblock Copolymers. *Macromolecules* **2017**, *50*, 6303–6313.

[88] Prhashanna, A.; Chen, S. B. Chain Exchange Kinetics between Linear ABA-Type Triblock Copolymer Micelles. *Polymer* **2017**, *118*, 22−29.

[89] Prhashanna, A.; Dormidontova, E. E. Tadpole and Mixed Linear/Tadpole Micelles of Diblock Copolymers: Thermodynamics and Chain Exchange Kinetics. *Macromolecules* **2017**, *50*, 1740−1748.

[90] Peters, A. J.; Lodge, T. P. Comparison of Gel Relaxation Times and End-Block Pullout Times in ABA Triblock Copolymer Networks. *Macromolecules* **2016**, *49*, 7340–7349.

[91] Lund, R.; Willner, L.; Pipich, V.; Grillo, I.; Lindner, P.; Colmenero, J.; Richter, D. Equilibrium Chain Exchange Kinetics of Diblock Copolymer Micelles: Effect of Morphology. *Macromolecules* **2011**, *44*, 6145−6154.

[92] Zhao, D.; Ma, Y.; Lodge, T. P. Exchange Kinetics for a Single Block Copolymer in Micelles of Two Different Sizes. *Macromolecules* **2018**, *51*, 2312−2320.

Chapter II.
Experiments

2.1 Synthesis of Block Copolymers

The polymers used in this work include poly(styrene) (PS) homopolymer, poly(styrene)-*b*-poly(ethylene-*alt*-propylene) (PS-PEP, or SEP in short) diblock, poly(ethylene-*alt*-propylene)-*b*-poly(styrene)-*b*-poly(ethylene-*alt*-propylene) (PEP-PS-PEP', or EPSEP') and poly(styrene)-*b*-poly(ethylene-*alt*-propylene)-*b*-poly(styrene) (PS-PEP-PS' , or SEPS') triblock copolymers (where PEP and PEP', and PS and PS' represent different chain lengths). The PS homopolymer was synthesized by anionic polymerization. For the diblocks and triblocks, sequential anionic polymerizations were conducted by adding styrene and isoprene in sequence, as illustrated in Figure 2.1. The sequence of adding monomers can be altered because poly(styrene) anion is able to initiate isoprene to propagate, and *vice versa*. Thus, poly(styrene)-*b*-poly(isoprene) (SI) diblock, poly(isoprene)-*b*-poly(styrene)-*b*-poly(isoprene) (ISI'), and poly(styrene)-*b*-poly(isoprene)-*b*-poly(styrene) (SIS') triblock copolymers were first obtained as precursors. We note that, in preparation of asymmetric ISI' triblocks, the shorter PI block was first polymerized, then followed by the midblock, and finally the longer PI' block that had the same type of monomer as the first block. Asymmetric SIS' triblocks were synthesized in the same way. Subsequently, the poly(isoprene) block of SI, ISI' and SIS' precursors were selectively saturated to form PEP blocks using a Ni/Al homogenous catalyst under 400 psi hydrogen H_2 or deuterium D_2. If the saturation was conducted under high-pressure deuterium, the resulting average repeat unit of PEP is $C_5D_{2.3}H_{7.7}$, where $D_{2.3}$ is a consequence of D_2 saturation and a small extent of H/D exchange. This partial deuteration of PEP blocks reduces the contrast to the solvent in the time-resolved small-angle neutron scattering (TR-SANS) experiments, and therefore, reduces the

scattering from PEP corona blocks. Since TR-SANS experiments require a pair of protonated and deuterated polymers, selectively deuterated equivalent polymers (dSEP, EPdSEP' and dSEPdS' respectively) were synthesized following the same protocol as protonated polymers. The difference is that deuterated styrene (Polymer Source, Inc.) monomer (C_8D_8) was used to polymerize the deuterated PS block (dS), with use of protonated isoprene.

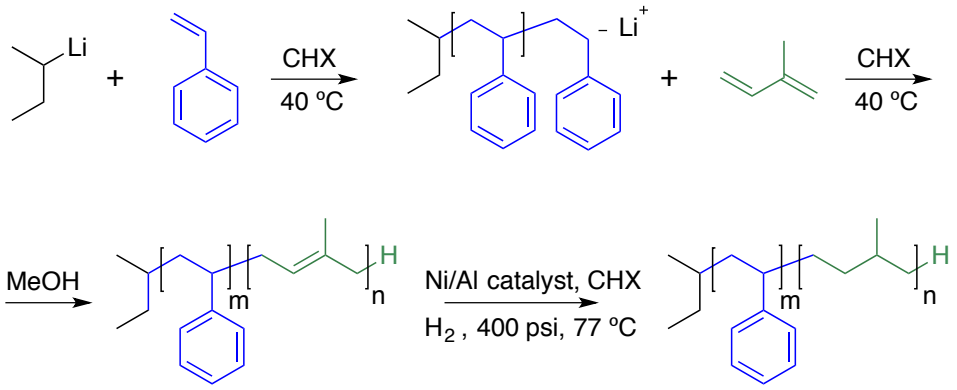

Figure 2.1 Illustration of synthesis of SEP diblock copolymers

2.1.1 Anionic Polymerization

Anionic polymerization is a living polymerization that enables synthesis of polymers with well-controlled architecture, e.g., diblock and triblock copolymers, and narrow molecular weight distribution (i.e., a Poisson distribution in the ideal case). The mechanism of anionic polymerization follows the kinetics of a chain-growth polymerization: initiation, propagation, and termination. The initiator, *sec*-butyllithium in our case, is a highly reactive agent in cyclohexane that initiates styrene or isoprene monomer to form the respective carbanions. The rate of initiation is significantly faster than the propagation rate, so that every chain is initiated at almost the same time, which enables a narrow dispersity of final chain lengths. The initiated anion then attacks additional monomers leading to chain propagation. In the absence of impurities, these

poly(styrene) and poly(isoprene) anions are living polymers with no termination or chain transfer. Living carbanions such as poly(styryllithium) can also initiate other monomers, e.g., isoprene when added to the system. The kinetics of chain propagation depends on the type of monomer. For example, isoprene is found to react faster than styrene, i.e., less time is required for polymerization. As poly(styrene) anion is able to initiate isoprene to propagate and *vice versa*, the sequence of adding styrene and isoprene monomers can be altered. Therefore, ISI' triblock copolymers can be polymerized by sequentially adding isoprene, styrene, and isoprene. Likewise, SIS' triblock copolymers can be obtained by just altering the monomer addition sequence. The termination step of these polyanions takes place by manually adding methanol, which end-caps the growing polymer chain with a proton.

The key factor in conducting anionic polymerization is to eliminate impurities, which can be from the monomers, solvents, and residual oxygen and moisture in the reactor. Polymerization of an SI diblock copolymer begins with purification of styrene and isoprene monomers. Taking SI 25-18 (precursor of SEP 25-19 where M_n of PS and PEP are 25 kg/mol and 19 kg/mol, respectively) for example, ~ 6 g styrene was weighed and poured into a purification flask or solvent flask. The styrene monomers were first degassed by applying the freeze-pump-thaw technique, which froze the monomer by immersing the flask into liquid nitrogen, then vacuum was applied to remove air. Finally, the monomers were thawed in warm water bath (~ 40 ºC) after isolating the flask from the vacuum line. After the freeze-pump-thaw process, most of the oxygen dissolved in styrene was removed. However, moisture, inhibitors and other high vapor pressure impurities need to be removed. Therefore, the styrene monomer was then transferred into a purification flask containing dibutyl-magnesium purification agent (dried from ~ 1.5 mL 1.0 M solution in heptane prior the monomer transfer). We note that the styrene was distilled under vacuum using a short pass glass tube to avoid liquid condensation. The

monomer transfer was driven by the vapor pressure difference between the monomer flask heated by a warm (ca. 40 °C) water bath and the purification agent flask cooled in liquid nitrogen. After the transfer, frozen styrene was thawed, and stirred over the dibutyl-magnesium for an hour in a warm water bath. This step was repeated twice to remove all of impurities. The purified styrene monomer was then transferred into a 50 mL burette. Prior to the monomer transfer, the empty burette was weighed and re-weighed after the monomer was added, then pressurized with ~ 3 psi argon. Isoprene monomer was purified following a similar protocol with several differences. First, isoprene has a higher vapor pressure than styrene, so transfer of isoprene can be quickly done with the Schlenk line. Second, the purification agent for isoprene was *n*-butyllithium, and the purification step took place in a salt ice water bath (ca. ~ –8 ºC) for 30 minutes. The lower temperature and shorter stirring time was applied to avoid potential polymerization of isoprene initiated by *n*-butyllithium. Note: If the isoprene solution containing *n*-butyllithium heats up during the purification process due to loss of cooling a runaway polymerization may occur, and this can lead to an explosion.

Purified cyclohexane (ca. ~ 400 mL) was collected from the solvent line. The cyclohexane is chosen to produce predominantly (~ 94%) 1,4-addition of isoprene in our work. The cyclohexane from the solvent line was pre-purified by degassing it under argon flow when refilling the solvent tank, and passing it through two purification columns: (i) one column packed with copper redox catalyst, and (ii) the other packed with activated alumina.

With monomers and solvent ready, a 1 L Pyrex glass reactor with 5 ports was assembled by attaching two monomer burettes (3 monomer burettes in the case of synthesizing ISI' and SIS' triblocks), a solvent flask, a thermocouple holder, and a 3-port connector in center. The top port of the connector was sealed with a septum for injecting the initiator, one of the other two ports was connected to the Schlenk line, while the other

was attached to a pressure gauge. Air and moisture in the reactor were removed by applying six cycles of vacuum with flame heating and argon filling. After the last cycle was completed, the reactor was pressurized with ~ 3 psi argon, and immersed in a water bath maintained at 40 ºC.

The cyclohexane was first added to the reactor, and stirred with a magnetic stir bar. The next important step was to inject the initiator, *sec*-butyllithium. The amount of *sec*-butyllithium can be precisely calculated by $V = m_S$ / ([initiator] × $M_{n,PS}$), where m_S is the mass of styrene monomer, [initiator] is the concentration of initiator, and $M_{n,PS}$ is the target molecular weight of the PS block. For example, we obtained 5 g styrene (1 g styrene was lost during purification), and the target molecular weight of PS was 26 kg/mol. Then, we should use 0.14 mL *sec*-butyllithium, assuming the concentration was 1.4 M as provided by the vendor. However, this value was usually underestimated for two reasons. First, the effective concentration would be lower than the given value because some initiators were deactivated during storage. Second, a small portion of the initiator was deactivated during the transfer from the glove box to reactor, and by reacting with remaining impurities in solvent as well. The former could be resolved by titrating the initiator just before the experiment, while the latter was empirical, usually adding 10% excess to account for the loss. This uncertainty in the actual amount of initiator that initiates the monomers leads to difficulty in precisely controlling the molecular weight of the product. That is the reason for the 10% difference in PS molecular weight (≈ 26 kg/mol) in SEP and EPdSEP' block polymers in Table 2.1, for example.

After an appropriate amount of *sec*-butyllithium was injected into the reactor using a 1 mL glass syringe containing a steel needle, 20 minutes equilibration time was given to react with remaining impurities in the solvent. Then, styrene monomer was slowly added from the burette. The solution turned red-yellowish due to the presence of poly(styrene)

anions. The solution was allowed to react for 8 hours to attain close to 100% conversion. Before adding the next monomer, a small aliquot of poly(styrene) anion was extracted from the reactor via a steal cannula and added to ~ 10 mL degassed methanol in a sealed flask. The first block, poly(styrene) in this case, was precipitated and characterized using SEC. Then, the second monomer isoprene was added, and allowed to polymerize for 5 hours. In the case of ISI' triblock synthesis, isoprene monomer corresponding to the shorter PI block was first added, then styrene, and finally isoprene from separate burettes. Two aliquots were taken out to determine the molecular weight and composition after each step. The first one is PI and the second one is the SI diblock. Likewise, the first PS and SI diblock grown during the synthesis of SIS' triblocks were sampled and characterized.

Termination of the reactions was carried out by adding ~ 20 mL degassed methanol, which was freeze-pump-thawed for 3 cycles prior to use. The reactor solution was cooled to room temperature and polymers were precipitated in excess methanol (~ 4 L), then dried in a bell jar under vacuum. The residual methanol was completely removed using the freeze-dry technique, where polymers were re-dissolved in benzene, together with small amount (~ 0.1 g) of butylated hydroxytoluene (BHT) as antioxidant, and then dried under vacuum after the polymer/benzene solution was frozen.

2.1.2 Selective Saturation

The PI blocks of the SI, ISI' and SIS' polymers were selectively saturated into PEP blocks to enhance the thermal and chemical stability, since some experiments were performed at about 200 ºC. This selective hydrogenation/deuteration was catalyzed by a Ni/Al homogenous catalyst, which is sensitive to air and moisture. Therefore, extra effort was paid to prepare a fresh Ni/Al catalyst just before the reaction, and to maintain an environment free of air and moisture throughout the reaction.

To prepare a fresh Ni/Al catalyst, 2 g 2-ethylhexanoate was degassed under vacuum, and dissolved in 40 mL cyclohexane collected from the solvent line. Then, 10 mL 1.0 M triethyl-aluminum solution in cyclohexane was transferred from the glove box using a glass syringe fitted with a steel needle, and injected into the 2-ethylhexanoate solution drop-by-drop. The reaction flask (a 250 mL 3-port flask with one port sealed with a septum for injection) was immersed in a salt ice water bath since this reaction is exothermic. The dark Ni/Al solution was stored in the cold bath for 30 minutes before use.

A typical reaction was conducted with 5 – 10 g of polymer dissolved in 500 mL of cyclohexane. To assure no air and moisture, the polymer was degassed and dissolved in purified cyclohexane. The reactor (a 1L stainless steel reactor) was connected to the Schlenk line with vacuum-argon cycles. It is worth noting that the reactor needs to be thoroughly cleaned to remove residual catalysts from other users, which could hydrogenate the PS block as well. The polymer solution was then transferred to the reactor in the liquid phase through a clean rubber tube. Similarly, the Ni/Al catalyst was injected into reactor via a steel cannula, while the polymer solution was stirring to mix with the catalyst.

After assuring that all valves were closed, the inlet valve of high-pressure hydrogen H_2 was slowly adjusted to fill the reactor at ~ 400 psi H_2. In the case of deuteration, high-pressure deuterium D_2 was used instead. The temperature of this reaction was gradually elevated to 77 ºC using a temperature-control heater. The reaction takes about 24 hours to finish. In some cases with high molecular weight precursors, a second hydrogenation was performed to fully hydrogenate the double bonds in PI blocks, which can be identified by ^{1}H-NMR spectroscopy (see Section 2.2.2).

After the reaction was completed, the reactor was cooled to room temperature and ~ 40 psi argon was flowed through the polymer/catalyst solution to purge the remaining H_2. The solution was poured into 1 L 80 g/L citric acid aqueous solution, and stirred for 2

days to deactivate the catalyst. The solution separated into two phases: (i) the upper phase is an organic phase containing saturated polymer products in cyclohexane, and (ii) the lower phase is an aqueous phase with deactivated catalyst which had a light blue color. The organic phase was separated from the solution, and was filtered through a layer of activated alumina held in a funnel to remove residual catalyst and salts. The final products were finally obtained by precipitating in excess methanol. Polymers were immediately dried and freeze-dried.

2.2 Characterization of Block Copolymers

The molecular weight and molecular weight distribution of the synthesized polymers were determined by size exclusion chromatography using a refractive index detector (SEC-RI), and another SEC instrument equipped with both RI and a multi-angle light scattering detector (SEC-MALS), and ^{1}H nuclear magnetic resonance spectroscopy (^{1}H NMR). Table 2.1 summarizes the characteristics of the polymers, including 1 PS homopolymer, 11 diblocks and 14 triblocks. The nomenclature of each polymer refers to the block molecular weights: e.g., SEP 25-19 indicates $M_n \approx 25$ kg/mol and 19 kg/mol for PS and PEP, respectively. All SEP diblocks (except the last two) have almost identical PS blocks, i.e., 26 kg/mol to within 10%, with PEP blocks varying by a factor of 8, from 19 kg/mol to 151 kg/mol. For EPSEP' triblocks, the molecular weights of the PS block and overall PEP + PEP' blocks are almost the same (26 kg/mol for PS and 70 kg/mol for overall PEP + PEP', within 10% variation). The ratio of shorter PEP over longer PEP' varies from 0.06 for the most asymmetric EPSEP' triblock to 1 for the symmetric EPSEP triblock. The core block asymmetry was designed in the SEPS' triblocks such that one PS block is similar with that of the symmetric SEPS while the other PS block is quite different. For example, asymmetric SEPS' 25-66-41 has one 41 kg/mol PS block which is comparable with that of symmetric SEPS 45-144-45, whereas the other PS block of the asymmetric SEPS' is much shorter.

Table 2.1 Characteristics of Synthesized Polymers (M_n in unit of kg/mol)

Homopolymers	$M_{n,\,PS}$ [a]			M_w/M_n [a]
PS 23	23			1.03
Diblock Copolymers	$M_{n,\,PS}$ [a]	$M_{n,\,PEP}$ [b]		M_w/M_n [a]
SEP 25-19	25	19		1.03
SEP 28-40	28	40		1.05
dSEP 30-41	30	41		1.07
SEP 26-70 [c]	26	70		1.04
dSEP 29-71 [c]	29	71		1.10
SEP 28-118	28	118		1.08
dSEP 25-95	25	95		1.06
SEP 26-151	26	151		1.09
dSEP 25-137	25	137		1.09
SEP 42-64 [c]	42	64		1.05
dSEP 47-67 [c]	47	67		1.10
Triblock Copolymers	$M_{n,\,PEP}$ [a]	$M_{n,\,PS}$ [b]	$M_{n,\,PEP'}$ [b]	M_w/M_n [a]
EPSEP' 4-29-74	4	29	74	1.05
EPSEP' 8-26-62	8	26	62	1.05
EPdSEP' 8-27-60	8	27	60	1.05
EPSEP' 15-28-52	15	28	52	1.04
EPdSEP' 15-28-55	15	28	55	1.03
EPSEP 30-24-30	30	24	30	1.07
EPdSEP 33-26-33	33	26	33	1.07
Triblock Copolymers	$M_{n,\,PS}$ [a]	$M_{n,\,PEP}$ [b]	$M_{n,\,PS'}$ [b]	M_w/M_n [a]
SEPS 17-53-17 [d]	17	53	17	1.04
SEPS' 19-61-26	19	61	26	1.04
SEPS' 25-66-41	25	66	41	1.06
dSEPdS' 26-71-46	26	71	46	1.13
SEPS 45-144-45 [e]	45	144	45	1.04
dSEPdS 49-133-49 [e]	49	133	49	1.05

Here, the molecular weights of polymers were converted from those of unsaturated SI and dSI diblock, ISI', IdSI', SIS', and dSIdS' triblock precursors that were directly measured by SEC and ^{1}H-NMR; and M_n of PEP blocks were calculated from the corresponding PI blocks in precursors assuming 100% saturation.

[a] The molecular weight of the first block was determined by SEC-RI with PS standards and another SEC-MALS instrument; the dispersity of the final polymer was determined by SEC-RI.

[b] The molecular weight of the second block and third block (in triblocks) was determined by ^{1}H-NMR spectroscopy and confirmed by SEC-MALS.

[c,d,e] These polymers were reproduced from previous work[1-3] (c) reference 1, (d) 2, and (e) 3.

2.2.1 Size Exclusion Chromatography (SEC)

SEC is a routine technique to characterize the molecular weight and molecular weight distribution of polymers. As a liquid chromatography, SEC has two phases, i.e., a mobile phase and a stationary phase. The mobile phase contains the polymer solution, 2 – 5 mg/mL polymer in tetrahydrofuran (THF), with 1 mL/min THF flow flushing the solution. The stationary phase is a column packed with porous material. When polymers with different hydrodynamic volumes (V_h) pass through the column, the largest polymer is excluded from pores to the highest extent, and therefore, elutes first. On the other hand, the smallest polymer is able to penetrate the pores in the column, so it elutes later than larger polymers. SEC separates polymers by size, i.e., hydrodynamic volume. The hydrodynamic volume of a polymer is related to its molecular weight by,

$$V_h \sim [\eta]M \sim kM^{1+a} \tag{2.1}$$

where $[\eta]$ is the intrinsic viscosity of the polymer that follows the Mark-Houwink relation, $[\eta] = kM^a$, with two empirical parameters k and a, and M is the molecular weight of the polymer.

Eluents are monitored for the appearance of polymers by one or several detectors, e.g., a refractive index (RI) detector and a multi-angle light scattering (MALS) detector. For dilute polymer solutions, the response of the RI detector reflects the polymer concentration c, given by,

$$n = n_s + \left(\frac{dn}{dc}\right)c \tag{2.2}$$

where n and n_s are refractive index of the eluent and solvent (THF) respectively, dn/dc is the refractive index increment, ≈ 0.187 mL/g for PS and ≈ 0.124 mL/g for PI in THF with wavelength of laser 637 nm at 25 ºC. If the SEC instrument is only equipped with an RI detector, the molecular weight of PS samples is given by the PS calibration standards, and by universal calibration for PI samples. One advantage of a MALS detector is to obtain the absolute molecular weight of polymer samples without any column calibration. The signal of the LS detector is proportional to the molecular weight and concentration of polymer.

$$I \sim \left(\frac{dn}{dc}\right)^2 cM \tag{2.3}$$

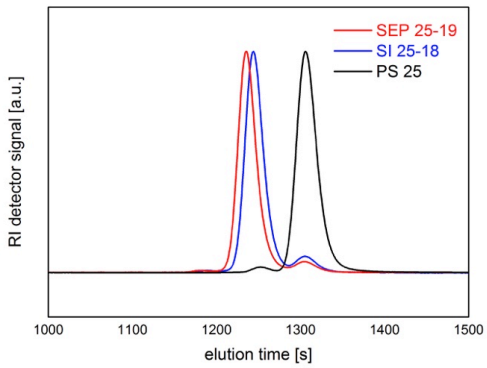

Figure 2.2 SEC traces of PS 25, SI 25-18 and SEP 25-19 polymers

Figure 2.2 shows the SEC traces of the first block PS 25 aliquot from the SI 25-18 precursor, along with the SI 25-18 and SEP 25-19 diblock copolymers. The molecular weight of PS is 25 kg/mol calibrated by a series of PS standards. Another SEC instrument gives the same value using multi-angle light scattering detector with dn/dc = 0.187 mL/g. It clearly shows a narrow distribution of molecular weight except a very small bump in earlier elution time than the primary peak. This bump is associated with chain coupling during termination of the PS aliquot, leading to a small fraction (< 1 wt% by the peak area in SEC trace) of PS with doubled molecular weight. The coupling during termination also occurred with the SI diblock copolymer, as observed in the blue curve. Moreover, a small fraction (≈ 1 wt%) of PS homopolymer is present in the sample due to spurious termination during the anionic polymerization (e.g., due to taking aliquots and adding another monomer). The red curve is the SEP diblock copolymer after selective saturation of the double bonds in the PI block. Compared to the trace of SI, the SEP curve shows almost the same shape but is shifted to slightly shorter elution time. Also, small amounts (< 2%) of coupled copolymer and PS homopolymer exist in the SEP sample. We argue that these minor amounts of coupled polymer and PS homoplymer should be inconsequential for the study of micelle structure and the chain exchange kinetics.

SEC-MALS can also directly measure the molecular weights of the block copolymers. This is especially useful with the deuterated polymers (e.g., dSEP) whose molecular weights cannot be determined by ^{1}H-NMR due to the absence of protons in dPS. The only requirement is to know the exact dn/dc value of the polymer solution in THF. A SEC instrument with both RI and LS detectors is able to determine the dn/dc value by inputting the exact concentration of injected polymer solution and assuming 100% sample recovery. Alternatively, one can also measure the dn/dc using a refractometry at the same wavelength and temperature as SEC.

Despite its wide use in polymer science, several limitations of SEC are noted here. First, the resolution of SEC is relatively low, compared to matrix-assisted laser desorption/ionization mass spectrometry (MALDI), which is able to distinguish chains with a resolution of one repeat unit. SEC can discriminate molecular weight with an accuracy of 5 to 10%. Second, the dispersity of an anionic polymerized polymer is usually overestimated by SEC due to the peak broadening effect. Even in the case of injecting an absolutely monodisperse sample, the SEC will show a molecular weight distribution, although narrow. Third, an appropriate range of molecular weights is typically from several kg/mol to several hundred kg/mol. For low molecular weight samples, MALDI and ^{1}H-NMR are needed to determine the molecular weight reliably.

2.2.2 Proton Nuclear Magnetic Resonance (^{1}H-NMR)

^{1}H-NMR spectroscopy detects various types of protons with different chemical shifts, and quantitatively determines the abundance of protons by the peak areas. We performed ^{1}H-NMR to determine the molecular weight of SI, ISI' and SIS' block copolymers, as well as the conversion of the hydrogenation reactions. Taking SI 25-18 as an example, about 0.6 mL polymer solution (10 – 20 mg/mL) in d-chloroform is prepared for a ^{1}H-NMR experiment. The black curve in Figure 2.3 represents an ^{1}H-NMR spectrum of SI 25-18, where broad peaks around chemical shifts 7.1 ppm (a) and 6.6 ppm (b) correspond to aromatic protons in PS, and the two peaks at 5.2 ppm (c) and 4.7 ppm (d) correspond to double-bond protons in 1,4-PI and 1,2-PI repeat units, respectively. Peaks at low chemical shifts (1.4 – 2.2 ppm) are associated with the remaining protons on saturated carbon atoms. With the molecular weight of the first block PS determined by SEC, the molecular weight of the second block PI ($M_{n,PI}$) can be determined from the ^{1}H-NMR spectra.

$$M_{n,PI} = M_I \times \frac{M_{n,PS}}{M_S} \times \frac{S_c + S_d / 2}{(S_a + S_b) / 5} \tag{2.4}$$

where M_I and M_S are molecular weights of isoprene and styrene monomers, respectively, $M_{n,PS}$ is the molecular weight of the PS block, i.e., 25 kg/mol from SEC, and S_a, S_b, S_c and S_d correspond to integrated areas of proton peaks in ^{1}H-NMR. The calculated $M_{n,PI}$ = 18 kg/mol agrees well with the feed ratio of isoprene and styrene monomers, indicating the conversion of anionic polymerization that we perform is essentially 100%. Similarly, the mole fraction of 1,4-PI repeat units can also be calculated as S_c / (S_c + S_d/2) = 93%. Therefore the saturated PI block contains 93% PEP repeat units when complete saturation is achieved.

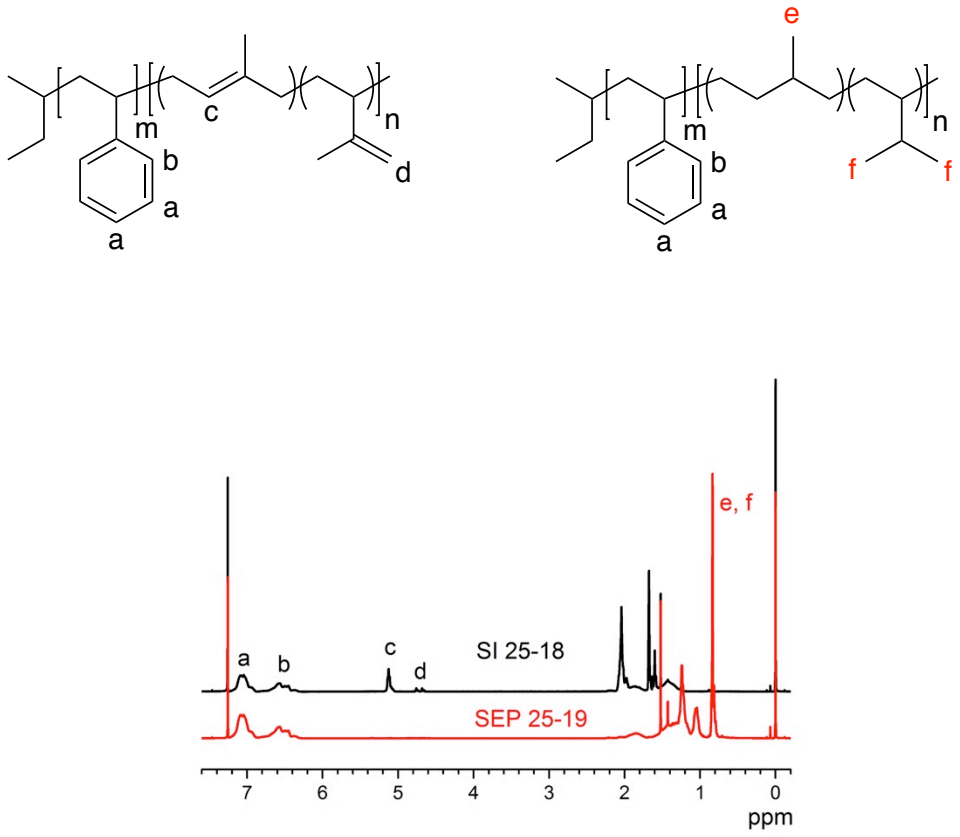

Figure 2.3 ^{1}H-NMR spectra of SI 25-18 and SEP 25-19, and their chemical structures

^{1}H-NMR was also performed to determine the extent of hydrogenation. As shown in Figure 2.3, the red curve represents SEP 25-19 after selective PI hydrogenation. The complete disappearance of the double-bond protons indicates full saturation of the PI blocks, while the aromatic protons of PS blocks are retained. The chemical shifts of the saturated protons in the PEP blocks appear around 0.8 ppm (peak e and f). Therefore, the molecular weight of the PEP blocks are calculated based on 100% saturation of the PI blocks.

It is worth noting that the molecular weights of the deuterated polymers (dSI, IdSI' and dSIdS') cannot be determined by ^{1}H-NMR due to the absence of aromatic protons in dPS repeat units. For these polymers, the molecular weights were determined by SEC-MALS, and compared with the calculated values assuming 100% conversion of the monomers fed to the reactor during the anionic polymerization.

2.3 Micelle Solution Preparation

Micelle solutions were prepared using a cosolvent procedure. Polymer was dissolved in squalane with a similar amount of dichloromethane as cosolvent. After the polymer completely dissolved, the solution was filtered through 0.2 μm hydrophobic PTFE filters to remove dust. The dichloromethane was then evaporated at room temperature for two days until constant weight was achieved. Micelles formed as the dichloromethane was removed, due to unfavorable enthalpy of mixing between the PS block and the solvent. The dilute solutions (≤ 1 wt%) were filtered again using 0.2 μm filters; the concentrated solutions did not permeate through the filter because of high viscosity. The solutions were degassed under vacuum for 5 min to remove air bubbles and residual dichloromethane. Micelle solutions were annealed at 160 ºC for 1 h to equilibrate, and then slowly cooled back to room temperature. Finally, micelle solutions were transferred to different sample holders for measurements, including LS glass tubes for static and

dynamic light scattering, capillaries and hermetic aluminum pans for small-angle X-ray scattering, and quartz banjo cells for small-angle neutron scattering experiments.

2.4 Light Scattering

2.4.1 Static Light Scattering (SLS)

Static and dynamic light scattering (SLS and DLS, respectively) are important techniques for studying polymer solutions. The excess scattering intensity from a dilute polymer solution is given by the Zimm equation, eqn 2.5.[4]

$$\frac{Kc}{R_\theta} = \frac{1}{M_w}\left(1 + \frac{1}{3}q^2 R_g^2\right) + 2A_2 c \tag{2.5}$$

$$R_\theta = r^2 \frac{I_p - I_s}{I_o} \tag{2.6}$$

$$K = \frac{4\pi^2 n^2 (dn/dc)^2}{\lambda^4 N_{av}} \tag{2.7}$$

$$q = \frac{4\pi n \sin(\theta/2)}{\lambda} \tag{2.8}$$

Here R_θ is the Rayleigh ratio defined by eqn 2.6, where the scattering intensity of a polymer solution, I_p, has been obtained by subtracting the solvent scattering I_s, and then this excess scattering intensity is normalized to the incident beam intensity I_o, as well as the square of sample-to-detector distance r^2. Note that R_θ has the unit of cm^{-1}. The constant K contains the solvent refractive index n and the refractive index increment (dn/dc) for the solution, laser wavelength in vacuum λ, and Avogadro's number N_{av}. The scattering wave vector q is defined by eqn 2.8, with a unit of inverse length. q depends on the scattering angle θ and laser wavelength. In the Zimm equation, eqn 2.5, M_w is the weight average molecular weight of the polymer, R_g is the radius of gyration of the

polymer chain in solution, A_2 is the second virial coefficient, and c is the polymer concentration.

One example of using Zimm approach is to determine the second virial coefficient A_2 of PS in pure squalane and the binary solvent mixture squalane and 1-phenyldodecane. The Flory-Huggins interaction parameter χ between PS and the solvent can be quantified by eqn 2.9,

$$\chi = \frac{1}{2} - \rho_p^2 v_1 A_2 \tag{2.9}$$

where ρ_p is the polymer density, and v_1 is the molar volume of the solvent, which is also taken as the reference volume.

In this experiment, a series of dilute PS (M_n = 23 kg/mol from SEC-MALS in Table 2.1) solutions in 1-phenyldodecane with various concentrations (10 – 50 mg/mL) were prepared, and sealed in LS glass tubes. The refractive indices of the solvent and the dn/dc values for the dilute PS solutions were measured using a refractometer operated with red light (≈ 650 nm), as shown in Figure 2.4a. The dashed lines gave the dn/dc value, 0.0989 mL/g, which was almost independent of temperature in the range of 23 – 60 ºC. With a dn/dc values known, these samples were investigated using a Brookhaven BI-200SM goniometer and laser light scattering system with λ = 637 nm. The instrument constant was calibrated using toluene at 23 ºC. Measurements were taken at multiple angles ranging from 50º to 130º with 10º increments, leading to a q range of 0.012 – 0.026 nm^{-1}. Figure 2.4b shows the Zimm plot obtained from these PS solutions. Kc/R_θ was independent of scattering angle because this polymer is rather small (R_g ≈ 4 nm in theta solvent), $qR_g \leq 0.1$, while Kc/R_θ decreased with increasing polymer concentration. The second virial coefficient $A_2 = -1.69\times10^{-4}$ cm^{3}mol/g^2 was obtained, indicating 1-phenyldodecane is a poor solvent for PS at 23 ºC. With ρ_p = 1.04 g/cm^3 for PS and v_1 =

288 cm^3/mol for 1-phenyldodecane, χ is calculated to be approximately 0.55 based on Flory-Huggins theory. By double extrapolation of angle and concentration to 0, the weight average molecular weight of this PS sample was determined to be 30 kg/mol, which is 20% larger than the molecular weight obtained from SEC-MALS.

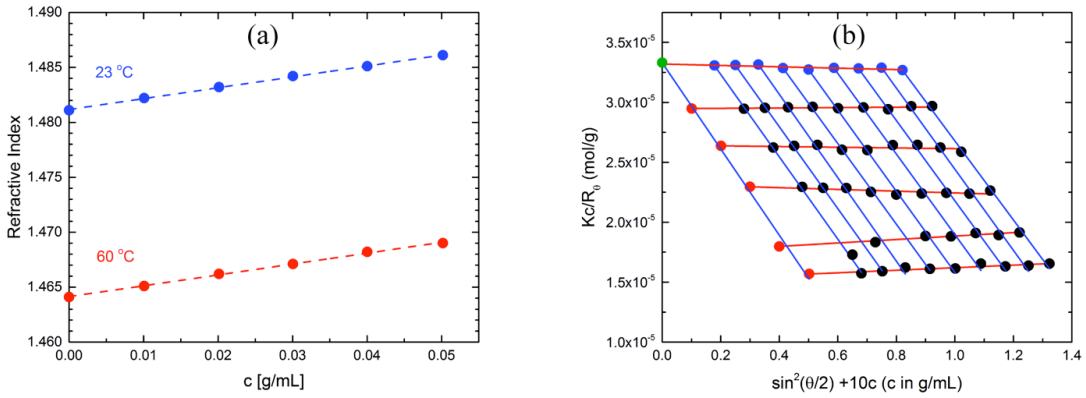

Figure 2.4. (a) Refractive indices vs concentration of dilute PS solutions in 1-phenyldodecane at 23 ºC and 60 ºC, and the slop (dashed line) gives the refractive index increment (d*n*/d*c*), and (b) Zimm plot of PS in 1-phenyldodecane at 23 ºC.

We note that SLS can also be used to measure the average molecular weight of micelles ($M_{w,mic}$) in SEP and EPSEP micelle solutions. Dividing by the molecular weight of one polymer chain ($M_{w,p}$), the average aggregation number of chains within a micelle is then obtained, i.e., $N_{agg} = M_{w,mic} / M_{w,p}$. Simultaneously, the radius of gyration (R_g) of the micelle is obtained from the Zimm plot as well, which is important information of micelle structure.

2.4.2 Dynamic Light Scattering (DLS)

DLS probes dynamic properties of polymer solutions such as the mutual diffusion coefficient (D_m) of micelles in solution. In the dilute limit, the hydrodynamic radius of micelles (R_h) is determined by the Stokes-Einstein equation,

$$R_h = \frac{kT}{6\pi\eta_s D_0} \tag{2.10}$$

where k, T, η_s, and D_0 are the Boltzmann constant, temperature, solvent viscosity, and tracer diffusion coefficient ($D_0 = D_m$ in the dilute limit), respectively.

Typically, 0.5 vol% (≈ 5 mg/mL) or even lower concentrations of micelle samples were prepared for DLS measurements to avoid micelle overlap. The room temperature measurement was conducted using the same instrument as SLS (a Brookhaven BI-200SM goniometer with λ = 637 nm). Measurements were taken at multiple angles ranging from 60º to 120º in increments of 15º. The acquisition time at each angle was 20 minutes for good statistics. The instrument recorded the history of detector counts and reported the intensity correlation function, which was converted to the field amplitude correlation function $g(1)(q,t)$. The data were processed using the regularized positive exponential sum (REPES) method,[5] which performs an inverse Laplace transform of $g(1)(q,t)$ resulting in a distribution function of relaxation times (τ),

$$\frac{1}{\tau} = \Gamma = q^2 D_m \tag{2.11}$$

where Γ is the decay rate in unit of s^{-1} and q is the scattering vector. Using the Stokes-Einstein equation, the distribution of micelle hydrodynamic radii R_h was obtained, as shown in Figure 2.5a. These micelles formed by the SEP 25-19 block copolymer have a narrow monomodal distribution with a mean hydrodynamic radius of 30 nm. With this information, a second cumulant fitting method was also employed to interpret the data from this disperse system with a single distribution, as shown in Figure 2.5b.

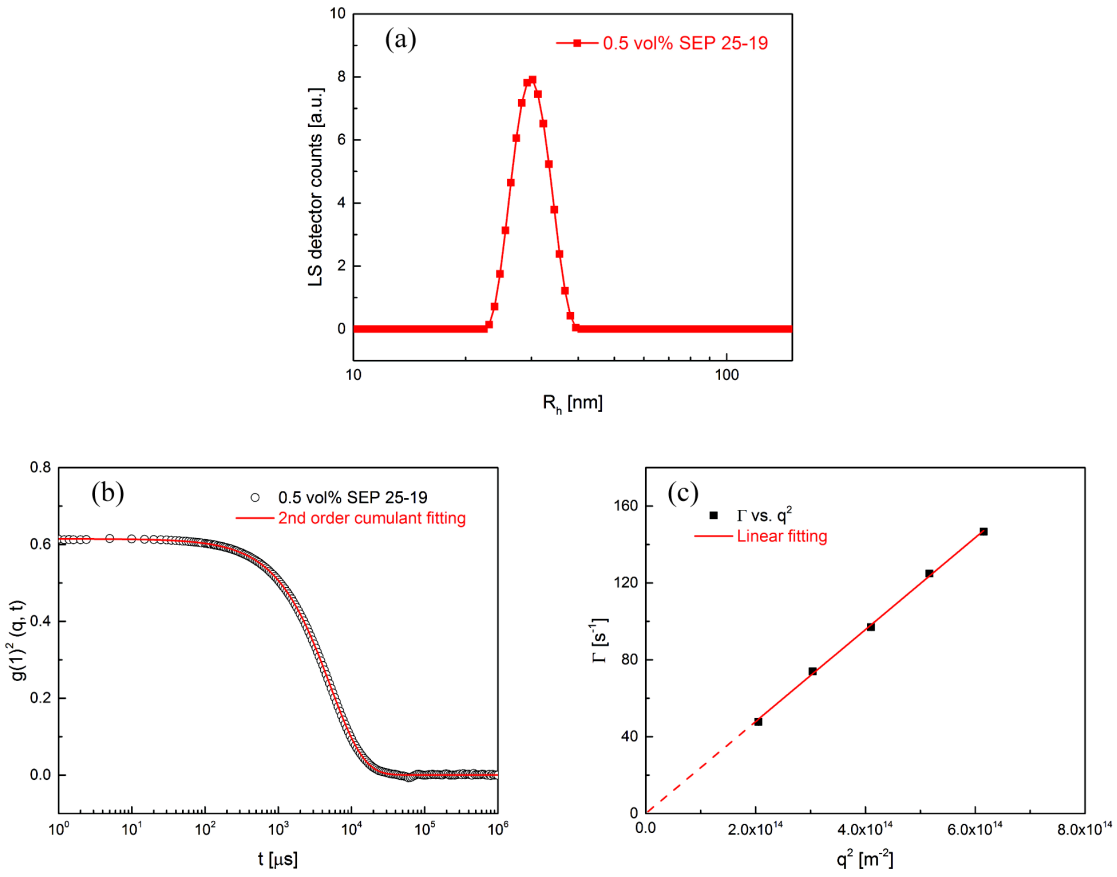

Figure 2.5 (a) The R_h distribution, (b) square of the amplitude correlation function $g(1)^2(q, t)$, and (c) decay rates Γ at multiple angles of SEP 25-19 micelles in 0.5 vol% solution

$$g(1)(q,t) = \exp\left(-\Gamma t + \frac{\mu_2}{2!}t^2\right) \tag{2.12}$$

Here the mean decay rate Γ and dispersity of particles (μ_2/Γ^2) can be obtained. Figure 2.5c shows the mean decay rates at multiple angles, from which D_m is determined as the slope. Note that the fitting line of Γ vs q^2 should go through the origin. Thus, the micelle hydrodynamic radius is calculated to be 30 nm with dispersity $\mu_2/\Gamma^2 = 0.10$, which is consistent with the value obtained by REPES.

High temperature DLS measurements were performed on a home-built light scattering instrument using silicon oil as a refractive index matching solvent, since the aforementioned instrument is not able to go alone 70 ºC. This home-built instrument can be operated at temperatures as high as 200 ºC. To obtain reliable data, the laser needs 2 hours stabilize prior use, with a wavelength 488 nm. A temperature ramp can be designed for micelle samples to determine the critical micelle temperature T_{CMT}, at which micelles dissolve into free chains, causing a drop in both scattering intensity and hydrodynamic radius. The scattering intensity is proportional to the molecular weight of: (i) micelles $M_{w,mic}$ at $T < T_{CMT}$, or free polymers $M_{w,p}$ at $T > T_{CMT}$. Therefore, the intensity changes by a factor of almost N_{agg} across the T_{CMT}. Figure 2.6 shows the temperature-dependent response of a 0.5 vol% SEP 26-70 solution upon heating (red curve) and cooling (blue curve). At each temperature, the sample was held for 10 minutes to thermally equilibrate. T_{CMT} is estimated to be around 130 ºC. When the temperature goes across T_{CMT}, about two orders of magnitude change was observed in the detector counts as shown in Figure 2.6a. Simultaneously, the apparent R_h value drops from 37 nm to 5 nm in Figure 2.6b. This change is thermally reversible as the cooling curve overlaps with the heating curve

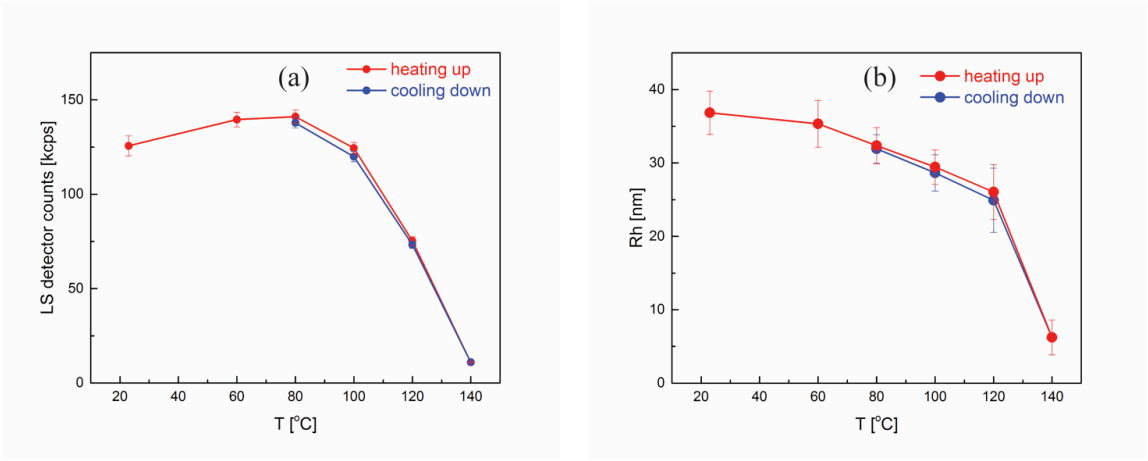

Figure 2.6 Temperature dependence of (a) the LS detector counts and (b) the hydrodynamic radius of 0.5 vol% SEP 26-70 polymer in the 25/75 vol% 1-phenyldodecane/squalane mixing solvent upon heating and cooling.

2.5 Small-Angle X-ray Scattering (SAXS)

Due to the limited q range (0.001 – 0.003 $Å^{-1}$), the light scattering technique cannot provide structural information of micelles at smaller length scales such as micelle core radius R_{core} (~ 10 nm). SAXS offers access to smaller structures because of higher q values, typically 0.001 $Å^{-1}$ – 1.0 $Å^{-1}$. We also note that the source of contrast in SAXS comes from the electron density difference ($\rho_p - \rho_{solvent}$, where ρ_p is electron density of polymer, either PS block or PEP block, and $\rho_{solvent}$ is that of solvent) rather than the refractive index increment (dn/dc) in light scattering. The contrast between the PS core block and squalane is calculated to be 0.123 mol e^-/cm^3, approximately five times that between PEP corona block and squalane, 0.025 mol mol e^-/cm^3. Therefore, the scattering from the micelle core is dominant in the overall scattering from this system.

SAXS was performed at the 5-ID-D beam line at the DuPont-Northwestern-Dow (DND-CAT) station at Argonne National Laboratory. A beam energy of 17 keV, corresponding to a wavelength 0.73 Å, and a sample-to-detector distance 8.5 m were selected to give a q range of 0.003 – 0.15 $Å^{-1}$. Due to the high flux with the synchrotron X-ray source, only a 1s exposure time was required, even for dilute micelle solutions. The solution samples ($c \leq 10$ vol%) were loaded and sealed into capillary tubes after the co-solvent procedure. Concentrated micelle solutions ($c > 10$ vol%) were loaded into hermetic aluminum pans by solvent casting, and then sealed under argon in a glove box. There are various kinds of sample stages to choose for both capillaries and aluminum pans. A 16-position room temperature capillary stage was available for room temperature, while an 8-position hot capillary stage works well for a temperature ramp from 25 ºC to 200 ºC. If precise control of temperature is required (± 0.5 ºC), the Linkam single capillary stage was used to heat and cool the sample. As for aluminum pans, a 32-position hot pan stage is good for heating and cooling samples, while the Linkam single pan stage is designed for better temperature control. At each temperature, samples were

annealed for 10 min to equilibrate thermally, and then exposed to X-rays. A pure solvent sample was measured as a background to be subtracted from micelle solution scattering. Since micelle samples are isotropic, two-dimensional scattering images were azimuthally averaged to the one-dimensional intensity $I(q)$ vs. q in arbitrary intensity units.

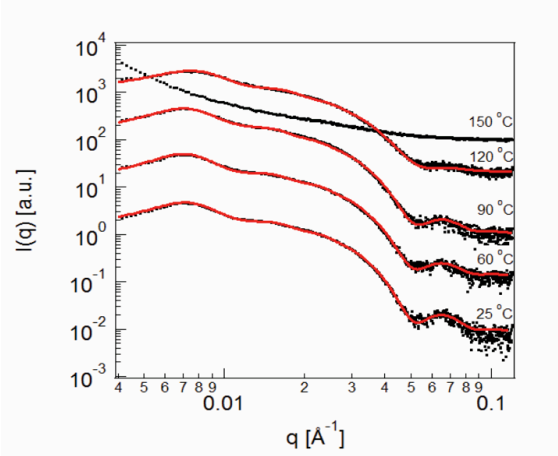

Figure 2.7 SAXS patterns of 1 vol% SEP 26-70 micelles in the solvent mixture of 25/75 vol% 1-phenyldodecane/squalane (vertically shifted for clarification). Red lines are the best fits to the hard sphere model.

Figure 2.7 shows the SAXS patterns of 1 vol% SEP 26-70 micelles in the solvent mixture of 25/75 vol% 1-phenyldodecane/squalane after the solvent background was subtracted. Low temperature scattering patterns show a distinct micelle form factor at high q with the first minimum $q_1 = 0.051$ Å^{-1}, and a small bump in the structure factor at low q (≈ 0.007 Å^{-1}) reflecting inter-micelle interactions. Based on the first minimum appearing at $q_1 = 0.051$ Å^{-1}, the micelle core radius R_{core} is estimated to be 8.8 nm at 25 ºC by applying the characteristic equation for the minima in the hard sphere form factor, i.e., $qR_{core} = 4.49$. The red lines in the figure are the best fits to the hard sphere model developed for BCP micelles, which is discussed in Section 2.6. The model fits give R_{core} = 8.8 nm with standard deviation of core radii $\sigma_{Rc} = 0.7$ nm, in good agreement with the

calculated results from the first minima. The model also provides the effective hard sphere radius R_{hs} = 31 nm for these micelles, which is close to their hydrodynamic radius 37 nm. At elevated temperatures, the micelle core radius and effective hard sphere radius do not show any appreciable change. However, more solvent penetrates into the core, leading to less contrast between the micelle core and solvent, as evidenced by weaker first minima in the SAXS patterns. Micelle features disappeared at 150 ºC, indicating no long-lasting micelle present at this temperature. The T_{CMT} is within the temperature window of 120 – 150 ºC, which is consistent with DLS results (≈ 130 ºC).

2.6 Hard Sphere Model for Block Copolymer Micelles

A hard sphere model was adopted to extract structural details for the SEP micelles, which was originally developed by Pedersen and co-workers,[6-10] and later adapted by Bang et al.[11] The model depicts each micelle as constructed of swollen Gaussian chains of corona blocks tethered on hard spheres formed by the core blocks, where the micelles also can interact with each other. The coherent scattering intensity $I(q)$ from BCP micelles is given by eqn 2.13, where R_{core} is the core radius with a Gaussian distribution of $D(R_{core})$ as given by eqn 2.14, $P_{mic}(q)$ is the micelle form factor (eqn 2.15), $A_{mic}(q)$ is the form factor amplitude (eqn 2.16), and $S(q)$ is the structure factor for hard spheres with the Percus–Yevick closure approximation.

$$I(q) = \int D(R_{core})\left(P_{mic}(q) + A_{mic}^2(q)[S(q)-1]\right)\mathrm{d}R_{core} \tag{2.13}$$

$$D(R_{core}) = \frac{1}{\sqrt{2\pi}\sigma_{Rc}}\exp\left[-\frac{\left(R_{core}-\left\langle R_{core}\right\rangle\right)^2}{2\sigma_{Rc}^2}\right] \tag{2.14}$$

$$P_{mic}(q) = N_{agg}^2 \beta_{core}^2 A_{core}^2(q) + N_{agg} \beta_{corona}^2 P_{chain}(q) + 2N_{agg}^2 \beta_{core} \beta_{corona} A_{core}(q) A_{corona}(q) + N_{agg}(N_{agg} - 1) \beta_{corona}^2 A_{corona}^2(q) \quad (2.15)$$

$$A_{mic}(q) = N_{agg} \left(\beta_{core} A_{core}(q) + \beta_{corona} A_{corona}(q) \right) \quad (2.16)$$

In eqn 2.14, $<R_{core}>$ is the mean core size and σ_{Rc} is the standard deviation of core sizes. The first term in $P_{mic}(q)$ (eqn 2.15) is the self-correlation of spherical micelle cores. N_{agg} is the aggregation number, and β_{core} is the contrast between the core block and solvent defined as $\beta_{core} = v_{PS}(\rho_{PS} - \rho_{sol})$ where v_{PS} is the volume of the PS core block, ρ_{PS} and ρ_{sol} are the scattering length density of the PS core block and solvent, respectively. $A_{core}(q)$ is the form factor amplitude for hard-sphere cores expressed by eqn 2.17 and eqn 2.18, where σ_{int} is the thickness of the core/corona interface.

$$A_{core}^2(q) = \Phi^2(qR_{core}) \exp(-q^2 \sigma_{int}^2) \quad (2.17)$$

$$\Phi(qR_{core}) = \frac{3[\sin(qR_{core}) - (qR_{core})\cos(qR_{core})]}{(qR_{core})^3} \quad (2.18)$$

The second term in eqn 2.15 is the self-correlation of the corona chains, which are assumed to be Gaussian coils. β_{corona} is the contrast between the core block and solvent defined in a similar way to the core block $\beta_{corona} = v_{PEP}(\rho_{PEP} - \rho_{sol})$. $P_{chain}(q)$ is the form factor of a corona chain described by the Debye function shown by eqn 2.19, where R_g is the radius of gyration of a corona chain within the micelle.

$$P_{chain}(q) = \frac{2[\exp(-q^2 R_g^2) - 1 + q^2 R_g^2]}{(q^2 R_g^2)^2} \quad (2.19)$$

The third term in eqn 2.15 represents the cross term between the spherical cores and the corona chains, while the fourth term is the cross term for different corona chains. $A_{\text{corona}}(q)$ appearing in both terms is the form factor amplitude of corona chains given by eqn 2.20.

$$A_{corona}(q) = \frac{4\pi \int \phi_{corona}(r) \frac{\sin(qr)}{qr} r^2 \, dr}{4\pi \int \phi_{corona}(r) r^2 \, dr} \exp(-q^2 \sigma_{\text{int}}^2 / 2) \tag{2.20}$$

$$\phi_{corona}(r) = \frac{\phi_1(r) + a\phi_2(r)}{1 + a} \tag{2.21}$$

Here, $\phi_{\text{corona}}(r)$ is the density distribution function of the corona chains. It can be expressed as a linear combination of two spline density functions $\phi_1(r)$ and $\phi_2(r)$ as shown in eqn 2.21,[11] where r is the radial distance from the center of the core, and a is an adjustable parameter ($-1 < a < 1$).

The hard sphere model quantitatively accounts for the SAXS patterns in Figure 2.7 as well as small-angle neutron scattering (SANS) data, and thus provides rich structural information for the micelles, including N_{agg}, R_{hs}, R_{core}, and σ_{Rc}.

2.7 Small-Angle Neutron Scattering (SANS) and time-resolved SANS (TR-SANS)

SANS is also able to cover a wide range of q values to probe detailed information of micelle systems. Compared to synchrotron X-rays, the neutron flux, however, is many orders of magnitude lower. Therefore, longer exposure times are required in SANS experiments, typically several minutes to hours. The spread in wavelengths ($\Delta\lambda/\lambda > 0.1$) is relatively large for neutrons, causing some smearing of features including Bragg peaks and maxima and minima of the hard sphere form factor. Neutron scattering contrast comes from the scattering length density difference between different components of the

micelle system, which can be tuned appreciably by deuterium labeling. Table 2.2 lists the scattering length densities (ρ) of hydrogenated and deuterated PS core block repeat units, the PEP corona repeat unit, and solvents including 1-phenyldodecane and squalane. We take advantage of the contrast matching technique to isolate and probe a particular component via selective labeling of individual polymer blocks and the solvent.

Table 2.2 The Scattering Length Densities of Polymers and Solvents

Chemical formula	b (10^{-12} cm)	v (10^{-22} cm^3)	ρ (10^{10} cm^{-2})
PS, C_8H_8	2.33	1.65	1.41
dPS, C_8D_8	10.66	1.65	6.46
PEP, $C_5D_{2.3}H_{7.7}$	1.98	1.36	1.46
squalane, $C_{30}H_{62}$	–3.24	8.65	–0.374
d-squalane, $C_{30}D_{62}$	61.30	8.65	7.08
1-phendodecane, $C_{18}H_{30}$	0.75	4.78	0.157
d-(1-phendodecane), $C_{18}D_{30}$	31.98	4.78	6.69

Here b is the coherent scattering length, v is the volume of the repeat unit, and $\rho = b/v$ is the scattering length density

Time-resolved SANS (TR-SANS) was performed to probe the micelle chain exchange kinetics. The experiments were conducted at the NG-7 30 m beam line at the Center for Neutron Research at the National Institute of Standards and Technology (NIST). A wavelength of λ = 6 Å and sample-to-detector distance 4.7 m were selected to achieve a q range of 0.008 – 0.08 Å^{-1}. As shown in Figure 2.8a, this q range captures the form factor of the micelle cores. A relatively wider wavelength width $\Delta\lambda/\lambda$ = 0.22 was chosen to increase the neutron flux, and thus to reduce the acquisition time. TR-SANS experiments were also performed at the CG-2 SANS beam line in the High Flux Isotope Reactor (HFIR), Oak Ridge National Laboratory. We used a wavelength of 4.75 Å with spread of $\Delta\lambda/\lambda$ = 0.13 and sample-to-detector distance 10 m to give an accessible q range

of 0.007 – 0.1 $Å^{-1}$. Micelle solutions were loaded into 1 mm quartz banjo cells, and fixed in a sample block for heating and cooling. Each scattering measurement takes 5 minutes, which is a compromise between obtaining a timely response versus accruing acceptable counting statistics. Sample transmission measurements take 3 minutes.

Kinetic experiments successively recorded the change of scattering intensity with time, which results from the chain exchange between micelles. To be quantitative, the evolution of excess scattering intensity is proportional to the change of contrast between the micelle cores and solvent: $I(t) - I(\infty) \sim (\rho_{core}(t) - \rho_{solvent})^2$, where I(t) is the instantaneous intensity at time t, and $I(\infty)$ is the intensity at infinite time (i.e., completely exchanged state), and ρ_{core} and $\rho_{solvent}$ are the scattering length density of the core block and solvent, respectively. We take the TR-SANS experiment of the 1 vol% hSEP 28-118/dSEP 25-95 micelle system to explain how the experiment works.[12] In this experiment, two types of 1 vol% micelles solutions were separately prepared using the co-solvent method: 1 vol% protonated micelles formed by hSEP 28-118 polymers and 1 vol% deuterated micelles formed by dSEP 25-95 polymers. A "postmixed" specimen was prepared by blending 50% by volume protonated and 50% deuterated micelles at room temperature. In this case, protonated and deuterated cores remain unmixed due to the glassy PS cores at room temperature. The scattering length density of the postmixed cores corresponds to $\rho_{postmixed} = \rho_{core}(t=0)$. A "premixed" specimen also was prepared by forming micelles from molecularly mixed 50/50 by volume of hSEP 28-118 and dSEP 25-95 polymers, so that every premixed core contains mixed PS and dPS chains. This represents the complete mixed state, where $\rho_{premixed} = \rho_{core}(t=\infty) = (\rho_{hPS}+\rho_{dPS})/2 = 3.93 \times 10^{10}$ cm^{-2}. Moreover, the scattering length density of the solvent is matched with the premixed cores, so that $\rho_{solvent} = \rho_{core}(t=\infty) = (\rho_{hPS}+\rho_{dPS})/2$. This is achieved by mixing the isotopic solvents, $\rho_{solvent} = f_{h\text{-}sol}\,\rho_{h\text{-}sol} + (1- f_{h\text{-}sol})\rho_{d\text{-}sol}$, where $f_{h\text{-}sol}$ is the volume fraction of protonated solvent in the solvent mixture. Using the values in Table 2.2, an

isotopic solvent mixture of 42 vol% h-squalane and 58 vol% d-squalane, i.e., $f_{\text{h-squalane}} = 0.42$, is used to match the scattering length density of a completely mixed core.

Thus, at $t = 0$, the excess scattering intensity is maximized due to the largest contrast between the unmixed cores and solvent, $I(0) - I(\infty) \sim [(\rho_{PS} - \rho_{solvent})^2 + (\rho_{dPS} - \rho_{solvent})^2]/2 \sim (\rho_{dPS} - \rho_{hPS})^2/4$. Here, the first term $(\rho_{PS} - \rho_{solvent})^2$ represents the contrast from protonated cores while the second term $(\rho_{dPS} - \rho_{solvent})^2$ is from deuterated cores. This is evidenced by the highest scattering intensity of the postmixed specimen, the red curve in Figure 2.8a. When the sample was heated to the target temperature, e.g., T = 97 ºC, polymer chains exchanged between micelles, resulting in $I(t) - I(\infty) \sim [((1-x)\rho_{hPS} + x\rho_{dPS}) - \rho_{solvent}]^2/2 + [(x\rho_{hPS} + (1-x)\rho_{dPS}) - \rho_{solvent}]^2/2 \sim (1/2-x)^2(\rho_{dPS} - \rho_{hPS})^2$, where x is the volume fraction of effectively exchanged chains into another type of cores, $0 < x < 1/2$. As shown in Figure 2.8a, the scattering intensity decreases with increasing x, since more chains exchanged. At $t = \infty$, protonated and deuterated chains would be completely mixed, i.e., $x = 1/2$. This situation is obtained with the premixed specimen since in practice an experiment cannot be run to infinite time. There is no excess scattering from premixed cores because of the matched contrast, i.e., $[(\rho_{hPS} + \rho_{dPS})/2 - \rho_{solvent}]^2 = 0$. The scattering intensity of the premixed specimen (blue curve in Figure 2.8a) is almost identical with the solvent background (black curve) except for the weak scattering from the micelle coronas in the low q region ($q < 0.01$ Å^{-1}). This is because the contrast of the corona blocks is not perfectly matched with the solvent in this experiment, although reduced by partial deuteration of the PEP blocks.

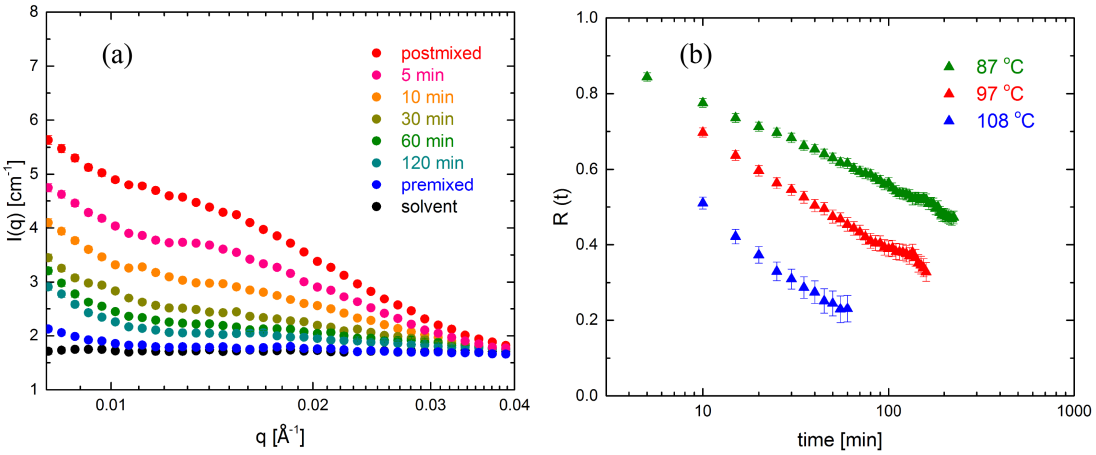

Figure 2.8 (a) Representative TR-SANS intensity evolution traces at T = 97 ºC, and (b) R(t) traces of 1 vol% SEP 28-118/dSEP 25-95 micelle system at different temperatures. This figure is reproduced from reference 11.

To quantitatively determine the rate of chain exchange, a normalized relaxation function $R(t)$ is defined as,

$$R(t) = \sqrt{\frac{I(t) - I(\infty)}{I(0) - I(\infty)}} \tag{2.22}$$

Here, all of $I(0)$, $I(t)$, $I(\infty)$ are integrated over a q range of 0.01 – 0.04 Å^{-1} for good statistics. As discussed above, $R(t)$ is proportional to the fraction of exchanged chains. Figure 2.8b shows that $R(t)$ decreases with time due to the reduced contrast between micelle cores and solvent. The decay of $R(t)$ directly reflects the rate of chain exchange, which increases at higher temperatures, indicating faster chain exchange kinetics. We also note that the error-bars in Figure 2.8b become larger at higher temperatures and longer times, i.e., at 108 ºC. The error $\delta R(t)$ is propagated as

$$\delta R(t) = \sqrt{\left[\frac{\partial R(t)}{\partial I(t)} \cdot \delta I(t)\right]^2 + \left[\frac{\partial R(t)}{\partial I(\infty)} \cdot \delta I(\infty)\right]^2 + \left[\frac{\partial R(t)}{\partial I(0)} \cdot \delta I(0)\right]^2} \qquad (2.23)$$

where $\delta I(t)$, $\delta I(\infty)$, and $\delta I(0)$ are errors in $I(t)$, $I(\infty)$, and $I(0)$, respectively. The errors in the intensities are averaged over a q range of 0.01 – 0.04 $Å^{-1}$. At higher temperatures and longer times, value of $R(t)$ get close to 0 by eqn 2.22, and therefore, the propagated error $\delta R(t)$ becomes larger. Due to this large uncertainty, the data with $R(t) < 0.1$ were not used for quantitative analysis.

2.8 References

[1] Choi, S.; Bates, F. S.; Lodge, T. P. Structure of Poly(styrene-*b*-ethylene-*alt*-propylene) Diblock Copolymer Micelles in Squalane. *J. Phys. Chem. B* **2009**, *113*, 13840–13848.

[2] Lu, J.; Bates, F. S.; Lodge, T. P. Remarkable Effect of Molecular Architecture on Chain Exchange in Triblock Copolymer Micelles. *Macromolecules* **2015**, *48*, 2667−2676.

[3] Peters, A. J.; Lodge, T. P. Comparison of Gel Relaxation Times and End-Block Pullout Times in ABA Triblock Copolymer Networks. *Macromolecules* **2016**, *49*, 7340–7349.

[4] Zimm, B. H. The Scattering of Light and the Radial Distribution Function of High Polymer Solutions. *J. Chem. Phys.* **1948**, *16*, 1093–1099.

[5] Jakeš, J. Regularized Positive Exponential Sum (REPES) Program – A way of Inverting Laplace Transform Data Obtained by Dynamic Light Scattering. *Collect. Czech. Chem. Commun.* **1995**, *60*, 1781−1797.

[6] Pedersen, J. S.; Gerstenberg, M. C. Scattering Form Factor of Block Copolymer Micelles. *Macromolecules* **1996**, *29*, 1363–1365.

[7] Pedersen, J. S.; Hamley, I. W.; Ryu, C. Y.; Lodge, T. P. Contrast Variation Small-Angle Neutron Scattering Study of the Structure of Block Copolymer Micelles in a Slightly Selective Solvent at Semidilute Concentrations. *Macromolecules* **2000**, *33*, 542–550.

[8] Pedersen, J. S. Structure Factors Effects in Small-Angle Scattering from Block Copolymer Micelles and Star Polymers. *J. Chem. Phys.* **2001**, *114*, 2839–2846.

[9] Pedersen, J. S.; Svaneborg, C. Scattering from Block Copolymer Micelles. *Curr. Opin. Colloid Interface Sci.* **2002**, *7*, 158–166.

[10] Pedersen, J. S.; Svaneborg, C.; Almdal, K.; Hamley, I. W.; Young, R. N. A Small-Angle Neutron and X-ray Contrast Variation Scattering Study of the Structure of Block Copolymer Micelles: Corona Shape and Excluded Volume Interactions. *Macromolecules* **2003**, *36*, 416–433.

[11] Bang, J.; Viswanathan, K.; Lodge, T. P.; Park, M. J.; Char, K. Temperature-Dependent Micellar Structures in Poly(styrene-*b*-isoprene) Diblock Copolymer Solutions near the Critical Micelle Temperature. *J. Chem. Phys.* **2004**, *121*, 11489–11500.

[12] Wang, E.; Lu, J.; Bates, F. S.; Lodge, T. P. Effect of Corona Block Length on the Structure and Chain Exchange Kinetics of Block Copolymer Micelles. *Macromolecules* **2018**, *51*, 3563–3571.

Chapter III.
Effect of Corona Block Length on the Structure and Chain Exchange Kinetics of Block Copolymer Micelles

Adapted with permission from

Wang, E.; Lu, J.; Bates, F. S.; Lodge, T. P. *Macromolecules* **2018**, *51*, 3563–3571.

3.1 Introduction

Block copolymers can self-assemble into micelles in selective solvents. These nanostructures enable a variety of important applications, including drug delivery,[1,2] ion gels,[3,4] viscosity modifiers,[5] and toughening of plastics.[6,7] Regardless of the application, molecular chain exchange plays a vital role in establishing the thermodynamic equilibrium state. However, compared to extensive studies[8,9] on thermodynamic properties, relatively little is known about the factors governing the chain exchange kinetics in block copolymer micelles, and particularly the dependence on corona block length (N_{corona}).

Halperin and Alexander[10] described the kinetics of block copolymer micelles near equilibrium, considering the roles of both the core and corona blocks. Their theory predicts the exchange process to follow an exponential time dependence with a characteristic relaxation time (τ), and in the limiting case of hairy micelles (*i.e.*, $N_{corona} >> N_{core}$), τ is expected to depend on both core block length and corona block lengths as:

$$\tau \sim N_{core}^{22/25} N_{corona}^{9/5} \exp(E_a / kT) \tag{3.1}$$

where E_a is an activation energy given by $\gamma N_{core}^{2/3} a^2$, where γ is the interfacial tension between the core block and the solvent, and a is the size of one core block repeat unit.

Recently, the mechanisms of chain exchange kinetics have been explored via time-resolved small-angle neutron scattering (TR-SANS) experiments[11-24] and dissipative particle dynamics (DPD) simulations.[25-29] Lund, Willner, Richter and coworkers[11,12] pioneered TR-SANS investigation for poly(ethylene-*alt*-propylene)-*b*-poly(ethylene oxide) (PEP-PEO) block copolymer micelles in water/DMF mixtures, and showed an apparently logarithmic time dependence of the chain exchange process. Later, Choi, Lodge, and Bates[13] attributed this logarithmic time dependence to the dispersity of core block length, based on TR-SANS results of dilute poly(styrene)-*b*-poly(ethylene-*alt*-propylene) (SEP) diblock copolymer micelles in squalane, a selective solvent for PEP. A theoretical model (eqn 3.3) was established to account for the dramatic influence of the core block length and its dispersity on chain exchange kinetics. However, this model does not address the effect of the corona block length. Although the role of the corona block is generally assumed to be less important than the core block, some experimental observations imply a significant role for the corona block in the chain exchange process, because the rate of chain exchange decreases in concentrated micelle solutions[14] and upon adding corona homopolymer chains,[15] while it increases in triblock micelles with one additional corona block compared to the diblock analog.[16] It was hypothesized that the exchange kinetics were accelerated by the relief of corona chain stretching upon chain expulsion.[16]

Dissipative particle dynamics (DPD) simulations by Li and Dormidontova[26] showed an acceleration of the chain exchange kinetics when increasing corona block length at constant core block length, which was attributed to a higher solubility and higher critical micelle concentration (CMC). However, Zinn *et al*.[30] found the kinetics to slow down as corona block length increased in the C_{27}-PEO_n/H_2O (n = number of repeat units of EO)

system. They attributed this slowing down to restricted chain diffusion through a thicker corona layer, as predicted by Halperin and Alexander for hairy micelles.[10]

These seemingly contradictory results motivate the current work to elucidate the role of corona block in micelle structure and chain exchange kinetics, as illustrated in Figure 3.1. We vary the corona block length by a factor of 8 ($<N_{corona}>$ = 256 – 2080) while keeping the core block length constant ($<N_{core}>$ ≈ 255). These systematic experimental results are used to generate an improved model that explicitly includes a corona term. With this improved model, we further discuss the unexplained but interesting observations in previous work associated with the role of the corona blocks.

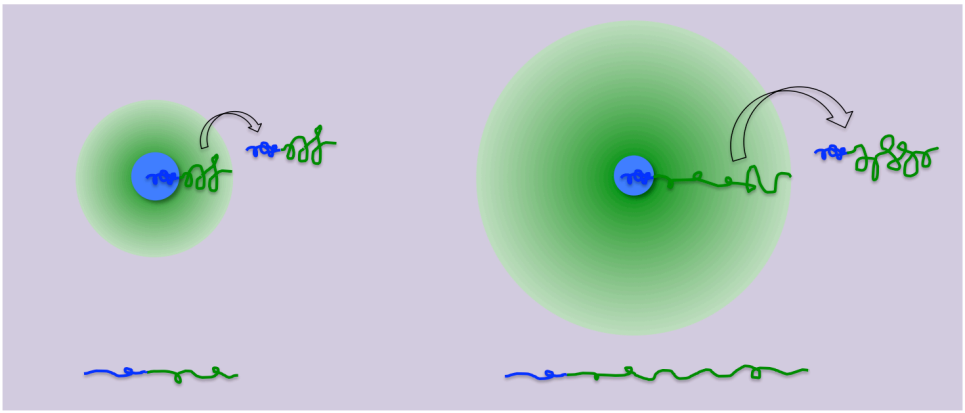

Figure 3.1 Schematic illustration of structure and chain exchange of micelles formed by block copolymers with shorter corona block (left) and with longer corona block (right) respectively, while the core block length is held constant.

3.2 Materials

A series of SEP diblock copolymers were prepared by anionic polymerization of polystyrene-*b*-1,4-polyisoprene, followed by selective saturation of the polyisoprene block using a Ni/Al catalyst under 400 psi deuterium D_2. The repeat unit of PEP is $C_5D_{2.3}H_{7.7}$, where $D_{2.3}$ is a consequence of D_2 saturation and a small extent of H/D exchange. Likewise, selectively deuterated equivalent polymers (dSEP) were synthesized using perdeuterated styrene (Polymer Source, Inc.) and protonated isoprene monomers.

Size exclusion chromatography using a refractive index detector (SEC-RI), and another SEC instrument equipped with RI and a light scattering detector (SEC-LS), and ^{1}H nuclear magnetic resonance spectroscopy (^{1}H NMR) were performed to determine the molecular weight and molecular weight distribution of SEP and dSEP diblock copolymers. Table 3.1 summarizes the characteristics of the SEP and dSEP polymers that were used in this work. The nomenclature of each SEP diblock copolymer refers to the block molecular weights: *e.g.*, SEP 25-19 indicates $M_n \approx 25$ kg/mol and 19 kg/mol for PS and PEP, respectively. All diblocks have almost identical PS blocks (26 kg/mol to within 10%), but PEP blocks varying by a factor of 8, from 256 repeat units to 2080. SEC traces of all SEP polymers are shown in Figure 3.2. Squalane ($C_{30}H_{62}$, Sigma-Aldrich), equivalent to 6 repeat units of EP, was used as a selective solvent for the PEP blocks.

Table 3.1 Characteristics of Diblock Copolymers

Polymers	$M_{n,\,PS}$ [a] (kg/mol)	$M_{n,\,PEP}$ [b] (kg/mol)	M_w/M_n [a]
SEP 25-19	25	19	1.03
SEP 28-40	28	40	1.05
dSEP 30-41	30	41	1.07
SEP 26-70[c]	26	70	1.04
dSEP 29-71[c]	29	71	1.10
SEP 28-118	28	118	1.08
dSEP 25-95	25	95	1.06
SEP 26-151	26	151	1.09
dSEP 25-137	25	137	1.09
SEP 42-64[c]	42	64	1.05
dSEP 47-67[c]	47	67	1.10

[a] Determined by SEC-RI with PS standards and SEC-LS
[b] Determined by ^{1}H-NMR spectroscopy and confirmed by SEC-LS
[c] Reproduced from reference 31

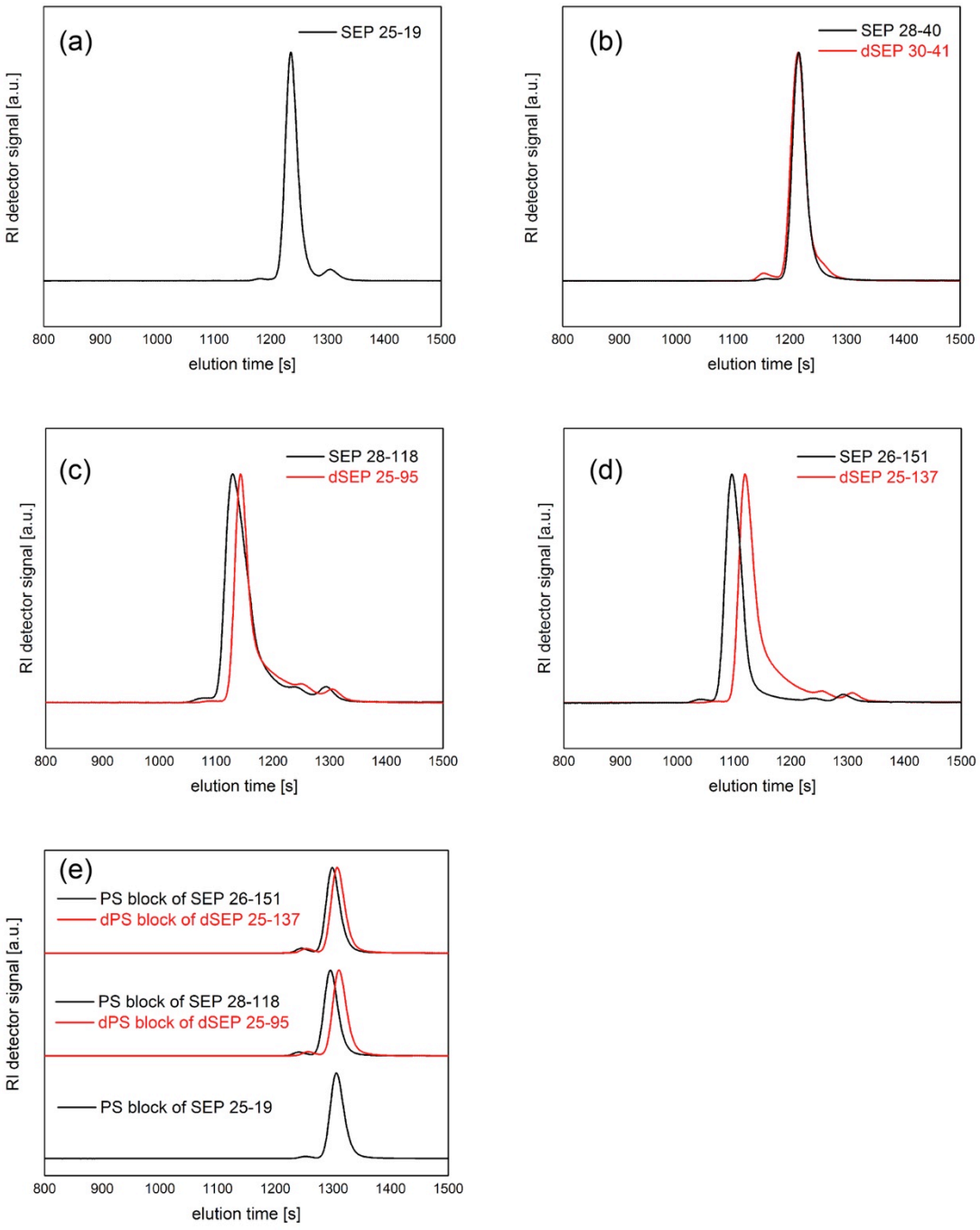

Figure 3.2 SEC traces of (a) SEP 25-19, (b) SEP 28-40 and dSEP 30-41, (c) SEP 28-118 and dSEP 25-95, (d) SEP 26-151 and dSEP 25-137 diblock copolymers, and (e) PS and dPS blocks of these SEP diblock copolymers.

3.3 Results and Discussion

3.3.1 Micelle Structure

The equilibrium structure of a micelle is determined by balancing the enthalpic gain of minimizing the interfacial contact between the core block and the corona/solvent environment, and the conformational entropic loss of polymer chains when confined into micelles. Table 3.2 summarizes the structural dimensions of dilute SEP diblock copolymer micelles: the core radius (R_{core}), standard deviation of the core radius (σ_{Rc}), aggregation number (N_{agg}), hydrodynamic radius (R_h), dispersity of the hydrodynamic radius (μ_2/Γ^2) and corona layer thickness (L_{corona}). The temperature dependence of these micelle structures is very weak when the temperature is far below the critical micelle temperature (CMT), which is above 150 ºC for these micelles. As shown in Figure 3.5, features of micelle structure in SAXS patterns do not show any appreciable change upon heating up to 120 ºC and cooling. Therefore, the values listed in Table 3.2 are valid over a wide temperature range, although they were determined at room temperature.

Table 3.2. Structure Dimensions of Dilute SEP Diblock Copolymer Micelles[a]

Micelles	R_{core}[b] (nm)	σ_{Rc}[b] (nm)	N_{agg}[c]	R_h[d] (nm)	μ_2/Γ^2[d]	L_{corona}[e] (nm)
SEP 25-19	11.2	0.8	147	30	0.10	19
SEP 28-40	10.1	0.7	96	33	0.09	23
SEP 26-70	9.0	0.4	74	43	0.08	34
SEP 28-118	8.8	0.7	64	56	0.11	47
SEP 26-151	8.4	0.5	60	66	0.12	58

[a] Measurements were made at room temperature and multiple high temperatures
[b] Determined by SAXS using BCP micelle model fit
[c] $N_{agg} = 4\pi R_{core}^3 / 3v_{core}$, where v_{core} is the volume of a core block
[d] Determined by DLS using 2nd order cumulant method
[e] $L_{corona} = R_h - R_{core}$

The mean micelle hydrodynamic radius (R_h) was determined by DLS using a 2nd order cumulant fit and the REPES Laplace inversion method. The values of R_h interpreted from the two methods agree well. For 0.25 vol% SEP 28-118 micelles, the 2nd cumulant fit gives a mean R_h = 56 nm with μ_2/Γ^2 = 0.11. The R_h distribution obtained by REPES shows a monomodal, narrow distribution with a peak value of $R_h \approx$ 60 nm, as shown in Figure 3.3. The R_h of SEP diblock micelles increases with increasing corona block length. This result is qualitatively expected by the scaling model[8,33,42] for hairy micelles, where the overall micelle radius is predicted to be proportional to $N_{corona}^{3/5}$.

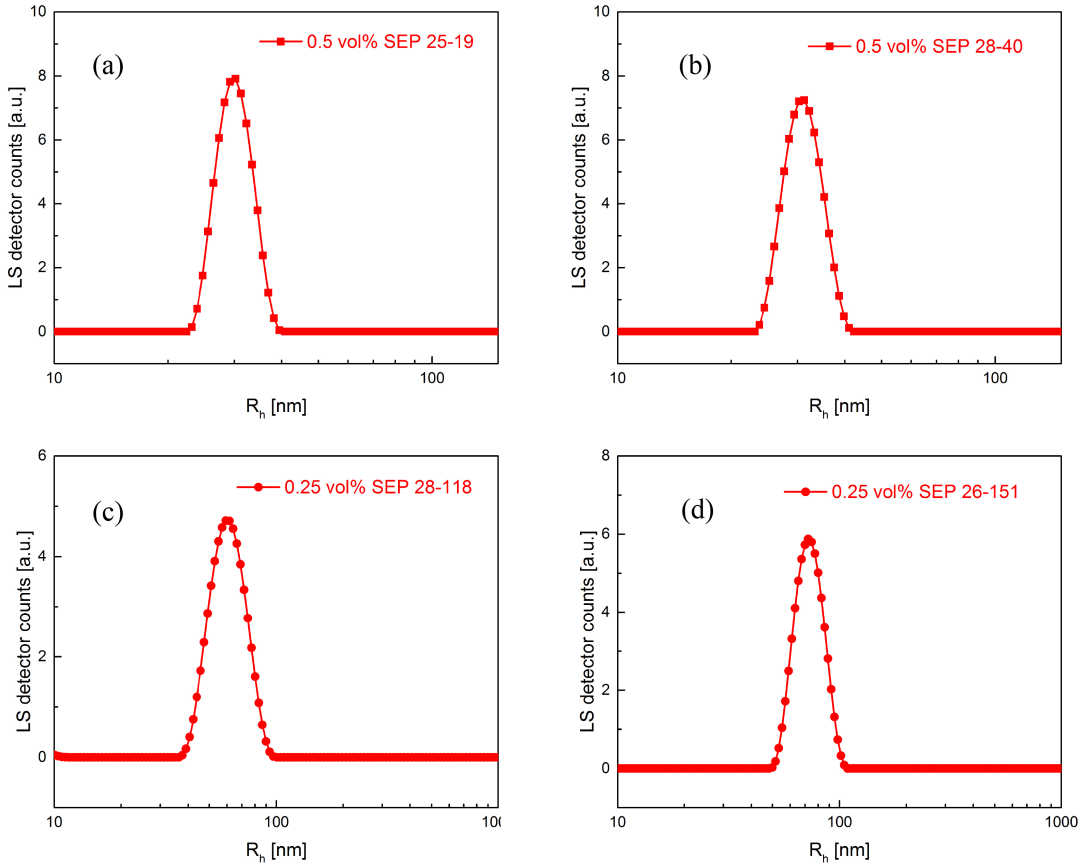

Figure 3.3 R_h distribution of (a) 0.5 vol% SEP 25-19, (b) 0.5 vol% SEP 28-40, (c) 0.25 vol% SEP 28-118 and (d) 0.25 vol% SEP 26-151 dilute micelle solutions.

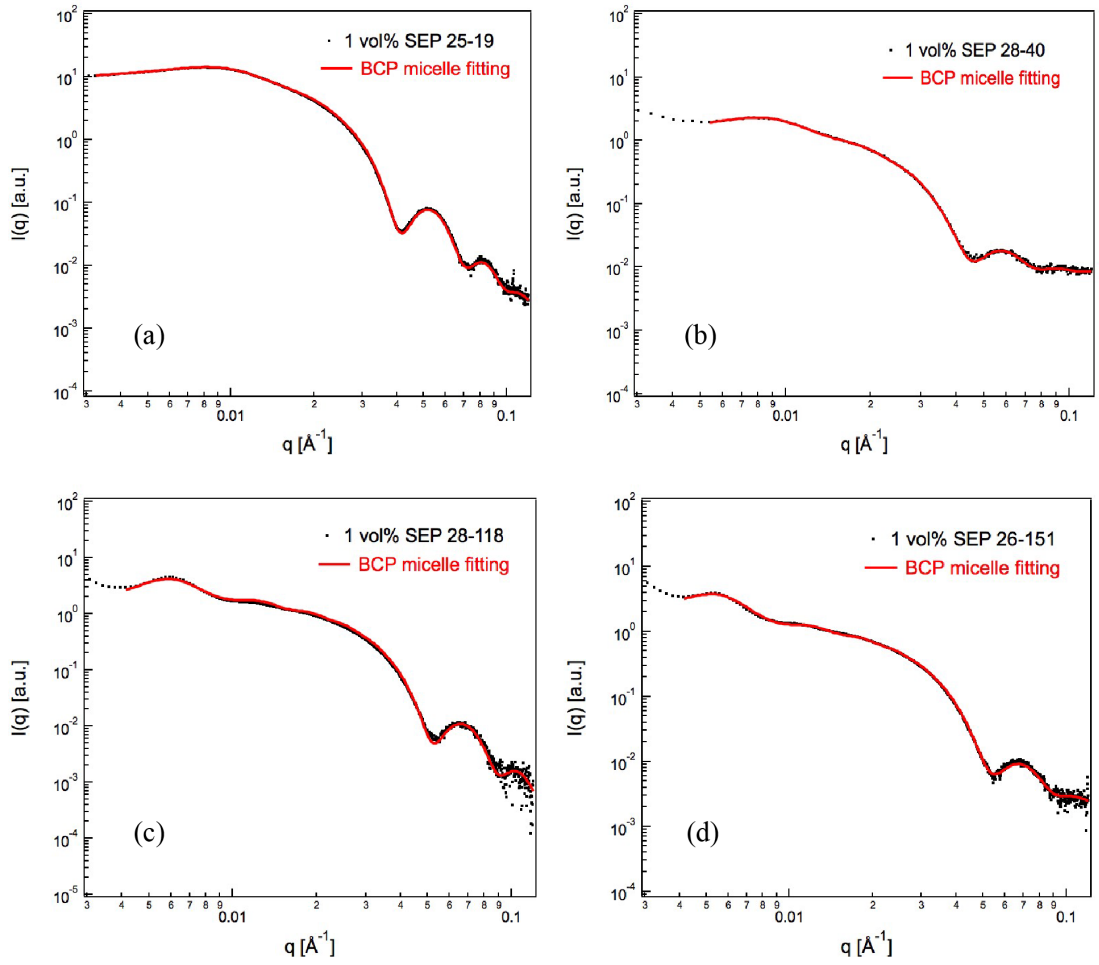

Figure 3.4 SAXS patterns of 1 vol% (a) SEP 25-19, (b) SEP 28-40, (c) SEP 28-118 and SEP 26-151 dilute micelle solutions with BCP micelle fittings. Measurements were made at room temperature.

As changes in R_h can reflect contributions from changes in both R_{core} and L_{corona}, more detailed SAXS analysis is used to decouple the effects of corona block length on core radius and corona layer thickness. Figure 3.4 displays the SAXS patterns of dilute SEP diblock micelle solutions after background subtraction. Each scattering pattern shows a distinct micelle form factor at high q, and a small bump in the structure factor at low q due to micelle-micelle interactions. For the 1 vol% SEP 28-118 micelles in Figure 3.4c,

the first minimum appears at q = 0.05 Å^{-1}, corresponding to R_{core} = 8.9 nm by applying the characteristic equation for the minima in the hard sphere form factor (qR_{core} = 4.49). This estimated value agrees well with the fitting results, R_{core} = 8.8 nm, as listed in Table 3.2. In each SAXS pattern, the red line represents the best fit to the data (ignoring the very low q region, ≤ 0.003 Å^{-1}) using the hard sphere model for BCP micelles as described in the Chapter II Experimental Section. The model also provides detailed information about micelle structure, such as standard deviation of the core radius σ_{Rc}.

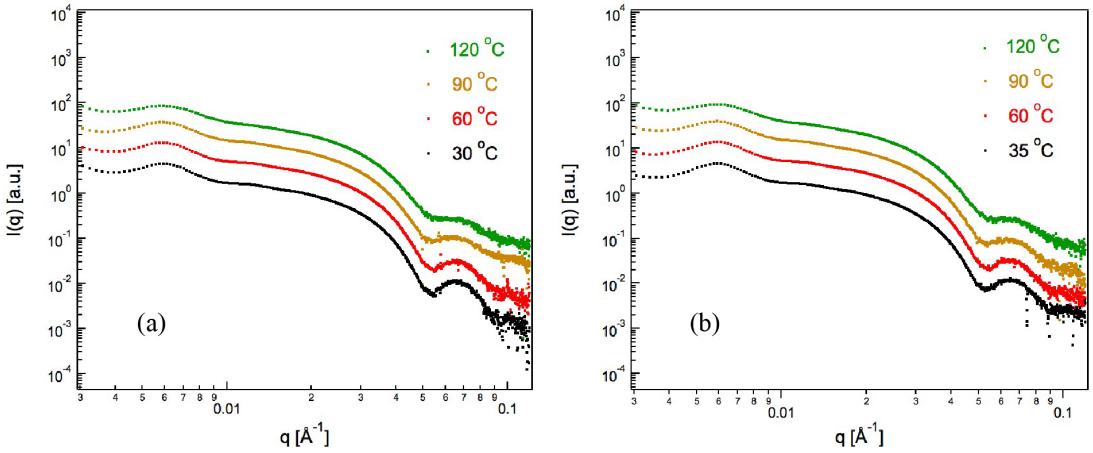

Figure 3.5 Temperature dependence of SAXS patterns of 1 vol% SEP 28-118 micelle solution upon (a) heating and (b) cooling.

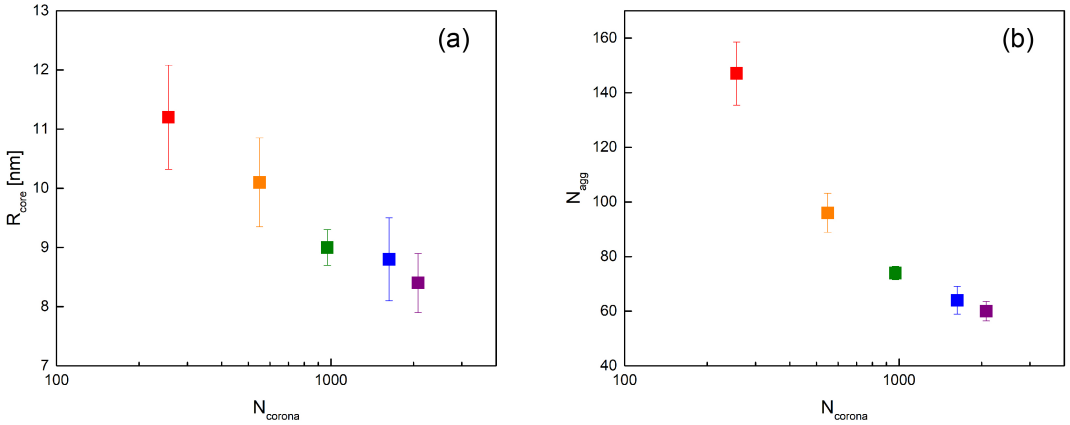

Figure 3.6 (a) Core radii and (b) aggregation numbers of dilute SEP block copolymer micelles in the sequence of increasing corona block length from left to right.

Qualitatively, the shift of the first minimum in the form factor to higher q indicates a smaller R_{core} as the corona block length increases. Figure 3.6a shows R_{core} decreasing with increasing N_{corona} for five SEP diblock micelles. Interestingly, R_{core} shows a relatively strong dependence on N_{corona} for SEP 25-19, SEP 28-40 and SEP 26-70, but no appreciable change for SEP with longer corona blocks (SEP 28-118 and SEP 26-151). With the assumption of a dry micelle core at room temperature, the micelle aggregation number (N_{agg}) can be calculated as $N_{agg} = 4\pi R_{core}^3 / 3v_{core}$, where v_{core} is the volume of a core block. Bang *et al*.[34] determined that almost no solvent penetrated into the core of a PS-PI (PS block 18 kg/mol) in tetradecane below 40 °C, below the glass transition temperature (T_g) of the PS block, which is approximately 70 °C.[35] As shown in Figure 3.5, the first minimum of the hard-sphere form factor, associated with the core size R_c, remained constant between 30 ºC and 120 ºC, consistent with the assumption that the micelle core contains little solvent over the range of temperatures associated with the TR-SANS experiments (as will be discussed later). Figure 3.6b shows N_{agg} decreasing with increasing N_{corona} for five SEP diblock micelles. This effect can be attributed to the higher solubility (higher CMC) of a diblock copolymer with a longer corona block. Therefore, there is a weaker tendency to aggregate into micelles in terms of the free energy. The CMC for SEP in squalane is difficult to measure accurately. Mok et al.[43] reported an increase of 1.5 times in the CMC (from 0.12 vol% to 0.18 vol%) when the PEO corona block length was increased by a factor of 2.6 (from 5 kg/mol to 13 kg/mol) at constant PS core block molecular weight (20 kg/mol) in a PS-PEO / [EMI][TFSA] system. We expect the same trend for the SEP system based on the observed decrease in N_{agg}. Similarly, N_{agg} shows a relatively strong dependence on N_{corona} when the corona block length is moderate (SEP 25-19, SEP 28-40 and SEP 26-70), but does not show appreciable change when corona block is long (SEP 28-118 and SEP 26-151). The simulation study by Li and Dormidontova[26] also reported a significant decrease in the equilibrium micelle

aggregation number (N_{agg}) with increasing number of B beads (N_{corona}) in an A_4B_x system (A is core block and B is corona block, and x = 4, 6 and 8). N_{agg} showed a stronger dependence on corona block length for diblocks with smaller mismatch between N_{corona} and N_{core}. For the C_{27}-PEO_n/H_2O system,[30] N_{agg} decreases with increasing n in diblocks with short PEO blocks, but does not show any appreciable decrease when PEO length is extremely long ($n > 200$).

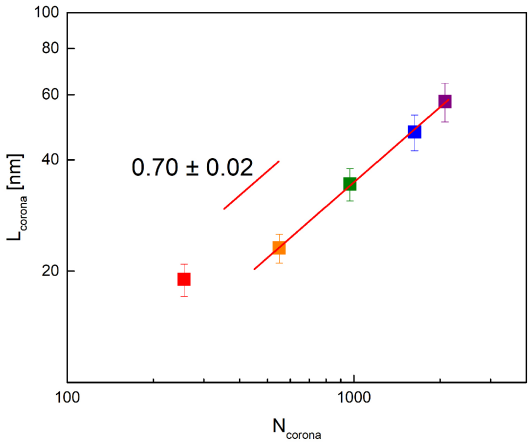

Figure 3.7 Relationship between the corona layer thickness and the corona block length.

A significant effect is observed on the corona layer thickness, L_{corona} (= $R_h - R_{core}$), with increasing corona block length, as shown in Figure 3.7. The red line in this figure shows a scaling exponent of 0.7 between L_{corona} and N_{corona} without including the data for SEP 25-19, because its corona block length does not satisfy the criterion for a hairy micelle ($N_{corona} >> N_{core}$). The fitting result qualitatively agrees with the scaling theory[8,33,42] which predicts an exponent of 0.6 for hairy micelles. The slightly higher scaling exponent indicates that the corona chains of the SEP micelles are stretched more than expected, as will be discussed subsequently.

3.3.2 Molecular Chain Exchange Kinetics

TR-SANS was conducted to probe the kinetics of molecular exchange. Figure 3.8a displays time-resolved neutron scattering patterns of the postmixed specimen (multiple colors) of 1 vol% hSEP 28-118/dSEP 25-95, the premixed specimen (blue) and the solvent (dark) at 97 ºC. The initial intensity (t = 0 min) is the highest because of the largest contrast between micelle cores and solvent. As micelles undergo chain exchange the intensity decreases over time due to the decrease of contrast. The intensity of the premixed micelle solution matches well with that of the solvent, and therefore accurately indicates a state of complete chain exchange.

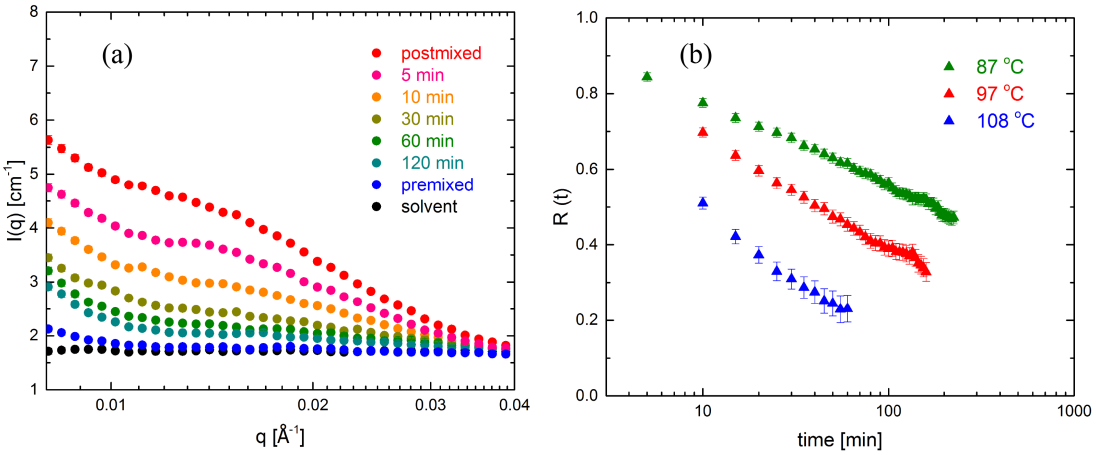

Figure 3.8 (a) Representative TR-SANS intensity evolution traces at T = 97 ºC, and (b) R(t) traces of 1 vol% SEP 28-118/dSEP 25-95 micelle system at different temperatures.

To quantify the rate of chain exchange, a normalized relaxation function, $R(t)$, is defined as

$$R(t) = \sqrt{\frac{I(t) - I(\infty)}{I(0) - I(\infty)}} \tag{3.2}$$

where $I(0)$ is the initial intensity, $I(t)$ is the instantaneous intensity at time t, and $I(\infty)$ is the intensity to infinite time, all of which are averaged over a q range of 0.01 – 0.04 $Å^{-1}$. Figure 3.8b shows $R(t)$ for 1 vol% SEP 28-118/dSEP 25-95 at 87 ºC, 97 ºC, and 108 ºC. $R(t)$ decays more rapidly at higher temperatures, indicating faster chain exchange kinetics.

As in all our previous work on this system, the time-temperature superposition (tTS) method is employed to construct a master curve of $R(t)$ with a reference temperature 125 ºC, as shown in Figure 3.9. The shift factors used in tTS method are shown in Figure 3.10. The rate of chain exchange increases with increasing corona block length but saturates for diblocks with relatively long corona blocks (SEP 28-118 and SEP 26-151). $R(t)$ of SEP 26-151 is more than two orders of magnitude faster than that of SEP 28-40, though its corona block is only four times longer. Therefore, the effect of corona block length is clearly significant for SEP diblock micelles, although it is a relatively minor factor compared to the core block length.

To quantify the effect of corona block length on kinetics, a theoretical model[13] is employed to describe $R(t)$ as

$$R(t) = \int P(N_{core}) \exp[-t \frac{6\pi^2 kT}{N_{core}^2 b^2 \zeta} \exp(-E_a / kT)] \mathrm{d}N_{core} \tag{3.3}$$

where N_{core} is the core block length, $P(N_{\mathrm{core}})$ is a Schulz-Zimm distribution function for disperse core blocks, ζ is the monomeric friction factor, b is the statistical segment length, and E_{a} is the activation energy for chain exchange. This model assumes the chain expulsion step to be rate-limiting in chain exchange, and depicts two consecutive

processes in the chain expulsion step: (*i*) motions of core blocks from buried core to the interface between micelle core and corona/solvent, which is governed by Rouse dynamics, *i.e.*, $\tau_1 \approx N_{core}^2 b^2 \zeta / 6\pi^2 kT$, and (*ii*) the expulsion of a polymer chain into corona/solvent by overcoming the activation energy (E_a/kT).

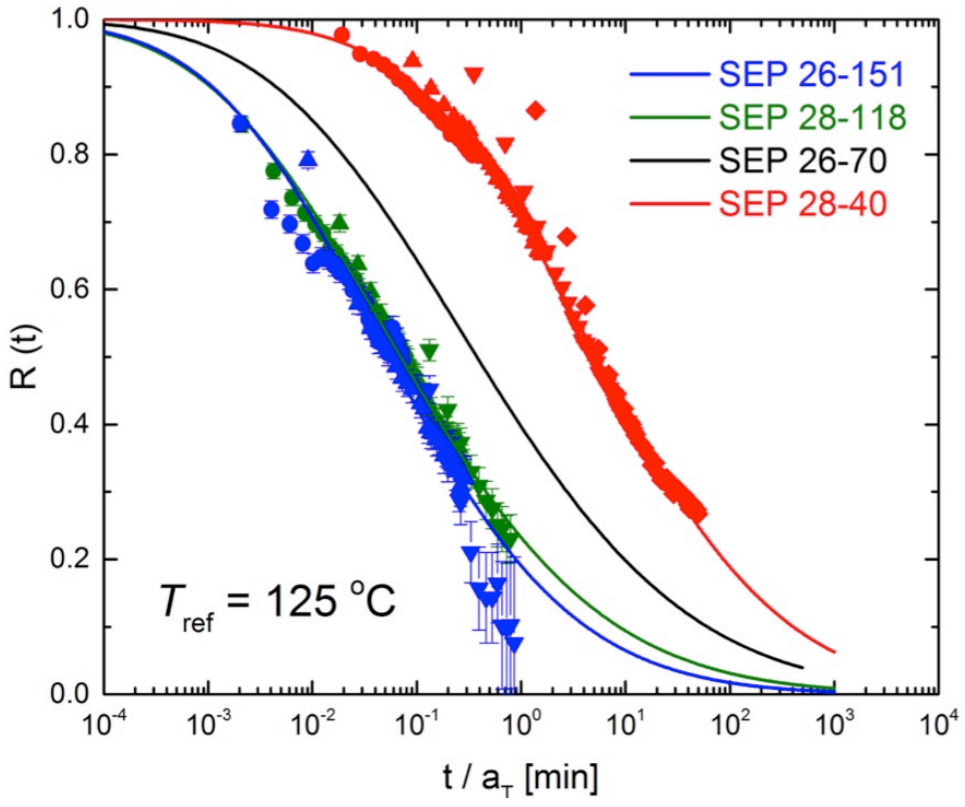

Figure 3.9 $R(t)$ master curves and theoretical model fits for 1 vol% SEP micelles with a reference temperature of 125 ºC (red for SEP 28-40, black for SEP 26-70, olive for SEP 28-118 and blue for SEP 26-151, and different symbols represent different temperatures). Original data of SEP 26-70 were published in reference 13, but not reproduced here.

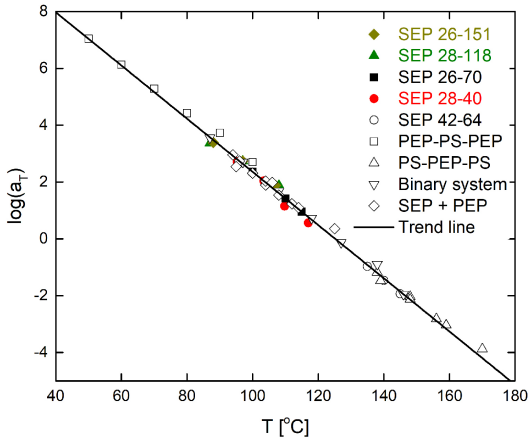

Figure 3.10 The shift factors $\log(a_T)$ and trend line as a function of temperature at a reference temperature of 125 ºC, together with the shift factors reported in our previous studies.

Table 3.3 Activation Energies for Chain Exchange in 1 Vol% Micelle Solutions

Micelle systems	$\langle N_{core} \rangle$	$\langle N_{corona} \rangle$	E_a / kT	s_{corona}
SEP 28-40 / dSEP 30-41	271	550	12.9	1.4_9
SEP 26-70 / dSEP 29-71	255	970	10.5	1.6_8
SEP 28-118 / dSEP 25-95	246	1470	8.8	1.8_0
SEP 26-151 / dSEP 25-137	237	1990	8.6	1.9_2
SEP 42-64 / dSEP 47-67	412	910	17.3	1.6_6

The solid lines in Figure 3.9 represent best fits to the data with two adjustable parameters, *i.e.*, dispersity of core block length (N_w/N_n) and activation energy (E_a/kT), by inputting the average core block length $\langle N_{core} \rangle$ of the micelle system considering a small mismatch in core block lengths between SEP and dSEP pairs. Table 3.3 shows the fitted values of activation energies of each micelle system. The E_a decreases by 4 kT (30% compared to that of SEP 28-40) when increasing average corona block length $\langle N_{corona} \rangle$

by only a factor of four. This result qualitatively differs from the C_{27}-PEO_n/H_2O system,[30] which showed an almost constant activation energy E_a (decreasing by 6% compared to that of shortest corona block) as the PEO block length increased by a factor of eight.

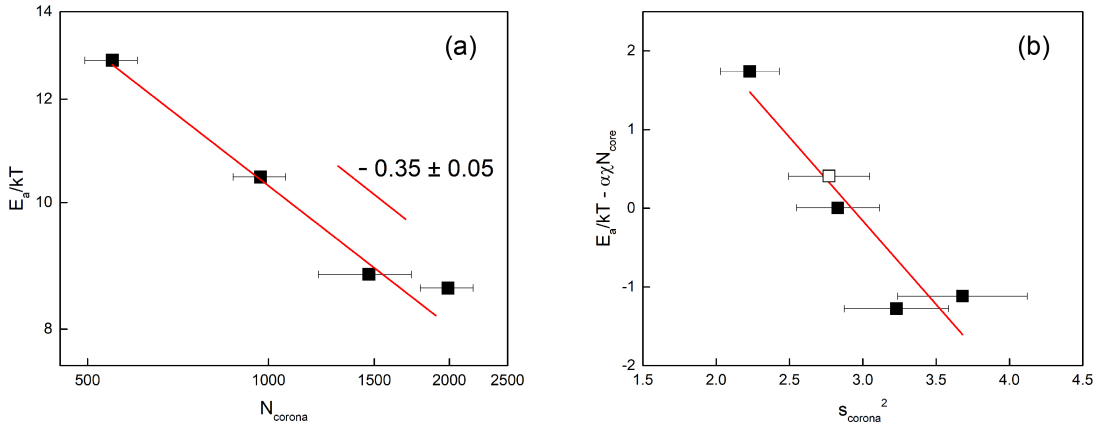

Figure 3.11 (a) Relationship between activation energy and corona block length, and (b) entropic gain arising from corona stretching relief in dilute SEP micelle systems. (The open square point represents SEP 42-64 / dSEP 47-67, which has a bigger N_{core} than the others).

Previous work[13] considered E_a/kT to reflect an enthalpic penalty associated with a diblock copolymer escaping a micelle, $\alpha\chi N_{core}$, where α is a constant and χ is the Flory-Huggins interaction parameter between the core block and solvent. This model did not address the effect of corona block length, although it successfully explained the effect of core block length and its dispersity on chain exchange kinetics in SEP diblock,[13,14] symmetric EPSEP and SEPS triblock[16] and poly(n-butyl methacrylate)-*b*-poly(methyl methacrylate) (PnBMA-PMMA) diblock micelles in ionic liquids.[36,37] Apparently, E_a/kT is not only a function of N_{core} but decreases with increasing N_{corona}, as shown in Figure 3.11a. The uncertainty of N_{corona} (approximately 10%) arises from a small mismatch between SEP and paired dSEP diblocks and the dispersity of the corona blocks. The scaling exponent of –0.35 indicates a relatively weak dependence on N_{corona} compared to

N_{core}, with perhaps an even weaker dependence for a SEP diblock system with longer corona blocks.

Recalling the slightly high scaling exponent between L_{corona} and N_{corona}, we note that chains are stretched in the micelle corona. Relief of corona chain stretching could reduce the activation energy for chain expulsion. Therefore, an entropy term associated with relief of corona chain stretching is added onto the total activation energy of chain exchange process. Assuming the corona chains follow Gaussian chain statistics,[38] E_a/kT can be expressed as

$$E_a / kT = \alpha\chi N_{core} - \frac{3}{2}\left(\frac{R_g^2}{R_{g,0}^2}\right)_{corona} = \alpha\chi N_{core} - \frac{3}{2}s_{corona}^2 \qquad (3.4)$$

where s_{corona} is the corona chain stretching parameter, $s_{corona} = R_g/R_{g,0}$, where R_g is the radius of gyration of corona chains in micelles and $R_{g,0}$ is the unperturbed value. R_g is estimated to be half of L_{corona} ($R_g = L_{corona}/2$) while $R_{g,0}$ is calculated for PEP with different molecular weights taking $R_{g,0} = 0.0392M^{1/2}$ (in nm) at 298 K,[39] where M is the PEP molecular weight. Figure 3.12 suggests that the excluded volume effect of PEP in squalane does not contribute significantly over the molecular weight range we investigated, based on the reported R_g values of syndiotactic-poly(propylene)-*b*-poly(ethylene-*alt*-propylene) (sPP-PEP) in decane.[41] As listed in Table 3.3, s_{corona} increases with increasing N_{corona} at fixed N_{core}, indicating that the corona chains of SEP micelles with longer corona blocks are more stretched than those with shorter blocks. We rationalize that at equilibrium the stronger stretching of the corona chains in SEP 26-151 micelle compensates for the larger interfacial energy per chain, which can be estimated as $\gamma(4\pi R_{core}^2)/N_{agg}$. Here, γ is the interfacial tension between the core block and the solvent,

and $4\pi R_{core}^2/N_{agg}$ approximates the area per chain, which increases from 13 nm^2 for SEP 28-40 to 15 nm^2 for SEP 26-151. Assuming the interfacial tension γ is roughly the same for all SEP micelles, the interfacial energy per chain of SEP 26-151 is 15% larger than SEP 28-40. During the chain exchange process, the entropic gain upon releasing a chain from SEP 26-151 micelles into solution, proportional to s_{corona}^2, is 65% more than SEP 28-40 micelles. We propose that this noticeable corona chain stretching plays a role in accelerating the chain exchange kinetics of SEP micelles. As shown in Figure 3.11b, E_a/kT of five SEP diblock micelle systems decreases with s_{corona}^2 following a linear trend within the uncertainty of the data E_a/kT and s_{corona} after the enthalpy term is subtracted (taking $\alpha\chi$ = 0.041 for each system as a constant[13]). More entropy is gained upon releasing a polymer chain from a micelle with larger extent of corona chain stretching, which ultimately accelerates the chain exchange kinetics.

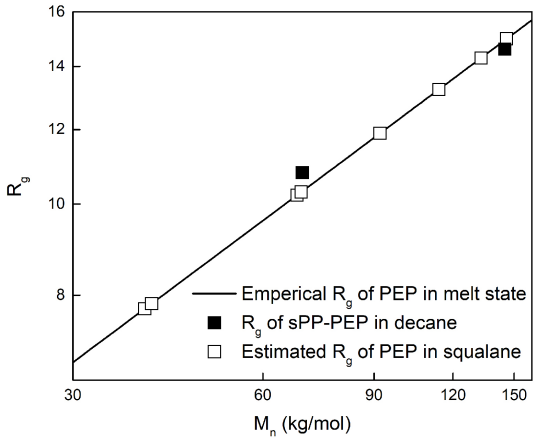

Figure 3.12 Radius of gyration of PEP in the melt, R_g of sPP-PEP in decane, and estimated R_g of PEP in squalane.

With this improved model incorporating a corona term, we are able to qualitatively explain the previous observations of a slowing down of chain exchange kinetics above

the overlap concentration of micelles[14] and upon adding corona homopolymer chains.[15] A crowded corona/solvent environment relieves the stretching of corona blocks in the micelle by screening excluded volume. Thus, less entropy benefit is gained when a polymer chain escapes from the micelle into the solution. The entropic gain argument can also be employed to discuss the results for triblock copolymer micelles. The chain exchange kinetics of 1 vol% PEP-PS-PEP (EPSEP 70-24-70)[16] is three orders of magnitude faster than that of 1 vol% SEP 26-70. The presence of one additional corona block in the triblock micelle leads to far more crowded corona environment than the diblock, when the aggregation number of triblock micelle (N_{agg} = 52) is slightly smaller than diblock (N_{agg} = 74). Dissipative particle dynamics simulations by Peters and Lodge[29] showed that B_1AB_2 triblocks exchange approximately one order of magnitude faster than AB diblocks, where A is the core block with the number of beads N_A = 6, B_1 and B_2 are two corona end-blocks of a triblock, and B is the corona block of a diblock with $N_{B1} + N_{B2} = N_B = 18$. This observation of accelerated chain exchange kinetics persists over various values of corona block asymmetries (N_{B1}/N_{B2}) and total corona length. One main cause is a higher density and stretching of corona blocks near the core surface in triblock micelles compared to diblock analogs. In such a scenario, the higher entropic gain upon releasing a polymer chain from a far more crowding corona of triblock micelle contributes to the faster kinetics of triblock micelle than diblock.

Our experimental results are also in good agreement with the simulation results of Li and Dormidontova,[26] in which chain exchange kinetics for A_4B_8 is faster than for A_4B_4. They observed an increase in critical micelle concentration (CMC) with increasing corona block length, indicating a larger population of free chains, which accounts for more rapid chain exchange kinetics. Although the CMC of the SEP system is difficult to detect, a decrease in micelle aggregation number was observed with increasing corona block length, indicating the same trend. However, our results appear to conflict with the

C_{27}-PEO_n/H_2O system[30] where the chain exchange kinetics slows down as the corona block length increases. The authors showed the pre-factor of the relaxation time (τ_0) to be proportional to $N_{corona}^{9/5}$ as predicted by Halperin and Alexander[10] for hairy micelles, which was attributed to slower chain diffusion through a thicker corona layer, while the activation energy did not show any appreciable decrease as corona block length increased. It is worth noting that this system differs from the one considered here in several aspects. For example, the alkane core block is crystalline at the measurement temperature, thereby introducing another term into the free energy balance. The short core blocks may make the Halperin-Alexander conjecture of a collapsed core block globule questionable. There are also multiple interaction parameters in play (core-solvent, core-corona, and corona-solvent), whereas in the PS-PEP/squalane system the chemical similarity of PEP and squalane effectively reduces the problem to a single χ. Nevertheless, it is not clear whether any of these considerations can account for a change in sign of the effect of corona length on chain exchange.

Very recently, Zhao *et al*.[40] observed an order of magnitude slower chain exchange kinetics in a PnBMA-PMMA/ionic liquid system when increasing N_{corona} from 250 to 840, while keeping constant $N_{core} \approx 246$. These results are apparently more in line with the C_{27}-PEO_n/H_2O system. Given that a core block with $N_{corona} = 0$ must surely exchange more slowly than one with a finite N_{corona}, there must be a regime where increasing N_{corona} increases the rate of chain exchange. Conceivably, there could then be an inversion as N_{corona} is increased further. There is a suggestion of this trend in Figure 3.9, where the corona block length effect saturates for SEP 28-118 and SEP 26-151 micelles. In such a scenario, the benefit of a lower activation energy of chain expulsion will be reduced while other competing mechanisms will be more evident. Clearly, the effects of the corona block on chain exchange in block copolymer micelles continues to be an

important and interesting fundamental question that warrants both additional theoretical and experimental attention.

3.4 Summary

We have investigated micelle structures and chain exchange kinetics for a series of SEP diblock copolymer micelles in squalane, with constant PS core block length ($<N_{core}>$ ≈ 255) but varying PEP corona block length ($<N_{corona}>$ = 256 – 2080). Smaller core radii and aggregation numbers, but significantly thicker corona layers and higher extents of corona chain stretching were observed with increasing corona block length. This effect agrees well with simulation results by Li and Dormidontova,[26] and with observations in a C_{27}-PEO_n system by Zinn *et al*.[30] Furthermore, a significant acceleration of chain exchange kinetics was detected with increasing corona block length. The activation energy of chain exchange was found to decrease as corona block length increases, which we attribute to the entropic gain arising from the relief of stretched corona chains upon chain expulsion. We extended a previous model by explicitly including a corona term associated with entropy change in the chain exchange process. With this improved model, previous results are successfully explained regarding the slowing down of the exchange kinetics as a consequence of increasing micelle concentration, added corona homopolymer chains, and speeding up with the presence of one additional corona block in triblock micelles compared to diblock analogs. Although qualitatively consistent with the simulations of Li and Dormidontova,[26] our results for chain exchange kinetics are seemingly contradictory to the theoretical predictions for hairy micelles[10] and experimental results for C_{27}-PEO_n/H_2O[30] and a PnBMA-PMMA/ionic liquid system.[40] These discrepancies are attributed to the differing significance of various mechanisms, indicating a need for more fundamental studies to elucidate the role of the corona block.

We also emphasize the simplicity of the current system to probe the chain exchange kinetics, in the nature of flexible coil-like polymer chains (both PS and PEP blocks are of high molecular weight), the amorphous nature of the core block, and the single χ interaction parameter (squalane has the same chemical structure with PEP). Overall, this work offers a better understanding of the role of corona blocks in the micelle structure and molecular chain exchange kinetics, which will aid in designing favorite block copolymer micelles (*i.e.,* core and corona block length, chain architecture and solvent selectivity) for specific applications.

3.5 References

[1] Kataoka, K.; Harada, A.; Nagasaki, Y. Block Copolymer Micelles for Drug Delivery: Design, Characterization and Biological Significance. *Adv. Drug Delivery Rev.* **2001**, *47*, 113−131.

[2] Li, Z.; Johnson L. M.; Ricarte R. G.; Yao, L. J.; Hillmyer M. A.; Bates, F. S.; Lodge, T. P. Enhanced Performance of Blended Polymer Excipients in Delivering a Hydrophobic Drug through the Synergistic Action of Micelles and HPMCAS. *Langmuir* **2017**, *33*, 2837−2848.

[3] Tang B.; White S. P.; Frisbie, C.D.; Lodge T. P. Synergistic Increase in Ionic Conductivity and Modulus of Triblock Copolymer Ion Gels. *Macromolecules* **2015**, *48*, 4942−4950.

[4] Tang B.; Schneiderman, D. K.; Bidoky, F. Z.; Frisbie, C.D.; Lodge T. P. Printable, Degradable, and Biocompatible Ion Gels from a Renewable ABA Triblock Polyester and a Low Toxicity Ionic Liquid. *ACS Macro Lett.* **2017**, *6*, 1083–1088.

[5] Anderson, W. Block Copolymers as Viscosity Index Improvers for Lubricating Oils. US3763044A, **1973**.

[6] Declet-Perez C.; Francis, L. F.; Bates, F. S. Deformation Processes in Block Copolymer Toughened Epoxy. *Macromolecules* **2015**, *48*, 3672–3684.

[7] Li, T.; Zhang J.; Schneiderman, D. K.; Francis, L. F.; Bates, F. S. Toughening Glassy Poly(lactide) with Block Copolymer Micelles. *ACS Macro Lett.* **2016**, *5*, 359−364.

[8] Halperin, A.; Tirrell, M.; Lodge, T. P. Tethered Chains in Polymer Microstructures. *Macromolecules: Synthesis, Order and Advanced Properties*; *Springer*: **1992**.

[9] Zhulina E. B.; Adam M.; LaRue I.; Scheiko S. S.; Rubinstein M. Diblock Copolymer Micelles in a Dilute Solution. *Macromolecules* **2005**, *38*, 5330–5351.

[10] Halperin, A.; Alexander, S. Polymeric Micelles: Their Relaxation Kinetics. *Macromolecules* **1989**, *22*, 2403−2412.

[11] Willner, L.; Poppe, A.; Allgaier, J.; Monkenbusch, M.; Richter, D. Time-resolved SANS for the Determination of Unimer Exchange Kinetics in Block Copolymer Micelles. *Europhys. Lett.* **2001**, *55*, 667–673.

[12] Lund, R.; Willner, L.; Stellbrink, J.; Lindner, P.; Richter, D. Logarithmic Chain-Exchange Kinetics of Diblock Copolymer Micelles. *Phys. Rev. Lett.* **2006**, *96*, 068302.

[13] Choi, S.; Lodge, T. P.; Bates, F. S. Mechanism of Molecular Exchange in Diblock Copolymer Micelles: Hypersensitivity to Core Chain Length. *Phys. Rev. Lett.* **2010**, *104*, 047802.

[14] Choi, S.; Bates, F. S.; Lodge, T. P. Molecular Exchange in Ordered Diblock Copolymer Micelles. *Macromolecules* **2011**, *44*, 3594−3604.

[15] Lu, J.; Bates, F. S.; Lodge, T. P. Addition of Corona Block Homopolymer Retards Chain Exchange in Solutions of Block Copolymer Micelles. *Macromolecules* **2016**, *49*, 1405−1413.

[16] Lu, J.; Bates, F. S.; Lodge, T. P. Remarkable Effect of Molecular Architecture on Chain Exchange in Triblock Copolymer Micelles. *Macromolecules* **2015**, *48*, 2667−2676.

[17] Lu, J.; Choi, S.; Bates, F. S.; Lodge, T. P. Molecular Exchange in Diblock Copolymer Micelles: Bimodal Distribution in Core-Block Molecular Weights. *ACS Macro Lett.* **2012**, *1*, 982−985.

[18] Lu, J.; Bates, F. S.; Lodge, T. P. Chain Exchange in Binary Copolymer Micelles at Equilibrium: Confirmation of the Independent Chain Hypothesis. *ACS Macro Lett.* **2013**, *2*, 451−455.

[19] Lund, R.; Willner, L.; Stellbrink, J.; Radulescu, A.; Richter, D. Role of Interfacial Tension for the Structure of PEP-PEO Polymeric Micelles. A Combined SANS and Pendant Drop Tensiometry Investigation, *Macromolecules* **2004**, *37*, 9984−9993.

[20] Lund, R.; Willner, L.; Stellbrink, J.; Radulescu, A.; Richter, D. Tuning of Structure and Kinetics of Chain Exchange in Star-Like PEP-PEO Block Copolymer Micelles. *Physica B* **2004**, *350*, 909−912.

[21] Lund, R.; Willner, L.; Richter, D.; Dormidontova, E. E. Equilibrium Chain Exchange Kinetics of Diblock Copolymer Micelles: Tuning and Logarithmic Relaxation. *Macromolecules* **2006**, *39*, 4566–4575.

[22] Lund, R.; Willner, L.; Richter, D.; Iatrou, H.; Hadjichristidisc, N.; Lindner, P. Unraveling the Equilibrium Chain Exchange Kinetics of Polymeric Micelles using Small-Angle Neutron Scattering – Architectural and Topological Effects. *J. Appl. Cryst.* **2007**, *40*, 327−331.

[23] Lund, R.; Willner, L.; Pipich, V.; Grillo, I.; Lindner, P.; Colmenero, J.; Richter, D. Equilibrium Chain Exchange Kinetics of Diblock Copolymer Micelles: Effect of Morphology. *Macromolecules* **2011**, *44*, 6145−6154.

[24] Zinn, T.; Willner, L.; Lund, R.; Pipich, V.; Richter, D. Equilibrium Exchange Kinetics in n-alkyl-PEO Polymeric Micelles: Single Exponential Relaxation and Chain Length Dependence. *Soft Matter* **2012**, *8*, 623−626.

[25] Li, Z.; Dormidontova, E. E. Kinetics of Diblock Copolymer Micellization by Dissipative Particle Dynamics. *Macromolecules* **2010**, *43*, 3521−3531.

[26] Li, Z.; Dormidontova, E. E. Equilibrium Chain Exchange Kinetics in Block Copolymer Micelle Solutions by Dissipative Particle Dynamics Simulations. *Soft Matter* **2011**, *7*, 4179–4188.

[27] Prhashanna, A.; Dormidontova, E. E. Tadpole and Mixed Linear/Tadpole Micelles of Diblock Copolymers: Thermodynamics and Chain Exchange Kinetics. *Macromolecules* **2017**, *50*, 1740−1748.

[28] Prhashanna, A.; Chen, S. B. Chain Exchange Kinetics between Linear ABA-Type Triblock Copolymer Micelles. *Polymer* **2017**, *118*, 22−29.

[29] Peters, A. J.; Lodge, T. P. Chain Exchange Kinetics of Asymmetric B_1AB_2 Linear Triblock and AB_1B_2 Branched Triblock Copolymers. *Macromolecules* **2017**, *50*, 6303–6313.

[30] Zinn, T.; Willner, L.; Pipich, V.; Richter, D.; Lund, R. Molecular Exchange Kinetics of Micelles: Corona Chain Length Dependence. *ACS Macro Lett.* **2016**, *5*, 884−888.

[31] Choi, S.; Bates, F. S.; Lodge, T. P. Structure of Poly(styrene-*b*-ethylene-*alt*-propylene) Diblock Copolymer Micelles in Squalane. *J. Phys. Chem. B* **2009**, *113*, 13840−13848.

[32] Pedersen, J. S.; Svaneborg, C.; Almdal, K.; Hamley, I. W.; Young, R. N. A Small-Angle Neutron and X-ray Contrast Variation Scattering Study of the Structure of Block Copolymer Micelles: Corona Shape and Excluded Volume Interactions. *Macromolecules* **2003**, *36*, 416–433.

[33] Halperin, A. Polymeric Micelles: A Star Model. *Macromolecules* **1987**, *20*, 2943–2946.

[34] Bang, J.; Viswanathan, K.; Lodge, T. P.; Park, M. J.; Char, K. Temperature-Dependent Micellar Structures in Poly(styrene-*b*-isoprene) Diblock Copolymer Solutions near the Critical Micelle Temperature. *J. Chem. Phys.* **2004**, *121*, 11489–11500.

[35] Lai, C.; Russel, W. B.; Register, R. A. Phase Behavior of Styrene-Isoprene Diblock Copolymers in Strongly Selective Solvents. *Macromolecules* **2002**, *35*, 841–849.

[36] Ma, Y.; Lodge, T. P. Poly(methyl methacrylate)-block-poly(n-butyl methacrylate) Diblock Copolymer Micelles in an Ionic Liquid: Scaling of Core and Corona Size with Core Block Length. *Macromolecules* **2016**, *49*, 3639−3646.

[37] Ma, Y.; Lodge, T. P. Chain Exchange Kinetics in Diblock Copolymer Micelles in Ionic Liquids: The Role of χ. *Macromolecules* **2016**, *49*, 9542−9552.

[38] Bates, F. S.; Fredrickson, G. H. Block Copolymers – Designer Soft Materials. *Physics Today* **1999**, *52*, 32–38.

[39] Fetters, L. J.; Lohse, D. J.; Richter, D.; Witten, T. A.; Zirkel, A. Connection between Polymer Molecular Weight, Density, Chain Dimensions, and Melt Viscoelastic Properties. *Macromolecules* **1994**, *27*, 4639–4647.

[40] Zhao, D.; Ma, Y.; Lodge, T. P. unpublished.

[41] Radulescu A.; Mathers R. T.; Coates G. W.; Richter D.; Fetters L. J. A SANS Study of the Self-Assembly in Solution of Syndiotactic Polypropylene Homopolymers, Syndiotactic Polypropylene-*block*-poly(ethylene-*co*-propylene) Diblock Copolymers, and

an Alternating Atactic-Isotactic Multisegment Polypropylene. *Macromolecules* **2004**, *37*, 6962–6971.

[42] Birshtein T. M.; Zhulina E. B. Scaling Theory of Supermolecular Structures in Block Copolymer-Solvent Systems: 1. Model of Micellar Structures. *Polymer* **1989**, *30*, 170–177.

[43] Mok M. M.; Thiagarajan R.; Flores M.; Morse D. C.; Lodge T. P. Apparent Critical Micelle Concentrations in Block Copolymer/Ionic Liquid Solutions: Remarkably Weak Dependence on Solvophobic Block Molecular Weight. *Macromolecules* **2012**, *45*, 4818–4829.

Chapter IV.
Effect of Solvent Selectivity on Chain Exchange Kinetics in Block Copolymer Micelles

4.1 Introduction

Self-assembled block copolymer (BCP) micelles in selective solvents offer useful solution properties. They are widely used in a variety of applications, including nanolithography,[1-3] drug delivery,[4-6] and viscosity modification.[7] The solvent quality is an important factor for both thermodynamics and dynamics of BCP micelles, which can be tuned by either changing the composition of binary solvent mixtures, or altering the temperature.

In terms of thermodynamic properties, the scaling model predicts the aggregation number of chains within a micelle (N_{agg}) to be proportional to the interfacial tension (γ) between the core block and solvent for crew-cut micelles, which have relatively longer core than corona block lengths (i.e., $N_{core} >> N_{corona}$).[8,9] For hairy micelles (i.e., $N_{core} >> N_{corona}$), a scaling of $N_{agg} \sim \gamma^{6/5}$ is proposed.[10,11] Quintana and coworkers studied the structures and thermodynamic properties of micelles formed by poly(styrene)-*b*-poly(ethylene-*alt*-propylene) (PS-PEP, or SEP) diblock copolymers in various solvent mixtures.[12-17] The authors reported lower aggregation numbers, smaller micelle sizes, lower critical micelle temperatures (CMT), and higher critical micelle concentrations (CMC) in less selective solvents, reflecting lower interfacial tension between the core block and solvent. Alternatively, changing the temperature is another way to adjust the solvent quality. Bang et al. showed a decrease in N_{agg} and core radius (R_{core}) of poly(styrene)-*b*-poly(isoprene) (PS-PI) micelles in tetradecane, and an increase of solvent fraction in the micelle core, when the temperature was elevated towards the CMT.[18,19] Recently, Choi et al. systematically investigated a series of PS-PEP diblock copolymers

in pure squalane and binary solvent mixtures of squalane and 1-phenyldodecane, where 1-phenyldodecane is a less selective solvent than squalane.[20,21] In good agreement with observations by Quintana et al. and Bang et al., the authors observed a smaller aggregation number, lower CMT, and higher solvent fraction in the core upon increasing the volume faction of 1-phenyldodecane in binary solvent mixtures.

The solvent quality also plays a critical role in equilibration dynamics of BCP micelles. Single chain exchange is believed to be the dominant mechanism for BCP micelles near equilibrium.[22-24] Both theory and experiment have shown a strong dependence of chain exchange kinetics on the solvent selectivity.[25-32] The scaling theory by Halperin and Alexander attributes the activation energy (E_a) of chain expulsion to the additional surface of a collapsed core block, i.e., $\gamma N_{core}^{2/3} a^2$, where γ reflects the effect of solvent selectivity, N_{core} is the number of core block repeat units, and a is the size of one repeat unit.[25,26] Following this theoretical prediction, Lund and coworkers showed an acceleration in chain exchange kinetics of poly(ethylene-*alt*-propylene)-*b*-poly(ethylene oxide) (PEP-PEO) micelles by reducing the interfacial tension between the PEP core block and solvent, by adding more *N*,*N*-dimethylformamide into water and/or increasing temperature.[27,28,29] Based on kinetic studies of dilute SEP diblock copolymer micelles in squalane, Choi and coworkers established a quantitative model (eqn 4.4) to account for the dramatic influence of the core block length, dispersity of core block length, and solvent selectivity.[30] This model attributes E_a to the unfavorable core block monomer–solvent interactions captured by $kT\chi N_{core}$, where χ is the Flory-Huggins interaction parameter between the core block and solvent. Dissipative particle dynamics (DPD) simulations by Li and Dormidontova[31] examined the effect of solvent selectivity by adjusting the pairwise repulsive interaction parameters, leading to the same form for E_a ($\sim \chi N_{core}$) as proposed by Choi et al.

However, there is a problem in this simple relation when considering the scenario near the CMT. At T_{CMT}, there should be literally no energy barrier for chain expulsion, i.e., $E_a \approx 0$. However, the solvent quality is approximately at the theta condition for the core block at T_{CMT}, i.e., $\chi \approx 0.5$, taking the solvent volume as the reference volume. To address this issue, Ma and Lodge[32] proposed an elaborate χ-dependent function $f(\chi)$ to replace χ, so that the adapted expression is $E_a \sim f(\chi)N_{core}$. The authors incorporated this modified function within Choi's model, and successfully interpreted the time-resolved small-angle neutron scattering (TR-SANS) data of poly(*n*-butyl methacrylate)-*b*-poly(methyl methacrylate) (PnBMA-PMMA) micelles in solvent mixtures of the ionic liquids 1- butyl-3-methylimidazolium:bis(trifluoromethylsulfonyl)imide ([BMIM][TFSI]) and 1-ethyl-3-methylimidazolium:bis(trifluoromethylsulfonyl)imide ([EMIM][TFSI]), which are lower critical micelle temperature (LCMT) systems.

This work aims to test the universality of this χ-dependent function with SEP micelles in binary mixed solvents of squalane and 1-phenyldodecane. In contrast to the previously studied PnBMA-PMMA/ionic liquids system, this SEP micelle system has an upper critical temperature (UCMT). We will show the consequences of varying the solvent composition and temperature on the rate of chain exchange using TR-SANS. An independent approach, static light scattering (SLS), has been adopted for direct measurements of χ between the core block and the solvent as a function of solvent composition and temperature. With TR-SANS and SLS results, we aim to determine the exact χ dependence of the activation energy associated with chain exchange. To our knowledge, this will be the first study that quantifies the effect of solvent selectivity on chain exchange kinetics for an UCMT micelle system.

4.2 Materials and Methods

4.2.1 Materials

Two polystyrene (PS) homopolymers were synthesized by anionic polymerization. The molecular weight and molecular weight distribution of PS with M_n = 1.3 kg/mol were characterized by matrix-assisted laser desorption/ionization mass spectroscopy (MALDI), and those of the other PS (M_n = 23 kg/mol) were characterized by size exclusion chromatography equipped with a refractive index detector and a multi-angle light scattering detector (SEC-MALS), as shown in Figure 4.1. Two pairs of SEP and core block deuterated dSEP diblock copolymers were reproduced from the previous work.[20,30] They were synthesized by sequential anionic polymerization of PS-PI and (d-PS)-PI, and then followed by selective saturation of the polyisoprene block using a Ni/Al catalyst under 400 psi deuterium D_2. The repeat unit of PEP is $C_5D_{2.3}H_{7.7}$ after the deuteration reaction, where $D_{2.3}$ is a result of D_2 saturation and a small extent of H/D exchange. SEC-MALS and proton nuclear magnetic resonance spectroscopy (^{1}H-NMR) were performed to determine the molecular weight and molecular weight distribution, which are displayed in Table 4.1. The number in the nomenclature of each polymer refers to the molecular weight, e.g., SEP 26-70 indicates $M_n \approx$ 26 kg/mol and 70 kg/mol for the PS and PEP blocks, respectively.

Squalane (sql) was used as a highly selective solvent for the PEP blocks, so that the PS blocks aggregate into the core while PEP blocks form the swollen corona. 1-phenyldodecane (phd), on the other hand, is relatively less selective, dissolving SEP diblock polymers as free chains. Binary solvent mixtures were prepared by mixing squalane with various volume fractions of 1-phenyldodecane, which were calculated using densities of squalane (0.810 g/mL) and 1-phenyldodecane (0.856 g/mL) at room temperature, assuming no volume change on mixing.

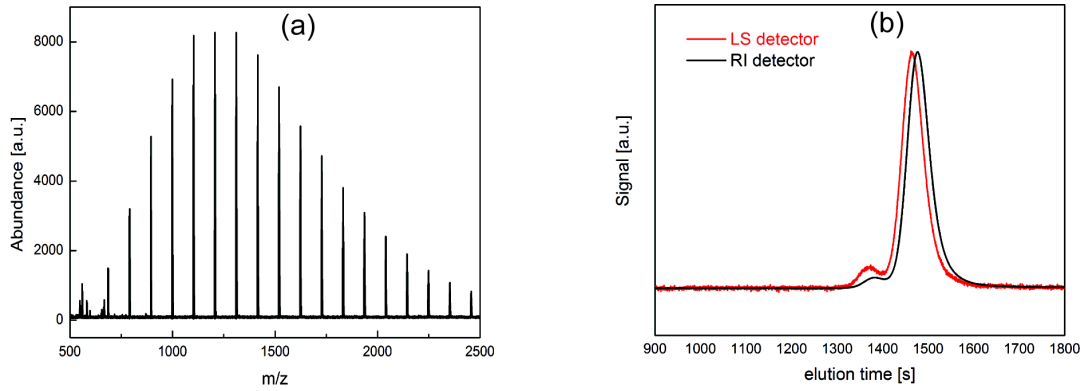

Figure 4.1 (a) MALDI spectra of 1.3 kg/mol PS, and (b) SEC trace of 23 kg/mol PS using RI detector and multi-angle LS detector

Table 4.1 Polymer Characteristics

Polymers	$M_{n,\,PS}$ [a] (kg/mol)	$M_{n,\,PEP}$ [b] (kg/mol)	M_w/M_n [a]
PS 1.3	1.3 [c]	–	1.10 [c]
PS 23	23	–	1.03
SEP 26-70	26	70	1.04
dSEP 29-71	29	71	1.10
SEP 42-64	42	64	1.05
dSEP 47-67	47	67	1.10

[a] Determined by SEC-MALS
[b] Determined by ^{1}H-NMR spectroscopy from the proton peaks of PS and PEP
[c] Determined by MALDI
Note: Characteristics of SEP and dSEP diblocks were reproduced from reference 20 and reference 30

4.2.2 Cloud Point Measurements

The cloud point measurements were performed on a home-built optical transmission apparatus, which consists of a helium–neon laser with wavelength $\lambda = 633$ nm, a sample heating stage, and a photodiode detector. Various volume fractions of 1.3 kg/mol PS were mixed with squalane into a glass ampule, which was then flame sealed under vacuum.

The sample was heated to 180 ºC or higher temperature, held for 30 minutes to completely dissolve, i.e., one phase solution, and followed by subsequently cooling at a rate of 1 ºC/min. The transmittance showed a sudden decrease when the solution phase separated. The cloud point was defined as the temperature at which the transmittance dropped to 80% of the transmittance of the one-phase solution.

4.2.3 Contrast Matching Method in TR-SANS Experiments

A contrast matching strategy is employed for the solvent used in TR-SANS experiments, such that the scattering density of the solvent matches that of completely mixed micelle cores. $\rho_{solvent} = \rho_{core}(t=\infty) = (\rho_{hPS} + \rho_{dPS})/2 = 3.93 \times 10^{10}$ cm^{-2}, using the values listed in Table 2.2. Isotopic solvent mixtures of h-(1-phenyldodecane), d-(1-phenyldodecane) h-squalane, and d-squalane were prepared using the calculated volume fractions as listed in Table 4.2.

Table 4.2 The Volume Fraction of Each Component in the Contrast Matching Solvent

Contrast Matching Solvents	h-phd	d-phd	h-sql	d-sql
50/50 vol% phd/sql	45 vol%	5 vol%	0	50 vol%
25/75 vol% phd/sql	25 vol%	0	19 vol%	56 vol%
0/100 vol% phd/sql	0	0	42 vol%	58 vol%

4.3 Results and Discussions

4.3.1 Micelle Chain Exchange Kinetics

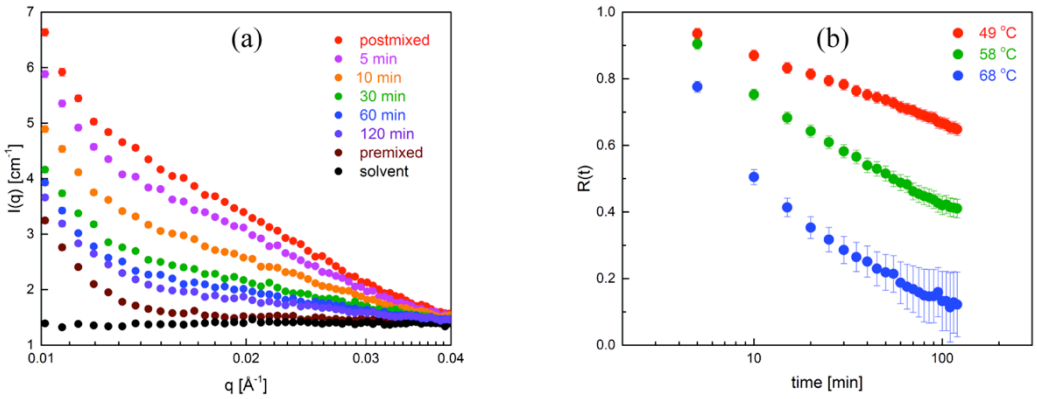

Figure 4.2 (a) Representative TR-SANS intensity evolution traces at 58 °C and (b) $R(t)$ traces of the 1 vol % SEP 26-70 micelles in the 25/75 vol% phd/sql solvent at different temperatures.

TR-SANS experiments were performed to probe the chain exchange kinetics of SEP block copolymer micelles in various solvent mixtures of squalane and 1-phenyldodecane. Figure 4.2a shows an example of time-dependent scattering intensities of 1 vol% SEP 26-70 micelles in the mixed solvent 25/75 vol% phd/sql at 58 ºC. The intensity of a postmixed specimen (red curve) was measured at room temperature where no chain exchange occurred, so it represents the initial state with unmixed cores, i.e., $I(0) = I_{\text{postmixed}}$. It showed the highest intensity because of the largest contrast between micelle cores (half of which were purely protonated cores while the other half were deuterated cores) and solvent. After the system was heated to the target temperature, 58 ºC for example, micelles exchanged chains with each other. Thus, the contrast between partially mixed cores and solvent decreases, leading to the decrease in scattering intensity over time, as shown in Figure 4.2a. The premixed micelle solution represents the state of complete chain exchange, i.e., $I(\infty) = I_{\text{premixed}}$, since the protonated and deuterated polymer chains were molecularly mixed in preparation. Under the contrast matching condition for mixed cores, the intensity of premixed specimen matches with that of the

solvent except in the low q regime (< 0.015 $Å^{-1}$), where there is a contribution from the corona scattering.

A normalized relaxation function, $R(t)$, is defined by the following equation to quantify the rate of chain exchange,

$$R(t) = \sqrt{\frac{I(t) - I(\infty)}{I(0) - I(\infty)}} \tag{4.1}$$

where $I(0)$, $I(t)$, $I(\infty)$ are the intensities at $t = 0$, at instantaneous time t, and at infinite time, respectively. The values of scattering intensities are integrated over a q range of 0.01 – 0.04 $Å^{-1}$. As shown in Figure 4.2b, $R(t)$ decays more rapidly at higher temperatures, which reflects faster chain exchange kinetics at higher temperatures. The error-bars of $R(t)$ in Figure 4b are propagated from the errors in the intensities, given by,

$$\delta R(t) = \sqrt{\left[\frac{\partial R(t)}{\partial I(t)} \cdot \delta I(t)\right]^2 + \left[\frac{\partial R(t)}{\partial I(\infty)} \cdot \delta I(\infty)\right]^2 + \left[\frac{\partial R(t)}{\partial I(0)} \cdot \delta I(0)\right]^2} \tag{4.2}$$

where $\delta I(t)$, $\delta I(\infty)$, and $\delta I(0)$ are instrumental uncertainties in measured values of $I(t)$, $I(\infty)$, and $I(0)$, respectively. $\delta I(t)$, $\delta I(\infty)$, and $\delta I(0)$ are integrated over the same q range of 0.01 – 0.04 $Å^{-1}$ as well. As shown in Figure 4.2b, the propagated errors of $R(t)$ became larger at higher temperatures and longer relaxation times, e.g., at 68 ºC and 100 minutes.

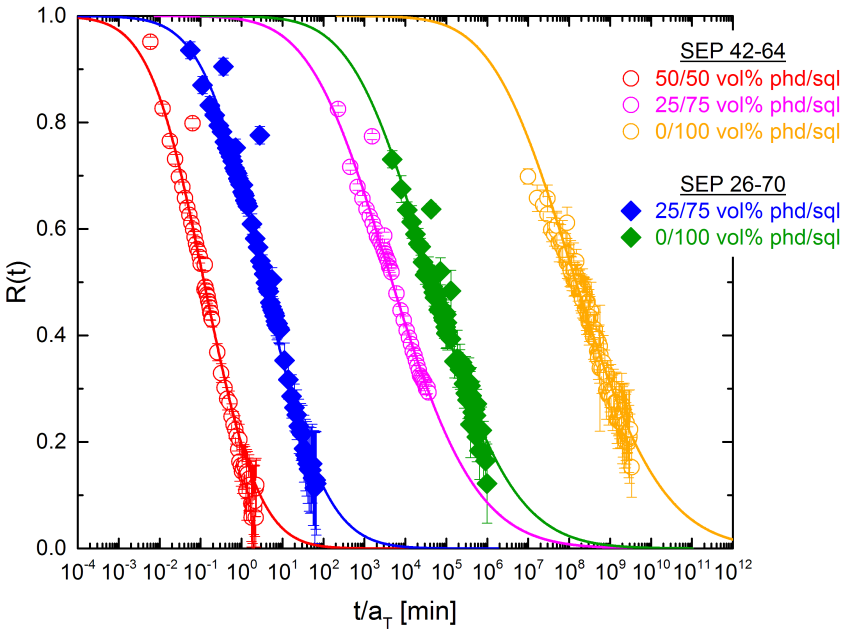

Figure 4.3 $R(t)$ master curves and theoretical model fits for 1 vol % SEP micelles in various binary mixed solvents at a reference temperature of 70 °C. Data of SEP micelles in pure squalane were adapted from reference 30.

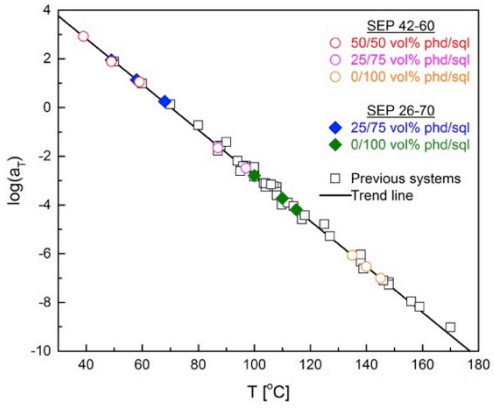

Figure 4.4 The shift factors $\log(a_T)$ and trend line as a function of temperature at a reference temperature of 70 ºC, open circles for SEP 42-64, and filled diamonds for SEP 26-70 in binary mixed solvents, together with the shift factors adapted from our previous studies.[30,33-35,42]

The time-temperature superposition (tTS) method is employed to construct $R(t)$ master curves with a reference temperature 70 ºC, as shown in Figure 4.3. The chain exchange rate increases significantly for both SEP micelle systems with reducing the solvent selectivity by mixing squalane with a higher volume fraction of 1-phenyldodecane. For instance, SEP 42-64 micelles exchange chains 10^5 times faster in 50 vol% squalane than in 75 vol% squalane, and furthermore, 10^{10} times faster than in pure squalane. The same trend was observed for SEP 26-70 micelles. The kinetics of chain exchange was accelerated by 5 orders of magnitude when only adding 25 vol% 1-phenyldodecane into squalane. The timescale of chain exchange is tremendously large in pure squalane, i.e., $\approx 10^5$ and 10^8 minutes at $R(t) = 0.5$ for SEP 26-70 and SEP 42-64 micelles, respectively. The main reason is that the reference temperature 70 ºC is approximately the glass transition temperature (T_g) of PS block in the micelle core,[36] where the PS chains are almost frozen in the core.

The empirical shift factors used in the tTS method are displayed in Figure 4.4. We note that the shift factors of previously studied micelle systems in pure squalane have been adapted from the reported values because the reference temperature was switched from 125 ºC to 70 ºC. Since the T_g of PS block in the core is about 70 ºC for micelles in pure squalane, the previous empirical trend line should still work, but needs shifting to the reference temperature 70 ºC, i.e., $\log(a_T) = -0.0936 \times (T - 70\ ºC)$. However, the T_g of the core block in binary mixed solvents will decrease with the increase of solvent fraction in the core region when the solvent selectivity is reduced. Therefore, the data of binary mixed solvents at multiple temperatures were empirically shifted to overlap with those obtained at 70 ºC.

The values of reduced T_g are estimated by the Fox equation where the unit of temperature is Kelvin.[37]

$$\frac{1}{T_{g,PS}^{wet}} = \frac{1-w}{T_{g,PS}^{dry}} + \frac{w}{T_{g,solvent}} \tag{4.3}$$

Here T_g^{wet} is the glass transition temperature of the core block in a wet core with a certain weight fraction of solvent w, while T_g^{dry} represents that of a dry core, ≈ 343 K (70 ºC). This is relatively lower than T_g of a bulk PS sample due to the significantly smaller size of PS domain in spherical micelles (<10 nm), where PS core block repeat units at the interface are plasticized by the solvent. The glass transition of the solvent ($T_{g,solvent}$) depends on the composition, which is estimated by the Fox equation as well, using $T_{g,squalane} \approx 168$ K and $T_{g,1\text{-phenyldodecane}} \approx 180$ K from the literature.[38,39,40] The solvent fraction in the core was reported in previous work for SEP 42-64 micelles in pure squalane and binary mixed solvents, using a combination of small-angle X-ray scattering and SANS.[20,21] There is almost no solvent within the core in pure squalane at experimental temperatures that are well below the CMT, while 13 vol% solvent was observed for the 25/75 vol% phd/sql binary solvent. In the latter case, the weight fractions of PS, squalane, and 1-phenyldodecane are 89 wt%, 3 wt% and 8 wt% in the core region, respectively. The glass transition temperature of the PS core block in such a wet core is estimated to be 37 ºC by eqn 4.3. As the solvent selectivity decreases, more solvent penetrates into the core, leading to a lower T_g of PS block, as shown in Table 4.3. Note that $T_{g,PS}$ in SEP 26-70 micelle cores is assumed to be the same as SEP 42-64 micelles in the same binary solvent because the molecular weight dependence of T_g is weak in this molecular weight range.[41]

As noted in Table 4.3, the TR-SANS experimental temperatures were designed for appropriate timescales from several minutes to hours, in order to capture the evolution of scattering intensities by SANS. These temperatures are at least 12 ºC higher than the glass transition temperature of the core block, so that the core blocks are able to relax in

the core. On the other hand, they are more than 50 ºC lower than the critical micelle temperature where the rate of chain exchange would be infinite large. T_{CMT} is determined by the sudden drop in micelle hydrodynamic radius, and simultaneously, the jump in scattering intensity, as shown in Figure 4.5.

To quantitatively describe the TR-SANS data, a theoretical model (eqn 4.4) has been established by previous studies on SEP diblock micelles.[30,42] This model makes the following assumptions: (i) single chain exchange is the dominant mechanism of kinetics near equilibrium; (ii) the chain expulsion step is the rate limiting step; (iii) the motion of core blocks follows Rouse dynamics when buried in the micelle cores; and (iv) the activation energy E_a of chain expulsion is a result of the enthalpy penalty from unfavorable interactions between the core blocks and corona/solvent matrix, and the entropy gain from the relief of stretched corona chains upon expulsion.

$$R(t) = \int P(N_{core}) \exp\left[-t \frac{6\pi^2 kT}{N_{core}^2 b^2 \zeta} \exp\left(-\alpha f(\chi) N_{core} + \frac{3}{2} s_{corona}^2 \right) \right] dN_{core} \tag{4.4}$$

$$P(N_i) = \frac{z^{z+1}}{\Gamma(z+1)} \frac{N_i^{z-1}}{N_n^z} \exp\left(-\frac{zN_i}{N_n} \right) \tag{4.5}$$

Here N_{core} is the degree of polymerization of core blocks, and $P(N_{core})$ is a Schulz-Zimm distribution function that accounts for disperse core blocks, given by eqn 4.5, where $z = [N_w/N_n - 1]^{-1}$, Γ is the gamma function, and N_w/N_n represents the dispersity of core blocks. Considering the small mismatch in the molecular weight of PS and dPS blocks from the isotopic pair of SEP and dSEP diblock copolymers, the SEP 26-40/dSEP 29-71 system has an averaged $<N_{core}> = 255$, while SEP 42-64/dSEP 47-67 has $<N_{core}> = 412$. N_w/N_n is taken as a fitting parameter to depict the slope of $R(t)$, as listed in Table 4.4.

The first term inside the first exponential term, $N_{core}^2 b^2 \zeta / 6\pi^2 kT$, represents the longest Rouse relaxation mode for the core blocks, where k is Boltzmann's constant, T = 343 K (70 ºC) is the temperature, ζ is the monomeric friction factor, and b = 0.67 nm is the statistical segment length of the core block. We assume that 26 and 42 kg/mol PS are not, or at most weakly, entangled since they are only three times bigger than the entanglement molecular weight. ζ is a strong temperature-dependent function described by the Williams-Landel-Ferry (WLF) equation.[43]

$$\log\left(\frac{\zeta_T}{\zeta_g}\right) = -\frac{C_1^g (T - T_g)}{C_2^g + (T - T_g)} \tag{4.6}$$

where $\zeta_g = 1.20 \times 10^{-3}$ Ns/m is the monomeric friction factor at T_g, and C_1^g = 11.0 and C_2^g = 69.8 ºC are two empirical constants, which are obtained from the rheological data of bulk PS homopolymer.[44] Since the T_g of PS in the micelle core varies with solvent composition, values of ζ at the reference temperature 70 ºC are calculated by eqn 4.6 for various binary mixed solvents. As listed in Table 4.4, ζ is more than 3 orders of magnitude lower with only 13 vol% solvent present in the core for micelles in the solvent of 75 vol% squalane, than in pure squalane. This decrease in the chain friction significantly facilitates the movements of core blocks in the core, and ultimately accelerates the kinetics of chain exchange.

The energy barrier for chain expulsion is expressed in the double exponential term. α is a pre-factor of order unity, and $f(\chi)$ is a χ-dependent function where χ represents the Flory-Huggins interaction parameter between the core block and solvent. Choi et al. originally assumed the enthalpy part to be $\alpha\chi N_{core}$.[30] Here the form of $\alpha f(\chi)$ is adopted as a fitting parameter, and the fitted results in Table 4.4 will be discussed with χ values obtained from SLS (see below). The entropic term arises from the increasing corona chain conformations after the polymer chain escapes from the micelle into solvent.[42]

Assuming the corona chains follow Gaussian chain statistics,[45] the corona chain stretching parameter (s_{corona}) is defined as $s_{corona} = R_g/R_{g,0}$, where R_g is the radius of gyration of corona chains in the micelle, and $R_{g,0}$ is the unperturbed value neglecting the excluded volume effect of PEP corona blocks in squalane.[46] R_g is estimated to be half of corona layer thickness (L_{corona}), i.e., $R_g = L_{corona}/2 = (R_h - R_{core})/2$, where R_h is the micelle hydrodynamic radius determined by DLS as shown in Figure 4.5b, and R_{core} is the core radius characterized by SAXS as demonstrated in Figure 4.6. These data were summarized in Table 4.3. $R_{g,0}$ is calculated by $R_{g,0} = 0.0392M^{1/2}$ ($R_{g,0}$ in unit of nm) at 298 K[47] with M = 70,000 and 64,000 for SEP 26-70 and SEP 42-64 micelles, respectively. As listed in Table 4.4, s_{corona} decreases with reduced solvent selectivity. This is attributed to less crowding of corona chains as the aggregation number decreases in a less selective solvent.

Table 4.3 Characteristics of SEP Micelles in Binary Mixed Solvents

Micelle systems	R_h [a] (nm)	R_{core} [b] (nm)	f_{sol} [c]	$T_{g,PS}$ [d] (ºC)	T_{CMT} [e] (ºC)	$T_{TR\text{-}SANS}$ [f] (ºC)
SEP 42-64 micelles in						
50/50 vol% phd/sql	34	10.1	≈ 0.21	≈ 20	110	39 – 59
25/75 vol% phd/sql	35	10.9	≈ 0.13	≈ 37	180	87 – 97
0/100 vol% phd/sql	43	11.0	≈ 0	≈ 70	> 200	135 – 145
SEP 26-70 micelles in						
25/75 vol% phd/sql	35	8.8	≈ 0.13	≈ 37	130	49 – 68
0/100 vol% phd/sql	43	9.0	≈ 0	≈ 70	≈ 200	100 – 115

[a,b] Micelle core radius and hydrodynamic radius at 70 ºC

[c] The volume fraction of solvent in the micelle core measured at room temperature

[d] The glass transition of PS core block in the core estimated by the Fox equation

[e] The critical micelle temperature determined by dynamic light scattering (DLS)

[f] The temperatures carried out in TR-SANS experiments

Note that f_{sol}, R_{core}, R_h and T_{CMT} data were reproduced from previous work,[20,21] except those of SEP 26-70 micelles in 25/75 vol% phd/sql, as shown in Figure 4.5 and 4.6.

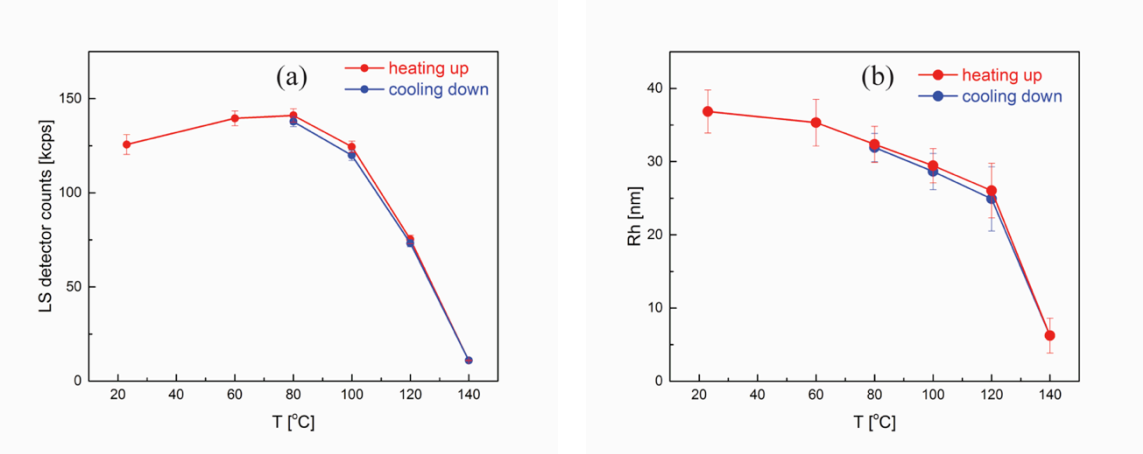

Figure 4.5 Temperature dependence of (a) the LS detector counts and (b) the hydrodynamic radius of 0.5 vol% SEP 26-70 polymer in the 25/75 vol% 1-phenyldodecane/squalane mixed solvent upon heating and cooling.

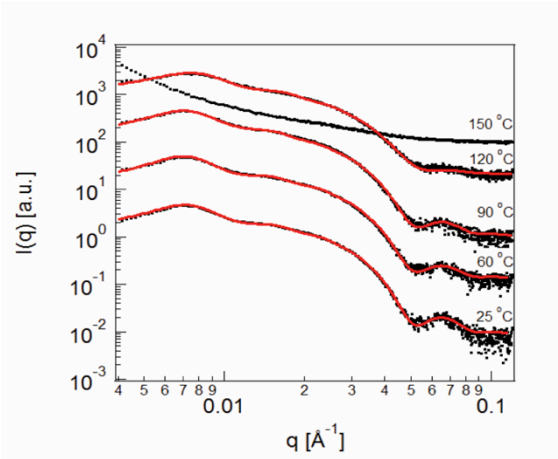

Figure 4.6 SAXS patterns of 1 vol% SEP 26-70 micelles in the 25/75 vol% phd/sql solvent at different temperatures (vertically shifted for clarification). Red lines are the best fits to the hard sphere model for BCP micelles[48-52] with R_{core} = 8.8 nm from 25 to 90 ºC.

Table 4.4 Parameters used in the Model

Micelle systems	$<N_{core}>$	$\zeta_{T=70\,^{o}C}$ (Ns/m)	s_{corona}	$\alpha f(\chi)^{fitted}$	$N_w/N_n{}^{fitted}$
SEP 42-64 micelles in					
50/50 vol% phd/sql	412	$3.0_8 \times 10^{-8}$	1.2_2	$2.3_4 \times 10^{-2}$	1.02
25/75 vol% phd/sql	412	$3.5_3 \times 10^{-7}$	1.2_3	$4.3_2 \times 10^{-2}$	1.04
0/100 vol% phd/sql	412	$1.2_0 \times 10^{-3}$	1.6_6	$5.3_3 \times 10^{-2}$	1.04
SEP 26-70 micelles in					
25/75 vol% phd/sql	255	$3.5_3 \times 10^{-7}$	1.2_8	$4.5_9 \times 10^{-2}$	1.02
0/100 vol% phd/sql	255	$1.2_0 \times 10^{-3}$	1.6_8	$5.8_9 \times 10^{-2}$	1.04

Table 4.4 summarizes the parameters used in this theoretical model and two adjustable fitting parameters, i.e., $\alpha f(\chi)$ and N_w/N_n. The solid lines in Figure 4.3 represent best fits to the TR-SANS data. The fitted $\alpha f(\chi)$ values decrease by more than a factor of 2 with decreasing the volume fraction of squalane in binary mixed solvents. This effect results from the reduced enthalpy of mixing between the core block and solvent. On the other hand, for a given solvent composition, $\alpha f(\chi)$ values are almost independent of the molecular characteristics of SEP block copolymers. The following paragraph will show the determination of χ using SLS and optical transmittance measurements as a function of solvent composition and temperature. Thus, the exact dependence of χ is quantified for the function $f(\chi)$.

4.3.2 Role of χ

SLS was performed to determine the χ between PS and the binary mixed solvent from the second virial coefficient A_2. Details of SLS experiments have been discussed in Chapter II. Figure 4.7 gives an example of obtaining the second virial coefficient A_2 of dilute PS (M_n = 23 kg/mol, M_w/M_n = 1.03, in Table 4.1) solutions in 1-phenyldodecane

from the Zimm plot. As shown in Figure 4.7a, the refractive index increment (dn/dc) was measured to be 0.0989 mL/g at both 23 ºC and 60 ºC, using a refractometer with red light (wavelength $\lambda \approx 650$ nm). With dn/dc values known, measurements were taken at multiple angles ranging from 50º to 130º with 10º increments using a laser light scattering system with $\lambda = 637$ nm, giving a q range of 0.012 – 0.026 nm^{-1}. As shown in Figure 4.7b, Kc/R_θ was independent of scattering angle because this polymer is rather small ($R_g \approx 4$ nm in theta solvent), $qR_g \leq 0.1$, while Kc/R_θ decreased with increasing of polymer concentration. The second virial coefficient $A_2 = (-1.69 \pm 0.10)\times10^{-4}$ cm^{3}mol/g^2 was obtained from the slope of Kc/R_θ vs c, indicating that 1-phenyldodecane is a poor solvent for PS at 23 ºC. By double extrapolation of angle and concentration to 0, the weight average molecular weight of this PS sample was determined to be 30 kg/mol, which is 20% larger than that obtained from SEC-MALS.

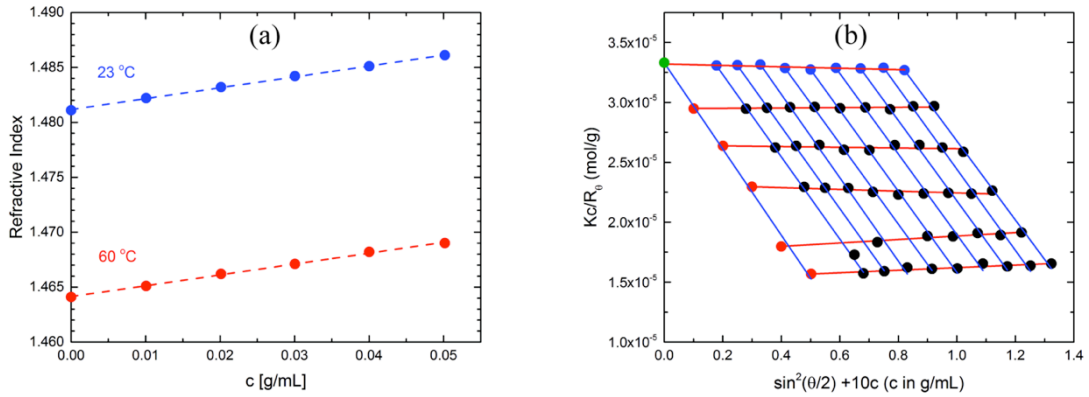

Figure 4.7 (a) Refractive indices vs concentration of dilute PS solutions in 1-phenyldodecane at 23 ºC and 60 ºC, and the slop gives the refractive index increment (dn/dc), and (b) Zimm plot of PS in 1-phenyldodecane at 23 ºC.

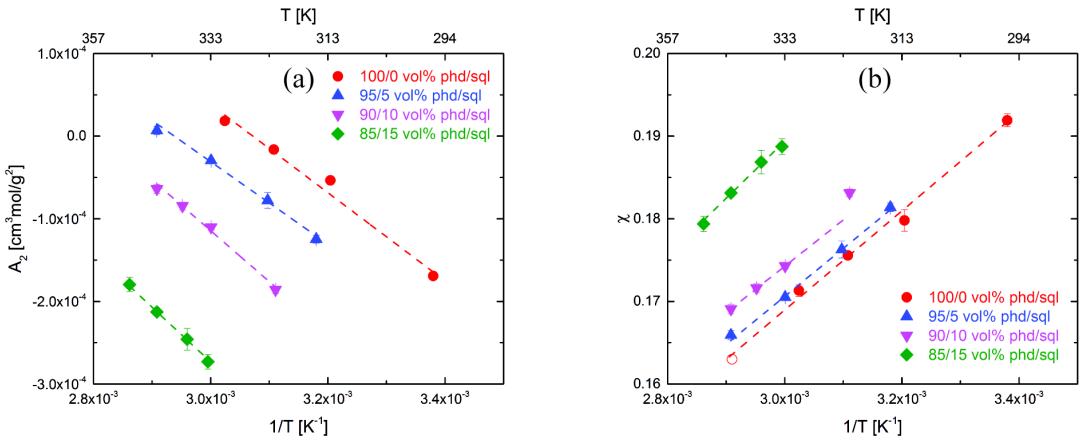

Figure 4.8 (a) The second virial coefficient (A_2) for PS in binary mixed solvents as a function of temperature and composition, and (b) calculated χ values from A_2, taking the PS repeat unit volume as the reference volume. The open circle is an extrapolation to 70 ºC.

$$\chi' = \frac{1}{2} - \rho_p^2 v_1 A_2 \qquad (v_0 = v_1) \qquad (4.7)$$

$$\chi = \frac{v_2}{v_1}\chi' \qquad (v_0 = v_2) \qquad (4.8)$$

Figure 4.8a summarizes the second virial coefficients obtained from SLS measurements. A_2 increases with increasing temperature, indicating higher solubility of PS in the solvent, which is an upper critical solution temperature (UCST) system. On the other hand, A_2 is strongly dependent on the solvent composition as well, decreasing with increasing volume fraction of squalane (ϕ_{sql}). Applying Flory-Huggins theory for dilute polymer solutions, χ values were calculated from A_2 by eqn 4.7, and then converted by eqn 4.8 taking the molar volume of PS repeat unit (v_2 = 100 cm^3/mol) as the reference volume v_0, instead of the molar volume of the solvent v_1 in the traditional definition, where ρ_p = 1.04 g/cm^3 is the density of PS. This is due to the use of the chemical degree

of polymerization in the fitting model (eqn 4.4) for TR-SANS data, i.e., $N_2 = N_{core}$ only if $v_0 = v_2$, where N_2 represents the volumetric degree of polymerization of PS block. Moreover, the values of χ were determined in binary mixed solvents of low squalane volume fraction ϕ_{sql} (= 0, 5, 10, and 15 vol%), whereas TR-SANS experiments were performed in the other extreme, i.e., ϕ_{sql} = 50, 75, and 100 vol%. It is mathematically convenient to extrapolate χ to high ϕ_{sql} solvents using a constant reference volume, since v_1 varies with solvent composition. If a linear relationship is assumed by v_1 = 288 and 522 cm^3/mol for 1-phenyldodecane and squalane, respectively, $v_1 = 288 + 234\phi_{sql}$ cm^3/mol is estimated for binary mixed solvents. As summarized in Figure 4.8b, χ decreases with increasing temperature, following the empirical relation $\chi = A/T + B$, where A is the enthalpic and B is the entropic part. The slope of χ vs $1/T$ was observed to be a weak function of solvent composition in this relatively narrow composition range, while the intercept showed appreciable changes due to different excess entropy of mixing.

Considering the uncertainty in extrapolation of χ vs solvent composition, optical transmittance experiments were performed to measure cloud points of PS solutions in squalane, and thus to determine χ between PS and pure squalane. A lower molecular weight PS (M_n = 1.3 kg/mol, M_w/M_n = 1.1) was used to obtain accessible cloud points. Figure 4.9a displays the temperature dependent transmittance of PS solutions. The transmittance showed a sudden when the solution phase separated. The cloud point was defined as the temperature at which the transmittance dropped to 80% of the transmittance of the one phase solution. Figure 4.9b summarizes cloud points of PS solutions at different PS volume fractions (ϕ_{PS}), ranging from 0.04 to 0.8. The black line was the coexistence curve calculated by Flory-Huggins theory, with two adjustable parameters (i.e., A and B) in χ, assuming $\chi = A/T + B$. Here the reference volume is $v_0 = v_2$ = 100 cm^3/mol, and N_1 = 5.2 and N_2 =12.5 are volumetric degrees of polymerization for squalane and 1.3 kg/mol PS, respectively. As shown in Figure 4.9b, $\chi = 287/T - 0.517$

gives the best fit. Therefore, $\chi = 0.32$ between PS and squalane at 70 ºC, with $v_0 = v_2 =$ 100 cm^3/mol, i.e., $\chi' = 1.67$ if converted by $v_0 = v_1 = 522$ cm^3/mol. This large quantity suggests the strong incompatibility between PS core blocks and the solvent, driving the segregation of PS blocks into micelle cores.

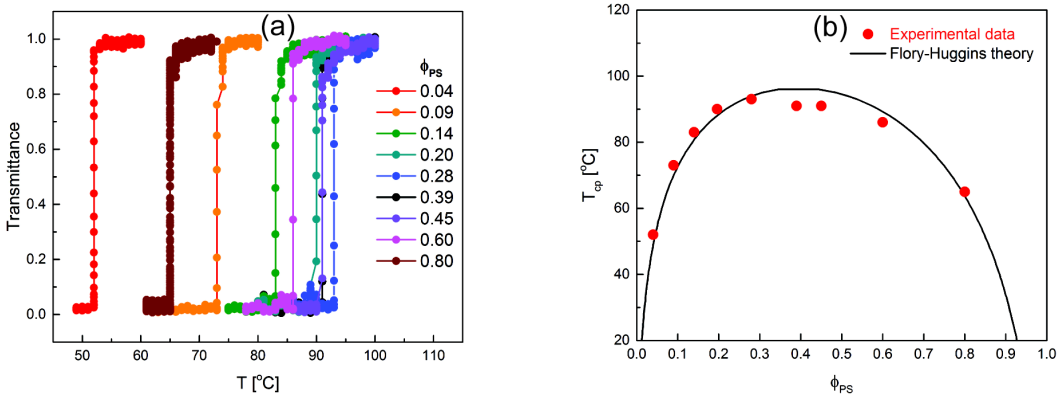

Figure 4.9 (a) Temperature dependent transmittance of PS solutions in squalane at different PS volume fractions, and (b) cloud points and coexistence curve calculated by Flory-Huggins theory with $\chi = 287/T - 0.517$.

Table 4.5 Enthalpic Interactions between the Core Block and Solvent

Micelle systems	χ' ($v_0 = v_2$)	χ ($v_0 = v_2$)	$a(\chi - v_2/v_1)\langle N_{core}\rangle$	$\alpha f(\chi)\langle N_{core}\rangle$
SEP 42-64 micelles in				
50/50 vol% phd/sql	1.2_4	0.23_8	$5._4$	$9._6$
25/75 vol% phd/sql	1.4_6	0.27_9	$15._1$	$17._8$
0/100 vol% phd/sql	1.6_7	0.32_0	$25._0$	$22._0$
SEP 26-70 micelles in				
25/75 vol% phd/sql	1.4_6	0.27_9	$9._3$	$11._7$
0/100 vol% phd/sql	1.6_7	0.32_0	$15._5$	$15._0$
Note that $a = 0.58$ gives best fit between $a(\chi - v_2/v_1)\langle N_{core}\rangle$ and $\alpha f(\chi)\langle N_{core}\rangle$				

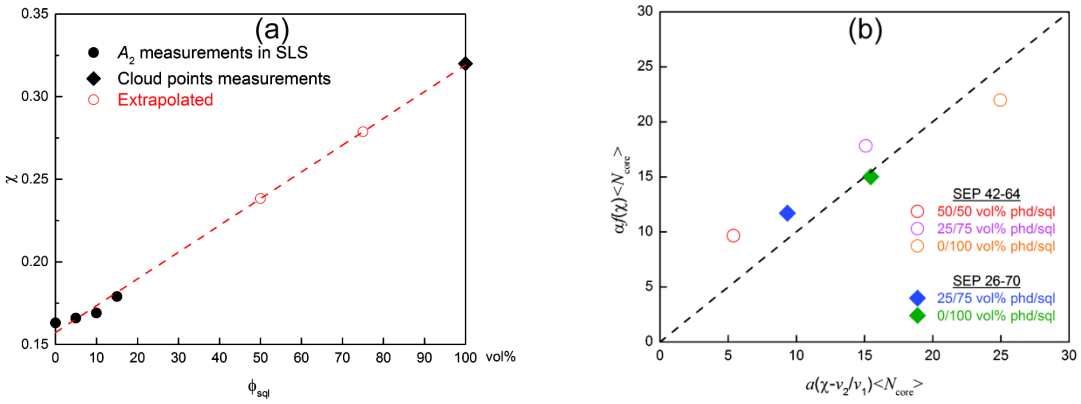

Figure 4.10 (a) χ values (black circles and diamond) between PS and binary mixed solvents as a function of composition at 70 ºC, and extrapolated values at ϕ_{sql} = 50, and 75 vol% (red circles), and (b) enthalpy penalty of chain expulsion for SEP micelles in binary mixed solvents, comparing the fitted results from TR-SANS ($\alpha f(\chi)<N_{core}>$) and calculated values by Flory-Huggins theory ($a(\chi - v_2/v_1)<N_{core}>$).

Figure 4.10a displays χ between PS and binary mixed solvents of various ϕ_{sql} at 70 ºC, where the data of ϕ_{sql} = 0, 5, 10, and 15 vol% were determined from A_2 measurements in SLS, ϕ_{sql} = 100 vol% was determined by cloud points measurements, and ϕ_{sql} = 50, and 75 vol% were obtained from the linear fitting between χ and ϕ_{sql}. We assume that the molecular weight dependence of χ is negligible in the range of 26 – 42 kg/mol. Hoarforst and coworkers showed that χ between PnBMA and the ionic liquid mixtures of [BMIM][TFSI] and [EMIM][TFSI] was almost constant when varying the molecular weight of PnBMA from 25 to 115 kg/mol.[53]

$$\Delta E / kT = a\left(\chi - \frac{v_2}{v_1}\right)N_{core} \qquad (v_0 = v_2) \qquad (4.9)$$

Ma and Lodge[32] derived the energy barrier of chain expulsion by the free energy difference (ΔE) between the core block within the micelle cores and in the solvent from Flory-Huggins theory, as given by eqn 4.9, where $v_0 = v_2$ and a is a constant. In their description, the micelle solution was treated as a two-phase system that is under equilibrium, with a polymer-rich phase within the micelle cores and a solvent-rich phase outside. For simplicity, the entropic contribution of the corona blocks was neglected in the derivation. Therefore, ΔE purely represents the enthalpic penalty from unfavorable core block monomer–solvent contacts. Figure 4.9b shows the enthalpy penalty of chain expulsion for SEP micelles in binary mixed solvents. The fitted results from TR-SANS (i.e., $\alpha f(\chi)<N_{core}>$) agree with the calculated values within 4 kT difference, i.e., $a(\chi - v_2/v_1)<N_{core}>$, where $a = 0.58$, $v_1 = 463.5$ cm^3/mol and $v_2 = 100$ cm^3/mol were used in the calculation. The validation of this expression is independent on molecular characteristics for two SEP block copolymers differing $<N_{core}>$ by a factor of 1.6.

A relatively big difference in fitted vs calculated values (5.4 vs 9.6) was noted for the 50/50 vol% phd/sql micelle system in Table 4.5. This discrepancy is attributed to the two strict assumptions in the derivation of eqn 4.9, that the solvent fraction in the core is close to zero, and that polymer fraction in the solvent is negligible. They are good assumptions for SEP micelles in pure squalane, where the micelle core is dry[20] and the CMC is estimated to be as low as 10^{-6} g/mL.[12] However, about 21 vol% solvent remain within SEP micelle cores in binary mixed solvent containing 50 vol% squalane, as shown in Table 4.3. Zhao et al. reported roughly 10 vol% solvent fraction in the core of PnBMA-PMMA micelles in the ionic liquid [EMIM][TFSI].[54] More solvent will penetrate into the core if χ between the core block and solvent is further reduced. Similarly, the significant drop in the CMT of SEP micelles reflects an increase of CMC in less selective solvents. So it might be invalid to neglect the polymer concentration in the solvent for SEP 42-64 micelles in 50/50 vol% phd/sql, which potentially causing the deviation from the theory.

In this case where χ is not large enough, a more complicated χ-dependent function is probably needed to account for the offset.

4.4 Summary

The chain exchange kinetics of SEP block copolymer micelles was investigated in pure squalane and binary solvent mixtures of squalane and 1-phenyldodecane by TR-SANS. The variation of solvent composition significantly influences the kinetics of chain exchange between micelles, where 5 orders of magnitude faster kinetics was observed when mixing squalane with only 25 vol% 1-phenyldodecane. This acceleration in the kinetics is attributed to two primary factors: (i) faster motion of core blocks in the core as more solvent penetrates into the core, serving as plasticizer; and (ii) reduced energy barrier of chain expulsion due to the higher solubility between the core block and solvent. By fitting the TR-SANS data to a theoretical model, the enthalpic penalty of chain expulsion was determined for SEP micelles in various binary mixed solvents, reflecting the change of Flory-Huggins interaction parameter χ between the core block and solvent. Alternatively, Ma and Lodge proposed a χ-dependent function for this energy barrier in a strong segregated micelle system by the Flory-Huggins theory. With a direct measurement of χ between the PS core block and solvent using SLS, the theoretically predicted values of activation energy agree with the experimental results obtained from TR-SANS. In summary, this work quantifies the role of χ in kinetics of chain exchange for an UCMT micelle system, and indicates the universality of this χ-dependent function for the activation energy, regardless of the thermodynamics and molecular characteristics of block copolymers. This potentially provides insights in selecting an appropriate solvent for design of micelles.

4.5 References

[1] Lazzari, M.; López-Quintela, M. A. Block Copolymers as a Tool for Nanomaterial Fabrication. *Adv. Mater*. **2003**, *15*, 1583−1594.

[2] Glass, R.; Möller, M.; Spatz, J. P. Block Copolymer Micelle Nanolithography. *Nanotechnology* **2003**, *14*, 1153−1160.

[3] Hamley, I. W. Nanostructure Fabrication using Block Copolymers. *Nanotechnology* **2003**, *14*, 39−54.

[4] Jeong, B.; Bae, Y. H.; Lee, D. S.; Kim, S. W. Biodegradable Block Copolymers as Injectable Drug-Delivery Systems. *Nature* **1997**, *388*, 860−862.

[5] Li, Z.; Johnson L. M.; Ricarte R. G.; Yao, L. J.; Hillmyer M. A.; Bates, F. S.; Lodge, T. P. Enhanced Performance of Blended Polymer Excipients in Delivering a Hydrophobic Drug through the Synergistic Action of Micelles and HPMCAS. *Langmuir* **2017**, *33*, 2837−2848.

[6] Li, Z.; Lenk T. I.; Yao, L. J.; Bates, F. S.; Lodge, T. P. Maintaining Hydrophobic Drug Supersaturation in a Micelle Corona Reservoir. *Macromolecules*, **2018**, *51*, 540–551.

[7] Anderson, W. Block Copolymers as Viscosity Index Improvers for Lubricating Oils. US3763044A, **1973**.

[8] de Gennes, P. G. Conformations of Polymers Attached to an Interface. *Macromolecules* **1980**, *13*, 1069–1075.

[9] Halperin, A.; Tirrell, M.; Lodge, T. P. Tethered Chains in Polymer Microstuctures. *Adv. Polym. Sci.* **1992**, *100*, 31–71.

[10] Daoud, M.; Cotton, J. P. Star Shaped Polymers: A Model for the Conformation and its Concentration Dependence. *J. Phys. France* **1982**, *43*, 531–538.

[11] Halperin, A. Polymeric Micelles: A Star Model. *Macromolecules* **1987**, *20*, 2943–2946.

[12] Quintana, J. R.; Villacampa, M.; Muñoz, M.; Andrio, A.; Katime, I. A. Micellization of a Polystyrene-*block*-poly(ethylene/propylene) Copolymer in *n*-Alkanes. 1. Thermodynamic Study. *Macromolecules* **1992**, *25*, 3125–3128.

[13] Quintana, J. R.; Villacampa, M.; Andrio, A.; Muñoz, M.; Katime, I. A. Micellization of a Polystyrene-*block*-poly(ethylene/propylene) Copolymer in *n*-Alkanes. 2. Structural Study. *Macromolecules* **1992**, *25*, 3129–3136.

[14] Quintana, J. R.; Villacampa, M.; Katime, I. A. Micellization of a Polystyrene-*b*-poly(ethylene/propylene) Block Copolymer in *n*-Dodecane/1.4-Dioxane Mixtures. 1. Thermodynamics of Micellization. *Macromolecules* **1993**, *26*, 601–605.

[15] Quintana, J. R.; Villacampa, M.; Katime, I. A. Micellization of a Polystyrene-*b*-poly(ethylene/propylene) Block Copolymer in *n*-Dodecane/1.4-Dioxane Mixtures. 2. Structure and Dimensions of Micelles. *Macromolecules* **1993**, *26*, 606–611.

[16] Quintana, J. R.; Jáñez, M. D.; Villacampa, M.; Katime, I. Diblock Copolymer Micelles in Solvent Binary Mixtures. 1. Selective Solvent/Precipitant. *Macromolecules* **1995**, *26*, 4139–4143.

[17] Villacampa, M.; de Apodaca, E. D.; Quintana, J. R.; Katime, I. Diblock Copolymer Micelles in Solvent Binary Mixtures. 2. Selective Solvent/Good Solvent. *Macromolecules* **1995**, *26*, 4144–4149.

[18] Bang, J.; Viswanathan, K.; Lodge, T. P.; Park, M. J.; Char, K. Temperature-Dependent Micellar Structures in Poly(styrene-*b*-isoprene) Diblock Copolymer Solutions near the Critical Micelle Temperature. *J. Chem. Phys.* **2004**, *121*, 11489–11500.

[19] Bang, J.; Jain, S.; Li, Z.; Lodge, T. P.; Pedersen, J. S.; Kesselman, E.; Talmon, Y.

Sphere, Cylinder, and Vesicle Nanoaggregates in Poly(styrene-*b*-isoprene) Diblock Copolymer Solutions. *Marcomolecules* **2006**, *39*, 1199–1208.

[20] Choi, S.; Bates, F. S.; Lodge, T. P. Structure of Poly(styrene-*b*-ethylene-*alt*-propylene) Diblock Copolymer Micelles in Squalane. *J. Phys. Chem. B* **2009**, *113*, 13840–13848.

[21] Choi, S.; Lee, W. B.; Lodge, T. P.; Bates, F. S. Structure of Poly(styrene-*b*-ethylene-*alt*-propylene) Diblock Copolymer Micelles in Binary Solvent Mixtures. *J. Polym. Sci. B: Polym. Phys.* **2016**, *54*, 22–31.

[22] Dormidontova, E. E. Micellization Kinetics in Block Copolymer Solutions: Scaling Model. *Macromolecules* **1999**, *32*, 7630–7644.

[23] Haliloğlu, T.; Bahar, I.; Erman, B.; Mattice, W. L. Mechanisms of the Exchange of Diblock Copolymers between Micelles at Dynamic Equilibrium. *Macromolecules* **1996**, *29*, 4764–4771.

[24] Rharbi, Y. Fusion and Fragmentation Dynamics at Equilibrium in Triblock Copolymer Micelles. *Macromolecules* **2012**, *45*, 9823−9826.

[25] Halperin, A.; Alexander, S. Polymeric Micelles: Their Relaxation Kinetics. *Macromolecules* **1989**, *22*, 2403–2412.

[26] Halperin, A. On Micellar Exchange: The Role of the Insertion Penalty. *Macromolecules* **2011**, *44*, 5072–5074.

[27] Lund, R.; Willner, L.; Stellbrink, J.; Radulescu, A.; Richter, D. Tuning of Structure and Kinetics of Chain Exchange in Star-Like PEP-PEO Block Copolymer Micelles. *Physica B* **2004**, *350*, 909−912.

[28] Lund, R.; Willner, L.; Richter, D.; Dormidontova, E. E. Equilibrium Chain Exchange Kinetics of Diblock Copolymer Micelles: Tuning and Logarithmic Relaxation. *Macromolecules* **2006**, *39*, 4566–4575.

[29] Lund, R.; Willner, L.; Stellbrink, J.; Lindner, P.; Richter, D. Logarithmic Chain-Exchange Kinetics of Diblock Copolymer Micelles. *Phys. Rev. Lett.* **2006**, *96*, 068302.

[30] Choi, S.; Lodge, T. P.; Bates, F. S. Mechanism of Molecular Exchange in Diblock Copolymer Micelles: Hypersensitivity to Core Chain Length. *Phys. Rev. Lett.* **2010**, *104*, 047802.

[31] Li, Z.; Dormidontova, E. E. Equilibrium Chain Exchange Kinetics in Block Copolymer Micelle Solutions by Dissipative Particle Dynamics Simulations. *Soft Matter* **2011**, *7*, 4179–4188.

[32] Ma Y.; Lodge, T. P. Chain Exchange Kinetics in Diblock Copolymer Micelles in Ionic Liquids: The Role of χ. *Macromolecules* **2016**, *49*, 9542−9552.

[33] Lu, J.; Choi, S.; Bates, F. S.; Lodge, T. P. Molecular Exchange in Diblock Copolymer Micelles: Bimodal Distribution in Core-Block Molecular Weights. *ACS Macro Lett.* **2012**, *1*, 982−985.

[34] Lu, J.; Bates, F. S.; Lodge, T. P. Remarkable Effect of Molecular Architecture on Chain Exchange in Triblock Copolymer Micelles. *Macromolecules* **2015**, *48*, 2667−2676.

[35] Lu, J.; Bates, F. S.; Lodge, T. P. Addition of Corona Block Homopolymer Retards Chain Exchange in Solutions of Block Copolymer Micelles. *Macromolecules* **2016**, *49*, 1405−1413.

[36] Lai, C.; Russel, W. B.; Register, R. A. Phase Behavior of Styrene-Isoprene Diblock Copolymers in Strongly Selective Solvents. *Macromolecules* **2002**, *35*, 841–849.

[37] Hiemenz, P. C.; Lodge, T. P. *Polymer Chemistry* (*2nd Ed.*), p492–495, Boca Raton, Florida: CRC Press **2007**.

[38] Richert, R.; Duvvuri, K.; Duong, L.-T. Dynamics of Glass-Forming Liquids. VII. Dielectric Relaxation of Supercooled *tris*-Naphthylbenzene, Squalane, and Decahydroisoquinoline. *J. Chem. Phys.* **2003**, *118*, 1828–1836.

[39] Hecksher, T.; Olsen, N. B.; Dyre, J. C. Model for the Alpha and Beta Shear Mechanical Properties of Supercooled Liquids and its Comparison to Squalane Data. *J. Chem. Phys.* **2017**, *146*, 154504.

[40] Milhet, M.; Pauly, J.; Coutinho, J. A.P.; Daridon, J.-L. Solid–Liquid Equilibria under High Pressure of Nine Pure *n*-Alkylbenzenes. *J. Chem. Eng. Data* **2008,** *53,* 233–237.

[41] Fox, T. G.; Flory, P. J. The Glass Temperature and Related Properties of Polystyrene. Influence of Molecular Weight. *J. Polym. Sci.* **1954**, *14*, 315–319.

[42] Wang, E.; Lu, J.; Bates, F. S.; Lodge, T. P. Effect of Corona Block Length on the Structure and Chain Exchange Kinetics of Block Copolymer Micelles. *Macromolecules* **2018**, *51*, 3563–3571.

[43] Williams, M. L.; Landel, R. F.; Ferry, J. D. The Temperature Dependence of Relaxation Mechanisms in Amorphous Polymers and Other Glass-forming Liquids. *J. Am. Chem. Soc.***1955**, *77*, 3701–3707.

[44] Chapman, B. R.; Hamersky, M. W.; Milhaupt, J. M.; Kostelecky, C.; Lodge, T. P. Structure and Dynamics of Disordered Tetrablock Copolymers: Composition and Temperature Dependence of Local Friction. *Macromolecules* **1998,** *31,* 4562–4573.

[45] Bates, F. S.; Fredrickson, G. H. Block Copolymers – Designer Soft Materials. *Physics Today* **1999**, *52*, 32–38.

[46] Radulescu A.; Mathers R. T.; Coates G. W.; Richter D.; Fetters L. J. A SANS Study of the Self-Assembly in Solution of Syndiotactic Polypropylene Homopolymers, Syndiotactic Polypropylene-*block*-poly(ethylene-*co*-propylene) Diblock Copolymers, and

an Alternating Atactic-Isotactic Multisegment Polypropylene. *Macromolecules* **2004**, *37*, 6962–6971.

[47] Fetters, L. J.; Lohse, D. J.; Richter, D.; Witten, T. A.; Zirkel, A. Connection between Polymer Molecular Weight, Density, Chain Dimensions, and Melt Viscoelastic Properties. *Macromolecules* **1994**, *27*, 4639–4647.

[48] Pedersen, J. S.; Gerstenberg, M. C. Scattering Form Factor of Block Copolymer Micelles. *Macromolecules* **1996**, *29*, 1363–1365.

[49] Pedersen, J. S.; Hamley, I. W.; Ryu, C. Y.; Lodge, T. P. Contrast Variation Small-Angle Neutron Scattering Study of the Structure of Block Copolymer Micelles in a Slightly Selective Solvent at Semidilute Concentrations. *Macromolecules* **2000**, *33*, 542–550.

[50] Pedersen, J. S. Structure Factors Effects in Small-Angle Scattering from Block Copolymer Micelles and Star Polymers. *J. Chem. Phys.* **2001**, *114*, 2839–2846.

[51] Pedersen, J. S.; Svaneborg, C. Scattering from Block Copolymer Micelles. *Curr. Opin. Colloid Interface Sci.* **2002**, *7*, 158–166.

[52] Pedersen, J. S.; Svaneborg, C.; Almdal, K.; Hamley, I. W.; Young, R. N. A Small-Angle Neutron and X-ray Contrast Variation Scattering Study of the Structure of Block Copolymer Micelles: Corona Shape and Excluded Volume Interactions. *Macromolecules* **2003**, *36*, 416–433.

[53] Hoarfrost, M. L.; He, Y.; Lodge, T. P. Lower Critical Solution Temperature Phase Behavior of Poly(n-butyl methacrylate) in Ionic Liquid Mixtures. *Macromolecules* **2013**, *46*, 9464−9472.

[54] Zhao, D.; Ma, Y.; Wang, E.; Lodge, T. P. Micellization of Binary Diblock Co-polymer Mixtures in an Ionic Liquid. *Macromolecules* **2019**, *52*, 4729−4738.

Chapter V.
Effect of Corona Block Length Asymmetry on Structure and Chain Exchange Kinetics in Triblock Copolymer Micelles

5.1 Introduction

Self-assembly of block copolymer (BCP) micelles has attracted attention in emerging technologies such as nanolithography,[1-3] drug delivery[4-6] and gene therapeutics.[7-10] Understanding the mechanism of chain exchange is crucial to properly control desirable structures of BCP micelles at equilibrium or in non-equlibrium states.

A variety of theories,[11-13] simulations,[14-18] and experiments[19-23] have been conducted to study chain exchange kinetics of BCP micelles, particularly on AB diblock copolymer micelles where A is the core-forming block and B is the corona block. The rate of chain exchange in micelles formed by poly(styrene)-*b*-poly(ethylene-*alt*-propylene) (PS-PEP, or SEP) in squalane was observed to be four orders of magnitude slower with the PS core block length increasing by only a factor of 1.6.[24] This significant retarding effect was attributed to a higher enthalpic penalty of extracting the core block from the core into corona/solvent matrix. On the other hand, two orders of magnitude faster kinetics of chain exchange was reported for PS-PEP micelles when the corona block length increased four times at constant core block length,[25] although this is relatively less significant than the influence of core block length. This effect was attributed to the PEP corona block accelerating the kinetics because of entropic gain from the relief of corona chain stretching upon chain expulsion.

Despite extensive studies on AB diblock copolymer micelles, the diversity of molecular architectures such as BAB triblock copolymer micelles with two corona blocks

has not been thoroughly explored in terms of chain exchange kinetics. Lund and coworkers first investigated the chain exchange kinetics of a symmetric poly(styrene)-*b*-(butadiene)-*b*-poly(styrene) (PB-PS-PB) triblock copolymer micelle, and reported a 10 times slower exchange rate compared to a PS-PB diblock micelle in *n*-alkane solvents that favor the PB blocks.[26] Since the triblock had double the molecular weight of the diblock with the same composition, the kinetics of the triblock micelle was primarily decelerated due to pulling out a twice longer core block. This was supported by Prhashanna and Chen's simulation result,[27] where slower kinetics was observed with an increase of the core block length in a series of symmetric BAB triblocks. Recently, Lu et al. found that a symmetric PEP-PS-PEP triblock copolymer with similar core block length but an additional PEP corona block exhibited three orders of magnitude faster rate than the equivalent PS-PEP diblock.[28] DPD simulations by Peters and Lodge also revealed faster exchange kinetics in symmetric and asymmetric B_1AB_2 triblocks than in the AB diblock analogs, where A is the core block and B is the corona block, and the B_1 and B_2 corona blocks are a different length with $B_1 + B_2 = B$.[29] One argument was based on the fact that PEP corona block speeds up the kinetics in PS-PEP diblock micelles. The presence of two corona blocks in the PEP-PS-PEP triblock micelle leads to a higher graft density of corona blocks at the interface, and thus stronger corona chain stretching than the diblock, which facilitates the chain expulsion from a crowded corona environment into the solvent. In addition, core blocks adopt loop conformations in the core of BAB-type triblock micelles, which further reduces the energy barrier by increasing chain conformations when the core block is ejected.

To explore this issue further deeply, this work systematically investigates the chain exchange kinetics of PEP-PS-PEP' (EPSEP') triblock micelles in squalane using time-resolved small-angle neutron scattering (TR-SANS), where PEP and PEP' have different

molecular weights, while the PS core block molecular weight ≈ 26 kg/mol and overall corona block molecular weight (PEP + PEP') ≈ 70 kg/mol are held constant. The TR-SANS results experimentally elucidate the effect of corona block length asymmetry on chain exchange kinetics in EPSEP' triblock micelles for the first time, and are compared with previous results from a SEP diblock with same core and corona block lengths, and a symmetric EPSEP triblock with two longer corona blocks.

5.2 Materials

Two asymmetric EPSEP' and one symmetric EPSEP triblock copolymers were prepared by sequential anionic polymerization of 1,4-poly(isoprene)-*b*-poly(styrene)-*b*-1,4-poly(isoprene) (ISI') precursors, and followed by selective saturation of the polyisoprene (PI) block using a homogenous Ni/Al catalyst under 400 psi deuterium D_2. We note that, in preparation of asymmetric ISI' triblocks, the shorter PI block was first polymerized, then followed by the midblock, and finally the longer PI' block with the same type of monomer as the first block. The average repeat unit of PEP after deuteration is $C_5D_{2.3}H_{7.7}$, where $D_{2.3}$ results from D_2 saturation and a small extent of H/D exchange. This partial deuteration of PEP blocks reduces the scattering from PEP corona blocks in TR-SANS experiments, see below. Since TR-SANS experiments require a pair of protonated and deuterated polymers, selectively deuterated analogs, i.e., EPdSEP' triblock copolymers, were synthesized via the same protocol except using perdeuterated styrene (C_8D_8, purchased from Polymer Source, Inc.) to grow dPS midblocks.

The molecular weights and molecular weight distributions of the synthesized polymers were determined by size exclusion chromatography using a refractive index detector (SEC-RI), and another SEC instrument equipped with both RI and a multi-angle light scattering detector (SEC-MALS), and proton nuclear magnetic resonance spectroscopy (^{1}H-NMR). Figure 5.1 displays SEC traces of three pairs of EPSEP' and

EPdSEP' triblock copolymers recorded by the RI detector. A small bump (≈ 1 wt% by the peak area in SEC trace) was observed at earlier elution time than the primary peak, which was attributed to chain coupling during termination of polyanions. Also, a small fraction (≈ 2 wt%) of SEP diblock and PI homopolymer is present in the sample due to spurious termination during the anionic polymerization.

Table 5.1 Polymer Characteristics

Polymers	$M_{n,\,PEP}$ (kg/mol) [a]	$M_{n,\,PS}$ (kg/mol) [b]	$M_{n,\,PEP'}$ (kg/mol) [b]	M_w/M_n [a]	r
SEP 26-70 [c]	–	26	70	1.04	0
dSEP 29-71 [c]	–	29	71	1.10	0
EPSEP' 8-26-62	8	26	62	1.05	0.13
EPdSEP' 8-27-60	8	27	60	1.05	0.13
EPSEP' 15-28-52	15	28	52	1.04	0.29
EPdSEP' 15-28-55	15	28	55	1.03	0.27
EPSEP 30-24-30	30	24	30	1.07	1
EPdSEP 33-26-33	33	26	33	1.07	1
EPSEP 72-24-72 [d]	72	24	72	1.06	1
EPdSEP 67-24-67 [d]	67	24	67	1.06	1

Here, the molecular weights of polymers were converted from those of unsaturated ISI'and IdSI' triblock precursors that were measured by SEC and ^{1}H-NMR; M_n of PEP blocks were calculated from the corresponding precursor PI blocks in precursors assuming 100% saturation.

[a] The molecular weight of the first block PI and the dispersity of final product EPSEP' were determined by two SEC instruments separately: SEC-RI and SEC-MALS.

[b] The molecular weights of the second and third block were determined by ^{1}H-NMR spectroscopy and confirmed by SEC-MALS.

[c,d] These polymers were reproduced from (c) reference 24 and (d) reference 28.

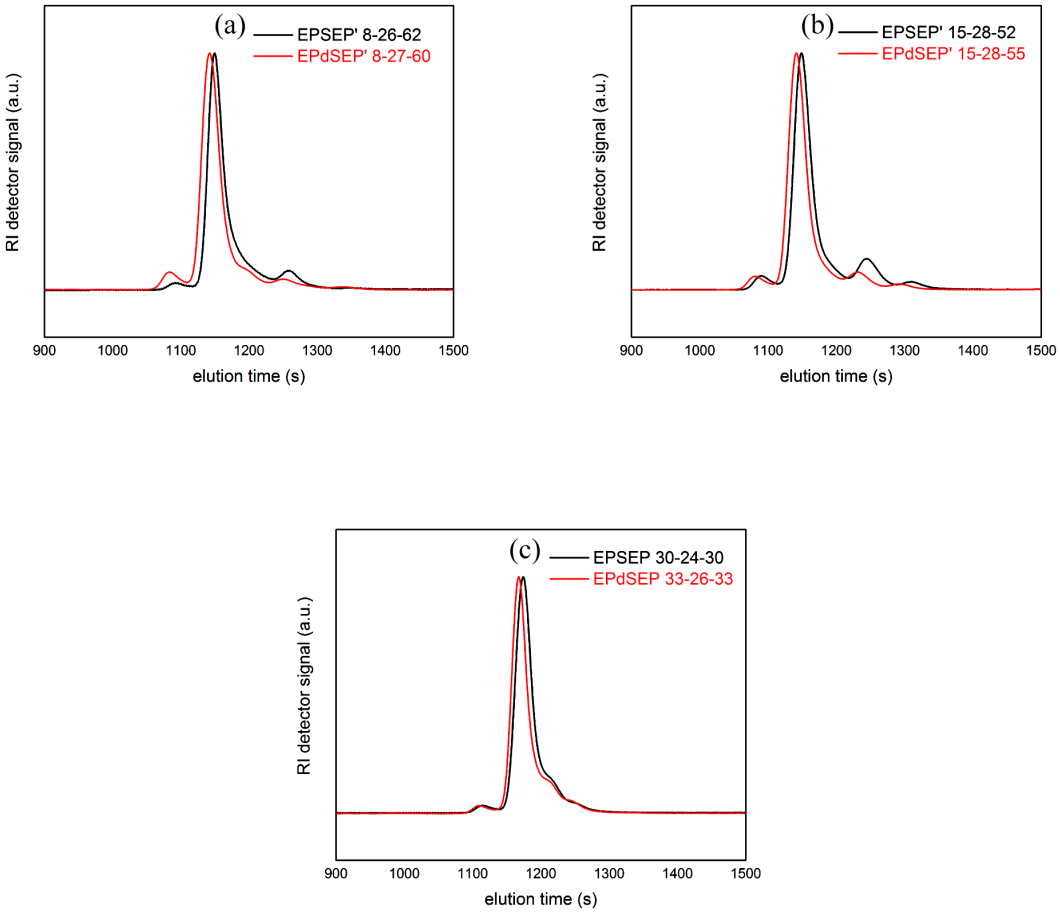

Figure 5.1 SEC traces of (a) EPSEP' 8-26-62 and EPdSEP 8-27-60, (b) EPSEP' 15-28-52 and EPdSEP 15-28-55, and (c) EPSEP 30-24-30 and EPdSEP 33-26-33 triblock copolymers

All polymer characteristics are summarized in Table 5.1, where the nomenclature of each polymer refers to the block molecular weights. For example, EPSEP' 8-26-62 indicates $M_n \approx 8$, 26, and 62 kg/mol for the shorter PEP block, PS midblock and the other relatively longer PEP block, respectively. Characteristics of SEP 26-70 and EPSEP 72-24-72 were reported in previous work.[24,28] For other EPSEP' triblocks, the molecular weights of the PS block and overall PEP + PEP' blocks are almost the same (≈ 26 kg/mol

for PS and ≈ 70 kg/mol for PEP + PEP', within 10% variation). The corona asymmetry parameter *r*, defined as the ratio of the shorter PEP over the longer PEP', varies from 0.13 for the most asymmetric EPSEP' 8-25-62 triblock to 1 for the symmetric EPSEP 30-24-30 triblock. The SEP 26-70 diblock can be considered as an extremely asymmetric triblock where one PEP block is infinitely short. Another symmetric EPSEP 72-24-72 triblock is a good comparison with EPSEP 30-24-30, to isolate the corona block length effect.

5.3 Results and Discussions

5.3.1 Structure and Thermodynamic Properties

The weight average molecular weights of SEP diblock and EPSEP' triblock micelles ($M_{w,mic}$) were determined by static light scattering (SLS) in dilute solution. Dividing by the weight average molecular weight of one polymer chain ($M_{w,p}$), the average aggregation number of chains within a micelle (N_{agg}) is obtained, i.e., $N_{agg} = M_{w,mic}/M_{w,p}$. A series of micelle solutions with concentrations ranging from 1.9 mg/mL to 9.5 mg/mL (≈ 1 vol%) were prepared by diluting the 9.5 mg/mL solution to lower concentrations at room temperature. We assume that the aggregation number does not change after dilution at room temperature, since the PS core blocks are kinetically frozen. The refractive index increment (dn/dc) values were measured using a refractometer with a red light source (≈ 650 nm), and found to be 0.047 mL/g and 0.053 mL/g for SEP 26-70 and EPSEP' 8-26-62 solutions in squalane, respectively. These values were expected from the calculation, $dn/dc \approx (n_P - n_S)/\rho_P \approx 0.052$ mL/g, where $n_P \approx 1.50$ is refractive index of block copolymer, $n_S = 1.452$ is refractive index of squalane, measured by the refractometer, and $\rho_P \approx 0.92$ g/mL is polymer density. Here n_P is estimated by weight-averaging refractive indices of PS and PEP blocks, i.e., $n_P \approx (M_{n,PS} \times n_{PS} + M_{n,PEP} \times n_{PEP})/(M_{n,PS} + M_{n,PEP}) \approx$

1.50, where $n_{PS} \approx 1.59$ and $n_{PEP} \approx 1.47$ were reproduced from a Polymer Data Handbook.[30]

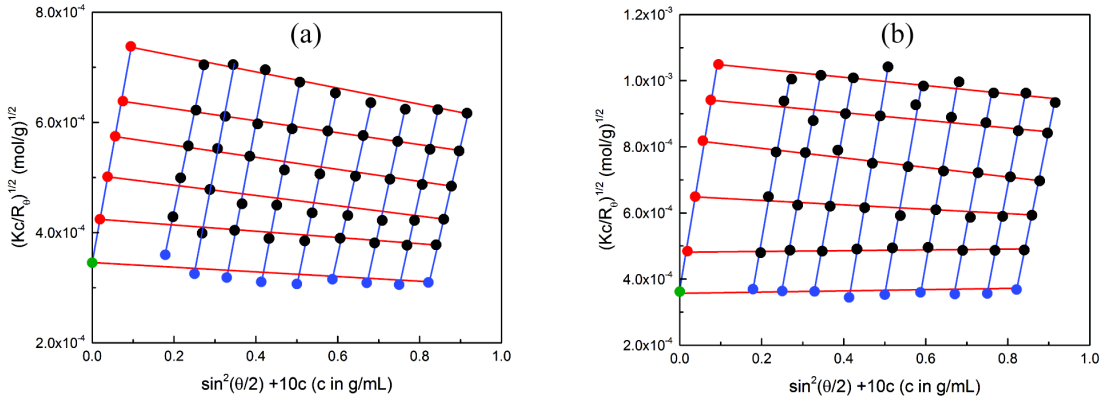

Figure 5.2 Berry plots of dilute (a) SEP 26-70 and (b) EPSEP' 8-26-62 micelles at 23 ºC

Table 5.2 Micelle Characteristics from Static Light Scattering

Micelles	A_2 (cm^{3}mol/g^2)	R_g (nm) [a]	$M_{w,mic}$ (kg/mol)	N_{agg}
SEP 26-70	1.4×10^{-5}	–	$(8.4 \pm 0.5)\times10^3$	84 ± 5
EPSEP' 8-26-62	2.7×10^{-5}	22 ± 10	$(7.6 \pm 0.3)\times10^3$	75 ± 3

[a] The uncertainty of R_g is large, so R_g cannot be extracted reliably.

Figure 5.2 shows the Berry plots of these micelle samples at multiple scattering angles 50º – 130º, giving a q range of 0.012 – 0.026 nm^{-1}. The concentration dependence of $(Kc/R_\theta)^{1/2}$ (blue lines in Figure 5.2) provides second virial coefficients (A_2) of these micelles in squalane, as listed in Table 5.2. They are positive, on order of 10^{-5} cm^{3}mol/g^2, indicating that squalane is good solvent for the micelles as expected. The radius of gyration of the micelle (R_g) cannot be extracted reliably from the angular dependence of

$(Kc/R_\theta)^{1/2}$, because $qR_g \approx 0.38 - 0.83$ is on the edge of SLS detection range, assuming micelles are hard spheres, i.e., $R_g \approx 0.77R_h \approx 32$ nm with $R_h \approx 42$ nm determined by dynamic light scattering. By double extrapolation of angle and concentration to 0, the weight average molecular weights of SEP 26-70 diblock and EPSEP' 8-26-62 triblock micelles were determined to be $(8.4 \pm 0.5)\times10^3$ kg/mol and $(7.6 \pm 0.3)\times10^3$ kg/mol, respectively. Taking $M_{w,p}$ = 100 kg/mol for SEP 26-70 and 101 kg/mol for EPSEP' 8-26-62, N_{agg} is calculated to be (84 ± 5) and (75 ± 3) for 1 vol% SEP 26-70 diblock and EPSEP' triblock micelles, respectively. In addition, N_{agg} of micelles can also be determined using small-angle neutron scattering (SANS) from the low q scattering intensity (see below).

Figure 5.3 displays the distribution of hydrodynamic radius (R_h) of dilute EPSEP' triblock micelles measured by dynamic light scattering (DLS) from room temperature to 190 ºC, where room temperature measurements were taken at angles from 60º to 120º with 15º increments and high temperature measurements were only taken at 90º. Data were interpreted by the regularized positive exponential sum (REPES) method.[31] All these triblock micelles have a narrow monomodal distribution with a mean hydrodynamic radius. For example, the asymmetric EPSEP' 8-26-62 micelles show a mean size of 38 nm, which agrees well with the value determined by the second cumulant fitting, i.e., R_h = 42 nm with dispersity (μ_2/Γ^2) = 0.06. This size is similar with the SEP 26-70 diblock micelle and the other asymmetric EPSEP' 15-28-52 triblock micelle, but larger than the symmetric EPSEP 30-24-30 triblock micelle (see Table 5.3). This is mainly because the corona block of the symmetric triblock is approximately half of the longer corona block in the asymmetric triblocks. However, another symmetric EPSEP 72-24-72 with two corona blocks of similar lengths showed a comparable hydrodynamic radius with the diblock.

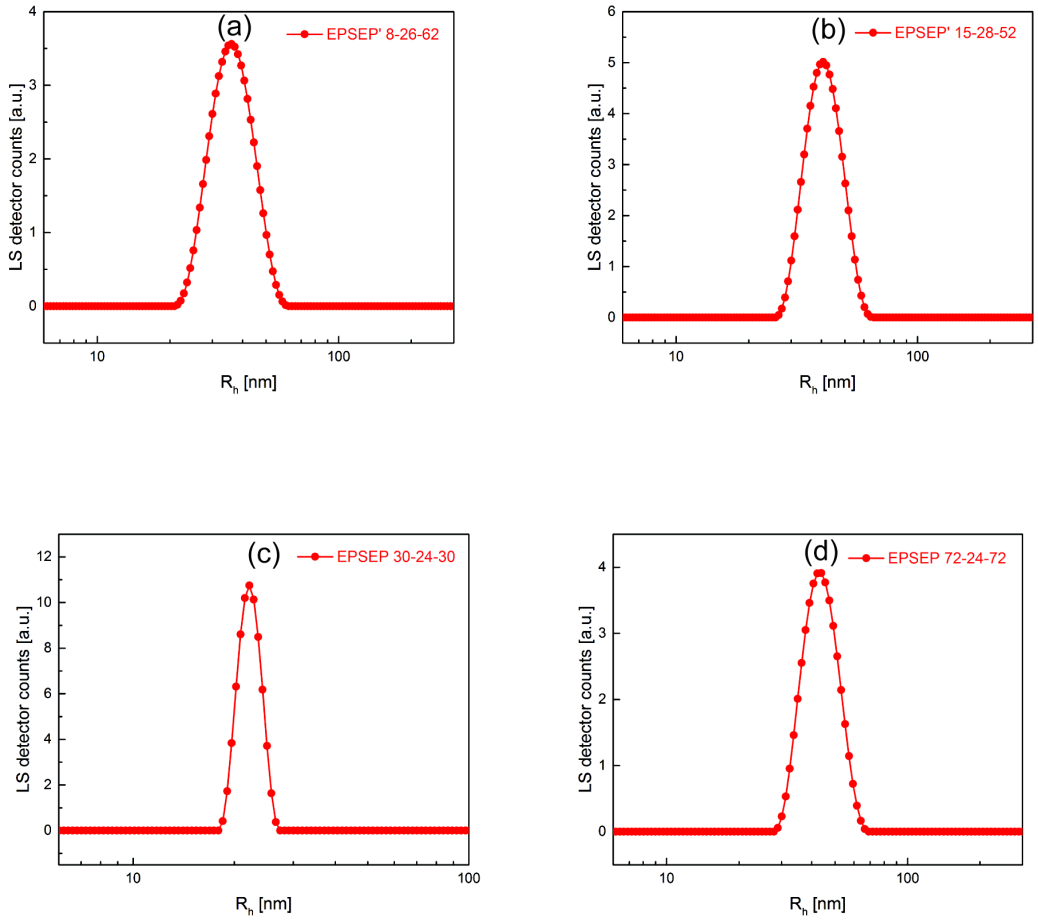

Figure 5.3 The distribution of hydrodynamic radius R_h at 90º angle of 0.5 vol% (a) EPSEP' 8-26-62, (b) EPSEP' 15-28-52, (c) EPSEP 30-24-30 and of 0.25 vol% (d) EPSEP 72-24-72 triblock micelles at 90 ºC.

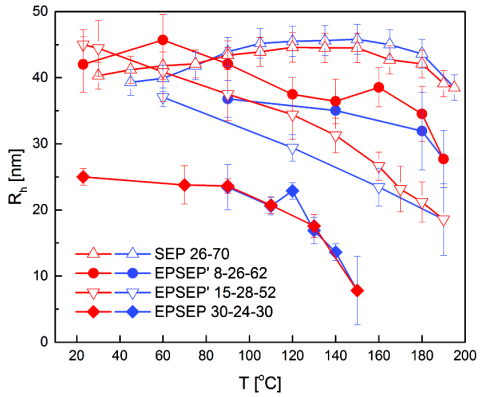

Figure 5.4 The temperature dependence of R_h for 0.5 vol% SEP diblock and EPSEP' triblock micelles upon heating (red) and cooling (blue). Data of SEP 26-70 were reproduced from previous work.[32]

Table 5.3 Micelle Hydrodynamic Radius at 90 ºC

Micelles	R_h (nm) [a]	R_h (nm) [b]	μ_2/Γ^2 [b]	T_{CMT} (ºC)
SEP 26-70 [c]	–	43	0.08	> 200
EPSEP' 8-26-62	38	42	0.10	≈ 190
EPSEP' 15-28-52	40	38	0.11	≈ 190
EPSEP 30-24-30	23	24	0.05	≈ 150
EPSEP 72-24-72	44	46	0.10	–

[a] Interpreted by REPES method
[b] Interpreted by second cumulant fitting
[c] R_h and T_{CMT} of SEP 26-70 were reported from reference 31.

As shown in Figure 5.4, R_h of SEP diblock and EPSEP' triblock micelles do not show appreciable change from room temperature to 90 ºC due to the glassy core. As temperature further increases, the micelle size decreases, reflecting the reduced interfacial tension between the core block and solvent. At the same time, a moderate fraction of solvent penetrates into the core. When the temperature is near the critical micelle temperature (T_{CMT}), a large number of polymer chains dissolve as free chains, causing a

drop in micelle size. The T_{CMT} of SEP 26-70 diblock micelles is expected to be higher than 200 ºC. The asymmetric EPSEP' 15-28-52 and 8-26-62 triblocks show comparable $T_{CMT} \approx 190$ ºC, while the symmetric EPSEP 30-24-30 triblock micelles tend to demicellize at $T_{CMT} \approx 150$ ºC. This decrease in the CMT suggests that the critical micelle concentration (CMC) increases from asymmetric to symmetric triblock micelles. Simulation results by Peters and Lodge also reported a higher unimer fraction in symmetric triblock micelle solutions than in the asymmetric triblocks.[29]

Compared to SLS and DLS, small-angle X-ray scattering (SAXS) is able to provide structural details at smaller length scales such as micelle core radius (R_{core}). Figure 5.6 displays the SAXS patterns of 1 vol% EPSEP' triblock micelles with the background subtracted at multiple temperatures from room temperature to 150 ºC. The scattering patterns show an evident spherical form factor with the first minimum at q_1, and a small structure factor peak at low q. For example, the first minimum of asymmetric EPSEP' 8-26-62 triblock micelle appeared at $q_1 = 0.051$ Å^{-1}, suggesting a core radius of 8.8 nm by the characteristic equation for the hard sphere form factor, i.e., $q_1 R_{core} = 4.49$. A hard sphere model was employed to fit the data, which describes block copolymer micelles as constructed of swollen corona chains tethered on hard spheres formed by core blocks.[33,34,35,36,37] The model gives the core radius $R_{core} = 8.8$ nm for asymmetric EPSEP' 8-26-62 triblock micelles with standard deviation of core radii $\sigma_{Rc} = 0.9$ nm, in good agreement with the estimate from hard sphere characteristic equation. Values of core radii are summarized in Table 5.4 and plotted in Figure 5.8b. The core radius of EPSEP' 15-28-52 is similar with EPSEP' 8-26-62, while that of symmetric EPSEP 30-24-30 is much smaller. As observed in R_h, the temperature dependence of R_{core} is not appreciable from room temperature to 90 ºC.

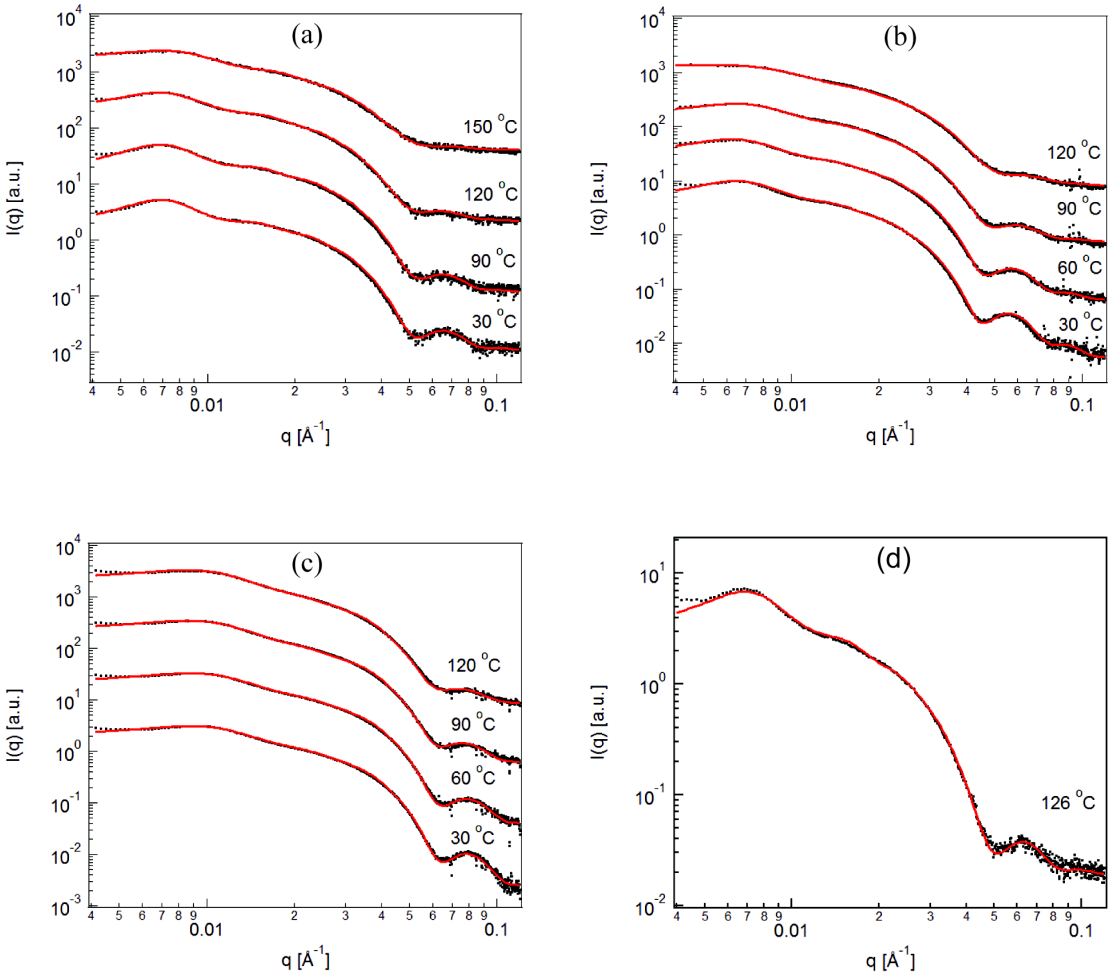

Figure 5.5 SAXS patterns and model fits of 1 vol% (a) EPSEP' 8-26-62, (b) EPSEP' 15-28-52, and (c) EPSEP 30-24-30 triblock micelles at multiple temperatures and (d) 1 vol% SEP 26-70 diblock micelle at 126 ºC. Note that data at different temperatures are vertically shifted for clarity.

Table 5.4 Micelle Core Radius from Small-Angle X-Ray Scattering

Micelles	R_{core} (nm) [a]	R_{core} (nm) [b]	σ_R (nm) [b]
SEP 26-70 at 126 ºC	9.2	9.2	0.8
EPSEP' 8-26-62 at 30 ºC	8.8	8.8	0.8
90 ºC	8.8	8.8	0.9
120 ºC	8.8	8.9	1.0
150 ºC	8.3	8.4	1.1
EPSEP' 15-28-52 at 30 ºC	10.2	10.2	0.9
60 ºC	9.8	10.0	0.9
90 ºC	9.4	9.6	1.0
120 ºC	9.2	9.1	1.2
EPSEP 30-24-30 at 30 ºC	7.5	7.3	0.7
60 ºC	7.5	7.3	0.7
90 ºC	7.6	7.5	0.8
120 ºC	7.5	7.6	0.9
EPSEP 72-24-72 at 80 ºC [d]	7.3	7.9	–

[a] Calculated by the characteristic equation for hard sphere, $q_1 R_{core} = 4.49$

[b] Fitted by the hard sphere model, where σ_R is standard deviation of core radii, and represents the overall hard sphere radius

[d] R_{core} of EPSEP 72-24-72 at 80 ºC were reported from reference 28.

Since SANS gives absolute intensities at low q, the aggregation number can be obtained from the low q scattering in SANS. Selectively deuterated dSEP 29-71 diblock and EPdSEP' 8-27-60 triblock copolymers were used to provide contrast in protonated squalane. Figure 5.7 shows the scattering patterns and model fits of dSEP diblock and EPdSEP' triblock micelles in dilute solutions, where the solvent background was subtracted. As shown in Figure 5.7, the hard sphere form factor is almost independent of concentration due to frozen cores at room temperature, where the 0.4 vol% solution was diluted from the 1 vol% solution. The fitted micelle core radii were 10.0 and 8.9 nm for

the dSEP 29-71 diblock and EPdSEP' 8-27-60 triblock micelles, respectively. These values agree with results obtained from SAXS. On the other hand, the scattering pattern of 0.4 vol% micelle solution displays a plateau at low q, whereas the 1 vol% sample shows an evident structure factor due to stronger inter-micellar interactions at higher concentration. By fitting the SANS data to the hard sphere model, the aggregation number was obtained for these micelles. For instance, N_{agg} = (71 ± 2) polymer chains per micelle was observed for 0.4 vol% EPdSEP 8-27-60, while N_{agg} = (74 ± 2) for the 1 vol% micelle solution. These values agree with the results obtained from SLS, as listed in Table 5.2.

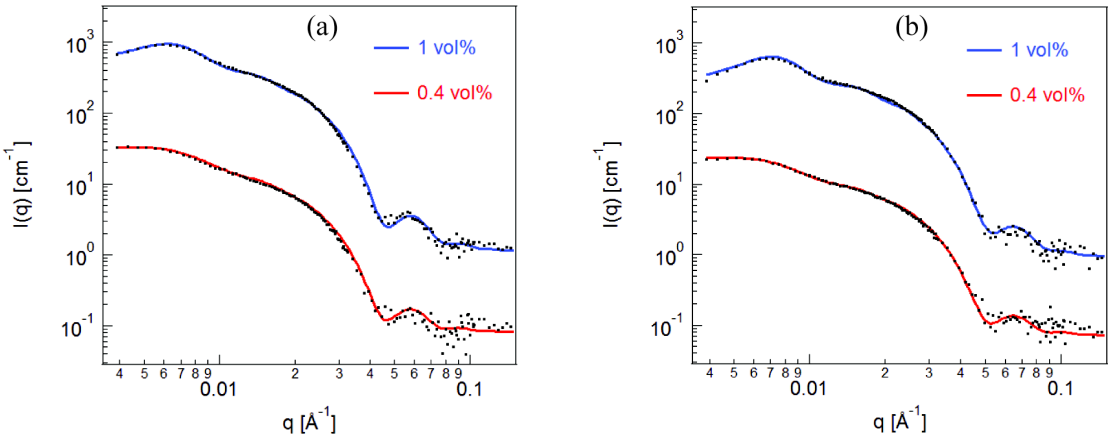

Figure 5.6 SANS patterns of dilute (a) dSEP 29-71 and (b) EPdSEP' 8-27-60 triblock micelles at 25 ºC. Data of 1 vol% samples are vertically shifted by a factor of 10.

Table 5.5 Micelle Characteristics from Small-Angle Neutron Scattering

Micelles	N_{agg} (nm)	R_{core} (nm)	σ_R (nm)
0.4 vol% dSEP 29-71	85 ± 3	10.0	0.8
1 vol% dSEP 29-71	98 ± 5	10.0	0.9
0.4 vol% EPdSEP' 8-27-60	71 ± 2	8.9	0.8
1 vol% EPdSEP' 8-27-60	74 ± 2	8.9	0.9

Table 5.6 summarizes the structural information of SEP diblock and EPSEP' triblock micelles at 90 ºC. As evidenced by DLS and SAXS, structures of EPSEP' triblock micelles do not change appreciably with temperature from 23 ºC to 90 ºC. Therefore, the aggregation numbers of SEP 26-70 and EPSEP 8-26-62 at 90 ºC are assumed the same as at room temperature where SLS and SANS were performed. The volume fraction of PS (φ_{PS}) in the core of SEP 26-70 diblock micelle is calculated by,

$$\varphi_{PS} = \frac{3N_{agg}v_{PS}}{4\pi R_{core}^3} \tag{5.1}$$

where N_{agg} = (84 ± 5) is aggregation number obtained from SLS, R_{core} = 9.2 nm is determined by SAXS, and v_{PS} = 41.3 nm^3 is the volume of 26 kg/mol PS core block[38] using 1.047 g/cm^3 for the melt density of a PS block. Thus, φ_{PS} = (1.06 ± 0.06) indicates no solvent in the core of SEP diblock at 90 ºC. φ_{PS} is estimated to be 1.07 using N_{agg} = 85 obtained from SANS, supporting this interpretation. Bang and coworkers observed dry cores for PS-PI micelles in *n*-tetradecane when the temperature is well below the T_{CMT}.[39]

We also examine the possibility of the shorter corona blocks mixed in the core of asymmetric EPSEP' 8-26-62 triblock micelle by calculating φ_{PS}. The volume of PS blocks in the core, $N_{agg}v_{PS} \approx 3.06 \times 10^3$ nm^3, matches the volume of core within 7% difference, $4\pi R_{core}^3/3 \approx 2.85 \times 10^3$ nm^3, where R_{core} = 8.8 nm characterized by SAXS, N_{agg} = 75 determined by SLS, v_{PS} = 40.8 nm^3 for the PS block in EPSEP' 8-26-62. Note that the volume of PS blocks also agrees well with $N_{agg}v_{PS} \approx 2.90 \times 10^3$ nm^3, taking N_{agg} = 71 from SANS. If the shorter PEP corona block was mixed with the core block in the core, then the volume of core and shorter corona blocks would be $N_{agg}(v_{PS} + v_{PEP}) \approx 4.16 \times 10^3$ nm^3, 1.5 times larger than the core volume, where v_{PEP} = 14.6 nm^3 is the volume of

the shorter PEP block using 0.881 g/cm^3 for density of PEP block in melts.[38] Therefore, the shorter corona block of asymmetric EPSEP' 8-26-62 is excluded from the core due to the considerable enthalpic cost. The corona of asymmetric triblock micelle is comprised of a dense layer near the interface that is occupied by the shorter corona block and inner part of the longer corona block, and a sparse layer that is filled only by the longer corona block. In this scenario, two ends of the core block must attach to the interface since they are chemically linked to two corona blocks, as illustrated in Figure 5.7. Prhashanna and Chen found that a majority of the core blocks adopted loop conformation rather than bridging across the core.[27]

Table 5.6 Summarized Micelle Characteristics at 90ºC

Micelles	N_{agg}	R_{core} (nm) [d]	R_h (nm) [e]	L_{corona} (nm)	φ_{PS}
SEP 26-70	84 ± 5, [a] 85 ± 3 [b]	9.2 ± 0.8	43 ± 2	34 ± 3	1.06 ± 0.06, [g] 1.07 ± 0.06 [h]
EPSEP' 8-26-62	75 ± 3, [a] 71 ± 2 [b]	8.8 ± 0.9	42 ± 3	33 ± 2	1.07 ± 0.07, [g] 1.04 ± 0.04 [h]
EPSEP' 15-28-52	82 ± 9 [c]	9.6 ± 1.0	38 ± 4	28 ± 3	1
EPSEP 30-24-30	47 ± 5 [c]	7.5 ± 0.8	24 ± 1	17 ± 1	1
EPSEP 72-24-72	54 [c]	7.9	46 ± 4	38 ± 4	1

Note that micelle structures are almost independent of temperature at 23 ºC – 90 ºC.

[a,b,c] The aggregation number determined by (a) SLS, (b) SANS, and (c) assuming the core contains purely PS blocks, i.e., no solvent or mixed corona blocks.

[d] Micelle core radius determined by SAXS, where the error represents the standard deviation of R_{core}. Note that R_{core} of SEP 26-70 was measured at 126 ºC, and R_{core} of EPSEP 72-24-72 at 80 ºC was reported from reference 28.

[e] Micelle hydrodynamic radius determined by DLS, where the error represents the dispersity of R_h. Data of SEP 26-70 were reproduced from reference 31.

[f] Corona layer thickness calculated by $L_{corona} = R_h - R_{core}$

[g,h] Volume fraction of PS in the core, defined by eqn 5.2, using N_{agg} obtained from (g) SLS and (h) SANS, and R_{core} obtiained from SAXS, respectively. $\varphi_{PS} = 1$ is assumed for EPSEP' 15-28-52, EPSEP 30-24-30 and EPSEP 72-24-72.

Figure 5.7 Illustration of asymmetric (left) and symmetric (right) EPSEP' triblock micelles, where blue region represents the core, the darker green for the inner corona layer, and the lighter green for outer layer.

As shown in Figure 5.8a, two asymmetric EPSEP' triblock micelles have comparable aggregation number with the diblock. However, the symmetric triblock micelle has much smaller aggregation number due to higher stretching of the corona blocks. A similar trend was observed in the core radius and hydrodynamic radius in Figure 5.8b. The corona layer thickness ($L_{corona} = R_h - R_{core}$) decreases with increasing r, as the length of longer corona block decreases from asymmetric to symmetric triblock.

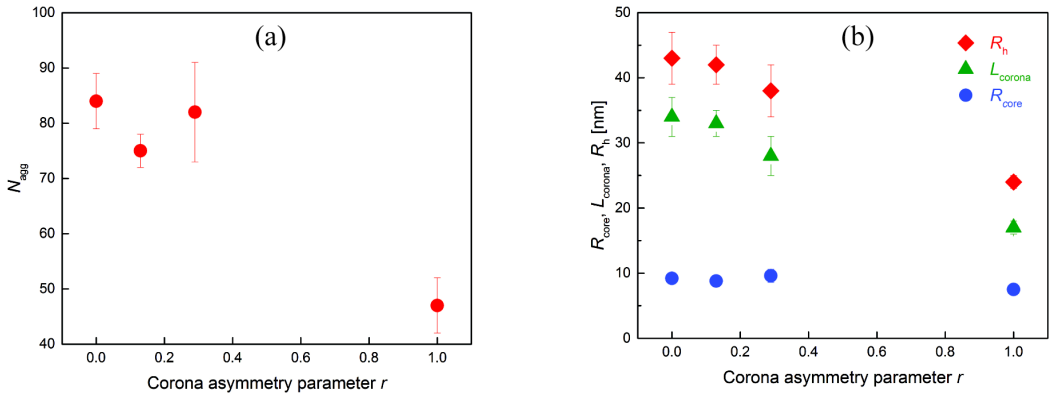

Figure 5.8 (a) The aggregation number, (b) core radius, hydrodynamic radius, and corona layer thickness of EPSEP' triblock micelles as a function of corona asymmetry parameter r.

5.3.2 Chain Exchange Kinetics

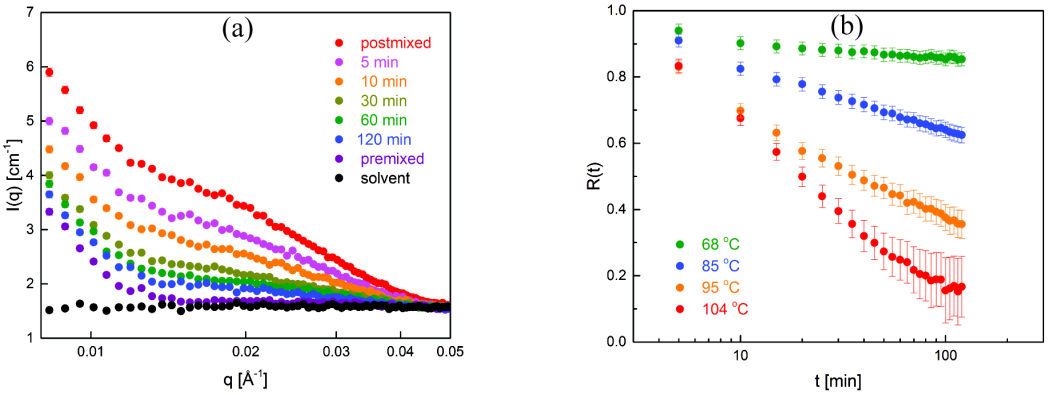

Figure 5.9 (a) The evolution of scattering intensities in EPSEP' 8-26-62 triblock micelle solutions in squalane at 95 ºC, and (b) normalized relaxation function $R(t)$ of EPSEP' 8-26-62 triblock micelle at various temperatures.

Time-resolved SANS (TR-SANS) was performed to study micelle chain exchange kinetics. Figure 5.9a displays the evolution of scattering intensities from 1 vol% asymmetric EPSEP' 8-26-62 triblock micelle solutions at 95 ºC. The postmixed sample (red) was measured at room temperature, where no chain exchange occurred. Its scattering intensity is the highest, reflecting the highest contrast between the micelle cores and the solvent at $t = 0$. As micelles undergo chain exchange, the contrast decreases, leading to decreases in intensity. The premixed sample represents the final state at $t = \infty$, where chains are completely exchanged. The scattering intensity of premixed sample (purple) matches with the solvent (black) since the contrast of mixed cores is matched with that of solvent, except that scattering from corona blocks is still present at low q (< 0.015 Å^{-1}), as the corona contrast is not matched.

A normalized relaxation function $R(t)$ is defined in eqn 5.2 to quantify the rate of chain exchange,

$$R(t) = \sqrt{\frac{I(t) - I(\infty)}{I(0) - I(\infty)}} \tag{5.2}$$

where $I(0)$, $I(t)$, $I(\infty)$ are scattering intensities at $t = 0$ (postmixed), t, and ∞ (premixed), respectively. The values of $I(0)$, $I(t)$, $I(\infty)$ are integrated over a q range of 0.01 – 0.04 $Å^{-1}$ for better statistics. $R(t)$ reflects the contrast decrease between micelle cores and solvent, which is proportional to the fraction of exchanged chains, since micelle structure does not change over time. As shown in Figure 5.9b, $R(t)$ decays more rapidly at higher temperatures, e.g., 104 ºC, indicating faster kinetics of chain exchange. Note that the error bars in the figure are propagated by eqn 5.3.

$$\delta R(t) = \sqrt{\left[\frac{\partial R(t)}{\partial I(t)} \cdot \delta I(t)\right]^2 + \left[\frac{\partial R(t)}{\partial I(\infty)} \cdot \delta I(\infty)\right]^2 + \left[\frac{\partial R(t)}{\partial I(0)} \cdot \delta I(0)\right]^2} \tag{5.3}$$

Here $\delta I(t)$, $\delta I(\infty)$, and $\delta I(0)$ are errors in $I(t)$, $I(\infty)$, and $I(0)$ from SANS, respectively, which are averaged over a q range of 0.01 – 0.04 $Å^{-1}$ as well. The propagated error $\delta R(t)$ becomes larger at higher temperatures and longer times, e.g., at 104 ºC with t = 120 minutes, where $R(t)$ is close to 0 and the derivative terms in eqn 5.3 get larger.

Applying the time–temperature superposition (tTS) method, $R(t)$ master curves of SEP diblock and EPSEP' triblock micelles are generated in Figure 5.10 with a reference temperature of 90 ºC. Data of SEP 26-70 diblocks and symmetric EPSEP 72-24-72 triblocks were adapted from references 24 and 28, respectively. Figure 5.11 shows the empirical shift factors used in the tTS method. They followed the trend line that was generated by fitting shift factors of previous studied micelle systems: $\log(a_T) = -0.0936 \times (T - 90\ ºC)$. The consistency verifies the feasibility of employing the tTS method to shift TR-SANS data of asymmetric EPSEP' triblock micelle systems.

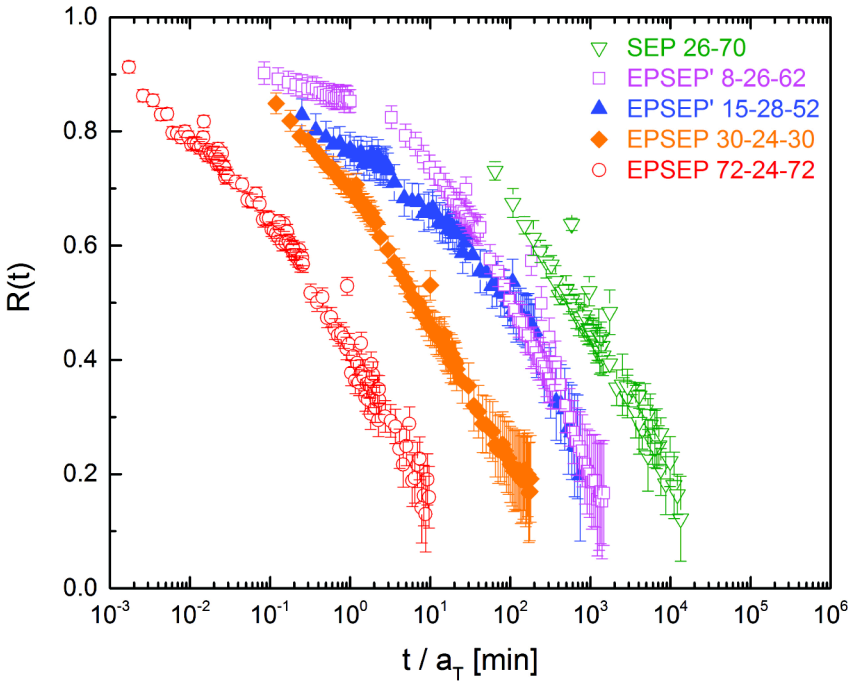

Figure 5.10 $R(t)$ master curves of 1 vol % SEP diblock and asymmetric EPSEP' and symmetric EPSEP triblock micelles at a reference temperature of 90 °C. Data of SEP 26-70 and EPSEP 72-24-72 micelles were adapted from reference 24 and 28, respectively.

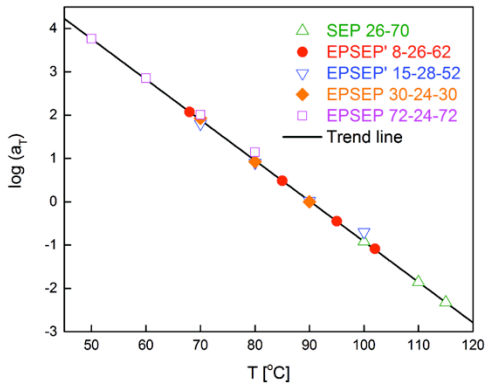

Figure 5.11 The shift factors $\log(a_T)$ as a function of temperature at a reference temperature of 90 ºC. The trend line was generated by fitting shift factors of previous studied micelle systems.[24,25,28,39-42]

As shown in Figure 5.10, the two asymmetric EPSEP' triblock micelles show comparable rates of chain exchange. Considering that the core block length of EPSEP' 15-28-52 is 10% larger than EPSEP' 8-26-62, a hypothetical EPSEP' 15-26-52 would exhibit approximately 2 – 3 times faster exchange rate. Both asymmetric EPSEP' triblocks exchanged chains approximately 10 times faster than the SEP 26-70 diblock, but 10 times slower than the symmetric EPSEP 30-24-30 triblock. Moreover, the symmetric EPSEP 72-24-72 exhibited one order of magnitude faster rate of chain exchange than EPSEP 30-24-30, where both corona blocks of EPSEP 72-24-72 are longer. Peters and Lodge reported the same trend in DPD simulations, where chain exchange kinetics was accelerated as the corona asymmetry parameter *r* increases from the diblock to asymmetric triblock, and to symmetric triblock. In the following paragraphs, we will discuss possible mechanisms to account for these observations.

Figure 5.12 Illustration of possible core block (blue chains) conformations in EPSEP' triblock micelle core: bridging (left), and looping (right). Green chains represent corona blocks that stay in the corona layer.

First, it is energetically unfavorable to drag the shorter corona block into the core when the other end of the core block is pulling out. The SLS, SAXS, and SANS results verify the exclusion of the shorter corona block from the core. Instead, the entire core block moves to the interface, and both ends of the core block cooperatively eject from the

core, as observed in simulation snapshots by Peters and Lodge.[29] Moreover, the probability that two or more than two core blocks crossover in "knots" is assumed to be negligible, since a large population of PS core blocks with average molecular weight 26 kg/mol are not entangled.

Second, the entropy gain upon expulsion of the core block is different between SEP diblock and EPSEP' triblock micelles. In SEP diblock micelles, core blocks are not stretched, behaving like a random coil in melts, $R_{core} \sim M_{PS}^{1/2}$.[32] This can also be verified by comparing the core radius with the unperturbed end-to-end distance of the core block (R_0) in melts. For the core block of SEP 26-70, R_{core} = 9.2 nm is even smaller than $R_0 = 0.0659 M_{PS}^{1/2}$ = 10.6 nm[38] with M_{PS} = 26,000 g/mol. The core stretching parameter $s_{core} = R_{core}/R_0 < 1$, indicating that core blocks are not necessarily stretched to touch the center of core. The entropy change of the core block upon chain expulsion can be neglected for SEP diblock micelle. By contrast, in EPSEP' triblock micelles, core blocks are looped to fill the space of core, while two ends are retained at the interface because they are chemically linked to two corona blocks. One limiting case is considered for asymmetric EPSEP' 8-26-62 micelles, where the core block bridges across the entire core, as illustrated in Figure 5.12. The bridging conformation of core blocks suggests a strong stretching, $s_{core} = 2R_{core}/R_0 = 1.7$, using R_{core} = 8.8 nm from SAXS and R_0 = 10.6 nm. In real practice, core blocks have higher probability of looping back on themselves to reduce core stretching, as illustrated in Figure 5.12. Yet, with two ends confined at the interface, the looped core block in EPSEP' triblock micelle core still loses some possible conformations that can be achieved by the one in a diblock. More entropy is gained upon ejecting the looped core block of triblock micelles, and thus facilitates the kinetics of chain exchange, comparing to the diblock. It was found by Peters and Lodge that a linear B_1AB_2 triblock with core blocks looped exhibited more rapid exchange kinetics than a

branched AB_1B_2, where A is the core block, and B_1 and B_2 are corona blocks of different lengths.[29] Prhashanna and Dormidontova designed a tadpole-shaped diblock copolymer that contains a loop-shaped core block and a linear corona block, and reported faster chain exchange in the tadpole-shaped diblock micelle than in the linear diblock micelle.[44]

Table 5.7 Interfacial Area, Graft Density and Stretching of Corona Blocks

Micelles	A_{int} (nm^2) [a]	σ (nm^{-2}) [b]	s_{corona} [c]	$\Delta S_{corona}/k$ [d]
SEP 26-70	13	0.07	1.6_5	4.1
EPSEP' 8-26-62	6.5	0.14	1.7_0	4.4
EPSEP' 15-28-52	7.1	0.14	1.5_8	3.8
EPSEP 30-24-30	7.5	0.13	1.2_7	4.9
EPSEP 72-24-72	7.3	0.14	1.8_8	10.6

[a] Interfacial area per junction: $A_{int} = 4\pi R_{core}^2/N_{agg}$ for diblock micelles, while $A_{int} = 2\pi R_{core}^2/N_{agg}$ for triblock micelles.
[b] Graft density of corona chains at interface: $\sigma = 1/A_{int}$
[c] Stretching of corona block, $s_{corona} = R_g/R_{g,0}$, where $R_g = L_{corona}/2$ is the radius of gyration of the longer corona block in the micelle, and $R_{g,0} = 0.0392 M_{PEP,}^{1/2}$ (in nm) represents unperturbed chain length.
[d] Entropy gain from the relief of corona chain stretching, assuming corona chains follow Gaussian statistics: $\Delta S_{corona}/k = 3s_{corona}^2/2$ for diblock and asymmetric triblock micelles; $\Delta S_{corona}/k = 3s_{corona}^2$ for symmetric triblock micelles.

In addition to the entropy gain from core blocks, stretching of corona blocks plays a significant role in EPSEP' triblock chain exchange, as it does for SEP diblock micelles. Comparing to the diblock, the interfacial area decreases from 13 to 7.5 nm^2 per junction in EPSEP' triblock micelles, since two corona chains are tethered on the interface per chain. The graft density of corona chains (σ) is doubled from 0.07 to 0.14 nm^{-2}, as listed

in Table 5.7. σ does not vary with the corona asymmetry r, implying high graft density for all EPSEP' triblock micelles. Note that σ counts the number of corona chains at the interface divided by the surface area of core, i.e., $\sigma = 2N_{agg}/4\pi R_{core}^2$, where the factor of 2 accounts for two corona blocks in the triblock. This significantly higher graft density leads to a more crowding corona environment at interface, pushing corona chains outwards.

To quantify the extent of corona chain stretching, a stretching parameter (s_{corona}) is defined as $s_{corona} = R_g/R_{g,0}$, where R_g is the radius of gyration of corona chain in the micelle, and $R_{g,0}$ is that of a corona chain in solvent. The entropy gain ($\Delta S_{corona}/k$) from releasing stretched corona blocks is proportional to s_{corona}^2, assuming corona chains follow Gaussian statistics.[45] In asymmetric EPSEP' triblock micelles, R_g of the longer corona block is estimated to be half of corona layer thickness, i.e., $R_g = L_{corona}/2$. Assuming the excluded volume effect of PEP corona blocks in squalane is insignificant,[46] $R_{g,0}$ is calculated using unperturbed chain length in melts, $R_{g,0} = 0.0392 M_{PEP'}^{1/2}$, where $M_{PEP'}$ is the longer corona block molecular weight, and the resulting $R_{g,0}$ is in unit of nm. Note that $M_{PEP'}$ is converted by a factor of 0.972 (= 70/72) in the calculation, which accounts for the partially deuterated PEP repeat unit $C_5D_{2.3}H_{7.7}$ with molecular weight of one repeat unit $M_0 = 72$ g/mol, replacing $M_0 = 70$ g/mol for the fully pronated PEP. We assume that stretching of the shorter corona block is negligible in mixed shorter and longer corona blocks in asymmetric triblock micelles. This assumption is supported by the observation that the shorter core block was almost not stretched in the core formed by bidisperse core blocks.[47] For symmetric EPSEP triblocks, two identical corona blocks are equally stretched to the outermost part of the corona layer.

As shown in Table 5.7, the two asymmetric EPSEP' triblocks exhibited comparable corona chain stretching, while the symmetric EPSEP 30-24-30 showed lower stretching

per corona block. However, there is more entropy gain ($\Delta S_{corona}/k$) from releasing two equally stretched corona chains upon chain expulsion in symmetric EPSEP 30-24-30 triblock micelles, accelerating the rate of chain exchange. This argument is supported by the fact that symmetric EPSEP 72-24-72 exchanged chains one order of magnitude faster than EPSEP 30-24-30. Both are symmetric triblocks with same core block length, but EPSEP 72-24-72 has longer corona blocks than EPSEP 30-24-30, which are significantly more stretched, as shown in Table 5.7. This suggests that the corona chain stretching effect is dominant over the diffusion effect in the kinetics of chain exchange in EPSEP' triblock micelles. Otherwise, the slower diffusion through a thicker corona layer will decelerate chain exchange rate, as predicted by theory.[11] Moreover, the symmetric EPSEP 72-24-72 exhibited more than three orders of magnitude faster kinetics than SEP 26-70, both of which have similar corona layer thickness and corona block length. However, entropy gain from corona chain stretching in EPSEP 72-24-72 triblock is more than twice of the diblock, due to the presence of one more corona block per chain in the triblock. These results agree with the observation in SEP diblock micelles, where the kinetics was accelerated by more than two orders of magnitude with increasing the corona block length by four times at the constant core block length.[25] Similar to the role of corona block played in SEP diblocks, the entropy benefit from releif of stretched corona chains accelerates the kinetics of chain exchange in EPSEP' triblock micelles.

5.4 Summary

Combining SLS, DLS, SAXS, SANS, and TR-SANS, we have systematically investigated the effect of corona block asymmetry on structure and chain exchange kinetics of EPSEP' triblock micelles, where PS core block length and overall corona block length (PEP + PEP') are held constant, ≈ 26 kg/mol and ≈ 70 kg/mol, respectively.

The aggregation number, core radius, and critical micelle temperature decreased from the diblock to asymmetric and to symmetric triblock micelles, indicating a higher tendency to dissolve as free chains. Similarly, smaller hydrodynamic radius and corona layer thickness was observed with decreasing the length of the longer corona block. On the other hand, chain exchange kinetics of EPSEP' triblock micelles were more than one order of magnitude faster than the equivalent diblock. Two asymmetric triblocks exhibited comparable exchange rates, while the symmetric triblock was 10 times faster. With increasing two corona block lengths by a factor of 2.4 times, the kinetics of symmetric EPSEP 72-24-72 triblock was further accelerated by 10 times, comparing to the symmetric EPSEP 30-24-30. These results indicate that the corona block facilitates chain exchange as it does for diblocks. The faster kinetics in triblock micelles is a consequence of more entropy gain from both core blocks and stretched corona blocks when a polymer chain escapes from the micelle. Our experimental results agree with observations in DPD simulations by Peters and Lodge, where the asymmetric triblock exchanged chains faster than the diblock, but slower than the symmetric triblock. In short, this work experimentally illustrates the possibility to tune the structure and chain exchange kinetics of block copolymer micelles by tailoring the molecular architecture of block copolymers.

5.5 References

[1] Lazzari, M.; López-Quintela, M. A. Block Copolymers as a Tool for Nanomaterial Fabrication. *Adv. Mater*. **2003**, *15*, 1583−1594.

[2] Glass, R.; Möller, M.; Spatz, J. P. Block Copolymer Micelle Nanolithography. *Nanotechnology* **2003**, *14*, 1153−1160.

[3] Hamley, I. W. Nanostructure Fabrication using Block Copolymers. *Nanotechnology* **2003**, *14*, 39−54.

[4] Jeong, B.; Bae, Y. H.; Lee, D. S.; Kim, S. W. Biodegradable Block Copolymers as Injectable Drug-Delivery Systems. *Nature* **1997**, *388*, 860−862.

[5] Li, Z.; Johnson L. M.; Ricarte R. G.; Yao, L. J.; Hillmyer M. A.; Bates, F. S.; Lodge, T. P. Enhanced Performance of Blended Polymer Excipients in Delivering a Hydrophobic Drug through the Synergistic Action of Micelles and HPMCAS. *Langmuir* **2017**, *33*, 2837−2848.

[6] Li, Z.; Lenk T. I.; Yao, L. J.; Bates, F. S.; Lodge, T. P. Maintaining Hydrophobic Drug Supersaturation in a Micelle Corona Reservoir. *Macromolecules* **2018**, *51*, 540–551.

[7] Kim, S. H.; Jeong, J. H.; Lee, S. H.; Kim, S. W.; Park, T. G. Local and Systemic Delivery of VEGF siRNA Using Polyelectrolyte Complex Micelles for Effective Treatment of Cancer. *J. Controlled Release* **2008**, *129*, 107−116.

[8] Tockary, T. A.; Osada, K.; Chen, Q.; Machitani, K.; Dirisala, A.; Uchida, S.; Nomoto, T.; Toh, K.; Matsumoto, Y.; Itaka, K.; Nitta, K.; Nagayama, K.; Kataoka, K. Tethered PEG Crowdedness Determining Shape and Blood Circulation Profile of Polyplex Micelle Gene Carriers. *Macromolecules* **2013**, *46*, 6585−6592.

[9] Yoshinaga, N.; Ishii, T.; Naito, M.; Endo, T.; Uchida, S.; Cabral, H.; Osada, K.; Kataoka, K. Polyplex Micelles with Phenylboronate/Gluconamide Cross-Linking in the Core Exerting Promoted Gene Transfection through Spatiotemporal Responsivity to Intracellular pH and ATP Concentration. *J. Am. Chem. Soc.* **2017**, *139*, 18567−18575.

[10] Jiang Y.; Lodge, T. P. Reineke, T. M. Packaging pDNA by Polymeric ABC Micelles Simultaneously Achieves Colloidal Stability and Structural Control. *J. Am. Chem. Soc.* **2018**, *140*, 11101−11111.

[11] Halperin, A.; Alexander, S. Polymeric Micelles: Their Relaxation Kinetics. *Macromolecules* **1989**, *22*, 2403–2412.

[12] Halperin, A. On Micellar Exchange: The Role of the Insertion Penalty. *Macromolecules* **2011**, *44*, 5072–5074.

[13] Dormidontova, E. E. Micellization Kinetics in Block Copolymer Solutions: Scaling Model. *Macromolecules* **1999**, *32*, 7630–7644.

[14] Haliloğlu, T.; Bahar, I.; Erman, B.; Mattice, W. L. Mechanisms of the Exchange of Diblock Copolymers between Micelles at Dynamic Equilibrium. *Macromolecules* **1996**, *29*, 4764–4771.

[15] Li, Z.; Dormidontova, E. E. Kinetics of Diblock Copolymer Micellization by Dissipative Particle Dynamics. *Macromolecules* **2010**, *43*, 3521−3531.

[16] Daza, F. A. G.; Avalos, J. B.; Mackie, A. D. Logarithmic Exchange Kinetics in Monodisperse Copolymeric Micelles. *Phys. Rev. Lett.* **2017**, *118*, 248001.

[17] Daza, F. A. G.; Avalos, J. B.; Mackie, A. D. Simulation Analysis of the Kinetic Exchange of the Copolymer Surfactants in Micelles. *Langmuir* **2017**, *33*, 6794–6803.

[18] Li, Z.; Dormidontova, E. E. Equilibrium Chain Exchange Kinetics in Block Copolymer Micelle Solutions by Dissipative Particle Dynamics Simulations. *Soft Matter* **2011**, *7*, 4179–4188.

[19] Underhill, R. S.; Ding, J.; Birss, V. I.; Liu, G. Chain Exchange Kinetics of Polystyrene-*block*-poly(2-cinnamoylethyl methacrylate) Micelles in THF/Cyclopentane Mixtures. *Macromolecules* **1997**, *30*, 8298–8303.

[20] Lund, R.; Willner, L.; Stellbrink, J.; Radulescu, A.; Richter, D. Tuning of Structure and Kinetics of Chain Exchange in Star-Like PEP-PEO Block Copolymer Micelles. *Physica B* **2004**, *350*, 909−912.

[21] Lund, R.; Willner, L.; Richter, D.; Dormidontova, E. E. Equilibrium Chain Exchange Kinetics of Diblock Copolymer Micelles: Tuning and Logarithmic Relaxation. *Macromolecules* **2006**, *39*, 4566–4575.

[22] Lund, R.; Willner, L.; Stellbrink, J.; Lindner, P.; Richter, D. Logarithmic Chain-Exchange Kinetics of Diblock Copolymer Micelles. *Phys. Rev. Lett.* **2006**, *96*, 068302.

[23] Zinn, T.; Willner, L.; Pipich, V.; Richter, D.; Lund, R. Molecular Exchange Kinetics of Micelles: Corona Chain Length Dependence. *ACS Macro Lett.* **2016**, *5*, 884−888.

[24] Choi, S.; Lodge, T. P.; Bates, F. S. Mechanism of Molecular Exchange in Diblock Copolymer Micelles: Hypersensitivity to Core Chain Length. *Phys. Rev. Lett.* **2010**, *104*, 047802.

[25] Wang, E.; Lu, J.; Bates, F. S.; Lodge, T. P. Effect of Corona Block Length on the Structure and Chain Exchange Kinetics of Block Copolymer Micelles. *Macromolecules* **2018**, *51*, 3563–3571.

[26] Lund, R.; Willner, L.; Richter, D.; Iatrou, H.; Hadjichristidisc, N.; Lindner, P. Unraveling the Equilibrium Chain Exchange Kinetics of Polymeric Micelles using Small-Angle Neutron Scattering – Architectural and Topological Effects. *J. Appl. Cryst.* **2007**, *40*, 327−331.

[27] Prhashanna, A.; Chen, S. B. Chain Exchange Kinetics between Linear ABA-Type Triblock Copolymer Micelles. *Polymer* **2017**, *118*, 22−29.

[28] Lu, J.; Bates, F. S.; Lodge, T. P. Remarkable Effect of Molecular Architecture on Chain Exchange in Triblock Copolymer Micelles. *Macromolecules* **2015**, *48*, 2667−2676.

[29] Peters, A. J.; Lodge, T. P. Chain Exchange Kinetics of Asymmetric B_1AB_2 Linear Triblock and AB_1B_2 Branched Triblock Copolymers. *Macromolecules* **2017**, *50*, 6303–6313.

[30] Kuo, A. C. M.; Mark, J. E. (Ed.) *Polymer Data Handbook*, p107 and p833, New York: Oxford University Press **1999**.

[31] Jakeš, J. Regularized Positive Exponential Sum (REPES) Program – A way of Inverting Laplace Transform Data Obtained by Dynamic Light Scattering. *Collect. Czech. Chem. Commun.* **1995**, *60*, 1781−1797.

[32] Choi, S.; Bates, F. S.; Lodge, T. P. Structure of Poly(styrene-*b*-ethylene-*alt*-propylene) Diblock Copolymer Micelles in Squalane. *J. Phys. Chem. B* **2009**, *113*, 13840–13848.

[33] Pedersen, J. S.; Gerstenberg, M. C. Scattering Form Factor of Block Copolymer Micelles. *Macromolecules* **1996**, *29*, 1363–1365.

[34] Pedersen, J. S.; Hamley, I. W.; Ryu, C. Y.; Lodge, T. P. Contrast Variation Small-Angle Neutron Scattering Study of the Structure of Block Copolymer Micelles in a Slightly Selective Solvent at Semidilute Concentrations. *Macromolecules* **2000**, *33*, 542–550.

[35] Pedersen, J. S. Structure Factors Effects in Small-Angle Scattering from Block Copolymer Micelles and Star Polymers. *J. Chem. Phys.* **2001**, *114*, 2839–2846.

[36] Pedersen, J. S.; Svaneborg, C. Scattering from Block Copolymer Micelles. *Curr. Opin. Colloid Interface Sci.* **2002**, *7*, 158–166.

[37] Pedersen, J. S.; Svaneborg, C.; Almdal, K.; Hamley, I. W.; Young, R. N. A Small-Angle Neutron and X-ray Contrast Variation Scattering Study of the Structure of Block Copolymer Micelles: Corona Shape and Excluded Volume Interactions. *Macromolecules* **2003**, *36*, 416–433.

[38] Fetters, L. J.; Lohse, D. J.; Richter, D.; Witten, T. A.; Zirkel, A. Connection between Polymer Molecular Weight, Density, Chain Dimensions, and Melt Viscoelastic Properties. *Macromolecules* **1994**, *27*, 4639–4647.

[39] Bang, J.; Viswanathan, K.; Lodge, T. P.; Park, M. J.; Char, K. Temperature-Dependent Micellar Structures in Poly(styrene-*b*-isoprene) Diblock Copolymer Solutions near the Critical Micelle Temperature. *J. Chem. Phys.* **2004**, *121*, 11489–11500.

[40] Choi, S.; Bates, F. S.; Lodge, T. P. Molecular Exchange in Ordered Diblock Copolymer Micelles. *Macromolecules* **2011**, *44*, 3594–3604.

[41] Lu, J.; Bates, F. S.; Lodge, T. P. Molecular Exchange in Diblock Copolymer Micelles: Bimodal Distribution in Core-Block Molecular Weights. *ACS Macro Lett.* **2012**, *1*, 982−985.

[42] Lu, J.; Bates, F. S.; Lodge, T. P. Chain Exchange in Binary Copolymer Micelles at Equilibrium: Confirmation of the Independent Chain Hypothesis. *ACS Macro Lett.* **2013**, *2*, 451−455.

[43] Lu, J.; Bates, F. S.; Lodge, T. P. Addition of Corona Block Homopolymer Retards Chain Exchange in Solutions of Block Copolymer Micelles. *Macromolecules* **2016**, *49*, 1405−1413.

[44] Prhashanna, A.; Dormidontova, E. E. Tadpole and Mixed Linear/Tadpole Micelles of Diblock Copolymers: Thermodynamics and Chain Exchange Kinetics. *Macromolecules* **2017**, *50*, 1740−1748.

[45] Bates, F. S.; Fredrickson, G. H. Block Copolymers – Designer Soft Materials. *Physics Today* **1999**, *52*, 32–38.

[46] Radulescu A.; Mathers R. T.; Coates G. W.; Richter D.; Fetters L. J. A SANS Study of the Self-Assembly in Solution of Syndiotactic Polypropylene Homopolymers, Syndiotactic Polypropylene-*block*-poly(ethylene-*co*-propylene) Diblock Copolymers, and an Alternating Atactic-Isotactic Multisegment Polypropylene. *Macromolecules* **2004**, *37*, 6962–6971.

[47] Zhao, D.; Ma, Y.; Wang, E.; Lodge, T. P. Micellization of Binary Diblock Co-polymer Mixtures in an Ionic Liquid. *Macromolecules* **2019**, *52*, 4729−4738.

Chapter VI.
Effect of Block Length Asymmetry on Phase Behavior of Triblock Copolymers in Selective Solvent

6.1 Introduction

Block copolymers are a special class of macromolecules containing two or more distinct chains linked end-to-end. The simplest example is an AB diblock copolymer that contains a long chain of type A monomers covalently bonded to a chain of type B monomers. The incompatibility between two distinct blocks, embodied in the Flory-Huggins interaction parameter χ_{AB}, drives microphase separation of block copolymers into various structures, including lamellae (LAM), bicontinuous gyroid (G), hexagonally packed cylinders (HEX), and body centered cubic spheres (BCC).[1,2] In terms of thermodynamics, these equilibrium structures are determined by enthalpic and entropic effects of both blocks.[3,4]

When dissolved in a selective solvent that favors one of the blocks, e.g., the B block, the associated domain will be swollen by the solvent, while the A domain will contain much less solvent. This preferential partitioning of solvent adjusts the interfacial tension between the two domains, stretching both A and B blocks, and therefore, adjusts the equilibrium structures and their characteristics such as domain spacing and intra-particle size.[5-12] For example, Choi and coworkers showed the series of transitions LAM–HEX–BCC in poly(styrene)-*b*-poly(ethylene-*alt*-propylene) (PS-PEP, or SEP) diblock copolymer solutions upon adding squalane, which is a highly selective solvent for PEP.[13] In addition, an increase in domain spacing occurred in the LAM, HEX, and BCC phases with increasing volume fraction of solvent, whereas a decrease in core radii of the cylinders and spheres was observed in the HEX and BCC phases.

The variation in molecular architectures of block copolymers mediates the phase behavior as well, such as linear triblock and multi-block copolymers.[14,15] Self-consistent field theory (SCFT) simulations by Matsen and Thompson showed that symmetric BAB triblock melts exhibited similar phase behavior with the AB diblock analog that was half the length of the triblock.[16] Asymmetric BAB' triblocks, however, shifted the phase boundaries between distinct ordered morphologies, and produced larger domain spacings than the symmetric triblock, where B and B' denote different lengths.[17] This was attributed to the reduced elastic energy of the B domain filled with a mixture of shorter and longer B blocks.

Immersing a triblock copolymer in a selective solvent expands the diversity of phases.[18-21] One intriguing question is: how will the bidipersity of solvophilic block lengths influence the self-assembled morphologies of asymmetric triblock copolymer solutions? In the dilute regime, micelles formed by asymmetric PEP-PS-PEP' (EPSEP') triblock copolymers in squalane exhibited a larger core radius and higher critical micelle temperature than the symmetric triblock micelle, where PEP and PEP' represent different block lengths. Following this work, here we reveal the consequences of varying the PEP block length asymmetry in concentrated PEP-PS-PEP' triblock copolymer solutions with polymer volume fraction ranging from 1 to 0.1, using small-angle X-ray scattering (SAXS).

6.2 Materials and Methods

6.2.1 Materials

The synthesis and characterization of SEP diblock and EPSEP' triblock polymers used in this study are detailed in Chapter V. Table 6.1 summarizes characteristics of these polymers, where the nomenclature refers to the molecular weight of each block. EPSEP'

8-26-62, for example, indicates $M_n \approx 8$, 26 and 62 kg/mol for the shorter PEP block, PS midblock and the other relatively longer PEP block, respectively. All these polymers hold similar molecular weights of the PS block and similar overall combined molecular weight PEP + PEP' (≈ 26 kg/mol for PS and ≈ 70 kg/mol for PEP + PEP', to within 10%). The PEP block asymmetry parameter r (= $M_{n,PEP}/M_{n,PEP'}$) varied from 0 (i.e., SEP diblock) to 1 (i.e., symmetric triblock). Squalane ($C_{30}H_{62}$) was used as a selective solvent for the PEP blocks, which is chemically equivalent to PEP. Densities of 1.047, 0.881, and 0.810 g/cm^3 for PS, PEP, and squalane at room temperature are used to calculate the volume fraction of PS in block polymer melts and the volume fraction of polymer in solutions, assuming additivity of volumes.

Table 6.1 Polymer Characteristics

Polymers	$M_{n,\,PEP}$ (kg/mol) [a]	$M_{n,\,PS}$ (kg/mol) [a]	$M_{n,\,PEP'}$ (kg/mol) [a]	M_w/M_n [b]	f_{PS} [c]	r
SEP 26-70 [c]	–	26	70	1.04	0.24	0
EPSEP' 8-26-62	8	26	62	1.05	0.24	0.13
EPSEP' 15-28-52	15	28	52	1.04	0.26	0.29
EPSEP 30-24-30	30	24	30	1.07	0.25	1

[a] Number average molecular weight of the shorter PEP, PS midblock, and the longer PEP block.

[b] Dispersity in polymer molecular weights, reported from size exclusion chromatography (SEC).

[c] Volume fraction of PS block in block copolymer melts, using 1.047 and 0.881 g/cm^3 for PS and PEP densities at room temperature, respectively.

[d] SEP 26-70 diblock has been reported in previous work.[22,23]

6.2.2 Small-Angle X-Ray Scattering

Polymers were dissolved in squalane using dichloromethane as a co-solvent. After dichloromethane was completely evaporated at room temperature for two days, polymer solutions were loaded into hermetic aluminum pans, and sealed under argon. Solutions were annealed at 180 ºC for 30 minutes, and then slowly cooled back to room temperature. A 32-position hot pan stage was used for heating and cooling samples to target temperatures (25 – 180 ºC) on the 5-ID-D beam line at the DuPont-Northwestern-Dow (DND-CAT) station in Argonne National Laboratory. At each temperature, samples were annealed for 10 min to thermally equilibrate before exposure to X-rays. A beam energy of 17 keV, corresponding to a wavelength 0.73 Å, and a sample-to-detector distance 8.5 m were selected to give a q range of 0.003 – 0.15 $Å^{-1}$.

6.2.3 Rheology

Rheology experiments were performed on a rotational rheometer (ARES, TA Instrument) with a 25 mm diameter parallel plate. Concentrated (> 10 vol%) micelle solution samples were loaded at 120 ºC under nitrogen, filling the gap (≈ 1 mm) between two parallel plates. Samples were first tested on a strain-sweep mode (0.1 – 100%) to find the onset of linear regime. At an appropriate strain (typically 1 – 10%), samples underwent frequency-sweep from 100 to 0.1 rad/s at multiple temperatures from 30 to 150 ºC. At each temperature, samples were annealed for 10 min to thermally equilibrate before dynamic shear measurements.

6.3 Results and Discussions

6.3.1 Phase Diagrams

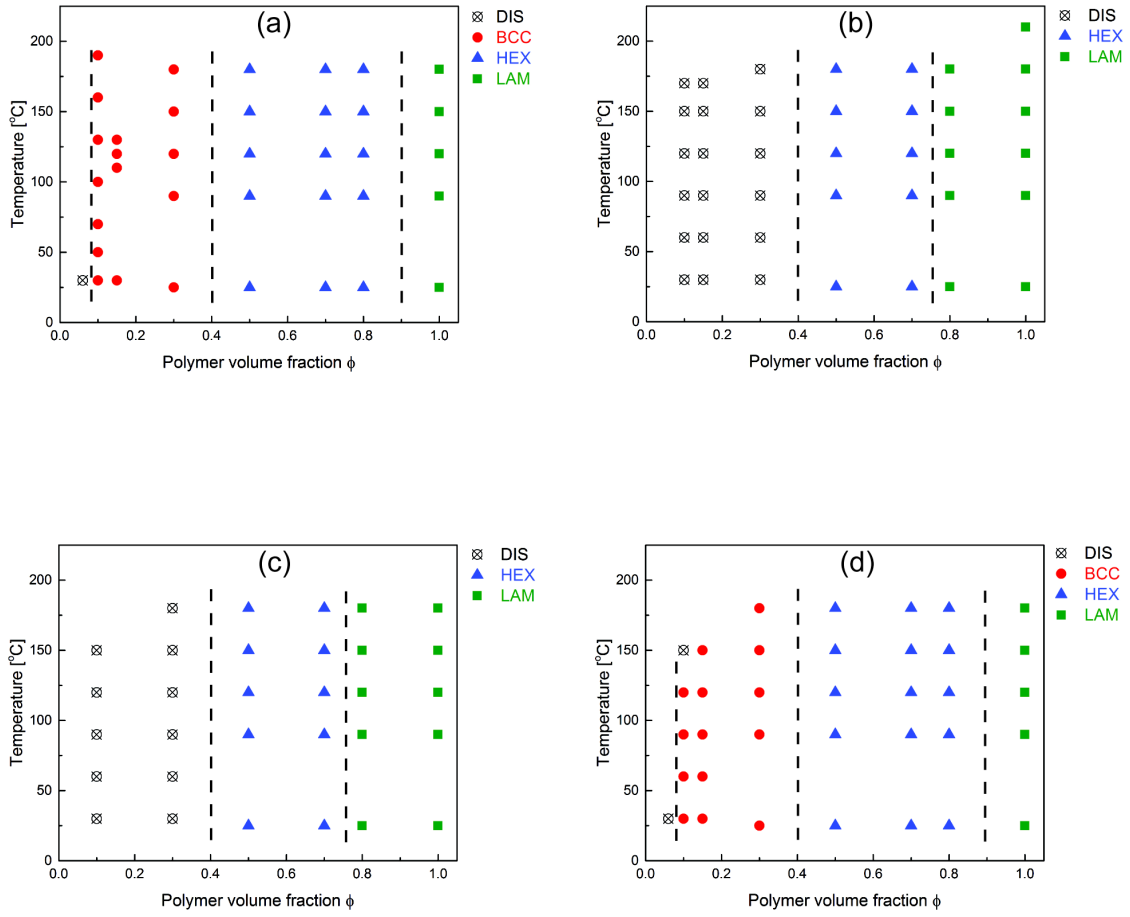

Figure 6.1 Phase diagrams of (a) SEP 26-70 diblock, (b) EPSEP' 8-26-62, (c) EPSEP' 15-28-52, and (d) EPSEP 30-24-30 triblock copolymers in squalane as a function of polymer volume fraction and temperature. LAM denotes lamellae (green squares), HEX for hexagonally packed cylinders (blue triangles), BCC for body-centered cubic spheres (red circles), DIS for disordered packing of spheres or ellipsoids (black crossed circles). Results of SEP 26-70 diblock copolymer solutions at ϕ = 0.06, 0.1, and 0.15 were reported in references 22 and 23, where details are avialable.

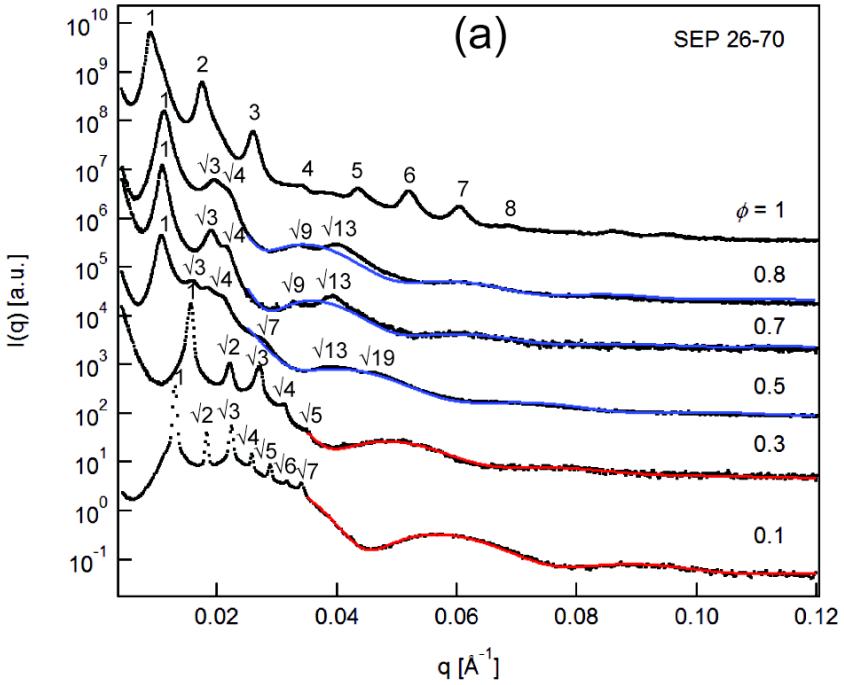
(a)
SEP 26-70
I(q) [a.u.]
q [Å^{-1}]
ϕ = 1
0.8
0.7
0.5
0.3
0.1

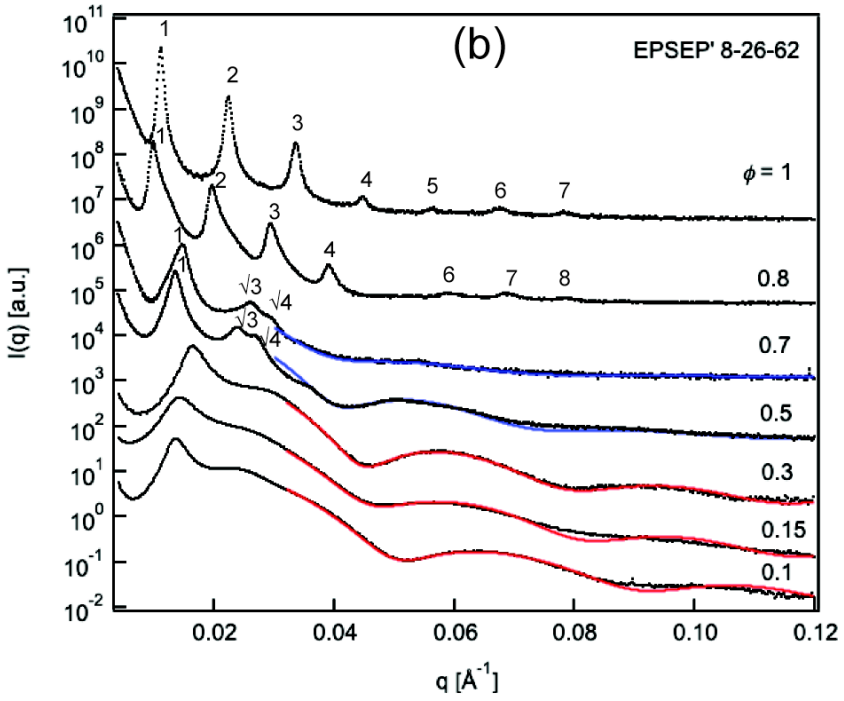
(b)
EPSEP' 8-26-62
I(q) [a.u.]
q [Å^{-1}]
ϕ = 1
0.8
0.7
0.5
0.3
0.15
0.1

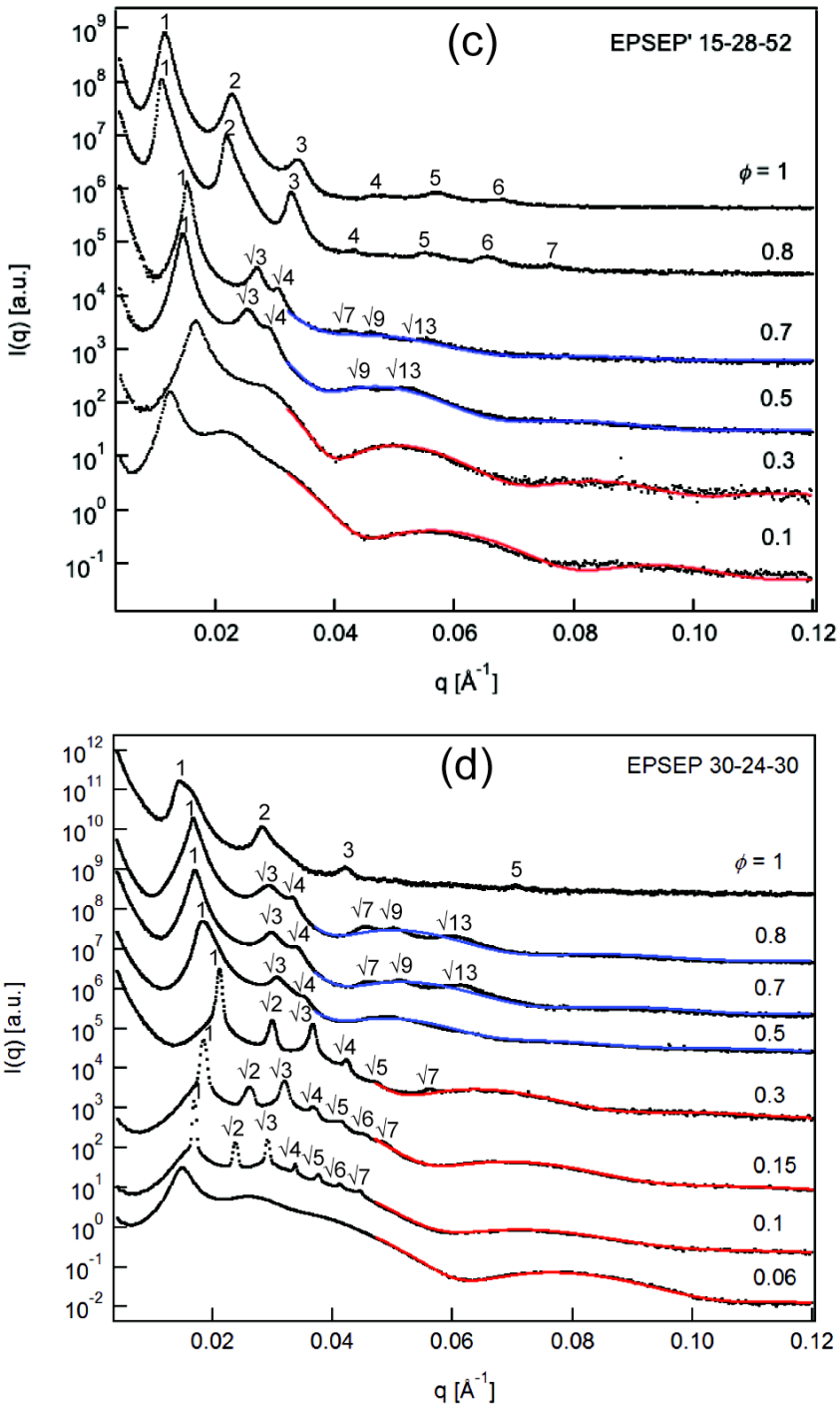

Figure 6.2 SAXS patterns and fittings to intra-particle form factors for (a) SEP 26-70 diblock, (b) EPSEP' 8-26-62, (c) EPSEP' 15-28-52, and (d) EPSEP 30-24-30 triblock copolymer solutions at different polymer volume fractions ϕ. Measurements were taken at 120 ºC.

Table 6.2 Domain Spacing and Internal Structure of SEP 26-70 Solutions at 120 ºC based on SAXS Results

ϕ =	Morphology	d (nm) [a]	R_c, R_s (nm) [b]	σ_R (nm) [c]	φ_{PS} [d]
1	LAM	71.0	–	–	–
0.8	HEX	56.6	14.4	2.0	1.09
0.7	HEX	58.2	14.2	1.6	1.04
0.5	HEX	59.0	12.1	2.2	1.05
0.3	BCC	40.4	11.9	1.1	0.95
0.1	BCC	48.5	10.2	0.8	0.87

[a] Domain spacing, $d = 2\pi/q^*$, where q^* represents the position of the primary peak.
[b] Radius of cylinder (R_c) in HEX phase and radius of sphere (R_s) in BCC phase, obtained by fitting SAXS data to cylindrical or spherical form factor.
[c] Standard deviation of radius of cylinders or spheres
[d] Volume fraction of PS in PS-rich domain: $\varphi_{PS} = \sqrt{3}a_{HEX}^2 f_{PS}\phi / (2\pi R_c^2)$ for HEX, where a_{HEX} is HEX unit cell dimension, $f_{PS} = 0.24$ is volume fraction of PS in melts, and ϕ is volume fraction of polymer in solutions; $\varphi_{PS} = 3a_{BCC}^3 f_{PS}\phi / (8\pi R_S^3)$ for BCC, where a_{BCC} is BCC unit cell size.

Figure 6.1a displays the phase diagram of SEP 26-70 in squalane as a function of polymer volume fraction and temperature. The SEP 26-70 diblock copolymer displayed a lamellar structure based on the indexing of Bragg peaks in Figure 6.2a, where the ratios of sequential peaks over the primary peak (q/q^*) were 1:2:3:4:5:6:7:8. The lamellar morphology is anticipated by theoretical predictions for SEP 26-70 melts,[24,25] which have PS volume fraction $f_{PS} = 0.24$, high segregation strength $\chi N \approx 150$ at 120 ºC, and slight conformational asymmetry $\varepsilon = (b_{PEP}/b_{PS})^2 = 1.29$. Here, $\chi = 73.9/T - 0.0576$ with reference volume $v_0 = (v_{PS} \times v_{PEP})^{1/2} = 89$ cm^3/mol, as reported in the literature,[13,26,27] and $N = 1147$, where $v_{PS} = 100$ cm^3/mol and $v_{PEP} = 80$ cm^3/mol are repeat unit volumes of PS and PEP, respectively. The conformation asymmetry parameter ε is defined as $\varepsilon =$

$(b_{PEP}/b_{PS})^2$, where b_{PEP} = 0.76 nm and b_{PS} = 0.67 nm are statistical segment lengths of PEP and PS repeat units, respectively.[28]

Upon adding squalane into the SEP diblock copolymer, a majority of this solvent partitions into the PEP domain and uniformly wets the PEP blocks; squalane is an oligomer of PEP.[29] Choi and coworkers reported more than 95 vol% squalane locating within the PEP domain in HEX and BCC phases formed by SEP 42-64 diblock copolymer in squalane.[13] This preferential partitioning of squalane changes the interfacial tension between the PS and PEP domains, and reduces the effective volume fraction of PS, $f_{eff} \approx f_{PS} \times \phi = 0.24 \times \phi$, assuming complete segregation of squalane within the PEP domain, where ϕ is the polymer volume fraction in solution. Both effects lead to the morphology transition from LAM to HEX in the presence of 20 vol% squalane, i.e., ϕ = 0.8, as shown in Figure 6.1a and 6.2a. The HEX phase was evidenced by Bragg peaks with q/q^* = 1:√3:√4:√9:√13 in the SAXS pattern, broad √7q^* and √12q^* peaks are also evident. The domain spacing ($d = 2\pi/q^*$) slightly increased from 57 to 59 nm in the HEX phase with decreasing polymer volume fraction from ϕ = 0.8 to 0.5, as listed in Table 6.2.

The form factor of cylinders $P_c(q)$ in the HEX phase was fitted using the disperse cylinder model provided by the NIST Igor Package,[30,31]

$$P_c(q) = \int f(R)\,dR \int_0^{\pi/2} \frac{2J_1(qR\sin\alpha)}{qR\sin\alpha} \frac{\sin(qL\cos\alpha/2)}{(qL\cos\alpha/2)} \sin\alpha\, d\alpha \tag{6.1}$$

$$f(R) = \frac{(z+1)^{z+1}}{\Gamma(z+1)} \frac{R^z}{R_c^{z+1}} \exp\left(-\frac{(z+1)R}{R_c}\right) \tag{6.2}$$

where R_c is the average cylinder radius, L is the cylinder length, $f(R)$ is a Schulz distribution function for disperse cylinder radii, given by eqn 6.2; $z = (R_c^2 - 1)/\sigma_R^2$, σ_R is standard deviation of radii and Γ is the gamma function. In the second integral of eqn 6.1,

J_1 is the first order Bessel function of the first kind, and $J_1(q_1R_c) = 0$ determines the first minimum q_1 in the scattering patterns, given by the characteristic equation $q_1R_c = 3.83$. For $\phi = 0.8$ sample, $q_1 = 0.029$ Å^{-1} indicates a 13.2 nm cylinder radius, which is used as initial guess for the fitting. The blue lines in Figure 6.2 represent best fits to the model with three adjustable parameters, i.e., R_c, σ_R, and L. The cylinder length L cannot be extracted from fitting reliably because the form factor in low q regime overlays with Bragg peaks. As listed in Table 6.2, the fitted result for cylinder radius R_c is 14.4 nm with standard deviation 2.0 nm, which agrees with the value calculated from the first minimum, i.e., $q_1R_c = 3.83$. In contrast to the increase in domain spacing d, the size of the PS domain decreases from 14.4 nm to 12.1 nm with decreasing polymer volume fraction from $\phi = 0.8$ to 0.5. Compared to the unperturbed end-to-end distance of 26 kg/mol PS in the melt state, $R_0 = 0.0659M^{1/2} = 10.6$ nm,[28] this decrease in R_c reduces stretching of the PS chains. However, the interfacial area per chain ($A_{int} = 2v_{PS}/R_c + 2v_{PS}/L$, where v_{PS} is the volume of PS block) simultaneously increases, and the PEP blocks becomes more stretched, as a consequence of the preferential partitioning of squalane within the PEP domain.

At higher squalane volume fraction, e.g., $\phi = 0.3$, a series of sharp peaks $q/q^* = 1{:}\sqrt{2}{:}\sqrt{3}{:}\sqrt{4}{:}\sqrt{5}$ indicate a cubic lattice. The higher order peak $q = \sqrt{7}q^*$ at $\phi = 0.1$ is consistent with a body-centered cubic (BCC) structure with long-range order. Similar to HEX, the domain spacing of BCC phases increased with added squalane, as shown in Table 6.2. A disperse hard sphere model[32,33] was employed to calculate the spherical form factor $P_s(q)$, (red lines in Figure 6.2),

$$P_s(q) = \int g(R)\left(\frac{3[\sin(qR) - (qR)\cos(qR)}{(qR)^3}\right)^2 dR \tag{6.3}$$

$$g(R) = \frac{1}{\sqrt{2\pi\sigma_R}} \exp\left[-\frac{(R - R_s)^2}{2\sigma_R^2}\right] \tag{6.4}$$

where R_s is the average sphere radius, $g(R)$ is a Gaussian distribution function for disperse radii, given by eqn 6.4, where σ_R is the standard deviation of radii. It was found that R_s decreased from 11.9 nm to 10.2 nm when the polymer concentration decreased from 30 vol% to 10 vol%, indicating the complete relaxation of PS blocks $R_s < R_0$ (= 10.6 nm), as observed in 1 vol% dilute solutions.[22] However, the interfacial area per chain ($A_{int} = 3v_{PS}/R_s$ for spheres) and PEP chain stretching increased as more squalane partitioned into the PEP domain.

The volume fraction of PS in the PS-rich domain φ_{PS} is calculated for the HEX and BCC phases based on the SAXS fitting results, as listed in Table 6.2. $\varphi_{PS} \approx 1$ confirms the assumption that the amount of squalane located in the PS domain is negligible, in good agreement with Choi's rsults.[13] Note that the uncertainty in φ_{PS} calculated for the BCC phases is larger than for the HEX phases because of significantly lower polymer volume fraction. Our observation of LAM to HEX, and HEX to BCC transitions in SEP 26-70 agrees with the phase behavior of other SEP diblock copolymers in squalane reported by Lai et al.,[26] and by Choi et al.[13] The gyroid phase was not observed, presumably because of the narrow concentration window for this structure in the strong segregation strength regime. No order–disorder transitions (ODTs) or order-order transitions (OOTs) were observed here, due to the limited polymer concentrations and temperatures that were investigated.

Table 6.3 Domain Spacing and Internal Structure of Asymmetric EPSEP' Triblock Copolymer Solutions at 120 ºC

EPSEP' 8-26-62 triblock copolymer solutions					
ϕ =	Morphology	d (nm) [a]	R_c (nm) [b]	σ_R (nm) [c]	φ_{PS} [d]
1	LAM	58.2	–	–	–
0.8	LAM	63.3	–	–	–
0.7	HEX	42.6	10.3	2.4	1.06
0.5	HEX	46.5	9.9	1.2	0.98
ϕ =	Morphology	d (nm) [a]	R_a (nm) [e]	R_b (nm) [e]	R_e (nm) [f]
0.3	DIS	38.0	12.5	9.2	10.2
0.15	DIS	43.7	19.2	9.0	11.6
0.1	DIS	46.0	11.9	8.2	9.3
EPSEP' 15-28-52 triblock copolymer solutions					
ϕ =	Morphology	d (nm) [a]	R_c (nm) [b]	σ_R (nm) [c]	φ_{PS} [d]
1	LAM	54.0	–	–	–
0.8	LAM	57.1	–	–	–
0.7	HEX	41.1	10.3	2.3	1.06
0.5	HEX	43.1	10.4	1.6	0.82
ϕ =	Morphology	d (nm) [a]	R_a (nm) [e]	R_b (nm) [e]	R_e (nm) [f]
0.3	DIS	37.6	14.3	10.4	11.6
0.1	DIS	49.9	13.9	9.2	10.6

[a] Domain spacing, $d = 2\pi/q^*$, where q^* represents the position of primary peak.

[b] Radius of cylinder (R_c) in HEX phase obtained by fitting SAXS data to cylindrical form factor.

[c] Standard deviation of radius of cylinders

[d] Volume fraction of PS in PS-rich domain: $\varphi_{PS} = \sqrt{3} a_{HEX}^2 f_{PS} \phi / (2\pi R_c^2)$ for HEX.

[e] Radius of ellipsoid (R_a and R_b, where R_a is along the rotational axis of ellipsoid) by fitting SAXS data to ellipsoidal form factor.

[f] The average radius of an ellipsoid (R_e) was calculated by $R_e^3 = R_a \times R_b^2$.

Similar to the diblock, the two asymmetric EPSEP' triblock copolymers showed lamellar morphologies in the pure melt state, as indicated in Figure 6.1b and c, based on the SAXS patterns in Figure 6.2b and c. For an asymmetric BAB' triblock with $f_B = 0.76$ strong segregation strength theory ($\chi N = 40$) [17] predicts the critical asymmetry $r_c \approx 0.06$, below which the shorter B block remains within the A domain. The most asymmetric triblock in this work, i.e., EPSEP' 8-26-62, has segregation strength $\chi N \approx 148$ at 120 ºC, and PEP block asymmetry $r = 0.13$, where $\chi \approx 0.13$ at 120 ºC, $N = 1142$. The stronger segregation strength between PS and PEP will push towards smaller r_c, due to higher energetic cost of placing the shorter PEP block in the PS domain, $\chi(N_{PS}+N_{PEP}) \approx 48$, where N_{PS} and N_{PEP} are the volumetric degrees of polymerization for PS and the shorter PEP block, respectively. For the most asymmetric triblock copolymers, EPSEP' 8-26-62 and EPSEP' 15-28-52, we assume the shorter PEP block is completely excluded from the PS domain (i.e., $r > r_c$).

We assume squalane is also completely segregated within the PEP domain in EPSEP' triblocks, based on the calculation $\varphi_{PS} \approx 1$ in the $\phi = 0.7$ and 0.5 asymmetric EPSEP' triblock copolymer solutions (Table 6.3). Therefore, the effective volume fraction of PS is estimated as $f_{eff} \approx f_{PS} \times \phi$, where f_{PS} is the volume fraction of the PS block in EPSEP' triblock melts, and ϕ is the volume fraction of EPSEP' triblock copolymer in solution. Lamellae persist at $\phi = 0.8$ in the asymmetric EPSEP' triblocks, with the q^* shifted towards lower q, indicating an increase in domain spacing. This result is in contrast to the HEX phase appearing in SEP 26-70 diblock and in symmetric EPSEP 30-24-30 triblock solutions (Figure 6.2d) at the same concentration. This is attributed to a stiffer layer of bidisperse PEP blocks near the interface in asymmetric triblocks, compared to that of monodisperse PEP blocks in the symmetric triblock. Moreover, the shorter PEP block mediates the spontaneous curvature by curving the interface away from the PS domain, as shown in asymmetric BAB' triblock melts by Matsen, where the boundary between LAM

and gyroid (and HEX) were shifted to lower volume fraction of A blocks.[17] Assuming that squalane is completely segregated within the PEP domain, the thickness of the PS domain in LAM phases can be estimated by $d_{PS} \approx d \times f_{eff} \approx d \times f_{PS} \times \phi$. For asymmetric EPSEP' 8-26-62 triblock copolymers (f_{PS} = 0.24) at ϕ = 0.8, the thickness of the PS domain was estimated as 12.2 nm, decreasing from 14.0 nm in melts, indicating a decrease in stretching of the PS blocks. Consequently, the interfacial area per chain increases, as along with additional PEP chain stretching, where $A_{int} = 2v_{PS}/d_{PS}$ for the LAM phase.

The HEX morphology appeared in the asymmetric triblocks at 70 and 50 vol% polymer concentration, as shown in Figure 6.2b and c. The domain size slightly increased with increasing the solvent volume fraction. By fitting to the cylindrical form factor (eqn 6.1 and 6.2), we found that the average core radius of cylinders slightly decreased with decreasing polymer volume fraction from ϕ = 0.7 to 0.5.

One intriguing phenomenon was the extinction of long-range ordered BCC structure in asymmetric EPSEP' triblock copolymer solutions at ϕ = 0.3 – 0.1. Based on the observation of distinct first minima in the SAXS patterns in Figures 6.2b and c, we suspect a disordered structure packed by ellipsoids. These ellipsoids failed to pack onto long-range ordered BCC morphology, as illustrated in Figure 6.3. These ellipsoids are stabilized in asymmetric triblock copolymer solutions because of a stiffer layer near the interface that resists being curved. This is supported by the observation that lamellae persisted at ϕ = 0.8 in the asymmetric EPSEP' triblocks. The ellipsoid is a compromise of mixed shorter and longer PEP blocks, where the shorter PEP blocks prefer a flatter curvature and the longer PEP blocks stay near sharper edges. By contrast, an ordered BCC morphology was observed in both SEP diblock and symmetric EPSEP triblock at these concentrations. It is worth noting that kinetic effects should be eliminated by

annealing these polymer solutions at 180 ºC for 30 minutes prior to measurements, which is much higher than the glass transition temperature of PS.

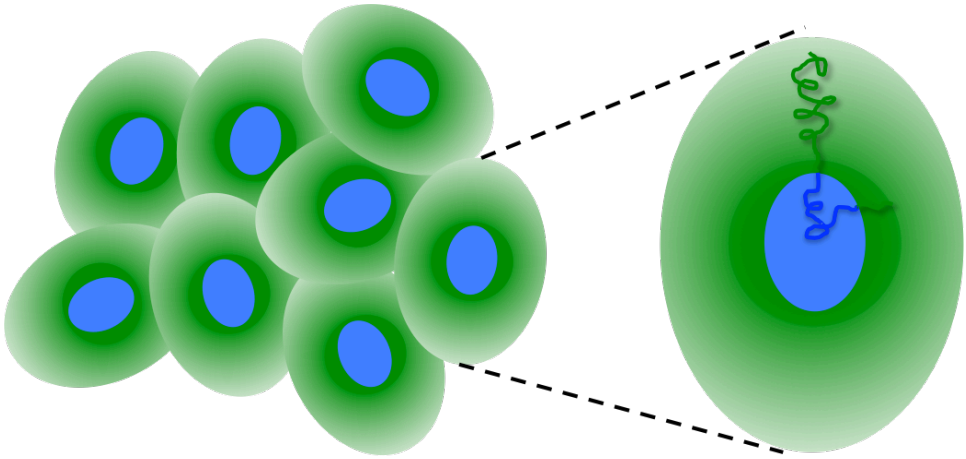

Figure 6.3 Illustration of disordered packed ellipsoids in asymmetric triblock copolymer solutions at $\phi = 0.3 - 0.1$.

The ellipsoid form factor $P_e(q)$ was employed to fit the SAXS data,[30,31] as shown in Figures 6.2b and c.

$$P_e(q) = \int_0^{\pi/2} \left(\frac{3[\sin(qR) - (qR)\cos(qR)}{(qR)^3} \right)^2 \sin\alpha d\alpha \tag{6.5}$$

$$R = R_b \left[\sin^2\alpha + \left(R_a / R_b \right)^2 \cos^2\alpha \right]^{1/2} \tag{6.6}$$

Here R_a and R_b are two adjustable fitting parameters, and R_a is along the rotational axis of ellipsoid, as listed in Table 6.3. Figure 6.4 shows an example to clarify the sensitivity of these two parameters. The red line using R_a = 12.5 nm and R_b = 9.2 nm best fits the SAXS data of EPSEP' 8-26-62 triblock copolymer solution at ϕ = 0.3, and $R_a > R_b$

suggests prolate ellipsoids with an elliptical ratio R_a/R_b = 1.4. The sharpness of the first minimum decreased if increasing R_a to 15 nm but holding R_b = 9.2 nm (green line), while the position of first minimum shifted to higher q if decreasing R_b to 8 nm but holding R_a = 12.5 nm (pink line). The blue line with R_a = R_b = 10.2 nm reproduced a sphere, matching the position of first minimum but deviating from the second minimum.

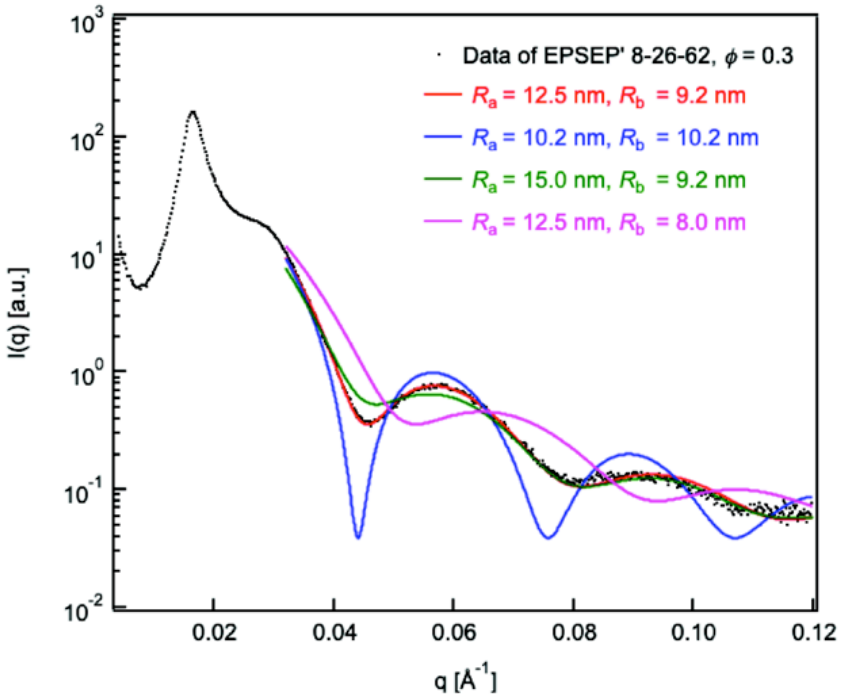

Figure 6.4 Example of ellipsoidal form factor fitting for EPSEP' 8-26-62 triblock copolymer solution at $\phi = 0.3$

The average radius of an ellipsoid (R_e) formed by asymmetric triblocks is calculated by $R_e^3 = R_a \times R_b^2$, where R_a and R_b are obtained by fitting SAXS data to the ellipsoid form factor, as listed in Table 6.3. With more squalane diluting these ellipsoids from $\phi = 0.3$ to 0.1, their radii decreased by 10% from 10.2 nm to 9.3 nm for the asymmetric EPSEP' 8-26-62 triblock, while the domain spacing increased by 21% from 38 nm to 46 nm. This

decrease in sphere radius and increase in domain spacing reflects reduced stretching of the PS blocks, but higher stretching of PEP blocks.

Table 6.4 Domain Spacing and Internal Structure of EPSEP 30-24-30 Solutions at 120 ºC

ϕ =	Morphology	d (nm) [a]	R_c, R_s (nm) [b]	σ_R (nm)[c]	φ_{PS} [d]
1	LAM	43.4	–	–	–
0.8	HEX	37.5	9.9	1.3	1.06
0.7	HEX	37.0	9.6	1.3	0.95
0.5	HEX	36.4	9.2	0.9	0.72
0.3	BCC	29.7	9.0	0.9	0.91
0.15	BCC	33.9	8.3	0.9	0.87
0.1	BCC	37.2	8.0	0.9	0.85
0.06	DIS	42.1	7.5	1.0	–

[a] Domain spacing, $d = 2\pi/q^*$, where q^* represents the position of primary peak.
[b] Radius of cylinder (R_c) in HEX phase and radius of sphere (R_s) in BCC phase, obtained by fitting SAXS data to cylindrical or spherical form factor.
[c] Standard deviation of radius of cylinder or spheres
[d] Volume fraction of PS in PS-rich domain: $\varphi_{PS} = \sqrt{3}a_{HEX}^2 f_{PS}\phi / (2\pi R_c^2)$ for HEX, and $\varphi_{PS} = 3a_{BCC}^3 f_{PS}\phi / (8\pi R_S^3)$ for BCC.

As displayed in Figure 6.1d, the symmetric EPSEP 30-24-30 exhibits phase behavior similar to the SEP diblock, which is anticipated by SCFT simulations.[16] The lamellae phase transitions to the HEX phase (ϕ = 0.8 – 0.5), and subsequently the BCC phase (ϕ = 0.3 – 0.1), as the polymer volume fraction decreases. As shown in Table 6.4, the domain spacing of the HEX phases does not change appreciably with polymer concentration, while that of the BCC structure increased from 30 nm to 37 nm as ϕ decreases from 0.3 to 0.1. The radii of the cylinders and spheres gradually decreased upon adding more squalane. At low polymer volume fractions, e.g., 0.06, the sphere size was nearly the

same as for the 1 vol% dilute spherical micelles. $\varphi_{PS} \approx 0.9$ in the BCC phase indicates that the PS cores might contain ≈ 10% solvent in the symmetric triblock, although the uncertainty of φ_{PS} is considerable at low polymer volume fractions. An order–disorder transition was observed in the $\phi = 0.1$ sample at 150 ºC, as shown in Figure 6.5, i.e., the BCC lattice melted. As more solvent penetrates into the PS cores at high temperature, the size dispersity of the spheres increases, ultimately leading to the disordered structure. Disorder is also induced by reducing the concentration to $\phi = 0.06$, as shown in Figure 6.2d.

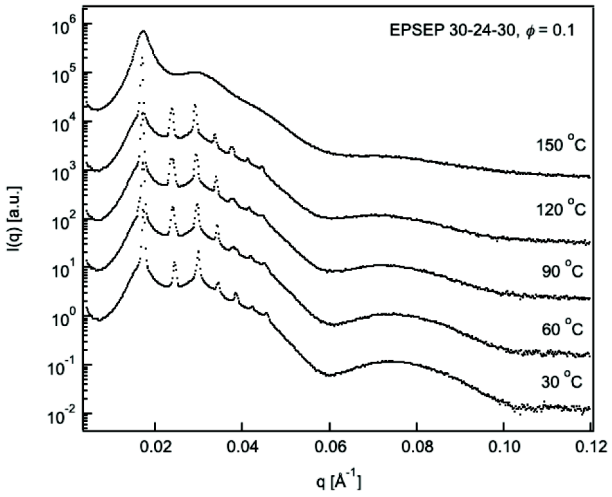

Figure 6.5 Temperature dependent SAXS results for 10 vol% EPSEP 30-24-30 triblock copolymer solution in squalane. Heating leads to disordering of the BCC morphology.

6.3.2 Block Length Asymmetry Effects

Figure 6.6a summarizes the domain spacing ($d = 2\pi/q^*$) in different morphologies formed by SEP 26-70, EPSEP' 8-26-62, EPSEP' 15-28-52, and EPSEP 30-24-30 triblock copolymer solutions at 120 ºC as a function of PEP block asymmetry parameter *r*. Here, we also present the domain spacing for the disordered structures (i.e., disordered

ellipsoids or spheres) in the asymmetric triblock copolymer solutions, although they literally lose long-range periodicity. At $\phi = 1$, in the LAM phase, the domain spacing decreased from diblock to asymmetric triblock and to symmetric triblock melts, which is in good agreement with SCFT predictions.[17] This is due to a stiffer layer of bidisperse PEP blocks near the interface in asymmetric triblocks, comparing to the symmetric triblock. Likewise, domain spacing decreases with increasing asymmetry parameter r at $\phi = 0.7$ and 0.5, where all these polymers formed HEX structures in squalane. In the sphere-forming region ($\phi = 0.3 - 0.1$), the dependence of domain spacing on the PEP block asymmetry was weaker than in the LAM and HEX phases, mainly due to the lower polymer volume fraction.

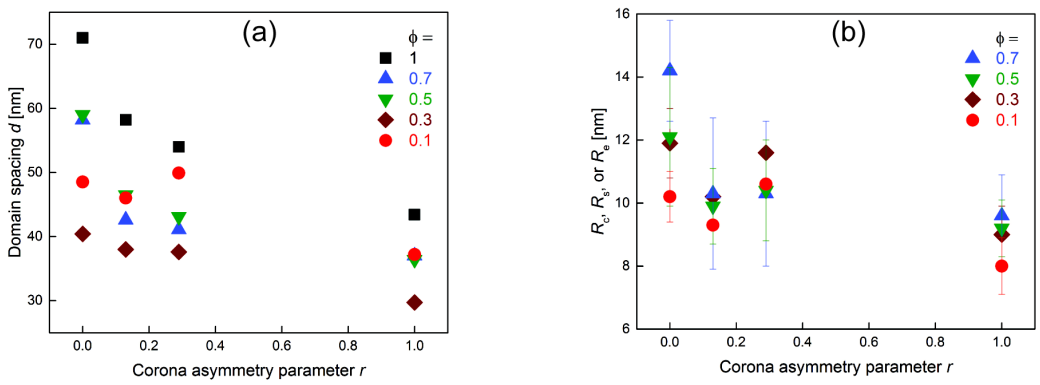

Figure 6.6(a) Domain spacing, and (b) Core radii of cylinders and spheres in SEP 26-70 diblock, asymmetric EPSEP' 8-26-62 and EPSEP' 15-28-52 triblocks and symmetric EPSEP 30-24-30 triblock copolymer solutions in squalane

As shown in Figure 6.6b, asymmetric and symmetric EPSEP' triblocks have smaller cylinder radii than the SEP diblock at $\phi = 0.7$ and 0.5. Similarly, triblocks showed smaller radii than the diblock in the sphere-forming region. It was observed in 1 vol% dilute solutions as well that the sphere size decreased with increasing PEP asymmetry

parameter *r*. This decrease in PS domain size reduces the stretching of PS chains in EPSEP triblocks, which were either looped or bridged across PS domains. The more entropy gain from relieving PS chain stretching compensated the higher interfacial energy caused by higher interfacial area per chain.

Another unexpected consequence of varying PEP block length asymmetry is that the mixed shorter and longer PEP blocks suppress long-range ordered packing of particles in asymmetric EPSEP' triblock copolymer solutions at $\phi = 0.3 - 0.1$. In this concentration range, BCC structures were observed for both diblock and symmetric triblock, both of which have narrow disperse PEP blocks. It is hypothesized that asymmetric EPSEP' triblocks form ellipsoids in the presence of a stiffer PEP layer near the interface, which resists bending. In these ellipsoids, the shorter PEP blocks preferentially distribute in middle with a flatter curvature, while the longer PEP blocks ditribute at shaper edges with more space. The dimensions of these ellipsoids were determined by fitting the SAXS data to the elliptical form factor, giving an elliptical ratio ≈ 1.5. Such a non-sphericity leads to the failure of long-range ordered packing structure.

Two SEP diblocks with similar PS block length but different PEP block lengths were mixed by equal number of polymer chains, i.e., SEP 26-70 and SEP 25-19, to mimic the mixed corona structure in the asymmetric EPSEP' triblock. As shown in Figure 6.7, the SAXS patterns of binary mixed diblocks showed sharp first minima at $\phi = 0.1$, and at $\phi = 0.01$ in dilute regime, indicating narrow dispersity spheres. By fitting the SAXS data to the spherical form factor, radius of spheres and standard deviation of radius were obtained in Table 6.5. The size of sphere was between that of pure SEP 26-70 diblock,[22] i.e., 9.0 nm, and that of pure SEP 25-19 diblock,[34] i.e., 11.2 nm, in 1 vol% dilute solutions. The small standard deviation of radius of spheres suggests that these two SEP diblocks are uniformly mixed and distributed, due to the almost identical core block lengths.[35] These spheres were slightly larger but still with narrow dispersity at 10 vol%

concentration, compared to in 1 vol% dilute solutions. In contrast to disordered packing of asymmetric EPSEP' ellipsoids, these narrow disperse spheres formed by binary mixed SEP diblocks packed onto ordered BCC structure, as shown in Figure 6.7.

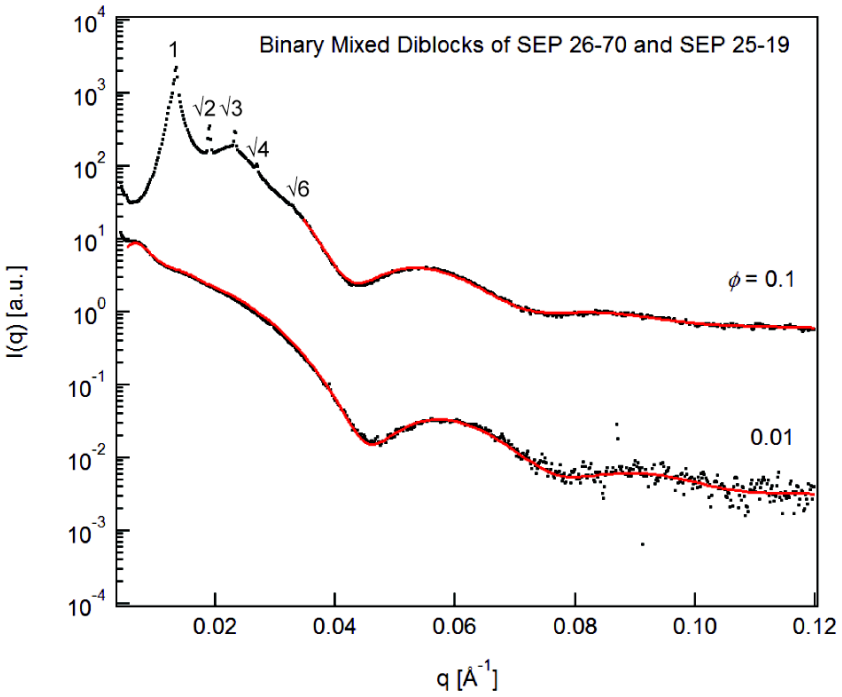

Figure 6.7 SAXS patterns of binary mixed diblocks of SEP 26-70 and SEP 25-19 by equal number of polymer chains at $\phi = 0.1$ and 0.01 at 30 ºC

Table 6.5 Domain Spacing and Structure of Binary Mixed Diblocks at 30 ºC

ϕ =	Morphology	d (nm) [a]	R_s (nm) [b]	σ_R (nm)[c]	φ_{PS} [d]
0.1	BCC	46.6	10.8	1.0	0.89
0.01	–	–	10.1	0.8	–

[a] Domain spacing, $d = 2\pi/q^*$, where q^* represents the position of primary peak.
[b] Radius of sphere (R_s) obtained by fitting SAXS data to spherical form factor.
[c] Standard deviation of radius of spheres
[d] Volume fraction of PS in PS-rich domain in BCC phase: $\varphi_{PS} = 3a_{BCC}{}^3 f_{PS}\phi / (8\pi R_S{}^3)$, where $f_{PS} = 0.33$ for binary mixed SEP 26-70 and SEP 25-19 diblocks by equal number of polymer chains.

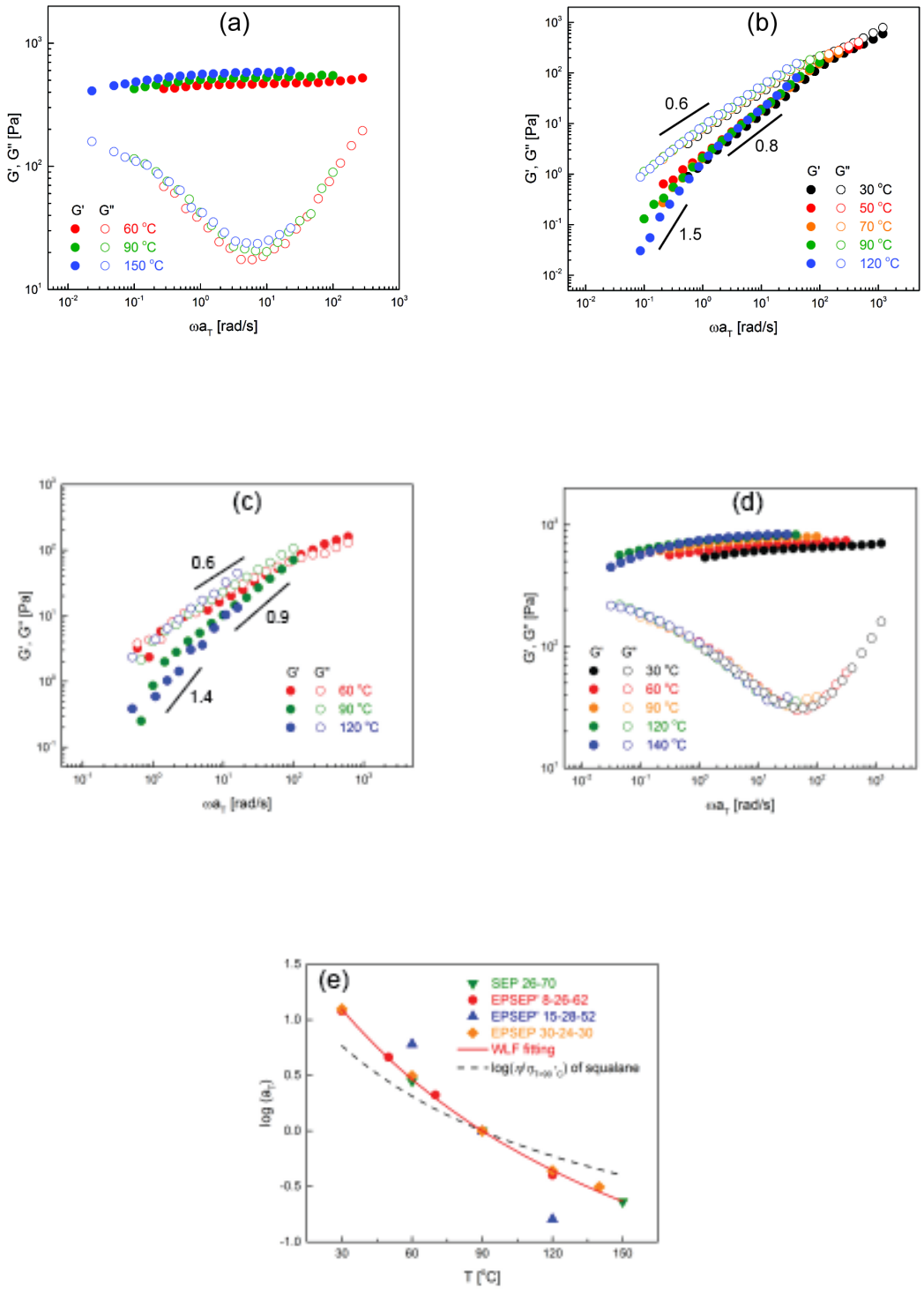

Figure 6.8 Viscoelastic behavior of (a) SEP 26-70, (b) EPSEP' 8-26-62, (c) EPSEP' 15-28-52, and (d) EPSEP 30-24-30 triblock copolymer solutions at $\phi = 0.1$ with a reference temperature of 90 ºC, and (e) shift factors used in the tTS method.

The loss of the BCC morphology influences the linear viscoelastic behavior of asymmetric EPSEP' triblock copolymer solutions. Dynamic rheological measurements were performed at low strain (1 – 10%) within the linear regime at multiple temperatures from 30 to 150 ºC. Applying the time-temperature superposition (tTS) method, data were shifted to a reference temperature of 90 ºC. As shown in Figures 6.8b and c, 10 vol% EPSEP' 8-26-62 and EPSEP' 15-28-52 solutions exhibited liquid-like behavior, where the viscous modulus was larger than elastic modulus from 30 to 120 ºC. However, the sample did not follow the characteristic response of Newtonian liquids, i.e., G' ~ ω^2, G" ~ ω^1, in low ω regime. By contrast, both SEP 26-70 and the symmetric EPSEP 30-24-30 triblock copolymer solutions showed a plateau of elastic modulus over several decades of frequency at the same concentration, as shown in Figures 6.8a and d. This is due to the presence of long-range ordered BCC structure.[36,37] The shift factors used in the tTS method were shown in Figure 6.8e, which were fitted to the WLF function: $\log(a_T) = -3(T - 90\ ºC)/(T + 136\ ºC)$. A slightly stronger temperature dependence was observed for SEP diblock, and asymmetric and symmetric EPSEP' triblock copolymer solutions than the squalane viscosity.

6.4 Summary

We have investigated the concentration dependent structures of an SEP diblock, two asymmetric EPSEP' triblocks, and a symmetric EPSEP triblock solutions in squalane, ranging in polymer volume fraction from 1 to 0.1 using SAXS measurements. Squalane is a selective solvent for the PEP blocks, and preferentially partitions within the PEP domain. A sequence of LAM–HEX–BCC morphologies was observed for both SEP diblock and symmetric EPSEP triblock copolymer solutions, which agrees with

theoretical and other experimental results.[13,16,26] The LAM-HEX phase boundary shifted to lower polymer fraction in asymmetric EPSEP' triblocks, compared to SEP diblock and the symmetric EPSEP triblock. Furthermore, a disordered packing of ellipsoids was observed at 10 – 30 vol% polymer concentration, instead of the BCC structure. The structure of ellipsoid was a compromise of mixed shorter and longer PEP in the asymmetric triblocks. The binary mixed SEP diblocks with similar PS block length but different PEP block lengths, however, formed narrow disperse spheres, and reproduced BCC packing at 10 vol% concentration. By varying the PEP block length asymmetry, smaller domain spacings and smaller PS domains were observed in LAM, HEX, and sphere forming region (BCC or DS) of symmetric triblock than those of asymmetric triblocks. This reflects an increase in PEP chain stretching and an increase in interfacial area per chain, but a decrease in PS chain stretching, from asymmetric to symmetric triblock. This result agrees with the observation in 1 vol% dilute micelle solutions, where the core size of symmetric triblock was smaller, but PEP chain stretching was stronger than the two asymmetric triblocks. In short, this work elucidates the effect of block length asymmetry on the phase behavior of triblock copolymers in selective solvent, and ultimately provides insights in design of block copolymer solutions.

6.5 References

[1] Bates, F. S. Polymer-Polymer Phase Behavior. *Science* **1991**, *251*, 898−905.

[2] Bates, F. S.; Fredrickson, G. H. Block Copolymers-Designer Soft Materials. *Phys. Today* **1999**, *52*, 32−38.

[3] Leibler, L. Theory of Microphase Separation in Block Copolymers. *Macromolecules* **1980**, *13*, 1602−1617.

[4] Bates, F. S.; Fredrickson, G. H. Block Copolymer Thermodynamics: Theory and Experiments. *Annu. Rev. Phys. Chem.* **1990**, *41*, 525–557.

[5] Sadron, C.; Gallot, B. Heterophases in Block-Copolymer/Solvent Systems in the Liquid and in the Solid State. *Makromol. Chem.* **1973**, *164*, 301−332.

[6] Douy, A.; Mayer, R.; Rossi, J.; Gallot, B. Structure of Liquid Crystalline Phases from Amorphous Block Copolymers. *Mol. Cryst. Liq. Cryst.* **1969**, *7*, 103–126.

[7] Grosius, P.; Gallot, Y.; Skoulios, A, Block Copolymers, Polystyrene/Polyvinyl-2 pyridine: Synthesis, Characterization and Study of Phases Mesomorphic. *Makromol. Chem.* **1969**, *127*, 94–112.

[8] McConnell, G. A.; Gast, A. P. Melting of Ordered Arrays and Shape Transitions in Highly Concentrated Diblock Copolymer Solutions. *Macromolecules* **1997**, *30*, 435−444.

[9] Hanley, K. J.; Lodge, T. P.; Huang, C.-I. Phase Behavior of a Block Copolymer in Solvents of Varying Selectivity. *Macromolecules* **2000**, *33*, 5918−5931.

[10] Lodge, T. P.; Pudil, B.; Hanley, K. J. The Full Phase Behavior for Block Copolymers in Solvents of Varying Selectivity. *Macromolecules* **2002**, *35*, 4707−4717.

[11] Laurati, M.; Stellbrink, J. Lund, R.; Willner, L.; Richter, D. Starlike Micelles with Starlike Interactions: A Quantitative Evaluation of Structure Factors and Phase Diagram. *Phys. Rev. Lett.* **2005**, *94*, 195504.

[12] Lai, C.; Russel, W. B.; Register, R. A. Phase Behavior of Styrene-Isoprene Diblock Copolymers in Strongly Selective Solvents. *Macromolecules* **2002,** *35,* 841–849.

[13] Choi, S.; Bates, F. S.; Lodge, T. P. Small-Angle X-ray Scattering of Concentration Dependent Structures in Block Copolymer Solutions. *Macromolecules* **2014**, *47*, 7978−7986.

[14] Widin, J. M.; Schmitt, A. K.; Schmitt, A. L. Im, K.; Mahanthappa, M. K. Unexpected Consequences of Block Polydispersity on the Self-Assembly of ABA Triblock Copolymers. *J. Am. Chem. Soc.* **2012**, *134*, 3834−3844.

[15] Ludwigs, S.; Böker, A.; Abetz, V.; Müller A. H.E.; Krausch, G. Phase Behavior of Linear Polystyrene-*block*-Poly(2-vinylpyridine)-*block*-Poly(tert-butyl methacrylate) Triblock Terpolymers. *Polymer* **2003**, *44*, 6815–6823.

[16] Matsen, M.W.; Thompson, R. B. Equilibrium Behavior of Symmetric ABA Triblock Copolymer Melts. *J. Chem. Phys.* **1999**, *111*, 7139–7146.

[17] Matsen, M.W. Equilibrium Behavior of Asymmetric ABA Triblock Copolymer Melts. *J. Chem. Phys.* **2000**, *113*, 5539–5544.

[18] Mortensen, K. Phase Behaviour of Poly(ethylene oxide)-Poly(propylene oxide)-Poly(ethylene oxide) Triblock-Copolymer Dissolved in Water. *Europhys. Lett.* **1992**, *19*, 599–604.

[19] Wanka, G.; Hoffmann, H.; Ulbricht W. Phase Diagrams and Aggregation Behavior of Poly(oxyethy1ene)-Poly(oxypropylene)-Poly(oxyethylene) Triblock Copolymers in Aqueous Solutions. *Macromolecules* **1994**, *27*, 4145–4159.

[20] Shusharina, N. P.; Alexandridis, P.; Linse, P.; Balijepalli, S.; Gruenbauer, H.J.M. Phase Behavior and Structure of an ABC Triblock Copolymer Dissolved in Selective Solvent. *Eur. Phys. J. E* **2003**, *10*, 45–54.

[21] Lodge, T. P.; Hillmyer, M. A.; Zhou, Z.; Yalmon, Y. Access to the Superstrong Segregation Regime with Nonionic ABC Copolymers. *Macromolecules* **2004**, *37*, 6680–6682.

[22] Choi, S.; Bates, F. S.; Lodge, T. P. Structure of Poly(styrene-*b*-ethylene-*alt*-propylene) Diblock Copolymer Micelles in Squalane. *J. Phys. Chem. B* **2009**, *113*, 13840–13848.

[23] Choi, S.; Bates, F. S.; Lodge, T. P. Molecular Exchange in Ordered Diblock Copolymer Micelles. *Macromolecules* **2011**, *44*, 3594–3604.

[24] Matsen, M. W.; Bates, F. S. Unifying Weak- and Strong-Segregation Block Copolymer Theories. *Macromolecules* **1996**, *29*, 1091−1098.

[25] Matsen, M. W.; Bates, F. S. Conformationally Asymmetric Block Copolymers. *J. Polym. Sci. Part B* **1997**, *35*, 945−952.

[26] Lai, C.; Russel, W. B.; Register, R. A.; Marchand, G. R.; Adamson, D. H. Phase Behavior of Styrene–Isoprene Diblock Derivatives with Varying Conformational Asymmetry. *Macromolecules* **2000**, *33*, 3461−3466.

[27] Lai, C. Block Copolymer Phase Behavior: From Melt to Solution. *Ph.D. Thesis*: Princeton University, Princeton, NJ, **1999**.

[28] Fetters, L. J.; Lohse, D. J.; Richter, D.; Witten, T. A.; Zirkel, A. Connection between Polymer Molecular Weight, Density, Chain Dimensions, and Melt Viscoelastic Properties. *Macromolecules* **1994**, *27*, 4639−4647.

[29] Matsen M. W. Phase Behavior of Block Copolymer/Homopolymer Blends. *Macromolecules* **1995**, *28*, 5765–5773.

[30] Kline, S. R. J. Reduction and analysis of SANS and USANS data using IGOR Pro. *Appl. Cryst.* **2006**, *39*, 895−900.

[31] Pedersen, J. S. Form Factors of Block Copolymer Micelles with Spherical, Ellipsoidal and Cylindrical Cores. *J. Appl. Crystallogr.* **2000**, *33*, 637−640.

[32] Pedersen, J. S.; Gerstenberg, M. C. Scattering Form Factor of Block Copolymer Micelles. *Macromolecules* **1996**, *29*, 1363–1365.

[33] Bang, J.; Viswanathan, K.; Lodge, T. P.; Park, M. J.; Char, K. Temperature-Dependent Micellar Structures in Poly(styrene-*b*-isoprene) Diblock Copolymer Solutions near the Critical Micelle Temperature. *J. Chem. Phys.* **2004**, *121*, 11489–11500.

[34] Wang, E.; Lu, J.; Bates, F. S.; Lodge, T. P. Effect of Corona Block Length on the Structure and Chain Exchange Kinetics of Block Copolymer Micelles. *Macromolecules* **2018**, *51*, 3563–3571.

[35] Zhao, D.; Ma, Y.; Wang, E.; Lodge, T. P. Micellization of Binary Diblock Co-polymer Mixtures in an Ionic Liquid. *Macromolecules* **2019**, *52*, 4729−4738.

[36] Kossuth, M. B.; Morse, D. C.; Bates, F. S. Viscoelastic Behavior of Cubic Phases in Block Copolymer Melts. *J. Rheol.* **1999**, *43*, 167–196.

[37] Fredrickson, G. H.; Bates, F. S. Dynamics of Block Copolymers: Theory and Experiment. *Annu. Rev. Mater. Sci.* **1996**, *26*, 501–550.

Chapter VII.
Conclusions and Future Work

7.1 Conclusions

This doctoral thesis has systematically studied mechanisms of chain exchange in block copolymer micelles. The block copolymers used in this work are PS-PEP (SEP) diblocks and PEP-PS-PEP' (EPSEP') and PS-PEP-PS' (SEPS') triblocks, where PEP and PEP' are in different chain lengths. Polymers were synthesized by sequential anionic polymerization of PS-PI precursors, and followed by selective saturation of PI blocks while PS blocks were retained. SEC and ^{1}H-NMR were employed to characterize the molecular characteristics of these block copolymers. Squalane and binary solvent mixtures of squalane and 1-phenyldodecane are used as selective solvents for the PEP block. Thus, spherical micelles are formed PS-PEP block copolymers, with the PS blocks aggregating into the core, while PEP blocks swelling as corona. Micelle structures and thermodynamic properties of micelle solutions were characterized by static and dynamic light scattering (SLS and DLS), small-angle X-ray scattering (SAXS) and small-angle neutron scattering (SANS). We have systematically investigated the kinetics of chain exchange in block copolymer micelles, using time-resolved small-angle neutron scattering (TR-SANS), as discussed in Chapters III, IV, and V.

Chapter III elucidated the effect of corona block length on micelle structures and chain exchange kinetics of SEP diblock copolymer micelles, where the PS core block length was held constant ($<N_{core}> \approx 255$) but the PEP corona block length varied ($<N_{corona}> = 256 - 2080$). We observed smaller core radii and aggregation numbers, but significantly thicker corona layers, with increasing corona block length. Moreover, two orders of magnitude faster kinetics was detected with increasing corona block length by four times. This is attributed to the entropic gain arising from the relief of stretched corona chains upon chain expulsion. With comparing the values of activation energy and

corona chain stretching, a more comprehensive model has been proposed with an explicit corona block length dependent term.

Chapter IV quantified the effect of solvent selectivity on kinetics of chain exchange between SEP micelles in binary mixed solvents of squalane and 1-phenyldodecane, where 10 orders of magnitude acceleration in kinetics was observed when mixing squalane with 50 vol% 1-phenyldodecane. This solvent selectivity effect originates from faster dynamics of core blocks in the core that are plasticized by the remaining solvent in the core, and reduced enthalpy penalty for chain expulsion. Combining the TR-SANS data and Flory-Huggins interaction parameter χ between the core block and different binary mixed solvents, the exact χ dependence of the activation energy in chain exchange kinetics has been determined.

With a better understanding of the role of the corona block, Chapter V explored the effect of corona block asymmetry on the kinetics of EPSEP' triblock copolymer micelles, where PEP and PEP' have different lengths, but PS ≈ 26 kg/mol and the overall corona molecular weight (PEP + PEP') ≈ 70 kg/mol are held constant. Smaller aggregation number, core radius, hydrodynamic radius, and lower critical micelle temperature were observed for symmetric triblock micelles, comparing to asymmetric triblocks and the diblock. The chain exchange kinetics of the two asymmetric triblocks was one order of magnitude faster than the diblock, while the symmetric triblock was two orders of magnitude faster still. Another symmetric EPSEP 72-24-72 triblock with two longer corona blocks exhibited 10 times faster rate of chain exchange than the symmetric EPSEP 30-24-30. The faster kinetics in triblock micelles is attributed to more entropy gain from looped core blocks and stretched corona blocks when a polymer chain escapes from the micelle.

As an extended study on EPSEP' triblock micelles, Chapter VI discussed the consequences of varying corona block asymmetry on the structure of triblock copolymer solutions at high concentrations. Smaller domain spacings and smaller PS domains were observed in LAM, HEX, and sphere forming region (BCC or DS) of symmetric triblock than those of asymmetric triblocks, reflecting a stronger PEP chain stretching, larger interfacial area per chain, but lower PS chain stretching in symmetric triblocks. Furthermore, the mixed shorter and longer PEP blocks in asymmetric EPSEP' triblocks suppressed the ordering structure up to 50 vol%, while the equivalent SEP diblocks and symmetric EPSEP triblocks packed onto body-centered cubic structure at 10 –30 vol% polymer concentration. We attributed this unexpected disordered structure to the non-sphericity of ellipsoids formed by asymmetric EPSEP' triblocks, where the shorter PEP blocks preferentially distribute in the middle area with a flatter curvature and the longer PEP blocks stay on the edges.

7.2 Future Work

In addition to the topics already discussed above, there are still several interesting questions not answered in the field of chain exchange kinetics in BCP micelles. For example, chain exchange behavior of SEPS' triblock copolymer micelles with two core blocks is not well understood, where PS and PS' have different lengths. Lu and coworkers previously reported a symmetric SEPS 45-144-45 triblock to exhibit 10^4 times slower kinetics than the equivalent SEP 42-64 diblock in dilute solution,[1] where the number after the nomenclature indicates the molecular weight of each block in unit of kg/mol. Due to the hypersensitivity of core block length that has been confirmed in the diblocks, pulling out two PS core blocks with comparable lengths significantly slowed down the dynamics of SEPS triblock micelles. Assuming two core blocks independently

extract from the core, the predicted rate of chain exchange by the diblock model, however, is much slower than that observed by TR-SANS. To interpret this result, Peters and Lodge examined the mechanism of core block pullout in PS-PEP-PS triblock micelles by measuring relaxation times of the SEPS triblock micellar gels at high concentration.[2] The authors attributed this faster kinetics than diblock model prediction to two factors. First, the PS block that is relatively shorter ejected from the core faster, because two PS blocks have dispersity in lengths even though the average lengths were almost the same. Second, the energy barrier for one core block expulsion was reduced in this triblock architecture by comparing the triblock relaxation time in rheology with the one core block expulsion time in TR-SANS.

To directly test this hypothesis, asymmetric SEPS' triblock micelles have been designed in Table 2.1 in Chapter II, where two PS blocks have different lengths. The asymmetric SEPS' 25-66-41 has one 41 kg/mol PS block that is comparable with that of symmetric SEPS 45-144-45, whereas the other PS block of the asymmetric SEPS' is much shorter. The 19 kg/mol PS block of asymmetric SEPS' 19-61-26 is similar with that of symmetric SEPS 17-53-17, while the other PS block of this asymmetric SEPS' is longer. In future work, TR-SANS will be performed to measure the rate of chain exchange in asymmetric SEPS' triblock micelles. Comparing to the results from symmetric SEPS triblock, the effect of core block asymmetry will be elucidated. It worth noting that SEPS 45-144-45 exhibited more than one order of magnitude slower rate of chain exchange when increasing polymer concentration from 0.25 to 0.5 vol%. We suspect that a certain fraction of SEPS triblock micelles are bridged by the long mid-block, leading to a higher local concentration within micelle clusters. Thus, this increase in local concentration retards the rate of chain exchange.[3-5] To suppress the clustering of SEPS' triblock micelles, SEP 42-64 diblock that has a comparable PS core block length will be mixed with SEPS' triblocks. The contrast of SEP 42-64 diblock pairing with

dSEP 47-67 can be matched with solvent, so that time dependent scattering intensity only reflects exchange of SEPS' triblock copolymer chains.

Another intriguing work would be to investigate kinetics of chain exchange between small and large micelles that are formed by narrow disperse short and long SEP diblock copolymers, respectively. Since small and large micelles are not at equilibrium, aggregation number of micelles and overall number of micelles will change over time until the system reach the equilibrium. Moreover, other mechanisms such as micelle fusion/fission might also contribute to this equilibration process.[6] Previous work by Lu blended SEP 26-70 micelles with dSEP 47-67 micelles by equal volume fraction of PS and dPS core blocks, given the total polymer concentration 1 vol%.[7] TR-SANS results showed that the initial relaxation function $R(t)$ was as anticipated, where the rate of pulling out a polymer chain, i.e., either a short or a long chain, was assumed to be identical with that in its pure micelles. However, slower kinetics was observed in the long time regime, which was more evident at a higher concentration, i.e., 3 vol%. In future work, time-resolved SAXS will be conducted to resolve the evolution of micelle sizes. By measuring time-dependent micelle sizes and overall number of micelles, we might be able to elucidate the role of chain exchange in equilibration kinetics of small and large micelles.

7.3 References

[1] Lu, J.; Bates, F. S.; Lodge, T. P. Remarkable Effect of Molecular Architecture on Chain Exchange in Triblock Copolymer Micelles. *Macromolecules* **2015**, *48*, 2667−2676.

[2] Peters, A. J.; Lodge, T. P. Comparison of Gel Relaxation Times and End-Block Pullout Times in ABA Triblock Copolymer Networks. *Macromolecules* **2016** *49*, 7340–7349.

[3] Halperin, A. On Micellar Exchange: The Role of the Insertion Penalty. *Macromolecules* **2011**, *44*, 5072–5074.

[4] Choi, S.; Bates, F. S.; Lodge, T. P. Molecular Exchange in Ordered Diblock Copolymer Micelles. *Macromolecules* **2011**, *44*, 3594–3604.

[5] Lu, J.; Bates, F. S.; Lodge, T. P. Addition of Corona Block Homopolymer Retards Chain Exchange in Solutions of Block Copolymer Micelles. *Macromolecules* **2016**, *49*, 1405−1413.

[6] Dormidontova, E. E. Micellization Kinetics in Block Copolymer Solutions: Scaling Model. *Macromolecules* **1999**, *32*, 7630–7644.

[7] Lu, J. Mechanisms of Chain Exchange in Block Copolymer Micelles. *Ph.D. Thesis*: University of Minnesota, Minneapolis, MN, **2015**.

Bibliography

Lazzari, M.; López-Quintela, M. A. Block Copolymers as a Tool for Nanomaterial Fabrication. *Adv. Mater*. **2003**, *15*, 1583−1594.

Glass, R.; Möller, M.; Spatz, J. P. Block Copolymer Micelle Nanolithography. *Nanotechnology* **2003**, *14*, 1153−1160.

Hamley, I. W. Nanostructure Fabrication using Block Copolymers. *Nanotechnology* **2003**, *14*, 39−54.

Jeong, B.; Bae, Y. H.; Lee, D. S.; Kim, S. W. Biodegradable Block Copolymers as Injectable Drug-Delivery Systems. *Nature* **1997**, *388*, 860−862.

Li, Z.; Johnson L. M.; Ricarte R. G.; Yao, L. J.; Hillmyer M. A.; Bates, F. S.; Lodge, T. P. Enhanced Performance of Blended Polymer Excipients in Delivering a Hydrophobic Drug through the Synergistic Action of Micelles and HPMCAS. *Langmuir* **2017**, *33*, 2837−2848.

Li, Z.; Lenk T. I.; Yao, L. J.; Bates, F. S.; Lodge, T. P. Maintaining Hydrophobic Drug Supersaturation in a Micelle Corona Reservoir. *Macromolecules* **2018**, *51*, 540–551.

Declet-Perez C.; Francis, L. F.; Bates, F. S. Deformation Processes in Block Copolymer Toughened Epoxy. *Macromolecules* **2015**, *48*, 3672–3684.

Li, T.; Heinzer, M. J.; Francis, L. F.; Bates, F. S. Engineering Superior Toughness in Commercially Viable Block Copolymer Modified Epoxy Resin. *J. Polym. Sci. B: Polym. Phys.* **2016**, *54*, 189–204.

Li, T.; Zhang J.; Schneiderman, D. K.; Francis, L. F.; Bates, F. S. Toughening Glassy Poly(lactide) with Block Copolymer Micelles. *ACS Macro Lett.* **2016**, *5*, 359−364.

Xu J.; Howard, M. J.; Mittal, V.; Bates, F. S. Block Copolymer Micelle Toughened Isotactic Polypropylene. *Macromolecules* **2017**, *50*, 6421–6432.

Anderson, W. Block Copolymers as Viscosity Index Improvers for Lubricating Oils. US3763044A, **1973**.

Lai C.; Russel, W. B.; Register, R. A. Phase Behavior of Styrene-Isoprene Diblock Copolymers in Strongly Selective Solvents. *Macromolecules* **2002**, *35*, 841–849.

de Gennes, P. G. Conformations of Polymers Attached to an Interface. *Macromolecules* **1980**, *13*, 1069–1075.

Daoud, M.; Cotton, J. P. Star Shaped Polymers: A Model for the Conformation and its Concentration Dependence. *J. Phys. France* **1982**, *43*, 531–538.

Halperin, A. Polymeric Micelles: A Star Model. *Macromolecules* **1987**, *20*, 2943–2946.

Halperin, A.; Tirrell, M.; Lodge, T. P. Tethered Chains in Polymer Microstuctures. *Adv. Polym. Sci.* **1992**, *100*, 31–71.

Zhulina, E. B.; Adam, M.; LaRue, I.; Sheiko, S. S.; Rubinstein, M. Diblock Copolymer Micelles in a Dilute Solution. *Macromolecules* **2005**, *38*, 5330–5351.

Nelson P. H.; Rutledge G. C.; Hatton T. A. On the Size and Shape of Self-Assembled Micelles. *J. Chem. Phys.* **1997**, *107*, 10777–10781.

Viduna, D.; Milchev, A.; Binder, K. Monte Carlo Simulation of Micelle Formation in Block Copolymer Solutions. *Macromol. Theory Simul.* **1998**, *7*, 649–658.

Milchev, A.; Bhattacharya A.; Binder K. Formation of Block Copolymer Micelles in Solution: A Monte Carlo Study of Chain Length Dependence. *Macromolecules* **2001**, *34*, 1881–1893.

Srinivas G.; Shelley J. C.; Nielsen, S. O.; Discher, D. E.; Klein M. L. Simulation of Diblock Copolymer Self-Assembly, Using a Coarse-Grain Model. *J. Phys. Chem. B* **2004**, *108*, 8153–8160.

Srinivas G.; Discher, D. E.; Klein M. L. Self-Assembly and Properties of Diblock Copolymers by Coarse-Grain Molecular Dynamics. *Nat. Mater*. **2004**, *3*, 638–644.

Ortiz, V.; Nielsen, S. O.; Discher, D. E.; Klein M. L. Lipowsky R.; Shillcock, J. Dissipative Particle Dynamics Simulations of Polymersomes. *J. Phys. Chem. B* **2005**, *109*,17708–17714.

Uneyama, T.; Doi, M. Calculation of the Micellar Structure of Polymer Surfactant on the Basis of the Density Functional Theory. *Macromolecules* **2005**, *38*, 5817–5825.

Jiang, Y.; Chen T.; Ye, F.; Liang, H.; Shi, A.-C. Effect of Polydispersity on the Formation of Vesicles from Amphiphilic Diblock Copolymers. *Macromolecules* **2005**, *38*, 6710–6717.

Price, C.; Hudd, A. L; Stubbersfield, R. B. A study of Micelle Formation by a Polystyrene-poly (ethylene/propylene) Block Copolymer in a Base Lubricating Oil. *Polymer* **1980**, *21*, 9.

Candau, F.; Heatley, F.; Price, C.; Stubbersfield, R. B. An Investigation of the Structure of Micelles Formed by a Polystyrene-*b*-poly(ethylene/propylene) Block Copolymer in Paraffinic Solvents using ^{1}H and ^{13}C-Nuclear Magnetic Resonance. *Eur. Polym. J.* **1984**, *20*, 685–690.

Quintana, J. R.; Villacampa, M.; Muñoz, M.; Andrio, A.; Katime, I. A. Micellization of a Polystyrene-*block*-poly(ethylene/propylene) Copolymer in *n*-Alkanes. 1. Thermodynamic Study. *Macromolecules* **1992**, *25*, 3125–3128.

Quintana, J. R.; Villacampa, M.; Andrio, A.; Muñoz, M.; Katime, I. A. Micellization of a Polystyrene-*block*-poly(ethylene/propylene) Copolymer in *n*-Alkanes. 2. Structural Study. *Macromolecules* **1992**, *25*, 3129–3136.

Quintana, J. R.; Villacampa, M.; Katime, I. A. Micellization of a Polystyrene-*b*-poly(ethylene/propylene) Block Copolymer in *n*-Dodecane/1.4-Dioxane Mixtures. 1. Thermodynamics of Micellization. *Macromolecules* **1993**, *26*, 601–605.

Quintana, J. R.; Villacampa, M.; Katime, I. A. Micellization of a Polystyrene-*b*-poly(ethylene/propylene) Block Copolymer in *n*-Dodecane/1.4-Dioxane Mixtures. 2. Structure and Dimensions of Micelles. *Macromolecules* **1993**, *26*, 606–611.

Quintana, J. R.; Jáñez, M. D.; Villacampa, M.; Katime, I. Diblock Copolymer Micelles in Solvent Binary Mixtures. 1. Selective Solvent/Precipitant. *Macromolecules* **1995**, *26*, 4139–4143.

Villacampa, M.; de Apodaca, E. D.; Quintana, J. R.; Katime, I. Diblock Copolymer Micelles in Solvent Binary Mixtures. 2. Selective Solvent/Good Solvent. *Macromolecules* **1995**, *26*, 4144–4149.

Choi, S.; Bates, F. S.; Lodge, T. P. Structure of Poly(styrene-*b*-ethylene-*alt*-propylene) Diblock Copolymer Micelles in Squalane. *J. Phys. Chem. B* **2009**, *113*, 13840–13848.

Choi, S.; Lee, W. B.; Lodge, T. P.; Bates, F. S. Structure of Poly(styrene-*b*-ethylene-*alt*-propylene) Diblock Copolymer Micelles in Binary Solvent Mixtures. *J. Polym. Sci. B: Polym. Phys.* **2016**, *54*, 22–31.

Pedersen, J. S.; Gerstenberg, M. C. Scattering Form Factor of Block Copolymer Micelles. *Macromolecules* **1996**, *29*, 1363–1365.

Pedersen, J. S.; Hamley, I. W.; Ryu, C. Y.; Lodge, T. P. Contrast Variation Small-Angle Neutron Scattering Study of the Structure of Block Copolymer Micelles in a Slightly Selective Solvent at Semidilute Concentrations. *Macromolecules* **2000**, *33*, 542–550.

Pedersen, J. S. Structure Factors Effects in Small-Angle Scattering from Block Copolymer Micelles and Star Polymers. *J. Chem. Phys.* **2001**, *114*, 2839–2846.

Pedersen, J. S.; Svaneborg, C. Scattering from Block Copolymer Micelles. *Curr. Opin. Colloid Interface Sci.* **2002**, *7*, 158–166.

Pedersen, J. S.; Svaneborg, C.; Almdal, K.; Hamley, I. W.; Young, R. N. A Small-Angle Neutron and X-ray Contrast Variation Scattering Study of the Structure of Block Copolymer Micelles: Corona Shape and Excluded Volume Interactions. *Macromolecules* **2003**, *36*, 416–433.

Wang, E.; Lu, J.; Bates, F. S.; Lodge, T. P. Effect of Corona Block Length on the Structure and Chain Exchange Kinetics of Block Copolymer Micelles. *Macromolecules* **2018**, *51*, 3563–3571.

LaRue, I.; Adam, M.; Zhulina, E. B.; Rubinstein, M.; Pitsikalis, M.; Hadjichristidis, N.; Ivanov, D. A.; Gearba, R. I.; Anokhin, D. V.; Sheiko, S. S. Effect of the Soluble Block Size on Spherical Diblock Copolymer Micelles. *Macromolecules* **2008**, *41*, 6555–6563.

McConnell, G. A.; Gast, A. P.; Huang, J. S.; Smith, S. D. Disorder-Order Transitions in Soft Sphere Polymer Micelles. *Phys. Rev. Lett.* **1993**, *71*, 2102.

McConnell, G. A.; Lin, E. K.; Gast, A. P.; Huang, J. S.; Lin, M. Y.; Smith, S. D. Structure and Interactions in Tethered-Chain Systems. *Faraday Discuss.* **1994**, *98*, 121–138.

Bang, J.; Viswanathan, K.; Lodge, T. P.; Park, M. J.; Char, K. Temperature-Dependent Micellar Structures in Poly(styrene-*b*-isoprene) Diblock Copolymer Solutions near the Critical Micelle Temperature. *J. Chem. Phys.* **2004**, *121*, 11489–11500.

Bang, J.; Jain, S.; Li, Z.; Lodge, T. P.; Pedersen, J. S.; Kesselman, E.; Talmon, Y. Sphere, Cylinder, and Vesicle Nanoaggregates in Poly(styrene-*b*-isoprene) Diblock Copolymer Solutions. *Marcomolecules* **2006**, *39*, 1199–1208.

LaRue, I.; Adam, M.; Pitsikalis, M.; Hadjichristidis, N.; Rubinstein, M.; Sheiko, S. S. Reversible Morphological Transitions of Polystyrene-*b*-polyisoprene Micelles. *Macromolecules* **2006**, *39*, 309–314.

Aniansson, E. A. G.; Wall, S. N. On the Kinetics of Step-Wise Micelle Association. *J. Phys. Chem.* **1974**, *78*, 1024–1030.

Aniansson, E. A. G.; Wall, S. N.; Almgren, M.; Hoffmann, H.; Kielmann, I.; Ulbricht, W.; Zana, R.; Lang, J.; Tondre, C. Theory of the Kinetics of Micellar Equilibria and Quantitative Interpretation of Chemical Relaxation Studies of Micellar Solutions of Ionic Surfactants. *J. Phys. Chem.* **1976**, *80*, 905–922.

Lessner, E.; Teubner, M.; Kahlweit, M. Relaxation Experiments in Aqueous Solutions of Ionic Micelles. 1. Theory and Experiments on the System H_2O-Sodium Tetradecyl Sulfate-$NaClO_4$. *J. Phys. Chem.* **1981**, *85*, 1529–1536.

Lessner, E.; Teubner, M.; Kahlweit, M. Relaxation Experiments in Aqueous Solutions of Ionic Micelles.2. Experiments on the System H_2O-NaDS-$NaClO_4$ and Their Theoretical Interpretation. *J. Phys. Chem.* **1981**, *85*, 3167–3175.

Halperin, A.; Alexander, S. Polymeric Micelles: Their Relaxation Kinetics. *Macromolecules* **1989**, *22*, 2403–2412.

Dormidontova, E. E. Micellization Kinetics in Block Copolymer Solutions: Scaling Model. *Macromolecules* **1999**, *32*, 7630–7644.

Haliloğlu, T.; Bahar, I.; Erman, B.; Mattice, W. L. Mechanisms of the Exchange of Diblock Copolymers between Micelles at Dynamic Equilibrium. *Macromolecules* **1996**, *29*, 4764–4771.

Rharbi, Y. Fusion and Fragmentation Dynamics at Equilibrium in Triblock Copolymer Micelles. *Macromolecules* **2012**, *45*, 9823−9826.

Halperin, A. On Micellar Exchange: The Role of the Insertion Penalty. *Macromolecules* **2011**, *44*, 5072–5074.

Choi, S.; Bates, F. S.; Lodge, T. P. Molecular Exchange in Ordered Diblock Copolymer Micelles. *Macromolecules* **2011**, *44*, 3594–3604.

Lu, J.; Bates, F. S.; Lodge, T. P. Addition of Corona Block Homopolymer Retards Chain Exchange in Solutions of Block Copolymer Micelles. *Macromolecules* **2016**, *49*, 1405−1413.

Honda, C.; Hasegawa, Y.; Hirunuma, R.; Nose, T. Micellization Kinetics of Block Copolymers in Selective Solvent. *Macromolecules* **1994**, *27*, 7660–7668.

Honda, C.; Abe, Y.; Nose, T. Relaxation Kinetics of Micellization in Micelle-Forming Block Copolymer in Selective Solvent. *Macromolecules* **1996**, *29*, 6778–6785.

Goldmints, I.; Holzwarth, J. F.; Smith, K. A.; Hatton, T. A. Micellar Dynamics in Aqueous Solutions of PEO-PPO-PEO Block Copolymers. *Langmuir* **1997**, *13*, 6130–6134.

Michels, B.; Waton, G.; Zana R. Dynamics of Micelles of Poly(ethylene oxide)-Poly(propylene oxide)-Poly(ethylene oxide) Block Copolymers in Aqueous Solutions. *Langmuir* **1997**, *13*, 3111–3118.

Kositza, M. J.; Bohne, C.; Alexandridis, P.; Hatton, T. A.; Holzwarth, J. F. Micellization Dynamics and Impurity Solubilization of the Block-Copolymer L64 in an Aqueous Solution. *Langmuir* **1999**, *15*, 322–325.

Kositza, M. J.; Bohne, C.; Alexandridis, P.; Hatton, T. A.; Holzwarth, J. F. Dynamics of Micro- and Macrophase Separation of Amphiphilic Block-Copolymers in Aqueous

Solution. *Macromolecules* **1999**, *32*, 5539–5551.

Waton, G.; Michels, B.; Zana, R. Dynamics of Block Copolymer Micelles in Aqueous Solution. *Macromolecules* **2001**, *34*, 907–910.

Lund, R.; Willner, L.; Monkenbusch, M.; Panine, P.; Narayanan, T.; Colmenero, J.; Richter, D. Structural Observation and Kinetic Pathway in the Formation of Polymeric Micelles. *Phys. Rev. Lett.* **2009**, *102*, 188301.

Procházka, K.; Bednář, B.; Mukhtar, E.; Svoboda, P.; Trněná, J.; Almgren, M. Nonradiative Energy Transfer in Block Copolymer Micelles. *J. Phys. Chem.* **1991**, *95*, 4563–4568.

Underhill, R. S.; Ding, J.; Birss, V. I.; Liu, G. Chain Exchange Kinetics of Polystyrene-*block*-poly(2-cinnamoylethyl methacrylate) Micelles in THF/Cyclopentane Mixtures. *Macromolecules* **1997**, *30*, 8298–8303.

Willner, L.; Poppe, A.; Allgaier, J.; Monkenbusch, M.; Richter, D. Time-Resolved SANS for the Determination of Unimer Exchange Kinetics in Block Copolymer Micelles. *Europhys. Lett.* **2001**, *55*, 667–673.

Lund, R.; Willner, L.; Stellbrink, J.; Radulescu, A.; Richter, D. Tuning of Structure and Kinetics of Chain Exchange in Star-Like PEP-PEO Block Copolymer Micelles. *Physica B* **2004**, *350*, 909−912.

Lund, R.; Willner, L.; Richter, D.; Dormidontova, E. E. Equilibrium Chain Exchange Kinetics of Diblock Copolymer Micelles: Tuning and Logarithmic Relaxation. *Macromolecules* **2006**, *39*, 4566–4575.

Lund, R.; Willner, L.; Stellbrink, J.; Lindner, P.; Richter, D. Logarithmic Chain-Exchange Kinetics of Diblock Copolymer Micelles. *Phys. Rev. Lett.* **2006**, *96*, 068302.

Lund, R.; Willner, L.; Richter, D.; Iatrou, H.; Hadjichristidisc, N.; Lindner, P. Unraveling the Equilibrium Chain Exchange Kinetics of Polymeric Micelles using Small-Angle Neutron Scattering – Architectural and Topological Effects. *J. Appl. Cryst.* **2007**, *40*, 327−331.

Choi, S.; Lodge, T. P.; Bates, F. S. Mechanism of Molecular Exchange in Diblock Copolymer Micelles: Hypersensitivity to Core Chain Length. *Phys. Rev. Lett.* **2010**, *104*, 047802–047804.

Lund, R.; Willner, L.; Stellbrink, J.; Lindner, P.; Richter, D. Erratum: Logarithmic Chain-Exchange Kinetics of Diblock Copolymer Micelles. *Phys. Rev. Lett.* **2010**, *104*, 049902.

Zinn, T.; Willner, L.; Lund, R.; Pipich, V.; Richter, D. Equilibrium Exchange Kinetics in n-alkyl–PEO Polymeric Micelles: Single Exponential Relaxation and Chain Length Dependence. *Soft Matter* **2012**, *8*, 623−626.

Lu, J.; Bates, F. S.; Lodge, T. P. Molecular Exchange in Diblock Copolymer Micelles: Bimodal Distribution in Core-Block Molecular Weights. *ACS Macro Lett.* **2012**, *1*, 982−985.

Lu, J.; Bates, F. S.; Lodge, T. P. Chain Exchange in Binary Copolymer Micelles at Equilibrium: Confirmation of the Independent Chain Hypothesis. *ACS Macro Lett.* **2013**, *2*, 451−455.

Daza, F. A. G.; Avalos, J. B.; Mackie, A. D. Logarithmic Exchange Kinetics in Monodisperse Copolymeric Micelles. *Phys. Rev. Lett.* **2017**, *118*, 248001.

Daza, F. A. G.; Avalos, J. B.; Mackie, A. D. Simulation Analysis of the Kinetic Exchange of the Copolymer Surfactants in Micelles. *Langmuir* **2017**, *33*, 6794–6803.

Zinn, T.; Willner, L.; Pipich, V.; Richter, D.; Lund, R. Effect of Core Crystallization and Conformational Entropy on the Molecular Exchange Kinetics of Polymeric Micelles. *ACS Macro Lett.* **2015**, *4*, 651−655.

König, N.; Willner, L.; Pipich, V.; Zinn, T.; Lund, R. Cooperativity during Melting and Molecular Exchange in Micelles with Crystalline Cores. *Phys. Rev. Lett.* **2019**, *122*, 078001.

Li, Z.; Dormidontova, E. E. Equilibrium Chain Exchange Kinetics in Block Copolymer Micelle Solutions by Dissipative Particle Dynamics Simulations. *Soft Matter* **2011**, *7*, 4179–4188.

Zinn, T.; Willner, L.; Pipich, V.; Richter, D.; Lund, R. Molecular Exchange Kinetics of Micelles: Corona Chain Length Dependence. *ACS Macro Lett.* **2016**, *5*, 884−888.

Ma Y.; Lodge, T. P. Chain Exchange Kinetics in Diblock Copolymer Micelles in Ionic Liquids: The Role of χ. *Macromolecules* **2016**, *49*, 9542−9552.

Lu, J.; Bates, F. S.; Lodge, T. P. Remarkable Effect of Molecular Architecture on Chain Exchange in Triblock Copolymer Micelles. *Macromolecules* **2015**, *48*, 2667−2676.

Peters, A. J.; Lodge, T. P. Chain Exchange Kinetics of Asymmetric B_1AB_2 Linear Triblock and AB_1B_2 Branched Triblock Copolymers. *Macromolecules* **2017**, *50*, 6303–6313.

Prhashanna, A.; Chen, S. B. Chain Exchange Kinetics between Linear ABA-Type Triblock Copolymer Micelles. *Polymer* **2017**, *118*, 22−29.

Prhashanna, A.; Dormidontova, E. E. Tadpole and Mixed Linear/Tadpole Micelles of Diblock Copolymers: Thermodynamics and Chain Exchange Kinetics. *Macromolecules* **2017**, *50*, 1740−1748.

Peters, A. J.; Lodge, T. P. Comparison of Gel Relaxation Times and End-Block Pullout Times in ABA Triblock Copolymer Networks. *Macromolecules* **2016**, *49*, 7340–7349.

Lund, R.; Willner, L.; Pipich, V.; Grillo, I.; Lindner, P.; Colmenero, J.; Richter, D. Equilibrium Chain Exchange Kinetics of Diblock Copolymer Micelles: Effect of Morphology. *Macromolecules* **2011**, *44*, 6145−6154.

Zhao, D.; Ma, Y.; Lodge, T. P. Exchange Kinetics for a Single Block Copolymer in Micelles of Two Different Sizes. *Macromolecules* **2018**, *51*, 2312−2320.

Zimm, B. H. The Scattering of Light and the Radial Distribution Function of High Polymer Solutions. *J. Chem. Phys.* **1948**, *16*, 1093–1099.

Jakeš, J. Regularized Positive Exponential Sum (REPES) Program – A way of Inverting Laplace Transform Data Obtained by Dynamic Light Scattering. *Collect. Czech. Chem. Commun.* **1995**, *60*, 1781−1797.

Kataoka, K.; Harada, A.; Nagasaki, Y. Block Copolymer Micelles for Drug Delivery: Design, Characterization and Biological Significance. *Adv. Drug Delivery Rev.* **2001**, *47*, 113−131.

Tang B.; White S. P.; Frisbie, C.D.; Lodge T. P. Synergistic Increase in Ionic Conductivity and Modulus of Triblock Copolymer Ion Gels. *Macromolecules* **2015**, *48*, 4942−4950.

Tang B.; Schneiderman, D. K.; Bidoky, F. Z.; Frisbie, C.D.; Lodge T. P. Printable, Degradable, and Biocompatible Ion Gels from a Renewable ABA Triblock Polyester and a Low Toxicity Ionic Liquid. *ACS Macro Lett.* **2017**, *6*, 1083–1088.

Declet-Perez C.; Francis, L. F.; Bates, F. S. Deformation Processes in Block Copolymer Toughened Epoxy. *Macromolecules* **2015**, *48*, 3672–3684.

Lund, R.; Willner, L.; Stellbrink, J.; Radulescu, A.; Richter, D. Role of Interfacial Tension for the Structure of PEP-PEO Polymeric Micelles. A Combined SANS and Pendant Drop Tensiometry Investigation, *Macromolecules* **2004**, *37*, 9984−9993.

Li, Z.; Dormidontova, E. E. Kinetics of Diblock Copolymer Micellization by Dissipative Particle Dynamics. *Macromolecules* **2010**, *43*, 3521−3531.

Ma, Y.; Lodge, T. P. Poly(methyl methacrylate)-block-poly(n-butyl methacrylate) Diblock Copolymer Micelles in an Ionic Liquid: Scaling of Core and Corona Size with Core Block Length. *Macromolecules* **2016**, *49*, 3639−3646.

Bates, F. S.; Fredrickson, G. H. Block Copolymers – Designer Soft Materials. *Physics Today* **1999**, *52*, 32–38.

Fetters, L. J.; Lohse, D. J.; Richter, D.; Witten, T. A.; Zirkel, A. Connection between Polymer Molecular Weight, Density, Chain Dimensions, and Melt Viscoelastic Properties. *Macromolecules* **1994**, *27*, 4639–4647.

Radulescu A.; Mathers R. T.; Coates G. W.; Richter D.; Fetters L. J. A SANS Study of the Self-Assembly in Solution of Syndiotactic Polypropylene Homopolymers, Syndiotactic Polypropylene-*block*-poly(ethylene-*co*-propylene) Diblock Copolymers, and an Alternating Atactic-Isotactic Multisegment Polypropylene. *Macromolecules* **2004**, *37*, 6962–6971.

Birshtein T. M.; Zhulina E. B. Scaling Theory of Supermolecular Structures in Block Copolymer-Solvent Systems: 1. Model of Micellar Structures. *Polymer* **1989**, *30*, 170–177.

Mok M. M.; Thiagarajan R.; Flores M.; Morse D. C.; Lodge T. P. Apparent Critical Micelle Concentrations in Block Copolymer/Ionic Liquid Solutions: Remarkably Weak Dependence on Solvophobic Block Molecular Weight. *Macromolecules* **2012**, *45*, 4818–4829.

Hiemenz, P. C.; Lodge, T. P. *Polymer Chemistry* (*2nd Ed.*), p492–495, Boca Raton, Florida: CRC Press **2007**.

Richert, R.; Duvvuri, K.; Duong, L.-T. Dynamics of Glass-Forming Liquids. VII. Dielectric Relaxation of Supercooled *tris*-Naphthylbenzene, Squalane, and Decahydroisoquinoline. *J. Chem. Phys.* **2003**, *118*, 1828–1836.

Hecksher, T.; Olsen, N. B.; Dyre, J. C. Model for the Alpha and Beta Shear Mechanical Properties of Supercooled Liquids and its Comparison to Squalane Data. *J. Chem. Phys.* **2017**, *146*, 154504.

Milhet, M.; Pauly, J.; Coutinho, J. A.P.; Daridon, J.-L. Solid–Liquid Equilibria under High Pressure of Nine Pure *n*-Alkylbenzenes. *J. Chem. Eng. Data* **2008,** *53,* 233–237.

Fox, T. G.; Flory, P. J. The Glass Temperature and Related Properties of Polystyrene. Influence of Molecular Weight. *J. Polym. Sci.* **1954**, *14*, 315–319.

Williams, M. L.; Landel, R. F.; Ferry, J. D. The Temperature Dependence of Relaxation Mechanisms in Amorphous Polymers and Other Glass-forming Liquids. *J. Am. Chem. Soc.* **1955**, *77*, 3701–3707.

Chapman, B. R.; Hamersky, M. W.; Milhaupt, J. M.; Kostelecky, C.; Lodge, T. P. Structure and Dynamics of Disordered Tetrablock Copolymers: Composition and Temperature Dependence of Local Friction. *Macromolecules* **1998,** *31,* 4562–4573.

Hoarfrost, M. L.; He, Y.; Lodge, T. P. Lower Critical Solution Temperature Phase Behavior of Poly(n-butyl methacrylate) in Ionic Liquid Mixtures. *Macromolecules* **2013**, *46*, 9464−9472.

Zhao, D.; Ma, Y.; Wang, E.; Lodge, T. P. Micellization of Binary Diblock Co-polymer Mixtures in an Ionic Liquid. *Macromolecules* **2019**, *52*, 4729−4738.

Kim, S. H.; Jeong, J. H.; Lee, S. H.; Kim, S. W.; Park, T. G. Local and Systemic Delivery of VEGF siRNA Using Polyelectrolyte Complex Micelles for Effective Treatment of Cancer. *J. Controlled Release* **2008**, *129*, 107−116.

Tockary, T. A.; Osada, K.; Chen, Q.; Machitani, K.; Dirisala, A.; Uchida, S.; Nomoto, T.; Toh, K.; Matsumoto, Y.; Itaka, K.; Nitta, K.; Nagayama, K.; Kataoka, K. Tethered PEG Crowdedness Determining Shape and Blood Circulation Profile of Polyplex Micelle Gene Carriers. *Macromolecules* **2013**, *46*, 6585−6592.

Yoshinaga, N.; Ishii, T.; Naito, M.; Endo, T.; Uchida, S.; Cabral, H.; Osada, K.; Kataoka, K. Polyplex Micelles with Phenylboronate/Gluconamide Cross-Linking in the Core Exerting Promoted Gene Transfection through Spatiotemporal Responsivity to Intracellular pH and ATP Concentration. *J. Am. Chem. Soc.* **2017**, *139*, 18567−18575.

Jiang Y.; Lodge, T. P. Reineke, T. M. Packaging pDNA by Polymeric ABC Micelles Simultaneously Achieves Colloidal Stability and Structural Control. *J. Am. Chem. Soc.* **2018**, *140*, 11101−11111.

Kuo, A. C. M.; Mark, J. E. (Ed.) *Polymer Data Handbook*, p107 and p833, New York: Oxford University Press **1999**.

Bates, F. S. Polymer-Polymer Phase Behavior. *Science* **1991**, *251*, 898−905.

Leibler, L. Theory of Microphase Separation in Block Copolymers. *Macromolecules* **1980**, *13*, 1602−1617.

Bates, F. S.; Fredrickson, G. H. Block Copolymer Thermodynamics: Theory and Experiments. *Annu. Rev. Phys. Chem.* **1990**, *41*, 525–557.

Sadron, C.; Gallot, B. Heterophases in Block-Copolymer/Solvent Systems in the Liquid and in the Solid State. *Makromol. Chem.* **1973**, *164*, 301−332.

Douy, A.; Mayer, R.; Rossi, J.; Gallot, B. Structure of Liquid Crystalline Phases from Amorphous Block Copolymers. *Mol. Cryst. Liq. Cryst.* **1969**, *7*, 103–126.

Grosius, P.; Gallot, Y.; Skoulios, A, Block Copolymers, Polystyrene/Polyvinyl-2 pyridine: Synthesis, Characterization and Study of Phases Mesomorphic. *Makromol. Chem.* **1969**, *127*, 94–112.

McConnell, G. A.; Gast, A. P. Melting of Ordered Arrays and Shape Transitions in Highly Concentrated Diblock Copolymer Solutions. *Macromolecules* **1997**, *30*, 435−444.

Hanley, K. J.; Lodge, T. P.; Huang, C.-I. Phase Behavior of a Block Copolymer in Solvents of Varying Selectivity. *Macromolecules* **2000**, *33*, 5918−5931.

Lodge, T. P.; Pudil, B.; Hanley, K. J. The Full Phase Behavior for Block Copolymers in Solvents of Varying Selectivity. *Macromolecules* **2002**, *35*, 4707−4717.

Laurati, M.; Stellbrink, J. Lund, R.; Willner, L.; Richter, D. Starlike Micelles with Starlike Interactions: A Quantitative Evaluation of Structure Factors and Phase Diagram. *Phys. Rev. Lett.* **2005**, *94*, 195504.

Choi, S.; Bates, F. S.; Lodge, T. P. Small-Angle X-ray Scattering of Concentration Dependent Structures in Block Copolymer Solutions. *Macromolecules* **2014**, *47*, 7978−7986.

Widin, J. M.; Schmitt, A. K.; Schmitt, A. L. Im, K.; Mahanthappa, M. K. Unexpected Consequences of Block Polydispersity on the SelfAssembly of ABA Triblock Copolymers. *J. Am. Chem. Soc.* **2012**, *134*, 3834−3844.

Ludwigs, S.; Böker, A.; Abetz, V.; Müller A. H.E.; Krausch, G. Phase Behavior of Linear Polystyrene-*block*-Poly(2-vinylpyridine)-*block*-Poly(tert-butyl methacrylate) Triblock Terpolymers. *Polymer* **2003**, *44*, 6815–6823.

Matsen, M.W.; Thompson, R. B. Equilibrium Behavior of Symmetric ABA Triblock Copolymer Melts. *J. Chem. Phys.* **1999**, *111*, 7139–7146.

Matsen, M.W. Equilibrium Behavior of Asymmetric ABA Triblock Copolymer Melts. *J. Chem. Phys.* **2000**, *113*, 5539–5544.

Mortensen, K. Phase Behaviour of Poly(ethylene oxide)-Poly(propylene oxide)-Poly(ethylene oxide) Triblock-Copolymer Dissolved in Water. *Europhys. Lett.* **1992**, *19*, 599–604.

Wanka, G.; Hoffmann, H.; Ulbricht W. Phase Diagrams and Aggregation Behavior of Poly(oxyethy1ene)-Poly(oxypropylene)-Poly(oxyethylene) Triblock Copolymers in Aqueous Solutions. *Macromolecules* **1994**, *27*, 4145–4159.

Shusharina, N. P.; Alexandridis, P.; Linse, P.; Balijepalli, S.; Gruenbauer, H.J.M. Phase Behavior and Structure of an ABC Triblock Copolymer Dissolved in Selective Solvent. *Eur. Phys. J. E* **2003**, *10*, 45–54.

Lodge, T. P.; Hillmyer, M. A.; Zhou, Z.; Yalmon, Y. Access to the Superstrong Segregation Regime with Nonionic ABC Copolymers. *Macromolecules* **2004**, *37*, 6680–6682.

Matsen, M. W.; Bates, F. S. Unifying Weak- and Strong-Segregation Block Copolymer Theories. *Macromolecules* **1996**, *29*, 1091−1098.

Matsen, M. W.; Bates, F. S. Conformationally Asymmetric Block Copolymers. *J. Polym. Sci. Part B* **1997**, *35*, 945−952.

Lai, C.; Russel, W. B.; Register, R. A.; Marchand, G. R.; Adamson, D. H. Phase Behavior of Styrene–Isoprene Diblock Derivatives with Varying Conformational Asymmetry. *Macromolecules* **2000**, *33*, 3461−3466.

Lai, C. Block Copolymer Phase Behavior: From Melt to Solution. *Ph.D. Thesis*: Princeton University, Princeton, NJ, **1999**.

Matsen M. W. Phase Behavior of Block Copolymer/Homopolymer Blends. *Macromolecules* **1995**, *28*, 5765–5773.

Kline, S. R. J. Reduction and analysis of SANS and USANS data using IGOR Pro. *Appl. Cryst.* **2006**, *39*, 895−900.

Pedersen, J. S. Form Factors of Block Copolymer Micelles with Spherical, Ellipsoidal and Cylindrical Cores. *J. Appl. Crystallogr.* **2000**, *33*, 637−640.

Kossuth, M. B.; Morse, D. C.; Bates, F. S. Viscoelastic Behavior of Cubic Phases in Block Copolymer Melts. *J. Rheol.* **1999**, *43*, 167–196.

Fredrickson, G. H.; Bates, F. S. Dynamics of Block Copolymers: Theory and Experiment. *Annu. Rev. Mater. Sci.* **1996**, *26*, 501–550.

Lu, J. Mechanisms of Chain Exchange in Block Copolymer Micelles. *Ph.D. Thesis*: University of Minnesota, Minneapolis, MN, **2015**.